NUREG/CR–6275
ANL–94/37

Mechanical Properties of Thermally Aged Cast Stainless Steels from Shippingport Reactor Components

Manuscript Completed: July 1994
Date Published: April 1995

Prepared by
O. K. Chopra and W. J. Shack

Argonne National Laboratory
9700 South Cass Avenue
Argonne, Illinois 60439

Prepared for
Division of Engineering
Office of Nuclear Regulatory Research
U.S. Nuclear Regulatory Commission
Washington, DC 20555
NRC FIN A2256

Mechanical Properties of Thermally Aged Cast Stainless Steels from Shippingport Reactor Components

by

O. K. Chopra and W. J. Shack

Abstract

Thermal embrittlement of static–cast CF–8 stainless steel components from the decommissioned Shippingport reactor has been characterized. Cast stainless steel materials were obtained from four cold–leg check valves, three hot–leg main shutoff valves, and two pump volutes. The actual time–at–temperature for the materials was ≈13 y at ≈281°C (538°F) for the hot–leg components and ≈264°C (507°F) for the cold–leg components. Baseline mechanical properties for as–cast material were determined from tests on either recovery–annealed material, i.e., annealed for 1 h at 550°C and then water quenched, or material from the cooler region of the component. The Shippingport materials show modest decreases in fracture toughness and Charpy–impact properties and a small increase in tensile strength because of relatively low service temperatures and ferrite content of the steel. The procedure and correlations developed at Argonne National Laboratory for estimating mechanical properties of cast stainless steels predict accurate or slightly lower values for Charpy–impact energy, tensile flow stress, fracture toughness J–R curve, and J_{IC} of the materials. The kinetics of thermal embrittlement and degree of embrittlement at saturation, i.e., the minimum impact energy achieved after long–term aging, were established from materials that were aged further in the laboratory. The results were consistent with the estimates. The correlations successfully predicted the mechanical properties of the Ringhals 2 reactor hot– and crossover–leg elbows (CF–8M steel) after service of ≈15 y and the KRB reactor pump cover plate (CF–8) after ≈8 y of service.

Contents

Nomenclature ix

Executive Summary xi

Acknowledgments xiii

1 Introduction 1

2 Material Characterization 2

3 Mechanical Properties 8

3.1 Baseline Mechanical Properties 9

3.2 Charpy–Impact Energy 12

3.3 Tensile Properties 13

3.4 Fracture Toughness 20

4 Estimati on of Mechanical Properties 20

4.1 Charpy–Impact Energy 20

4.2 Fracture Toughness 31

4.3 Tensile Properties 33

5 Ringhals Reactor Elbows 40

6 KRB Reactor Pump Cover Plate 46

7 Conclusions 48

References 51

Appendix A: Charpy–Impact Energy 55

Appendix B: Tensile Properties 65

Appendix C: J–R Curve Characterization 67

List of Figures

1. Photographs of check valve, main shutoff valve, and spare pump volute from the Shippingport reactor 3

2. Microstructure along axial section of Loop A check valve from the Shippingport reactor 5

3. Microstructure along axial section of Loop B main shutoff valve from the Shippingport reactor 6

4. Microstructure along axial section of the spare volute from the Shippingport reactor 6

5. Ferrite morphology of cast materials from Loops A, B, and C cold–leg check valves from the Shippingport reactor 7

6. Ferrite morphology of cast materials from Loops A, B, and C hot–leg main shutoff valves from the Shippingport reactor 7

7. Ferrite morphology of cast materials from the cold–leg and spare pump volutes from the Shippingport reactor 8

8. Effect of annealing for 1 h at 550°C and then water quenching on Charpy–transition curves for laboratory–aged Heats 69, 68, and 75, and service–aged KRB pump cover plate 10

9. Effect of annealing on Charpy–transition curve of cast material from the hot–leg main shutoff valve 12

10. Charpy transition curves for Loop A and B cold–leg check valves after 13 y of service at 264°C 14

11. Charpy transition curves for Loop A hot–leg main shutoff valve after 13 y of service at 281°C 15

12. Charpy transition curves for Loop A pump volute after 13 y of service at 264°C 16

13. Charpy transition curves for materials from the spare pump volute and cooler region of the main shutoff valve before and after aging for 10,000 h at 400°C........ 17

14. Yield and ultimate stresses estimated from Charpy–impact data and obtained from tensile tests for cold–leg check valve and pump volute, and estimated tensile stresses of annealed materials........ 18

15. Yield and ultimate stresses estimated from Charpy–impact data and obtained from tensile tests for hot–leg main valve, and estimated tensile stresses of annealed materials 19

16. Yield and ultimate stresses estimated from Charpy–impact data and obtained from tensile tests for spare pump volute and hot–leg main valve before and after aging for 10,000 h at 400°C 21

17. Fracture toughness J–R curves at room temperature and 290°C for annealed, service–aged, and laboratory–aged material from the cold–leg check valve 22

18. Fracture toughness J–R curves at room temperature and 290°C for unaged, service–aged, and laboratory–aged material from the hot–leg main shutoff valve...... 23

19. Fracture toughness J–R curves at room temperature and 290°C for annealed, service–aged, and laboratory–aged material from the cold–leg pump volute 24

20. Fracture toughness J–R curves at room temperature and 290°C for unaged and laboratory–aged material from the spare pump volute 25

21. Flow diagram for estimating mechanical properties of cast materials obtained from the Shippingport reactor 26

22. Variations of estimated room–temperature Charpy–impact energy with service time for Loop A cold–leg check valve CA4 and pump volute PV 30

23. Variations of estimated room–temperature Charpy–impact energy with time for materials from cooler region of the hot–leg main valve MA9 and spare pump volute VR........ 31

24. Variation of estimated room–temperature Charpy–impact energy with service time for Loop A hot–leg main valve MA1 32

25. Estimated and measured fracture toughness J–R curves for the cold–leg check valve in the annealed, 13–y service at 264°C, and fully embrittled or saturation condition 34

26. Estimated and measured fracture toughness J–R curves for the hot–leg main shutoff valve in essentially unaged, 13–y service at 281°C, and fully embrittled or saturation condition........ 35

27. Estimated and measured fracture toughness J–R curves for the cold–leg pump volute in the annealed, 13–y service at 264°C, and fully embrittled or saturation condition 36

28. Estimated and measured fracture toughness J–R curves for the spare pump volute in the unaged and fully embrittled or saturation condition........ 37

29. Estimated and measured tensile stress–vs.–strain curves at room temperature and 290°C for the cold–leg check valve after service for ≈13 y at 264°C 41

30. Estimated and measured tensile stress–vs.–strain curves at room temperature and 290°C for the hot–leg main shutoff valve after service for ≈13 y at 281°C 42

31. Estimated and measured tensile stress–vs.–strain curves at room temperature and 290°C for the cold–leg pump volute after service for ≈13 y at 264°C 43

32. Estimated and measured tensile stress–vs.–strain curves at room temperature and 290°C for material from cooler regions of the hot–leg main shutoff valve in the unaged and fully embrittled or aged condition.. 44

33. Estimated and measured tensile stress–vs.–strain curves at room temperature and 290°C for the spare pump volute in the unaged and fully embrittled or aged condition 45

34. Estimated and experimentally observed room–temperature Charpy–impact energy for the Ringhals hot– and crossover–leg elbows 46

35. Estimated fracture toughness J–R curves for the Ringhals hot– and crossover–leg elbows in the unaged condition, after service, and at saturation............................. 47

36. Variation of estimated room–temperature Charpy–impact energy with service time for the KRB pump cover plate... 48

37. Estimated and measured tensile stress–vs.–strain curves at room temperature and 290°C for the KRB pump cover plate in the annealed condition and after 8 y of service at 284°C 49

38. Estimated and measured fracture toughness J–R curve for the KRB pump cover plate in the annealed or unaged condition, after service, and at saturation.............. 50

List of Tables

1. Chemical composition, ferrite morphology, and hardness of cast stainless steel components from the Shippingport, KRB, and Ringhals reactors 5

2. Values of constants in Eq. 1 for Charpy transition curve of CF–8 cast SSs from the Shippingport reactor and KRB pump cover plate.. 13

3. Measured and estimated Charpy–impact properties of cast stainless steel materials from the Shippingport, KRB, and Ringhals reactors 29

4. Measured and estimated tensile yield and flow stresses and J_{IC} values for service– and laboratory–aged cast stainless steels.. 39

Nomenclature

b	Uncracked ligament of Charpy–impact specimen (mm).
B	Thickness of Charpy–impact speciemn (mm).
C	Coefficient of power–law J–R curve expressed as $J_d = C(\Delta a)^n$.
Cr_{eq}	Chromium equivalent for a material (wt.%).
C_V	Room–temperature "normalized" Charpy–impact energy, i.e., Charpy–impact energy per unit fracture area, at any given service and aging time (J/cm^2). Fracture area for a standard Charpy V–notch specimen (ASTM Specification E 23) is 0.8 cm^2. Divide the value of impact energy in J by 0.8 to obtain "normalized" impact energy.
C_{Vint}	Initial room–temperature "normalized" Charpy–impact energy of a material, i.e., unaged material (J/cm^2).
C_{Vsat}	Room–temperature "normalized" Charpy–impact energy of a material at saturation, i.e., minimum impact energy that would be achieved for the material after long–term service (J/cm^2).
CMTR	Certified material test record.
E	Modulus of elasiticity (MPa).
J_d	Deformation J per ASTM Specification E 813-85 or E 1152–87 (kJ/m^2).
n	Exponent of power–law J–R curve.
n_1	Ramberg–Osgood parameter.
Ni_{eq}	Nickel equivalent for a material (wt.%).
P	Aging parameter, i.e., log of time of aging at 400°C.
P_m	Maximum load for instrumented Charpy–impact test (N).
P_y	Yield load for instrumented Charpy–impact test (N).
Q	Activation energy for process of thermal embrittlement (kJ/mole).
R_f	Ratio of tensile flow stress of aged and unaged cast stainless steel.
R_y	Ratio of tensile yield stress of aged and unaged cast stainless steel.
t	Service or aging time (h).
T_s	Service or aging temperature (°C).
W	Width of Charpy–impact specimen (mm).
α	Shape factor of curve for change in room–temperature Charpy–impact energy with time and temperature of aging.
α_1	Ramberg–Osgood parameter.
β	Half the maximum change in room–temperature Charpy–impact energy.
δ_c	Ferrite content calculated from chemical composition of a material (%).
Δa	Crack extension (mm).

ε	Engineering strain.
ε_o	Reference strain in Ramberg–Osgood equation.
Φ	Material parameter.
θ	Aging behavior at 400°C, i.e., log of time to achieve β reduction in impact energy at 400°C.
σ_f	Engineering flow stress expressed as average value of yield and ultimate stress, i.e., $(\sigma_y + \sigma_u)/2$ (MPa).
σ_o	Reference stress in Ramberg–Osgood equation (MPa).
σ_u	Engineering ultimate stress (MPa).
σ_y	Engineering yield stress (MPa).

In this report, all values of impact energy are considered to be for a standard Charpy–V–notch specimen per ASTM Specification E 23, i.e., 10 x 10–mm cross section and 2–mm V notch. Impact energies obtained on subsize specimens should be normalized with respect to the actual cross–sectional area and appropriate correction factors should be applied to account for size effects. Similarly, impact energy from other standards, e.g., U–notch specimen, should be converted to a Charpy–V–notch value by appropriate correlations.

SI units of measure have been used in this report. Conversion factors for measurements in British units are as follows:

To convert from	to	multiply by
in.	mm	25.4
J*	ft·lb	0.7376
kJ/m^2	$in.–lb/in.^2$	5.71015
kJ/mole	kcal/mole	0.239

*When impact energy is expressed in J/cm^2, first multiply by 0.8 to obtain impact energy of a standard Charpy V–notch specimen in J.

Executive Summary

Cast duplex stainless steels are used extensively in the nuclear industry for valve bodies, pump casings, and primary coolant piping. The ferrite phase in the duplex structure of austenitic–ferritic stainless steels increases the tensile strength and improves the soundness of casting, weldability, and resistance to stress corrosion cracking of these steels. However, these steels are susceptible to thermal embrittlement after extended service at reactor operating temperatures. Recent data have shown that thermal embrittlement of cast stainless steel components can occur during the reactor design life of 40 y. Thermal aging of cast stainless steels at these temperatures causes an increase in hardness and tensile strength; a decrease in ductility, impact strength, and fracture toughness of the material; and a shift of the Charpy transition curve to higher temperatures. In general, the low–C CF–3 steels are the most resistant to thermal embrittlement, and the Mo–bearing, high–C CF–8M steels are the least resistant.

Therefore, mechanical–property degradation due to thermal embrittlement must be assessed so that the performance of cast stainless steel components during prolonged exposure to service temperatures can be evaluated, because rupture of the primary pressure boundary could lead to a loss–of–coolant accident and possible exposure of the public to radiation. A procedure and correlations have been developed at Argonne National Laboratory for estimating fracture toughness, tensile, and Charpy–impact properties of cast stainless steel components from known material information. Mechanical properties of a specific cast stainless steel are estimated from the extent and kinetics of thermal embrittlement. Because the embrittlement mechanisms and kinetics are complex, mechanical testing of actual component materials that have completed long in–reactor service is necessary to ensure that the mechanisms observed in accelerated aging experiments are the same as those occurring in reactors. Cast stainless steel materials from the decommissioned Shippingport reactor offered a unique opportunity to validate the correlations and benchmark the laboratory studies. The mechanical–property degradation of cast stainless steel components from the Shippingport reactor is characterized in this report. The results are compared with estimates from accelerated laboratory aging studies.

Cast stainless steel materials were obtained from four cold–leg check valves, three hot–leg main shutoff valves, and two pump volutes. The actual time–at–temperature for the materials was ≈13 y at ≈281°C (538°F) for the hot–leg components and ≈264°C (507°F) for the cold–leg components. The various cast materials were analyzed to determine their chemical composition, hardness, grain structure, and ferrite content and distribution. All materials from the Shippingport reactor are CF–8 cast stainless steel, with ferrite contents in the range of 2–16%. In general, hardness increases with increases in the ferrite content of the steel. Some differences in hardness and ferrite content were observed for material from different locations in the casting. Such differences appear to be related to compositional variations. All valve materials have a radially oriented columnar grain structure. The pump volutes exhibit a mixed grain structure of columnar and equiaxed grains. The materials contain a lacy ferrite with a mean ferrite spacing in the range of 150–300 μm. The check–valve materials show a significant amount of carbides at the ferrite/austenite phase boundaries.

Charpy-impact, tensile, and fracture toughness properties of several cast stainless steel materials from the Shippingport reactor have been characterized. Baseline mechanical properties of the unaged material were determined from tests on either recovery–annealed material, i.e., material that had been annealed for 1 h at 550°C and then water quenched, or on material from a cooler region of the component. The Shippingport materials exhibited modest degradation of mechanical properties, as would be expected at the relatively low operating temperatures. The room–temperature Charpy–impact energies of the materials are relatively high and the mid–shelf Charpy transition temperatures are very low. Check valve materials were weaker than main valve materials because of the presence of phase–boundary carbides.

Some materials were aged further in the laboratory to determine the kinetics of embrittlement and the saturation or minimum fracture properties of a specific material. The results indicate that the Shippingport cast stainless steels are not very susceptible to thermal embrittlement at reactor operating temperatures. Even at saturation or fully embrittled condition, the room–temperature impact energy of the materials is >60 J/cm^2 (>35 ft·lb) and the room–temperature J_d value is >600 kJ/m^2 (>3400 in.–lb/$in.^2$) at 5–mm crack extension.

The values obtained for the reactor–aged materials show good agreement with estimations based on accelerated laboratory aging studies. The procedure and correlations for estimating thermal aging degradation of cast stainless steels predict accurate or slightly conservative values for Charpy–impact energy, tensile flow stress, fracture toughness J–R curve, and J_{IC}. The correlations also successfully predict the mechanical properties of the Ringhals reactor hot– and crossover–leg elbows after ≈15 y of service and the KRB reactor pump cover plate after ≈8 y of service.

Acknowledgments

This work was supported by the Office of the Nuclear Regulatory Research in the U.S. Nuclear Regulatory Commission (NRC), under FIN A2256, Program Manager: Edward O. Woolridge. The authors are grateful to A. Sather, L. Y. Bush, T. M. Galvin, G. M. Dragel, P. T. Toben, and W. F. Burke for their contribution to the experimental effort. The methodology and correlations for estimating mechanical properties of aged cast stainless steels have been developed as part of a program entitled “Long–Term Embrittlement of Cast Stainless Steels in LWR Systems,” sponsored by the U.S. NRC, under FIN A2243, Program Manager: Joe Muscara.

1 Introduction

Cast duplex stainless steels (SSs) are used extensively in the nuclear industry for valve bodies, pump casings, and primary coolant piping. The ferrite phase in the duplex structure of austenitic–ferritic SSs increases the tensile strength and improves the soundness of casting, weldability, and resistance to stress corrosion cracking of these steels. However, these steels are susceptible to thermal embrittlement after extended service at reactor operating temperatures, i.e., typically 282°C (540°F) for boiling water reactors, 288–327°C (550–621°F) for pressurized water reactor (PWR) primary coolant piping, and 343°C (650°F) for PWR pressurizers. Thermal aging of cast SSs at these temperatures causes an increase in hardness and tensile strength; decrease in ductility, impact strength, and fracture toughness of the material; and a shift of the Charpy transition curve to higher temperatures. Therefore, to evaluate the performance of cast SS components during prolonged exposure to service temperatures, we must assess the mechanical–property degradation that is due to thermal embrittlement, because rupture of the primary pressure boundary could lead to a loss–of–coolant accident and possible exposure of the public to radiation.

Investigations at Argonne National Laboratory (ANL)[1–8] and elsewhere[9–16] have shown that thermal embrittlement of cast SSs (i.e., ASTM Specification A–351 grades* CF–3, CF–3A, CF–8, CF–8A, and CF–8M) can occur during the reactor design life of 40 y. Cast SS components with even modest ferrite content, e.g., 10–15% ferrite, may show significant thermal embrittlement. For example, the hot–leg elbow from the Ringhals 2 reactor showed poor fracture properties, e.g., room–temperature (RT) Charpy–impact energy of 36 J (≈26 ft·lb) and fracture toughness J_{IC} values of 150–330 kJ/m^2 (856–1884 in·lb/in^2).[17] In general, various grades and heats of cast SS exhibit varying degrees of thermal embrittlement. The low–C CF–3 steels are the most resistant to thermal embrittlement, and the Mo–bearing, high–C CF–8M steels are the least resistant.

Thermal embrittlement of cast SSs results in brittle fracture associated with either cleavage of the ferrite or separation of the ferrite/austenite phase boundary. Aging of cast SSs at temperatures <500°C (<932°F) leads to precipitation of additional phases in the ferrite, e.g., formation of a Cr–rich α' phase by spinodal decomposition; nucleation and growth of α'; precipitation of a Ni– and Si–rich G phase, $M_{23}C_6$, and γ_2 (austenite); and additional precipitation and/or growth of existing carbides at the ferrite/austenite phase boundaries. Thermal embrittlement is caused primarily by formation of the Cr–rich α' phase and, to some extent, by precipitation and growth of carbides at the phase boundaries. Formation of the α' phase increases strain hardening and local tensile stress. Consequently, the critical stress level for brittle fracture is attained at higher temperatures. Predominantly brittle failure occurs when either the ferrite phase is continuous (e.g., in cast material with a large ferrite content) or the ferrite/austenite phase boundary provides an easy path for crack propagation (e.g., in high–C grades of cast steel with large phase–boundary carbides). The amount, size, and distribution of the ferrite phase in the duplex structure, and the presence of phase–boundary carbides are important parameters in controlling the degree or extent of thermal embrittlement.

---

*In this report, grades CF–3A and CF–8A are considered equivalent to CF–3 and CF–8, respectively. The A designation represents high tensile strength. The chemical composition of CF–3A and CF–8A are further restricted within the composition limits of CF–3 and CF–8, respectively, to obtain a ferrite/austenite ratio that results in higher ultimate and yield strengths.

A procedure and correlations have been developed for estimating fracture toughness, tensile, and Charpy–impact properties of cast SS components from known material information.[5–8] Mechanical properties of a specific cast SS are estimated from the extent and kinetics of thermal embrittlement. The extent of thermal embrittlement is characterized by the RT Charpy–impact energy. A correlation for the extent of thermal embrittlement at "saturation," i.e., the minimum impact energy that would be achieved for the material after long–term aging, is given in terms of the chemical composition. The extent of thermal embrittlement as a function of time and temperature of reactor service is estimated from the extent of embrittlement at saturation and from the correlations that describe the kinetics of embrittlement, which are also given in terms of chemical composition. The fracture toughness J–R curve for the material is then obtained from the correlation between the fracture toughness parameters and the RT Charpy–impact energy that is used to characterize the extent of thermal embrittlement. Tensile yield and flow stresses, and Ramberg/Osgood parameters for tensile strain hardening are estimated from the flow stress of the unaged material and the kinetics of embrittlement. Fracture toughness J_{IC} and tearing modulus can then be determined from the estimated J–R curve and tensile flow stress.

Because the embrittlement mechanisms and kinetics are complex, mechanical testing of actual component materials that have completed long in–reactor service is necessary to ensure that the mechanisms observed in accelerated aging experiments are the same as those that occur in reactors. Cast SS materials from the decommissioned Shippingport reactor offered a unique opportunity to validate the correlations and benchmark the laboratory studies. Degradation of the mechanical properties of cast SS components from the Shippingport reactor has been characterized in this report. The results are compared with estimates from accelerated laboratory aging studies.

Degradation of the mechanical properties of cast SS materials from the hot–leg and crossover–leg elbows of the Ringhals 2 reactor in Sweden and from the recirculating–pump cover assembly of the KRB reactor in Gundremmingen, Germany, is also assessed and compared with experimental data. The elbows, constructed of CF–8M steel, were in service for ≈13 y at 325°C (617°F) for the hot leg and at 291°C (556°F) for the crossover leg, and at hot standby for ≈2 y at 303°C (577°F) for the hot leg and at 274°C (525°F) for the crossover leg. The recirculating–pump cover assembly of the KRB reactor was constructed of CF–8 steel and was in service for ≈8 y at 284°C (543°F).

2 Material Characterization

Cast SS materials were obtained from four cold–leg check valves, three hot–leg main shutoff valves, and two pump volutes. One of the volutes was a "spare" that had seen service only during the first core loading; the other was in service for the entire life of the plant. The actual time–at–temperature for the materials was ≈13 y at ≈281°C (538°F) for the hot–leg components and ≈264°C (507°F) for the cold–leg components. The components were in a hot–standby condition of ≈204°C (399°F) for an additional ≈2 y. Photographs of the check valve, main shutoff valve, and spare pump volute are shown in Fig. 1.

The various cast materials were characterized to determine their chemical composition, hardness, grain structure, and ferrite content and distribution. Samples were obtained from different locations of the casting and from different regions across the thickness of the wall.

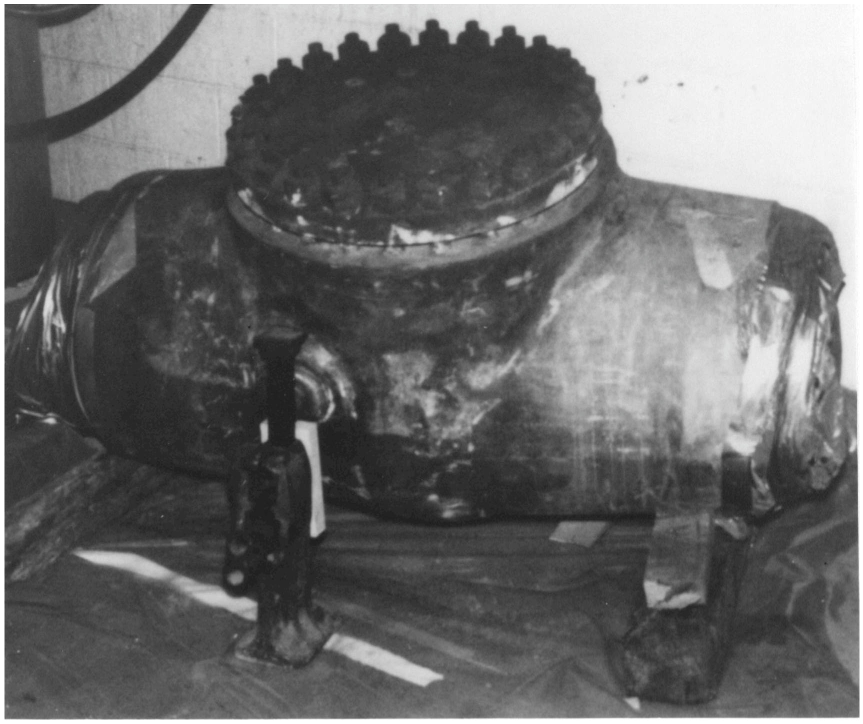

(a)

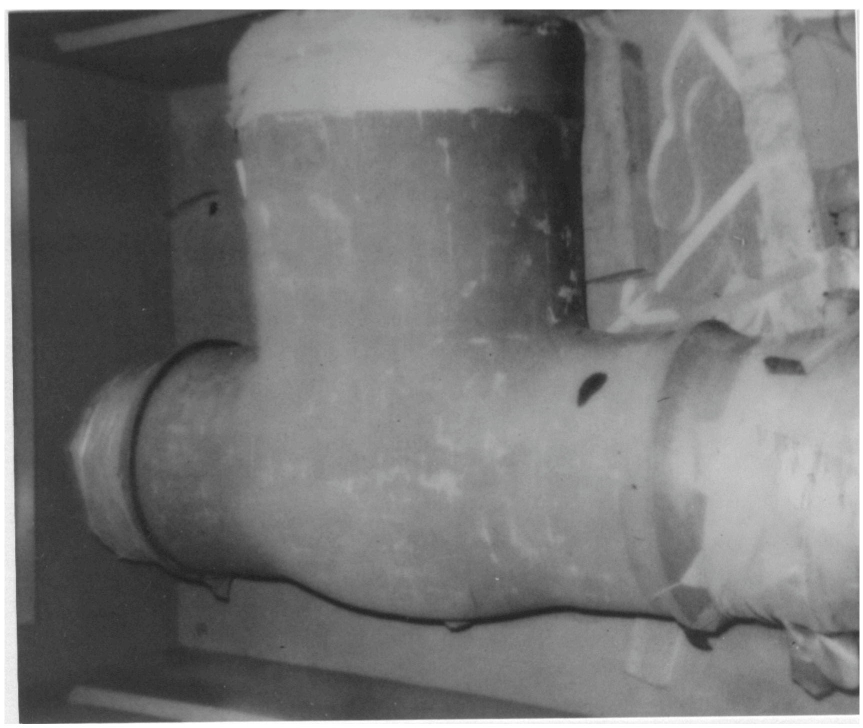

(b)

Figure 1. Photographs of (a) check valve, (b) main shutoff valve, and (c) spare pump volute from the Shippingport reactor

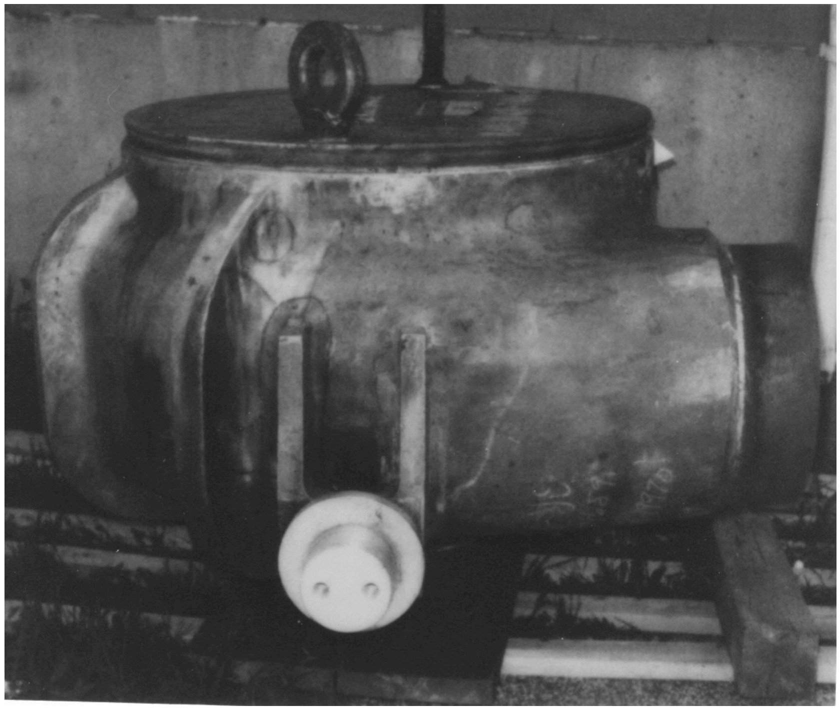

(c)

Figure 1. (Contd.)

The chemical composition, hardness, and amount and distribution of ferrite for the cast materials are given in Table 1. The chemical composition and ferrite content of the hot–leg and crossover–leg elbows from the Ringals 2 reactor and the pump cover plate from the KRB reactor are also included in Table 1. All materials from the Shippingport reactor are CF–8 cast SS with ferrite content in the range of 2–16%. In general, hardness increases with increases in ferrite content of the steel. Some differences in hardness and ferrite content were observed for material from different locations in the casting. Such differences appear to be related to compositional variations.

All valve materials exhibit a radially oriented columnar grain structure. Typical examples of the grain structure for the check valves and main shutoff valves are shown in Figs. 2 and 3, respectively. The inner surface of all of the valves contained repair welds; an example is shown in Fig. 3. The pump volutes display a mixed grain structure of columnar and equiaxed grains, Fig. 4. The ferrite morphologies of the check valves, main shutoff valves, and the pump volutes are shown in Figs. 5, 6, and 7, respectively. The materials contain a lacy ferrite with a mean ferrite spacing in the range of 150–300 μm. The check valve materials show a significant amount of carbides at the ferrite/austenite phase boundaries. Furthermore, most of the phase boundaries have migrated. The original phase boundaries are decorated with carbides, which most likely formed during production heat treatment of the casting.

Microstructural examination indicates that the mechanism of low–temperature embrittlement of the cast materials is the same as that of laboratory–aged materials.[18,19] All materials showed spinodal decomposition of ferrite to form a Cr–rich α' phase. In addition, the materials from the check valve contained a Ni– and Si–rich G phase in the ferrite, and $M_{23}C_6$ carbides at the austenite/ferrite phase boundary. An unexpected microstructural feature, i.e., σ–phase

Table 1. Chemical composition, ferrite morphology, and hardness of cast stainless steel components from the Shippingport, KRB, and Ringhals reactors

Mater. ID[a]	Composition, wt.% C	N	Si	Mn	P	S	Ni	Cr	Mo	Cu	Ferrite,% Calc.	Meas.	Ferrite Spacing, µm	Hardness, R_B
Cold–Leg Check Valve[b]														
CA4	0.056	0.041	1.45	1.10	0.018	0.009	8.84	20.26	0.01	0.07	10.8	10.9	157	79.8
CA7	0.058	0.041	1.43	1.09	0.018	0.009	8.72	20.22	0.01	0.07	10.9	10.0	148	78.6
CB7	0.052	0.053	1.36	1.07	0.018	0.011	8.85	19.12	0.02	0.06	5.9	3.2	296	75.0
Hot–Leg Main Shutoff Valve[b]														
MA1	0.052	0.049	0.22	0.72	0.039	0.013	10.50	20.74	0.24	0.13	5.2	9.5	217	76.9
MA9	0.052	0.051	0.24	0.72	0.041	0.011	10.54	20.78	0.24	0.13	5.1	10.0	245	77.6
MB2	0.042	0.073	0.51	0.72	0.043	0.017	10.77	19.74	0.19	0.12	2.6	1.9	–	74.2
Pump Volute[c]														
VR	0.046	0.049	1.14	0.50	0.027	0.017	9.56	20.79	0.04	0.07	9.8	16.2	181	82.9
PV	0.108	0.027	0.89	1.11	0.032	0.008	9.30	19.83	0.38	0.25	4.7	13.0	–	–
KRB Pump Cover Plate[d]														
KRB	0.062	0.038	1.17	0.31	–	–	8.03	21.99	0.17	–	27.7	34.0	–	–
Ringhals Reactor Elbows[e]														
H	0.037	0.044	1.03	0.77	0.022	0.008	10.60	20.00	2.09	0.17	13.0	20.1	–	–
C	0.039	0.037	1.11	0.82	0.020	0.012	10.50	19.60	2.08	0.08	12.3	19.8	–	–

[a] For the valves, the second letter indicates the loop where the valve was located and the number designates the segment of the component from which the material was removed. Segments 1, 2, and 7 are from the top half of the valve body and segment 4 is from the bottom half. Segment 9 of the main shutoff valves is from a cooler region, i.e., casing for valve stem and bonnet.
[b] In service for ≈13 y at 264°C for cold leg and at 281°C for hot leg.
[c] Spare pump volute VR in service only during initial core loading and PV in service for ≈13 y at 264°C.
[d] In service for ≈8 y at 284°C.
[e] In service for ≈13 y at 325°C for hot leg and at 291°C for crossover leg, and at hot standby for ≈2 y at 303°C for hot leg and 274°C for crossover leg.

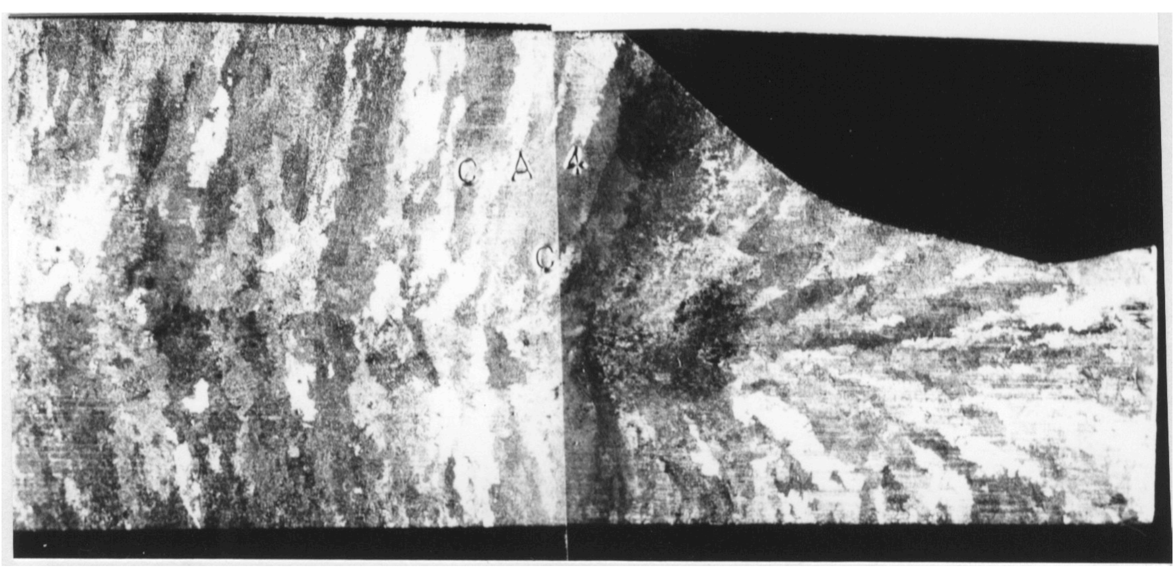

Figure 2. Microstructure along axial section of Loop A check valve from the Shippingport reactor

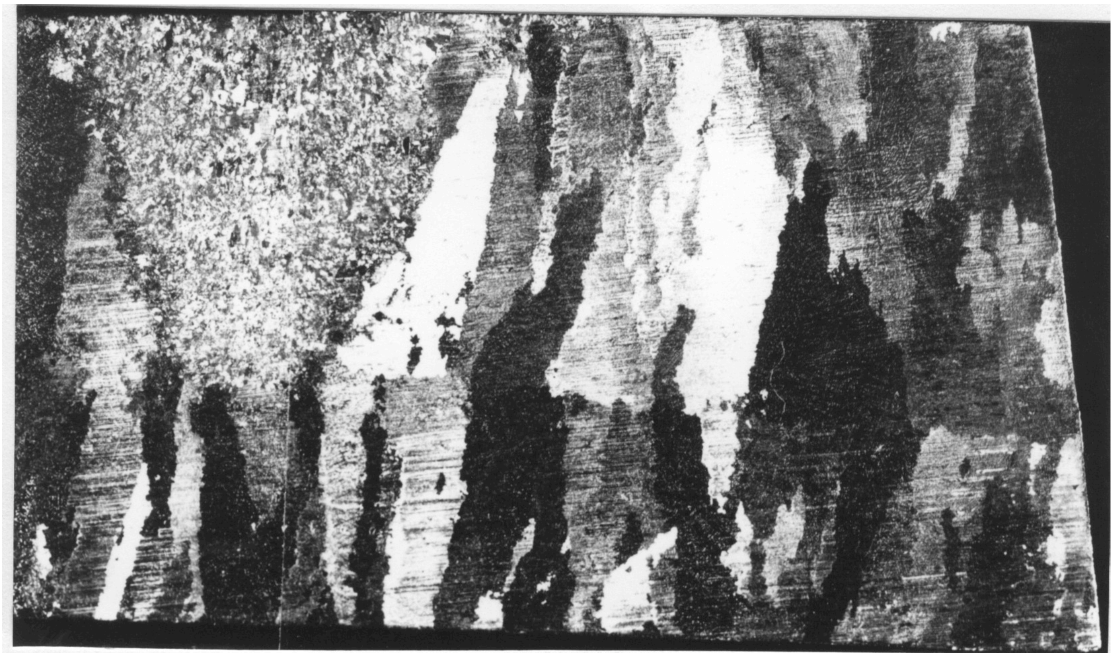

Figure 3. Microstructure along axial section of Loop B main shutoff valve from the Shippingport reactor. A repair weld is also seen on the outer diameter of the valve.

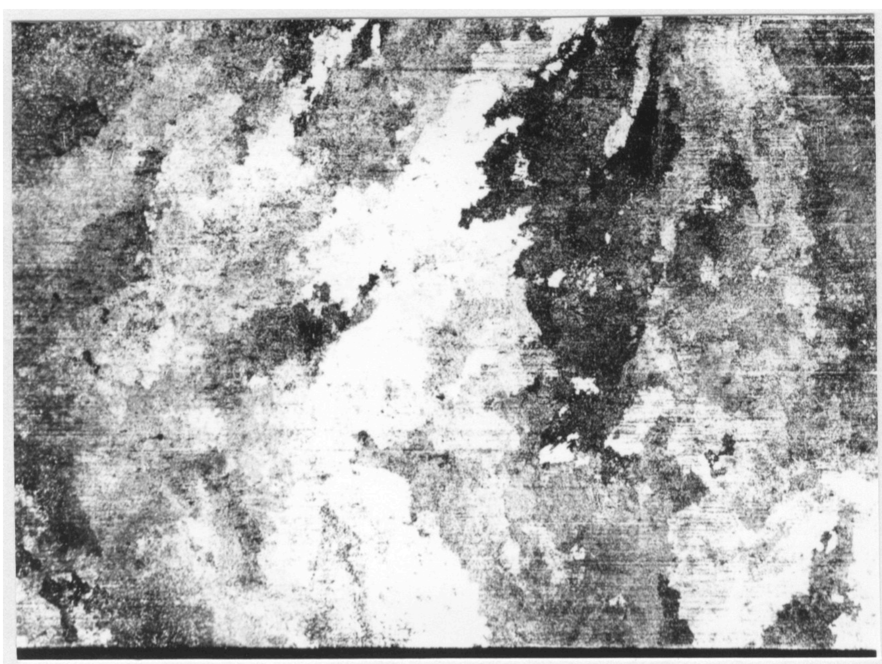

Figure 4. Microstructure along axial section of the spare volute from the Shippingport reactor

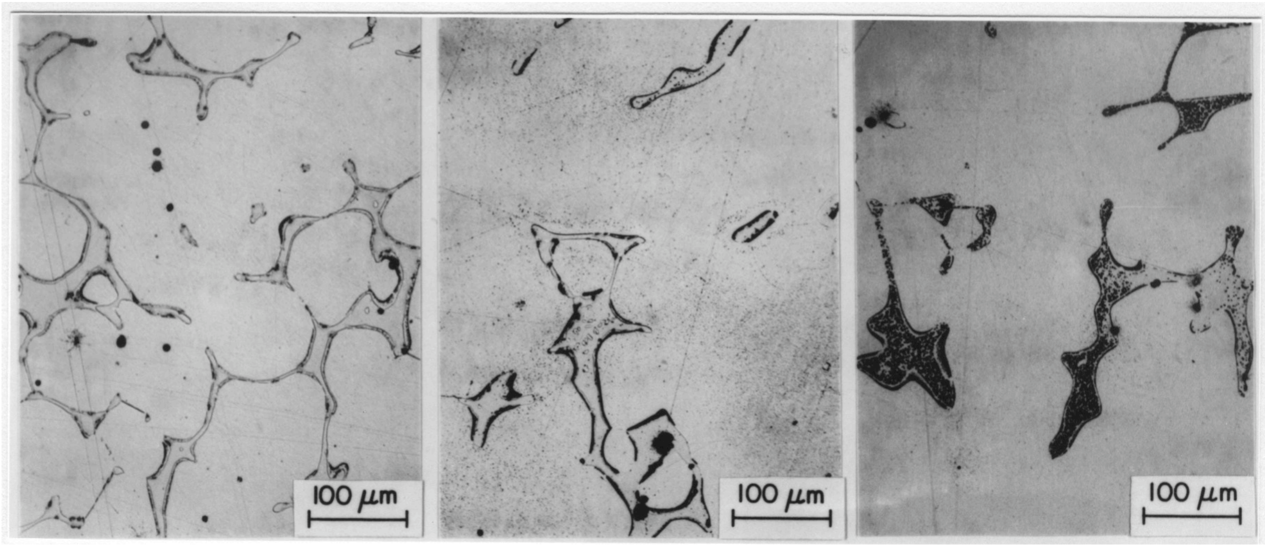

Loop A Loop B Loop C

Figure 5. Ferrite morphology of cast materials from Loops A, B, and C cold–leg check valves from the Shippingport reactor

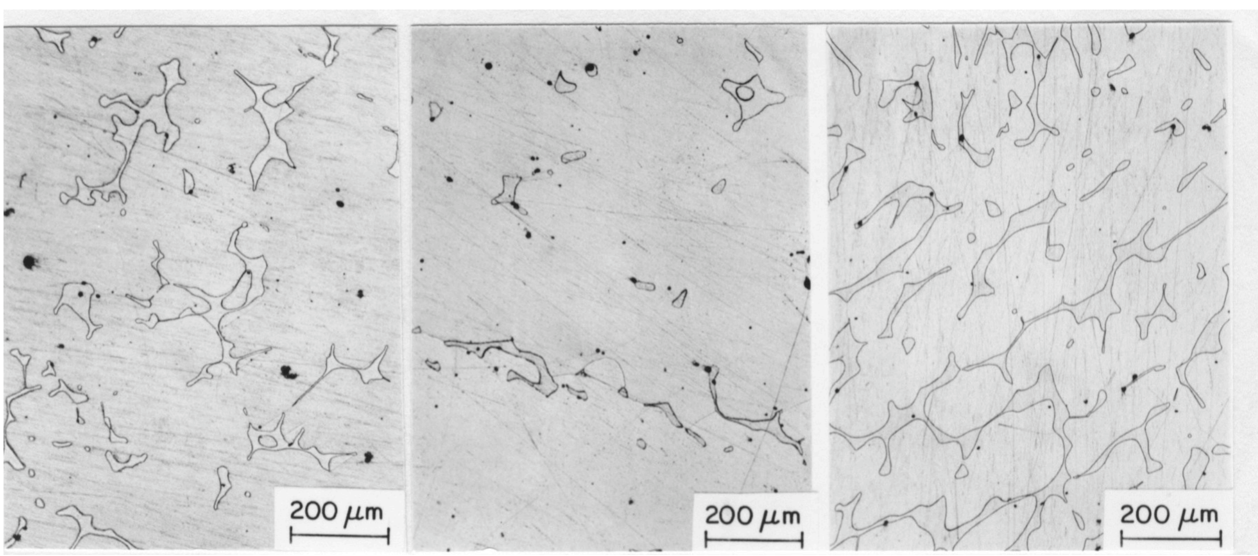

Loop A Loop B Loop C

Figure 6. Ferrite morphology of cast materials from Loops A, B, and C hot–leg main shutoff valves from the Shippingport reactor

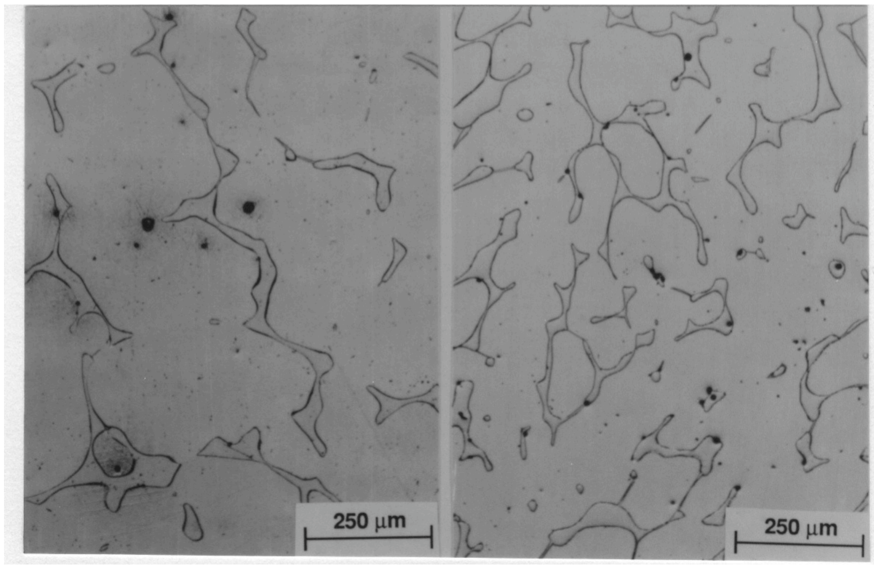

Cold–Leg Pump Volute *Spare Pump Volute*

Figure 7. Ferrite morphology of cast materials from the cold–leg and spare pump volutes from the Shippingport reactor

precipitates on slip bands and stacking faults, was also observed in the austenite of the check valve material. Precipitation of σ phase generally occurs at temperatures >550°C (1022°F). The presence of σ phase and phase–boundary migration indicate significant differences between the production heat treatment of the check valves and that of the other materials.

3 Mechanical Properties

Specimens for Charpy–impact, tensile, and fracture toughness tests were obtained from different locations across the thickness of the various components. All specimens were in the LC orientation.* Impact tests were conducted on standard Charpy V–notch specimens machined according to ASTM Specification E 23. A Dynatup Model 8000A drop–weight impact machine with an instrumented tup and data readout system was used for the tests. Tensile tests were performed on cylindrical specimens with a diameter of 5 mm and a gage length of 20 mm. The tests were conducted at an initial strain rate of 4×10^{-4} s^{-1}. The fracture toughness J–R curve tests were conducted according to ASTM Specifications E 813–85 and E 1152–87. Compact–tension specimens, 25.4 mm thick, were used for the tests. The experimental procedure and test results for the Charpy–impact, tensile, and fracture toughness tests are given in Appendices A, B, and C, respectively. Preliminary results from this study have been presented earlier.[20–22]

* The first letter represents the direction normal to the plane of the crack; the second indicates the direction of crack propagation. L = longitudinal and C = circumferential.

3.1 Baseline Mechanical Properties

The baseline mechanical properties for the unaged materials must be known to establish the effects of thermal aging during reactor service. Microstructural and annealing studies[3,4,18,19] on laboratory– and reactor–aged materials have been conducted to investigate the possibility of recovering the mechanical properties of embrittled materials. The formation of the α' phase by spinodal decomposition is the primary mechanism of thermal embrittlement. The α' phase is not stable at temperatures >550°C (1022°F). The mechanical properties can be recovered by annealing the embrittled cast stainless steels for 1 h at 550°C and then water quenching to dissolve the α' phase while avoiding the formation of σ phase.

The influence of annealing on the Charpy transition curves of three laboratory–aged heats and service–aged material from the KRB reactor is shown in Fig. 8. Heats 68, 69, and 75 were aged for 10,000 h at 400°C and the KRB pump cover plate was in service for ≈70,000 at 284°C. The Charpy–transition curve for the aged material is represented by dashed lines and open circles in Fig. 8. The thermally embrittled material was annealed for 1 h at 550°C and then water queched. The results indicate an essentially complete recovery from thermal embrittlement; the transition curves for the annealed materials agree well with those for the unaged steel. Microstructural examination of the annealed material showed no α' phase, but the size and distribution of the G phase were the same as in the aged material.[18,19] The results indicate that baseline mechanical properties of unaged material can be determined from recovery–annealed material.

Charpy–impact tests were also conducted on material from a cooler region of the Shippingport Loop A main shutoff valve to obtain baseline properties. The Charpy transition curves of MA9 and recovery–annealed material from MA9 and MA1 are shown in Fig. 9. These materials are from the same valve, although MA9 is from a cooler region of the valve. The results indicate that the MA9 material suffered no thermal embrittlement; annealing had no effect on the transition curves. The results for annealed MA1 material also show good agreement with the transition curve for MA9. The upper–shelf energy (USE) of both materials is not constant but decreases with an increase in temperature. The average impact energies at room temperature and at 290°C (554°F), respectively, are 356 and 253 J/cm^2 for MA9, and 320 and 254 J/cm^2 for annealed MA1. The Charpy data were fitted with a hyperbolic tangent function of the form

$$C_V = K_o + B\left\{1 + \tanh\left(\frac{T - C}{D}\right)\right\}, \tag{1}$$

where K_o is the lower–shelf energy, T is the test temperature in °C, B is half the distance between the upper– and lower–shelf energy, C is the mid–shelf Charpy transition temperature (CTT) in °C, and D is the half width of the transition region. The best–fit curves for MA9, with or without annealing, and for annealed MA1 indicate that the latter is marginally weaker; the CTT is ≈10°C higher and the average USE is ≈30 J/cm^2 lower for MA1. Such differences in impact energy are most likely due to minor variations in composition and structure of the materials from different locations of the casting. The Charpy data for MA9 and annealed MA1 may be represented by a single transition curve; the best–fit curve is shown in Fig. 9.

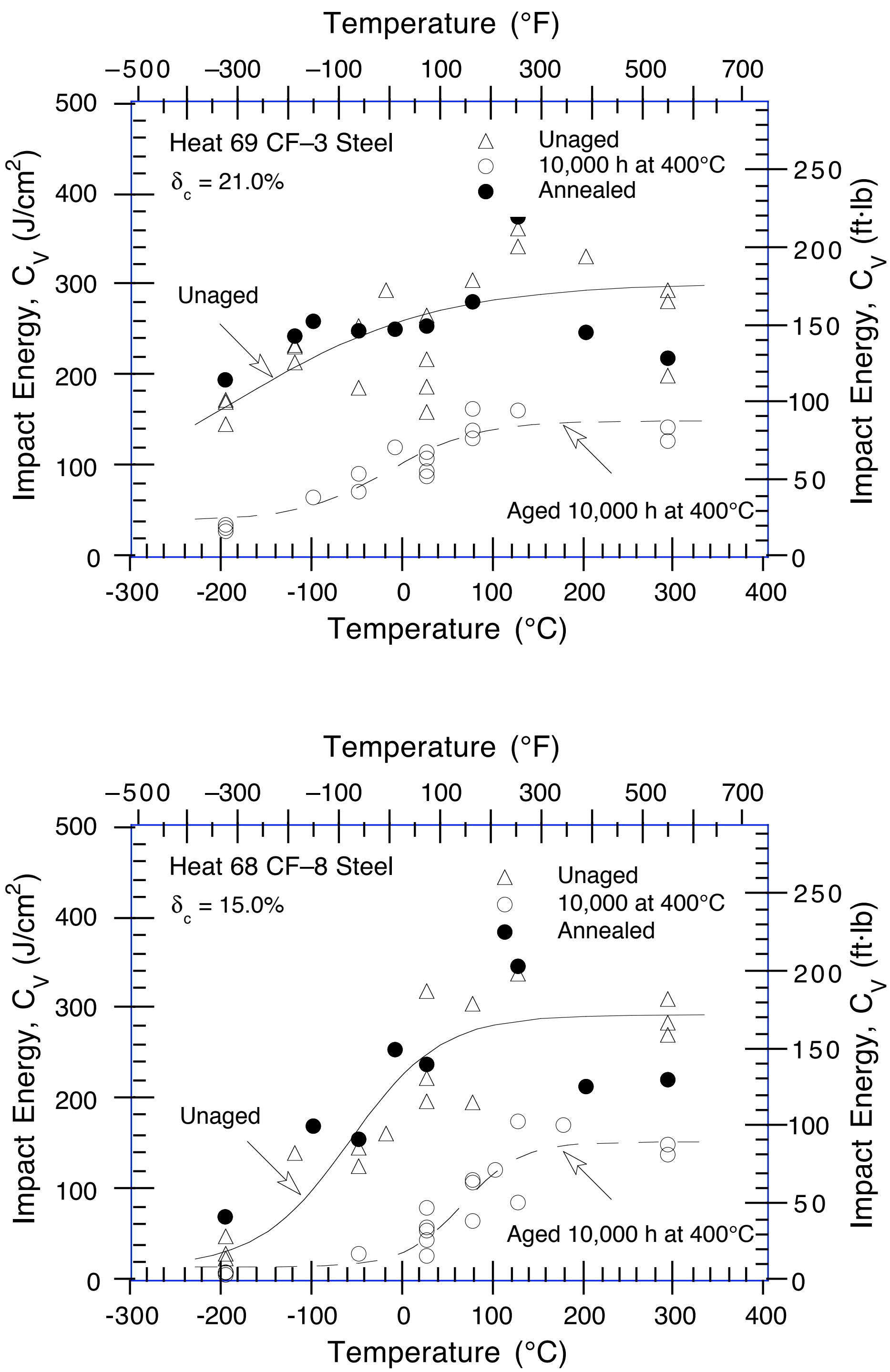

Figure 8. Effect of annealing for 1 h at 550°C and then water quenching on Charpy–transition curves for laboratory–aged Heats 69, 68, and 75, and service–aged KRB pump cover plate. The dashed lines and open circles represent the transition curve before the annealing treatment. (Solid and dashed lines are best–fit curves.)

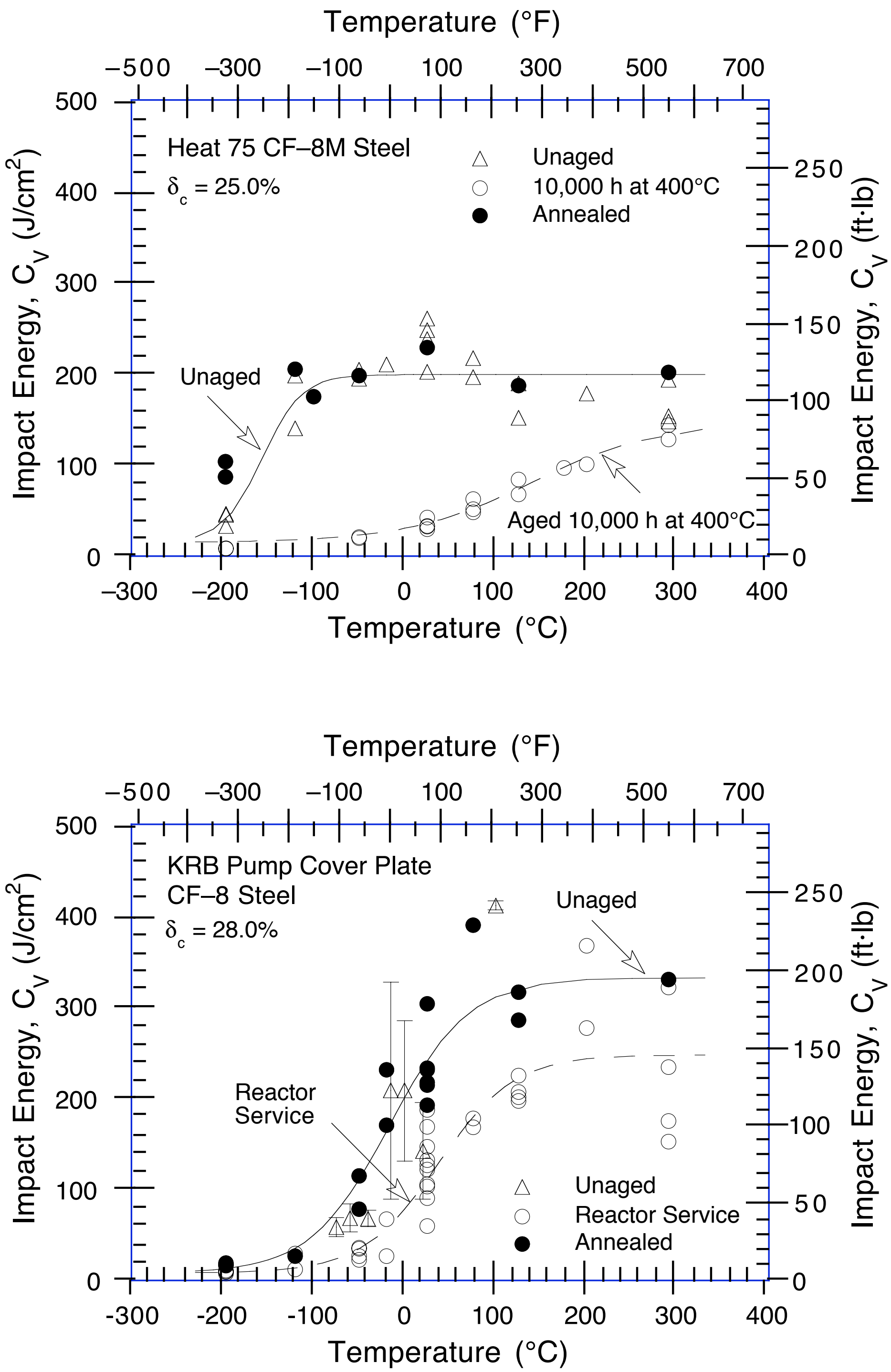

Figure 8. (Contd.)

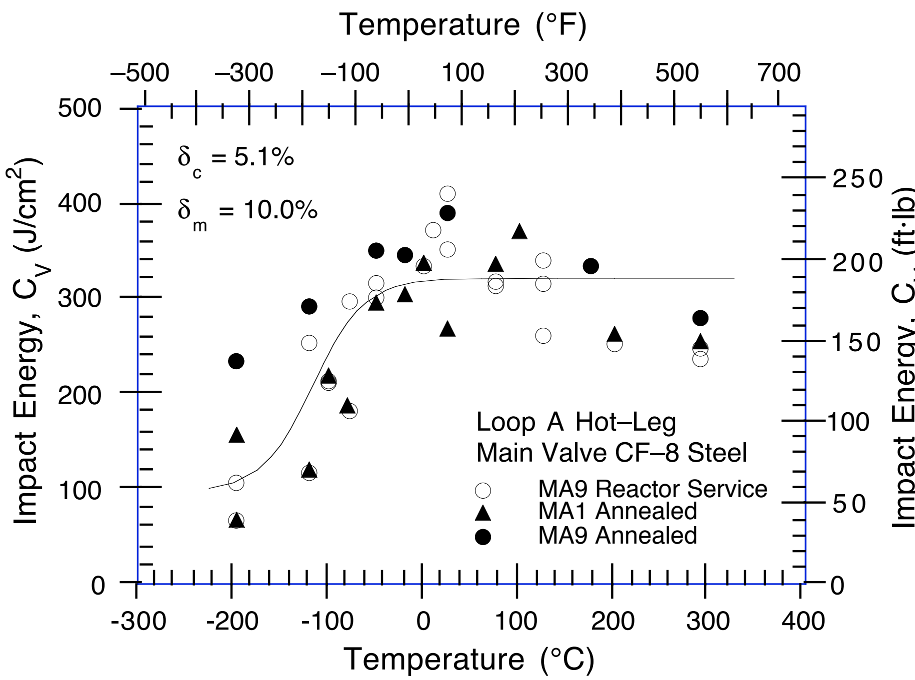

Figure 9. Effect of annealing on Charpy–transition curve of cast material from the hot–leg main shutoff valve. Material MA9 is from a cooler region of the valve. (Solid line is best–fit curve.)

3.2 Charpy–Impact Energy

Charpy impact data for the various cast materials from the Shippingport reactor are given in Appendix A and the Charpy transition curves are shown in Figs. 10–12. The results for MA9 and recovery–annealed MA1 materials are shown as the baseline Charpy transition curve for MA1 in Fig. 10. The baseline transition curves for CA4 and PV are represented by the results for recovery–annealed materials. The Charpy data were fitted with the hyperbolic tangent expression given in Eq. 1; the values of the constants for the various materials are given in Table 2. The results indicate that the RT impact energy of the materials is relatively high and the mid–shelf CTT, i.e., constant C in Eq. 1, is very low. The check valve materials CA4 and CB7 are weaker than MA1 and PV, e.g., the mid–shelf CTT is ≈100°C higher for CA4 and CB7. The higher CTTs are due to the presence of phase–boundary carbides in the check valve materials (Fig. 5). The carbides weaken the phase boundaries and thus promote failure by phase–boundary separation.

The decrease in impact strength from ≈13 y of service at reactor temperatures is minimal for the materials. The RT Charpy–impact energy decreased from 188 to 145 J/cm^2 (111 to 86 ft·lb) for check valve CA4, 320 to 299 J/cm^2 (189 to 176 ft·lb) for main valve MA1, and 424 to 322 J/cm^2 (250 to 190 ft·lb) for pump volute PV. The large difference in USE for the unaged and service–aged materials from Row 1 of MA1 (Fig. 10), is not due to thermal aging. The inner–15–mm region of the MA1 valve body contains a high density of inclusions/flaws and is inherently weak. The inner surface of all of the valves contained repair welds. However, no significant difference was noted in the chemical composition or ferrite content of the material across the thickness of the valve body.

Table 2. Values of constants in Eq. 1 for Charpy transition curve of CF–8 cast SSs from the Shippingport reactor and KRB pump cover plate

Material ID	Service Condition: Temp., °C	Service Condition: Time, y	Constants: K_o, J/cm²	Constants: B, J/cm²	Constants: C, °C	Constants: D, °C
Cold–Leg Check Valves						
CA4	Annealed	–	25	98.6	–37.0	97.9
CA4	264	113,900	25	79.2	–20.1	81.8
CB7	264	113,900	76	108.8	6.0	65.2
Hot–Leg Main Shutoff Valve						
MA9[a]	Annealed	–	96	112.0	–116.3	54.1
MA9	<200	113,900	83	110.1	–110.7	48.3
MA9	400	10,000	10	90.8	–23.6	127.8
MA1/23[a]	Annealed		96	112.0	–116.3	54.1
MA1/23[b]	281	113,900	73	87.6	–114.2	29.8
MA1/1[c]	281	113,900	69	63.7	–137.0	38.6
Pump Volutes						
PV	Annealed	–	150	116.2	–151.9	109.7
PV	264	113,900	75	109.4	–141.9	49.5
VR	Unaged	–	61	88.1	–112.4	38.5
VR	400	10,000	23	46.3	14.5	91.2
Pump Cover Plate[d]						
KRB	Annealed	–	8	161.9	–16.5	87.2
KRB	284	8	8	119.7	36.8	83.2

[a] Determined from combined data for MA9 and annealed MA9 and MA1.
[b] Material from Rows 2 & 3, which corresponds to 15– 45–mm region of the wall.
[c] Material from Row 1, which corresponds to inner–5–mm region of the wall.
[d] Obtained from the KRB reactor in Gundremmingen, Germany.

Unaged material from the spare pump volute and MA9 material from cooler regions of the main shutoff valve were aged in the laboratory for 10,000 h at 400°C; the results are shown in Fig. 13. Both steels show a significant decrease in impact energy after thermal aging. The USE decreases from ≈320 to 190 J/cm² for MA9 and from ≈235 to 115 J/cm² for VR material. The mid–shelf CTT increases by 90 and 120°C for MA9 and VR materials, respectively. These curves represent the saturation condition, i.e., the minimum Charpy–impact energy that would be achieved by these materials after long–term aging.

3.3 Tensile Properties

Tensile tests were conducted at room temperature and at 290°C on service–aged materials from the Loop A cold–leg check valve and pump volute and from the hot–leg main shutoff valve; results are given in Appendix B. The results indicate that thermal aging during ≈15 y of reactor service had no effect on yield stress and that the increase in ultimate stress is minimal for the three materials.

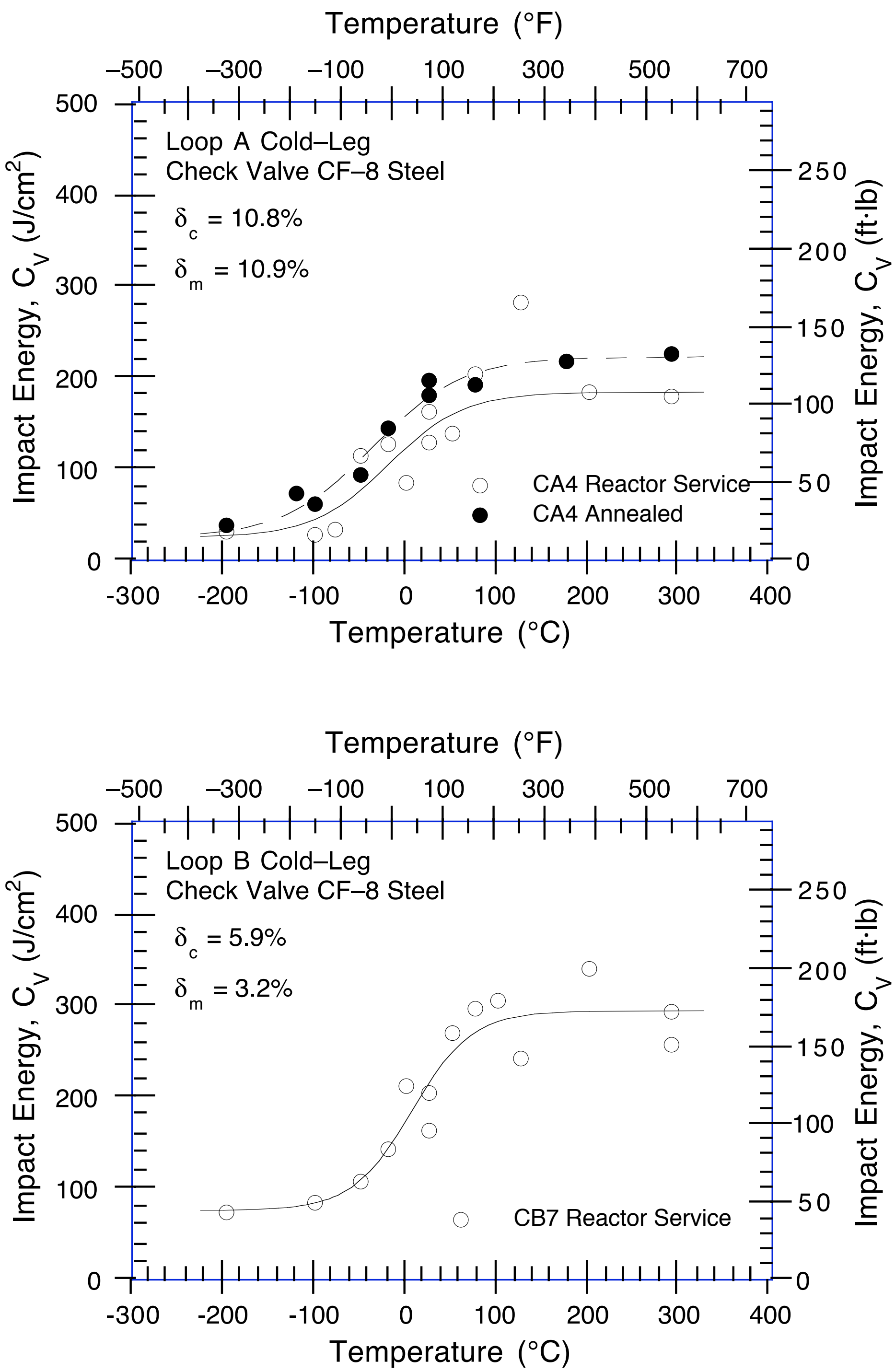

Figure 10. Charpy transition curves for Loop A and B cold–leg check valves after 13 y of service at 264°C. (Solid and dashed lines represent best–fit curves for service–aged and annealed materials, respectively.)

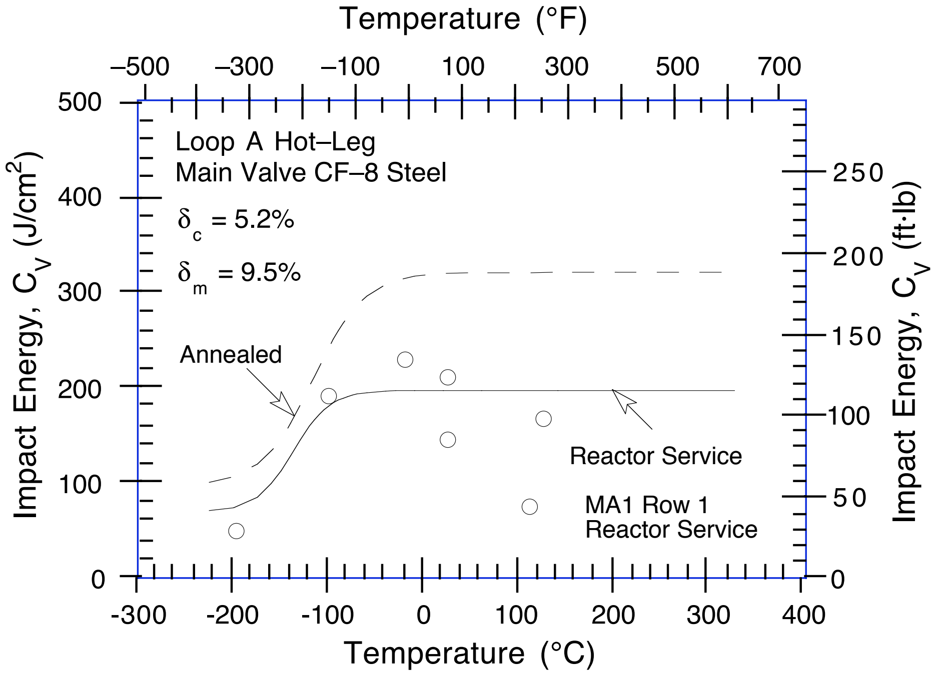

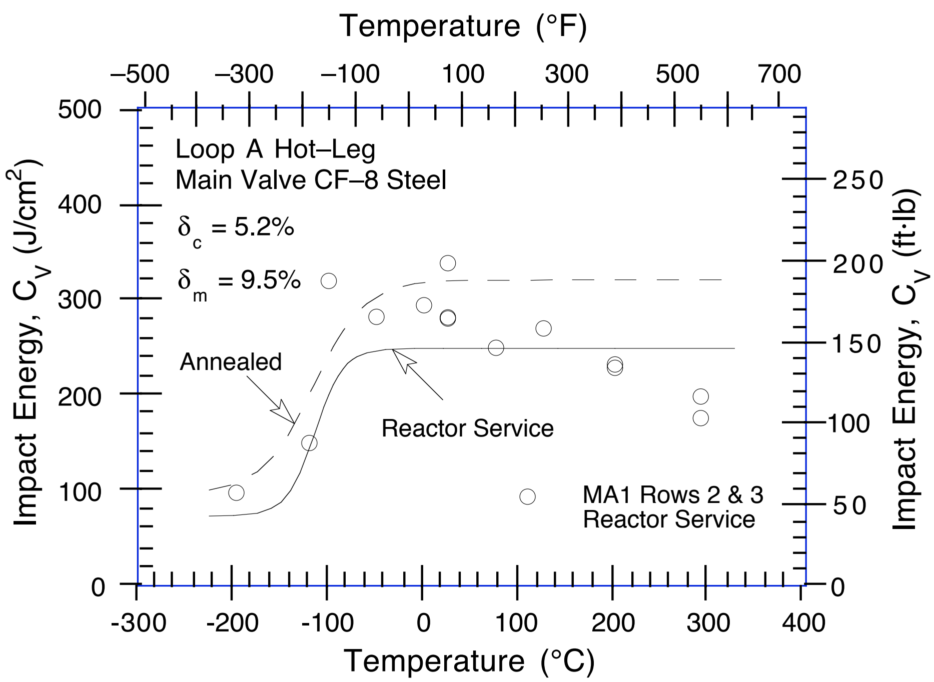

Figure 11. Charpy transition curves for Loop A hot–leg main shutoff valve after 13 y of service at 281°C. Row 1 corresponds to inner 15–mm region and rows 2 and 3 represent 15– to 50–mm region of the valve body. (Solid and dashed lines are best–fit curves.)

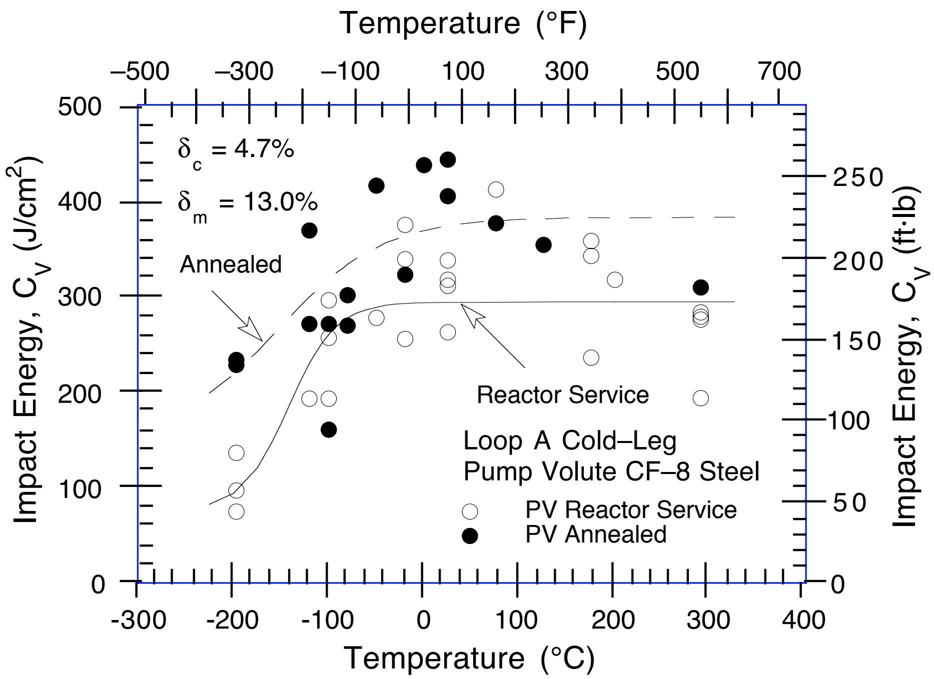

Figure 12. Charpy transition curves for Loop A pump volute after 13 y of service at 264°C. (Solid and dashed lines represent best–fit curves for service–aged and annealed materials, respectively.)

Tensile properties were also estimated from the instrumented Charpy–impact test data.[1,2,4] For a Charpy specimen, yield stress is given by

$$\sigma_y = 1.50P_y\left(\frac{B}{Wb^2}\right), \tag{2}$$

and ultimate stress by

$$\sigma_u = 2.28P_m\left(\frac{B}{Wb^2}\right), \tag{3}$$

where P_y and P_m are the yield and maximum loads obtained from the load–time traces of the instrumented Charpy–impact test, W is the specimen width, B is the specimen thickness, and b is the uncracked ligament.[23] The estimated values of yield and ultimate stress, the values obtained from tensile tests, and estimated tensile stresses for recovery–annealed materials are shown in Figs. 14 and 15. For all of the materials, the estimated tensile properties are in good agreement with measured values. The tensile strength of CA4, PV, and MA1 materials is comparable. Two specimens of MA1 (Fig. 15) showed low ultimate strength (and also poor ductility). These specimens were obtained from the inner–15–mm region of the valve body. The poor tensile properties are caused by inclusions in the material. As discussed above, the RT impact energy of Row 1 specimens is also low, e.g., ≈177 ±33 J/cm², compared with ≈299 ±33 J/cm² for specimens from other regions of the valve body.

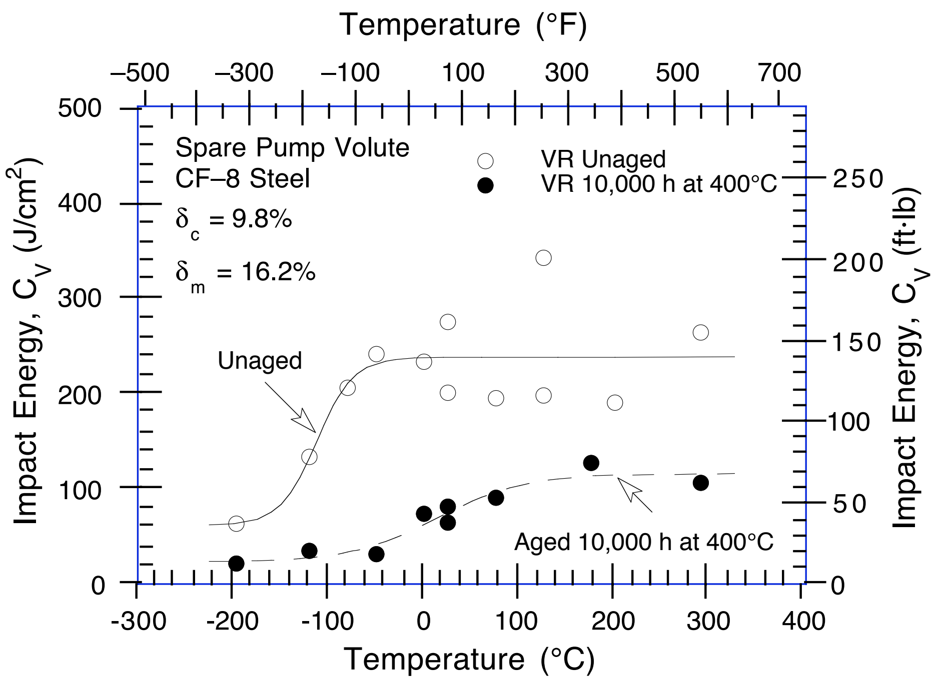

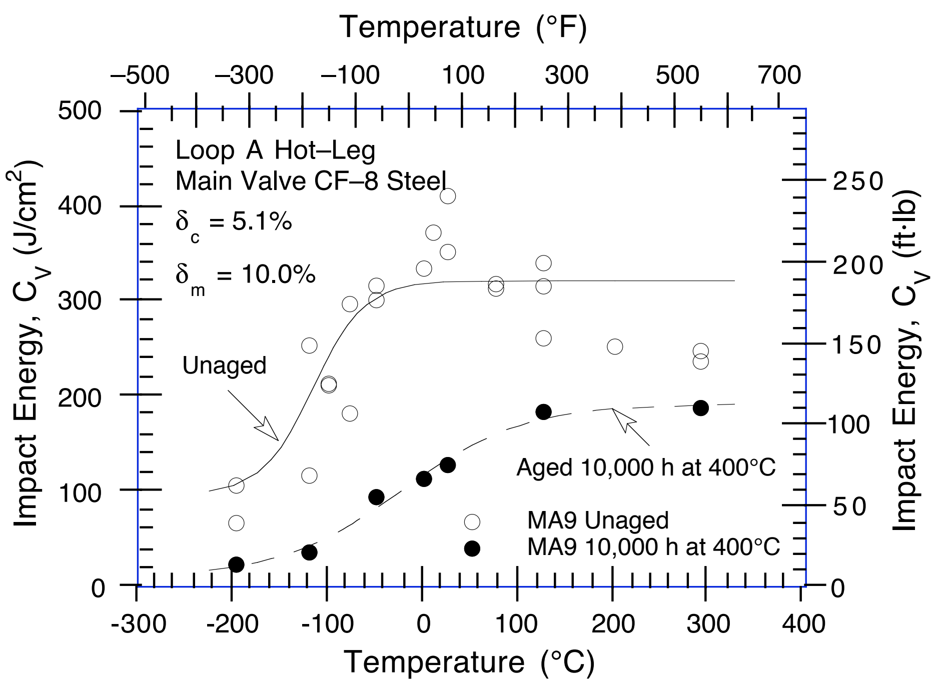

Figure 13. Charpy transition curves for materials from the spare pump volute and cooler region of the main shutoff valve before and after aging for 10,000 h at 400°C. (Solid and dashed lines represent unaged and aged materials, respectively.)

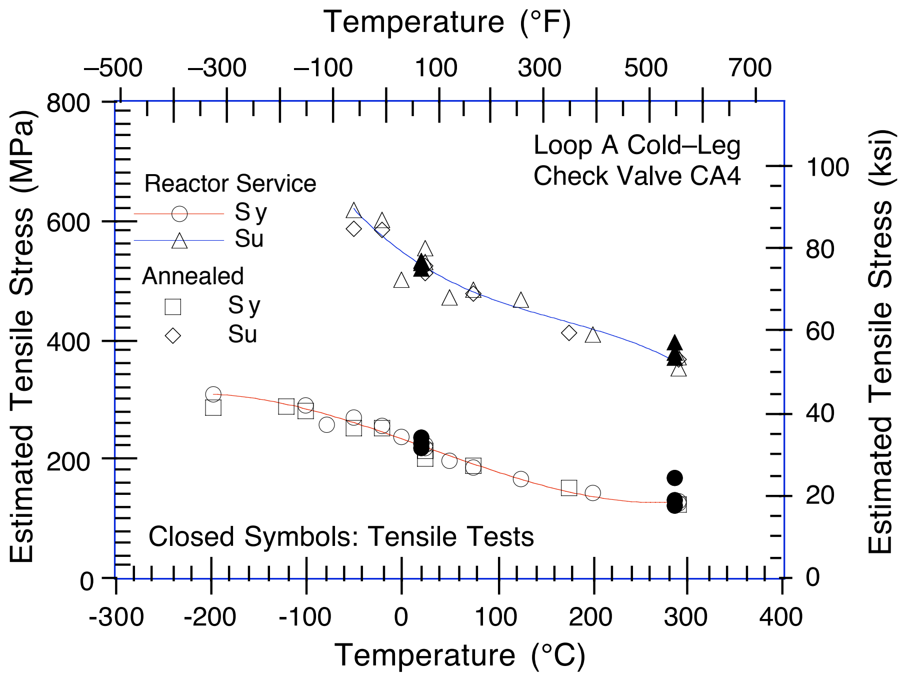

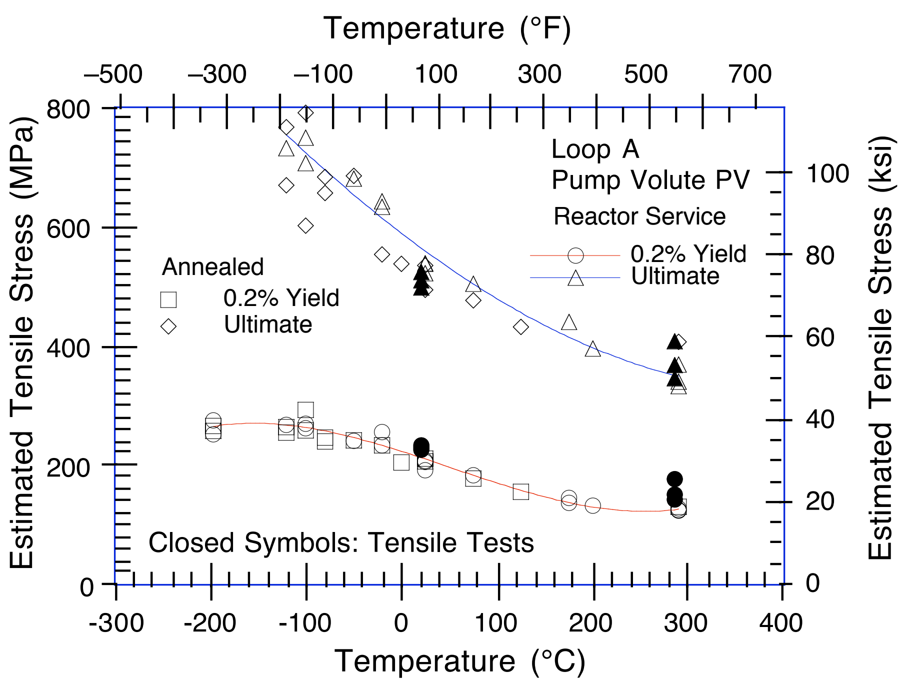

Figure 14. Yield and ultimate stresses estimated from Charpy–impact data and obtained from tensile tests for cold–leg check valve and pump volute, and estimated tensile stresses of annealed materials

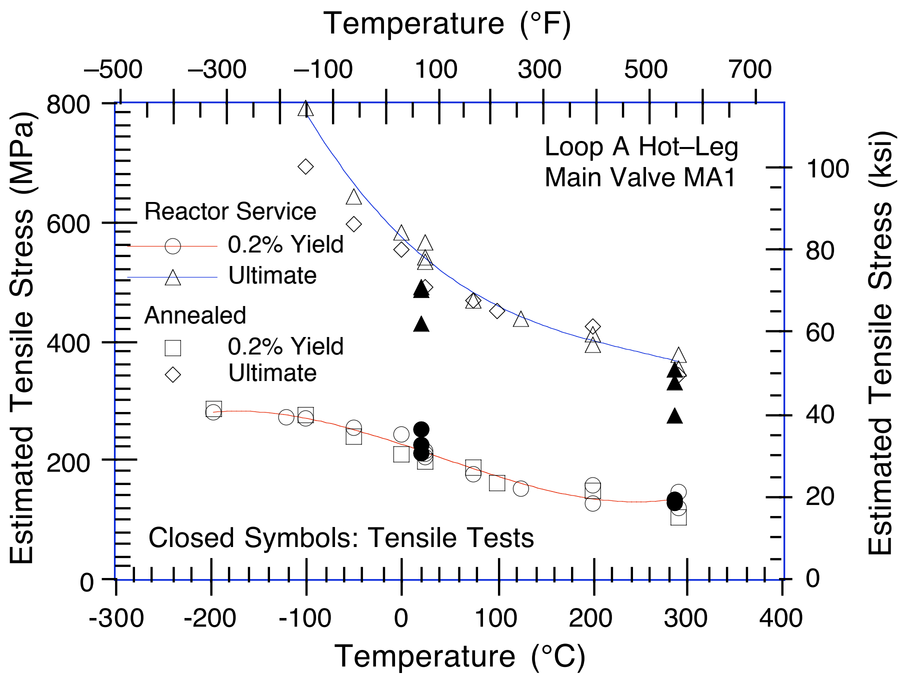

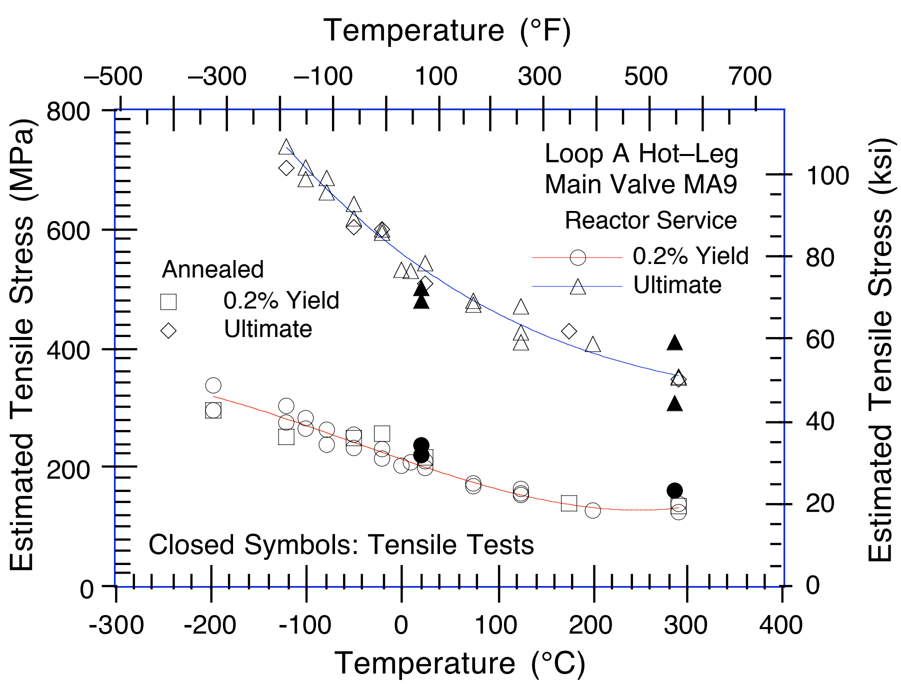

Figure 15. Yield and ultimate stresses estimated from Charpy–impact data and obtained from tensile tests for hot–leg main valve, and estimated tensile stresses of annealed materials. Material MA9 is from a cooler region of the valve.

Tensile tests were also conducted on MA9 and VR materials before and after aging for 10,000 h at 400°C. The experimental values of yield and ultimate stress and values estimated from the Charpy–impact data are shown in Fig. 16. These curves represent the saturation condition, i.e., the maximum increase in tensile strength achieved by these materials after long–term aging. The results indicate that, for both steels, the increase in yield stress is minimal and ultimate stress is increased by ≈4% for MA9 and by ≈15% for VR.

3.4 Fracture Toughness

Fracture toughness J–R curve tests were conducted at room temperature and 290°C on materials from the cold–leg check valve and pump volute, hot–leg main shutoff valve, and the spare pump volute; results are given in Appendix C. The test data, as well as an analysis and qualification of the data, are also presented in Appendix C. The baseline J–R curves for unaged materials were obtained from tests on material from cooler regions of the component, e.g., material MA9, or from material that was annealed for 1 h at 550°C and water quenched to recover the aging degradation. Tests were also conducted on materials that were aged further in the laboratory for 10,000 h at 400°C to determine the saturation fracture toughness, i.e., the minimum toughness that will be achieved for the specific materials after long–term service.

The effect of thermal aging, either during service or in the laboatory, on the fracture toughness J–R curves of the various materials are shown in Figs. 17–20. The J–R curves are expressed by the power–law relation $J_d = D(\Delta a)^n$ per ASTM Specifications E 813–85 and E 1152–87. The results indicate that the decrease in fracture toughness from reactor service is relatively small because of the low operating temperatures and/or low ferrite content of the materials. Even the decrease in toughness at saturation is minimal for these materials, particularly at 290°C. Only the saturation RT J–R curves for materials from pump volute PV and spare volute VR show a significant change in fracture toughness.

4 Estimation of Mechanical Properties

A procedure and correlations have been developed for estimating mechanical properties of cast SS components during reactor service from known material information.[7,8] A flow diagram for estimating Charpy–impact energy and fracture toughness J–R curves of cast SS components is shown in Fig. 21. Section B of Fig. 21 describes the estimation of Charpy–impact energy and fracture toughness J–R curves at “saturation,” i.e., the minimum impact energy and fracture toughness that would be achieved for the material after long–term aging. The only information needed for these estimations is the chemical composition of the material. Estimation of mechanical properties at any given time and temperature of service is described in Section C of Fig. 21. The initial impact energy of the unaged material is required for these estimations. A detailed description of the procedure and the correlations for estimating Charpy–impact, fracture toughness, and tensile properties of cast SS have been presented elsewhere;[6–8] for convenience, the correlations are repeated in the following sections.

4.1 Charpy–Impact Energy

When a certified materials test record (CMTR) is available, the saturation RT impact energy of a specific cast SS is determined from the chemical composition and ferrite content of the

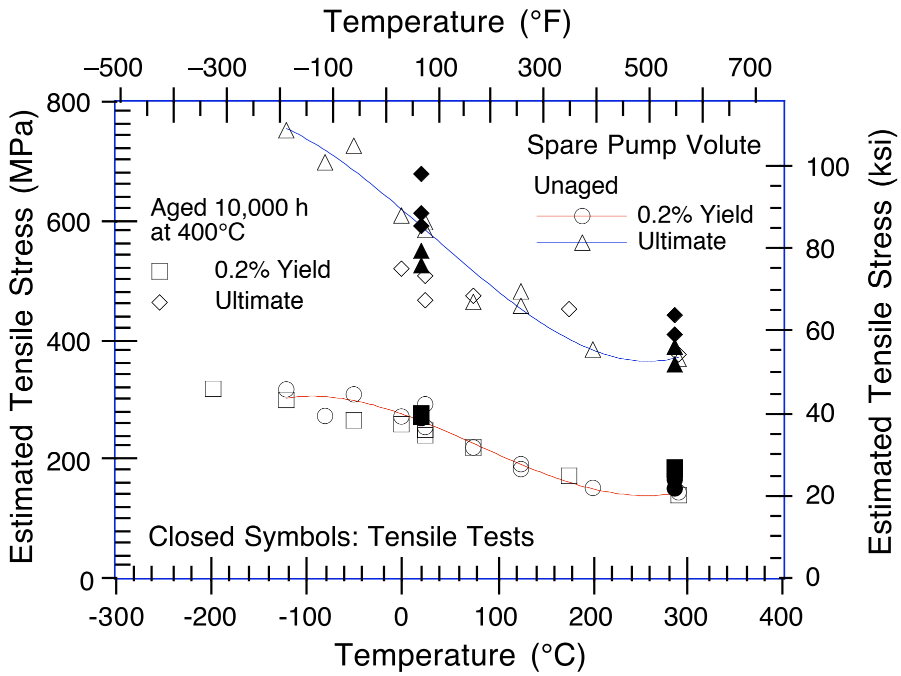

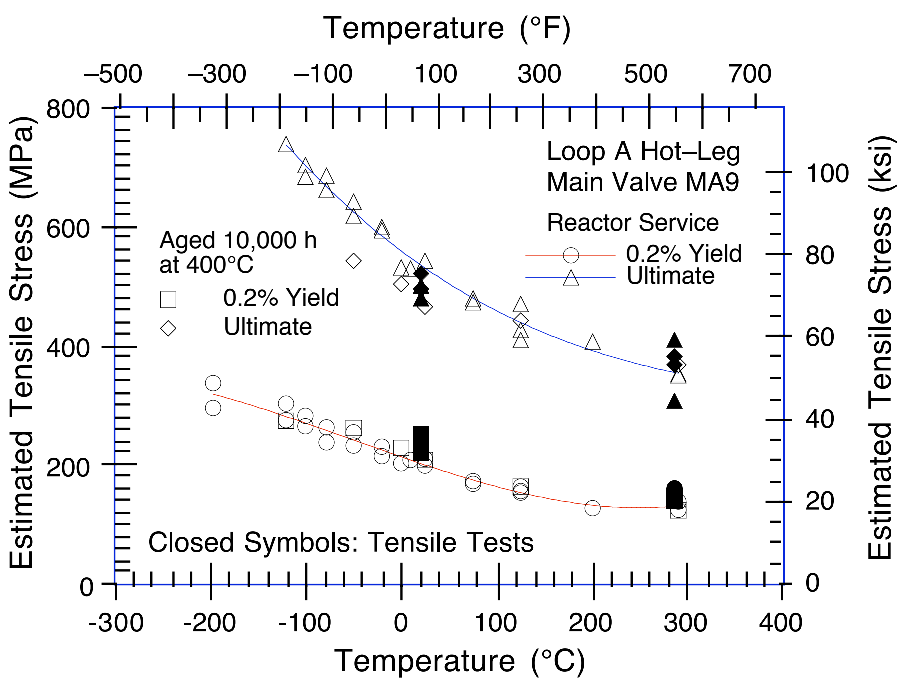

Figure 16. Yield and ultimate stresses estimated from Charpy–impact data and obtained from tensile tests for spare pump volute and hot–leg main valve before and after aging for 10,000 h at 400°C

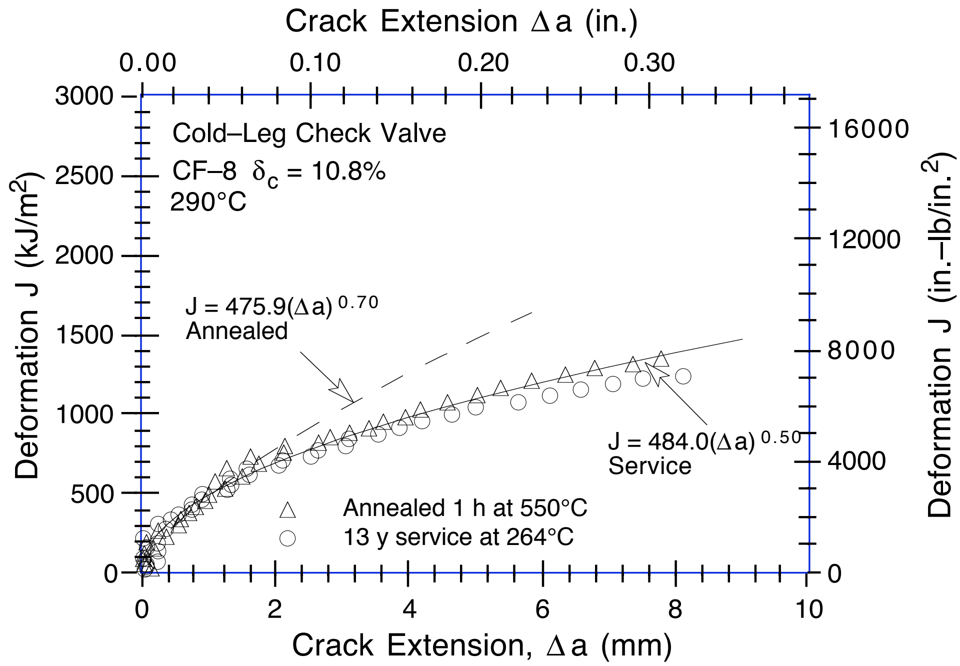

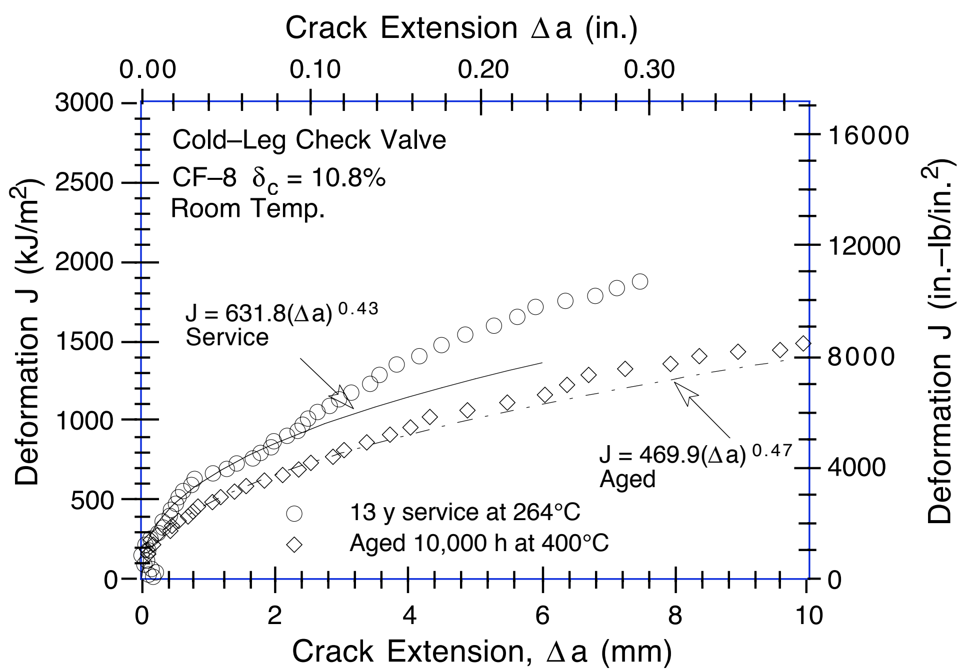

Figure 17. Fracture toughness J–R curves at room temperature and 290°C for annealed, service–aged, and laboratory–aged material from the cold–leg check valve. (Dashed, solid, and chain–dot lines are the best–fit power–law J–R curves for the annealed, service–aged, and laboratory–aged materials, respectively.)

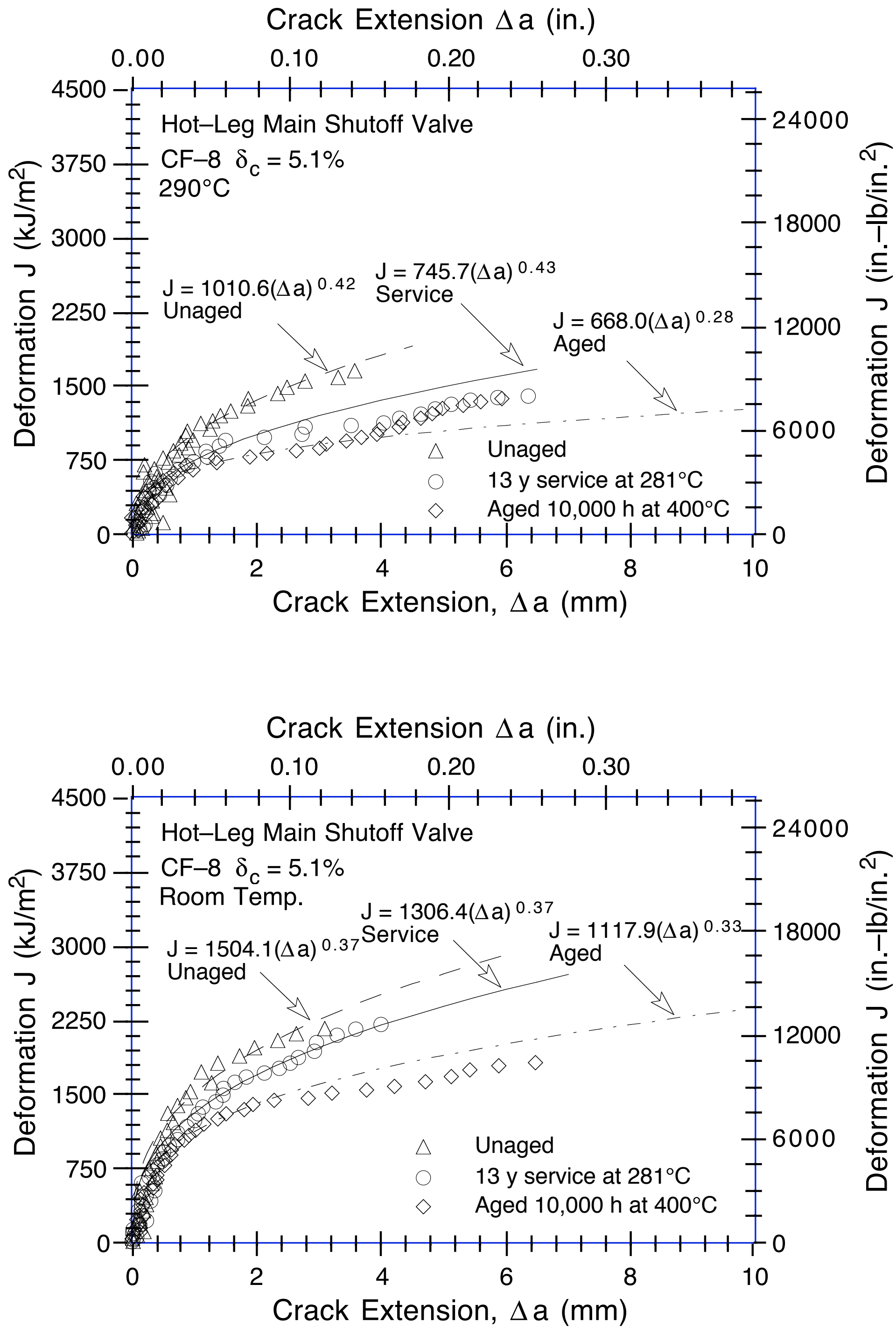

Figure 18. Fracture toughness J–R curves at room temperature and 290°C for unaged, service–aged, and laboratory–aged material from the hot–leg main shutoff valve. (Dashed, solid, and chain–dot lines are the best–fit power–law J–R curves for the unaged, service–aged, and laboratory–aged materials, respectively.)

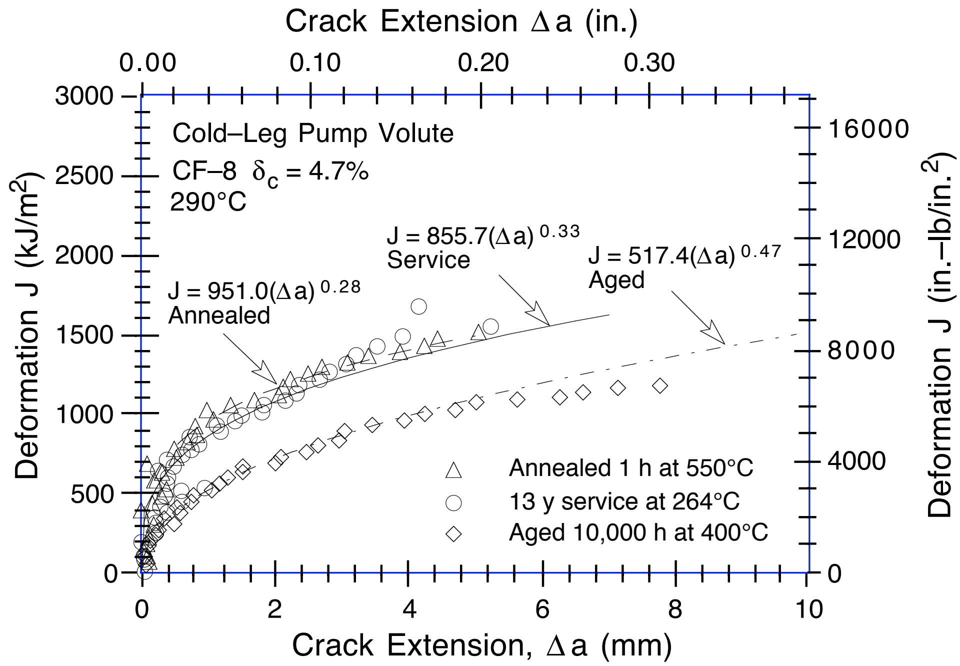

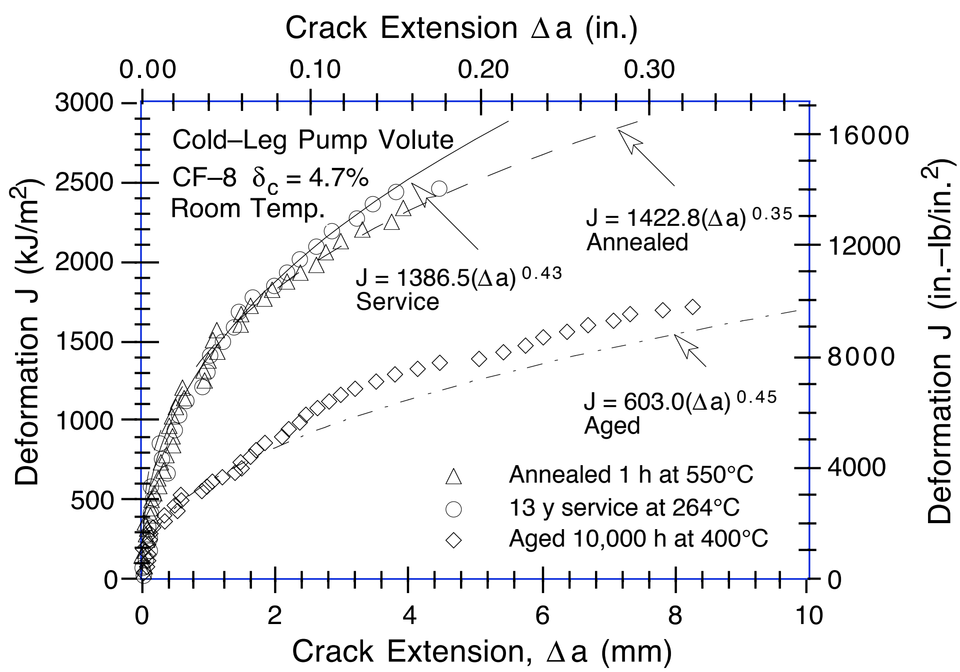

Figure 19. Fracture toughness J–R curves at room temperature and 290°C for annealed, service–aged, and laboratory–aged material from the cold–leg pump volute. (Dashed, solid, and chain–dot lines are the best–fit power–law J–R curves for the annealed, service–aged, and laboratory–aged materials, respectively.)

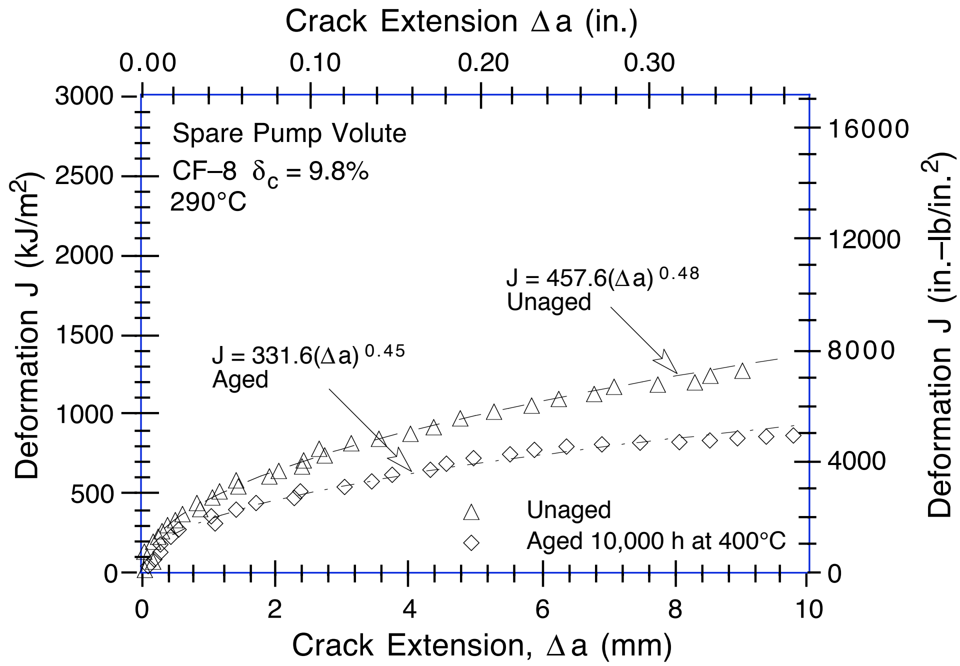

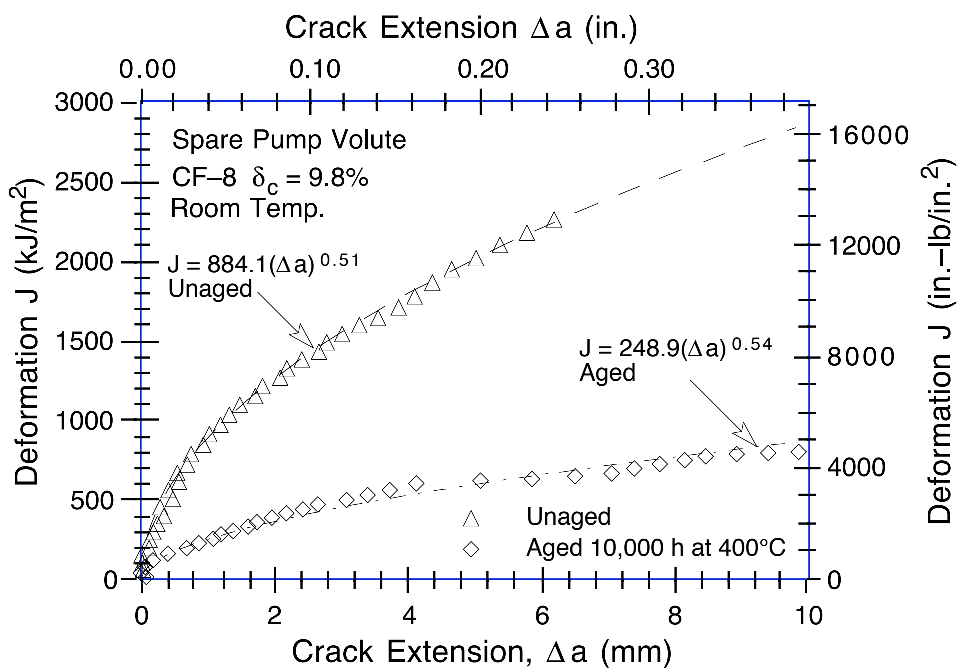

Figure 20. Fracture toughness J–R curves at room temperature and 290°C for unaged and laboratory–aged material from the spare pump volute. (Dashed and chain–dot lines are the best–fit power–law J–R curves for the unaged and laboratory–aged materials, respectively.)

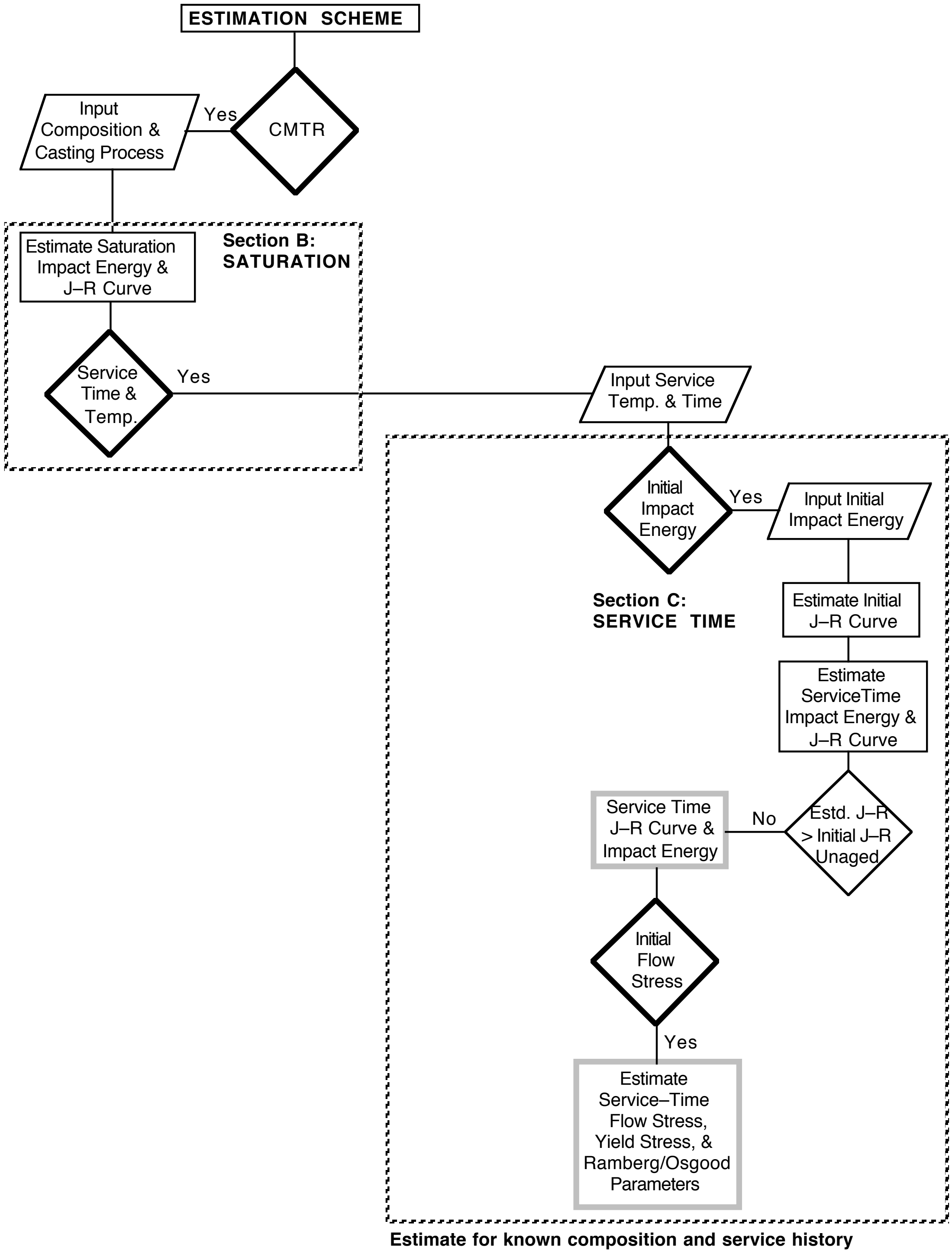

Figure 21. Flow diagram for estimating mechanical properties of cast materials obtained from the Shippingport reactor

material. The ferrite content is calculated from chemical composition in terms of the Hull's equivalent factors[24]

$$Cr_{eq} = Cr + 1.21(Mo) + 0.48(Si) - 4.99 \quad (4)$$

and

$$Ni_{eq} = (Ni) + 0.11(Mn) - 0.0086(Mn)^2 + 18.4(N) + 24.5(C) + 2.77. \quad (5)$$

The ferrite content δ_c is given by

$$\delta_c = 100.3(Cr_{eq}/Ni_{eq})^2 - 170.72(Cr_{eq}/Ni_{eq}) + 74.22. \quad (6)$$

The saturation RT impact energy for a specific cast SS is determined by two expressions, and the lower value is used for estimating fracture properties. For CF–3 and CF–8 steels, the saturation value of RT impact energy C_{Vsat} is the lower value determined from

$$\log_{10}C_{Vsat} = 1.15 + 1.36\exp(-0.035\Phi), \quad (7)$$

where the material parameter Φ is expressed as

$$\Phi = \delta_c(Cr + Si)(C + 0.4N), \quad (8)$$

and from

$$\log_{10}C_{Vsat} = 5.64 - 0.006\delta_c - 0.185Cr + 0.273Mo - 0.204Si + 0.044Ni - 2.12(C + 0.4N). \quad (9)$$

For CF–8M steel with <10% Ni, the saturation value of RT impact energy C_{Vsat} is the lower value determined from

$$\log_{10}C_{Vsat} = 1.10 + 2.12\exp(-0.041\Phi), \quad (10)$$

where the material parameter Φ is expressed as

$$\Phi = \delta_c(Ni + Si + Mn)^2(C + 0.4N)/5, \quad (11)$$

and from

$$\log_{10}C_{Vsat} = 7.28 - 0.011\delta_c - 0.185Cr - 0.369Mo - 0.451Si - 0.007Ni - 4.71(C + 0.4N). \quad (12)$$

For CF–8M steel with >10% Ni, the saturation value of RT impact energy C_{Vsat} is the lower value determined from

$$\log_{10}C_{Vsat} = 1.10 + 2.64\exp(-0.064\Phi), \quad (13)$$

where the material parameter Φ is expressed as

$$\Phi = \delta_c(Ni + Si + Mn)^2(C + 0.4N)/5, \quad (14)$$

and from

$$\log_{10}C_{Vsat} = 7.28 - 0.011\delta_c - 0.185Cr - 0.369Mo - 0.451Si - 0.007Ni - 4.71(C + 0.4N). \quad (15)$$

If not known, the N content can be assumed to be 0.04 wt.%. The RT impact energy as a function of time and temperature of aging of a specific cast SS is determined from its estimated RT saturation impact energy C_{Vsat} and the kinetics of embrittlement. The decrease in RT Charpy–impact energy C_V with time is expressed as

$$\log_{10} C_V = \log_{10} C_{Vsat} + \beta\left\{1 - \tanh\left(\frac{P - \theta}{\alpha}\right)\right\}, \quad (16)$$

where the aging parameter P is defined by

$$P = \log_{10}(t) - \frac{1000Q}{19.143}\left(\frac{1}{T_s + 273} - \frac{1}{673}\right). \quad (17)$$

The constants α and β can be determined from the initial impact energy C_{Vint} and saturation impact energy C_{Vsat} as follows:

$$\alpha = -0.585 + 0.795\log_{10}C_{Vsat} \quad (18)$$

and

$$\beta = (\log_{10}C_{Vint} - \log_{10}C_{Vsat})/2. \quad (19)$$

The value of θ varies with service temperature; it is 3.3 for temperatures <280°C (<536°F), 2.9 for temperatures between 280 and 330°C (536 and 626°F), and 2.5 for temperatures between 330 and 360°C (626 and 680°F). Activation energy for thermal embrittlement is expressed in terms of both chemical composition and the constant θ. The activation energy Q is given by

$$Q = 10\,[74.52 - 7.20\,\theta - 3.46\,Si - 1.78\,Cr - 4.35\,I_1\,Mn + (148 - 125\,I_1)\,N - 61\,I_2\,C], \quad (20)$$

where the indicators $I_1 = 0$ and $I_2 = 1$ for CF–3 or CF–8 steels and assume the values of 1 and 0, respectively, for CF–8M steels. Equation 20 is applicable to compositions within ASTM Specification A 351, with an upper limit of 1.2 wt.% for Mn content. Actual Mn content is used when materials contain up to 1.2 wt.% Mn; for steels that contain >1.2 wt.% Mn, 1.2 wt.% is assumed. Furthermore, the values of Q predicted from Eq. 20 should be between 65 kJ/mole (15.5 kcal/mole) minimum and 250 kJ/mole (59.8 kcal/mole) maximum; Q is assumed to be 65 kJ/mole if the predicted values are lower, and 250 kJ/mole if the predicted values are higher.

Room–temperature impact energies of the various service–aged materials from the Shippingport reactor were estimated from Eqs. 4–20. The initial impact energy of the unaged

Table 3. Measured and estimated Charpy–impact properties of cast stainless steel materials from the Shippingport, KRB, and Ringhals reactors

Material ID	Initial Impact Energy C_{Vint}[a] (J/cm² [ft·lb])	Saturation Impact Energy C_{Vsat} (J/cm² [ft·lb]) Meas.	Saturation Impact Energy C_{Vsat} (J/cm² [ft·lb]) Estd.	Activation Energy (kJ/mole [kcal/mole]) Calculated from Meas. θ[b]	Activation Energy Calculated from Meas. θ	Activation Energy Calculated from Estd. θ[c]	β	α	P[d]	Service Time Impact Energy C_V (J/cm² [ft·lb]) Meas.	Service Time Impact Energy C_V Estd.
Shippingport Cold Leg											
CA4	188 (111)	64 (38)	59 (35	2.65	170 (41)	123 (29)	0.252	0.822	2.632	145 (86)	155 (91)
CB7	–	–	107 (63	–	–	167 (40)	–	1.028	–	183 (108	–
CC4	–	–	71 (42	–	–	166 (40)	–	0.887	–	122 (72)	–
PV	424 (250)	–	106 (63	–	–	98 (23)	0.302	1.023	3.132	322 (190	237 (140
Shippingport Hot Leg											
MA1	320 (189)	141 (83	127 (75	3.40	164 (39)	200 (48)	0.201	1.087	1.715	299 (176	292 (172
MB2	–	–	175 (10	–	–	250 (60)	–	1.198	–	–	–
Unaged Material											
MA9	357 (210)	128 (76	124 (73	2.70	216 (52)	202 (48)	0.230	1.078	–	357 (210	–
VR	237 (140)	64 (38)	62 (37)	2.40	207 (50)	171 (41)	0.290	0.842	–	237 (140	–
KRB Pump Cover Plate											
KRB	232 (137)	23 (14)	24 (14)	2.44	156 (37)	123 (29)	0.488	0.519	2.849	131 (77)	84 (50)
Ringhals Elbows											
Hot–Leg	262 (155)	–	56 (33)	–	–	121 (29)	0.334	0.807	3.714	45 (27)	67 (40)
Xover–Leg	253 (149)	–	65 (38)	–	–	122 (29)	0.295	0.857	3.072	107 (63)	112 (66)

[a] Obtained from recovery–annealed material.
[b] Experimental values determined from material that was aged further at 400°C.
[c] The value of θ in Eq. 20 is 3.3 for <280°C, 2.9 for 280–330°C, and 2.5 for 330–360°C.
[d] Values correspond to activation energies obtained with estimated values of θ and the following service conditions:
Shippingport Cold–Leg Components: 113,900 h at 264°C.; Hot–Leg Components: 113,900 h at 281°C.
KRB Pump Cover Plate: 68,000 h at 284°C.
Ringhals Hot–Leg Elbow: 78,650 h at 325°C (70,000 h at 325°C and 22,000 h at 303°C).
Ringhals Crossover–Leg Elbow: 79,760 h at 291°C (70,000 h at 291°C and 22,000 h at 274°C).

materials was determined from the data for recovery–annealed material. Some materials were aged further in the laboratory at 320, 350, and 400°C (608, 662, and 752°F) to validate the estimates of the saturation impact energy C_{Vsat} and kinetics of thermal embrittlement for the materials. The results are summarized in Table 3. The change in estimated Charpy–impact energy with aging time at temperatures between reactor service temperature and 400°C is shown in Figs. 22–24. The high–temperature aging data for CA4 and MA1 materials represent service–aged material that was aged further in the laboratory; aging times were adjusted to include the effect of aging at reactor temperature. For example, service of ≈13 y at a cold–leg temperature of 264°C corresponds to 234 h at 400°C for the CA4 material, and service of ≈13 y at a hot–leg temperature of 281°C corresponds to 113 h at 400°C for MA1 material.

The changes in impact energy that were estimated from activation energies obtained with experimental values of θ show very good agreement with the experimental data at all temperatures; those estimated from activation energies with assumed values of θ show good agreement at temperatures ≤360°C.

The impact energy for the main valve MA1 was estimated from the compositions of MA1 and MA9 materials; the differences in the compositions of the two materials are minor.

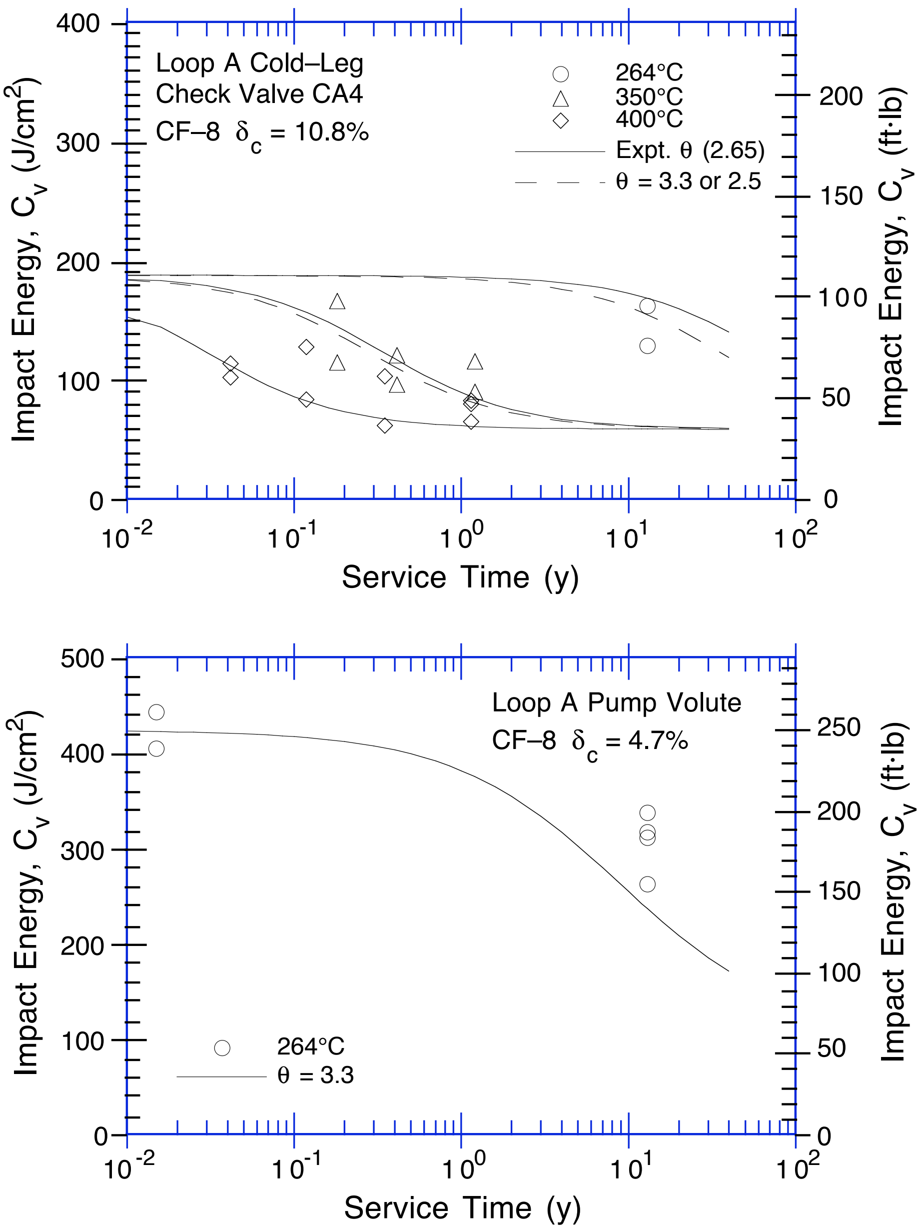

Figure 22. Variations of estimated room–temperature Charpy–impact energy with service time for Loop A cold–leg check valve CA4 and pump volute PV

Figures 23 and 24 show that, although the aging behavior at 400°C and the kinetics of embrittlement for MA1 and MA9 are significantly different, the estimates based on MA1 and MA9 agree well with the observed values for ≈13 y of service at 281°C. The aging behavior estimated from MA9 is slightly slower than that estimated from MA1.

The predicted minimum saturation RT impact energies also are in excellent agreement with the experimental data. The measured impact energies for the CA4, VR, MA1, and MA9 materials aged at 400°C achieve saturation at the predicted values.

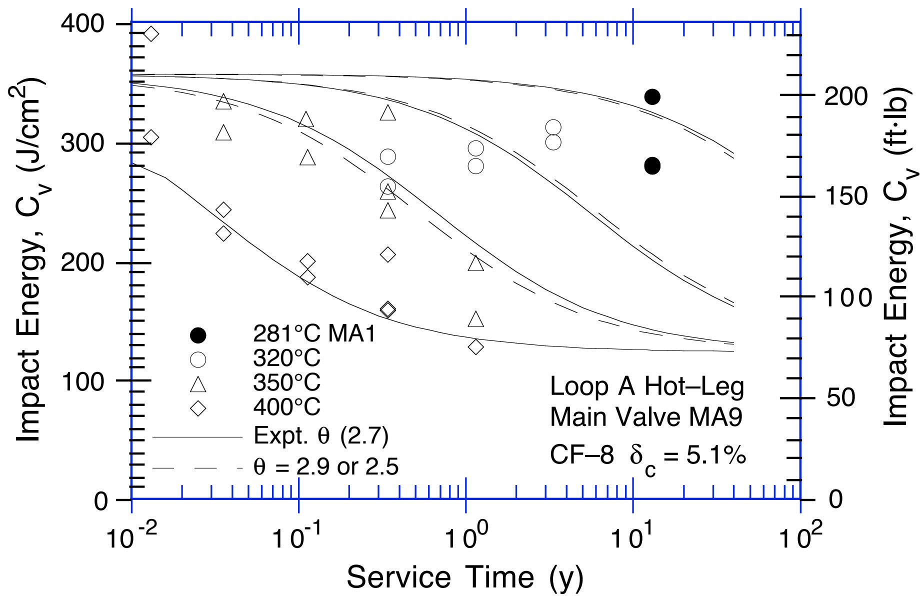

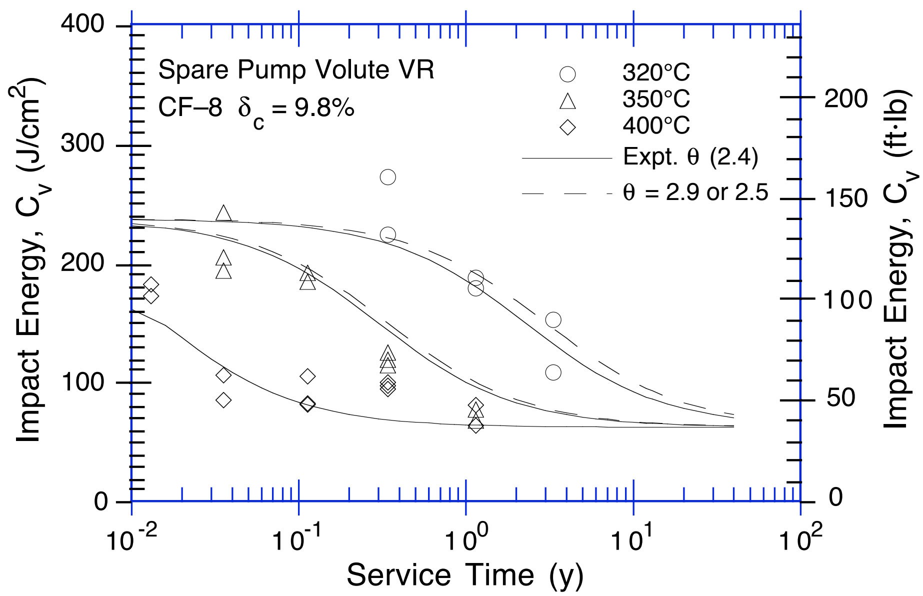

Figure 23. Variations of estimated room–temperature Charpy–impact energy with time for materials from cooler region of the hot–leg main valve MA9 and spare pump volute VR

4.2 Fracture Toughness

The fracture toughness J–R curve for a specific cast SS can be estimated from its RT Charpy–impact energy, C_V. The J–R curve is expressed by the power–law relation $J_d = C\Delta a^n$ per ASTM Specifications E 813–85 and E 1152–87. At room temperature, the fracture toughness J–R curve for static–cast CF–8 steel is given by

$$J_d = 49[C_V]^{0.52}[\Delta a]^n, \quad (21)$$

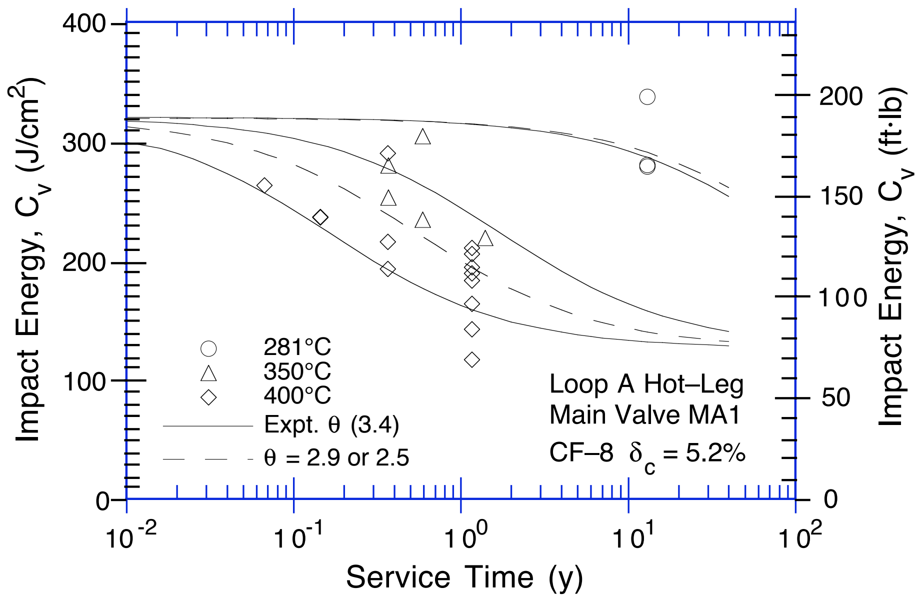

Figure 24. Variation of estimated room–temperature Charpy–impact energy with service time for Loop A hot–leg main valve MA1

where the exponent n is expressed as

$$n = 0.20 + 0.12\log_{10}[C_V]; \tag{22}$$

and for static–cast CF–8M steel, by

$$J_d = 16[C_V]^{0.67}[\Delta a]^n, \tag{23}$$

where the exponent n is expressed as

$$n = 0.23 + 0.08\log_{10}[C_V]. \tag{24}$$

At 290°C (554°F), the fracture toughness J–R curve for static–cast CF–8 steels is given by

$$J_d = 102[C_V]^{0.28}[\Delta a]^n, \tag{25}$$

where the exponent n is expressed as

$$n = 0.21 + 0.09\log_{10}[C_V]; \tag{26}$$

and for static–cast CF–8M steel, by

$$J_d = 49[C_V]^{0.41}[\Delta a]^n, \tag{27}$$

where the exponent n is expressed as

$$n = 0.23 + 0.06\log_{10}[C_V]. \tag{28}$$

The J–R curve at any intermediate temperature can be linearly interpolated from the estimated values of C and n at room temperature and at 290°C.

The fracture toughness J–R curves for the CA4, MA1, and PV materials after reactor service were estimated from Eqs. 7–28 and RT Charpy–impact energies for the materials were determined by the procedure described in Section 4.1. For all materials, the saturation fracture toughness J–R curve, i.e., the minimum J–R curve that would be achieved for the specific composition after long–term aging, was estimated from Eqs. 7–28 and saturation RT impact energy, C_{Vsat}. However, the initial fracture toughness J–R curve was used as an upper bound for the material. The correlations described in Eqs. 7–28 account for the degradation of mechanical properties of typical heats of cast SS. They do not consider the initial fracture properties of the unaged material. Some heats of cast SSs may exhibit a low initial fracture toughness, and the estimated J–R curve may be higher than the initial curve. When the estimated J–R curve is higher than the initial fracture toughness J–R curve, the latter is used as the J–R curve of the material. The failure mechanism of materials with low initial fracture toughness is controlled by processes other than those that cause thermal embrittlement of cast SSs; such materials will undergo little or no change in fracture toughness because of thermal aging during service.

The CMTR for a specific cast SS component provides information on chemical composition, tensile strength, and possibly Charpy–impact energy of the material; fracture toughness is not available in CMTRs. The fracture toughness J–R curve for unaged material was obtained by using the initial RT Charpy–impact energy, C_{Vint}, instead of C_V in Eqs. 21–28. The estimated and experimental fracture toughness J–R curves at room temperature and at 290°C for the CA4, MA1, PV, and VR materials in the unaged or recovery–annealed condition, after service, and at saturation, are shown in Figs. 25–28.

The estimated J–R curves either show good agreement, e.g., CA4 and VR materials, or are slightly lower (30–50%) than the experimental results, e.g., MA1 and PV materials. The somewhat conservative estimates are expected for some compositions of cast SSs; the criteria used in developing the estimation scheme ensure that the estimated mechanical properties are adequately conservative for cast SSs as defined by ASTM Specification A–351.[5–8] They do not consider the effects of metallurgical differences that may arise from differences in production heat treatment or casting processes and, therefore, may be overly conservative for some steels. The estimates are consistent with the experimental data. For example, the estimation scheme predicts relatively modest decreases in fracture toughness for the materials after reactor service. Also, the correlations predicted that the spare pump volute VR would exhibit the observed saturation fracture toughness, which was lower than that for the other materials.

4.3 Tensile Properties

Thermal aging of cast SSs increases their tensile strength, particularly their ultimate stress. The increase in yield or flow stress of aged cast SSs is estimated from a correlation between the ratio of tensile yield or flow stress of aged, and unaged material and the aging parameter, P.[6,8] At room temperature, the tensile–flow–stress ratio $R_f = (\sigma_{f_{aged}}/\sigma_{f_{unaged}})$ for CF–8 steel is given by

$$R_f = 0.84 + 0.08P \qquad (1.00 \le R_f \le 1.16); \qquad (29)$$

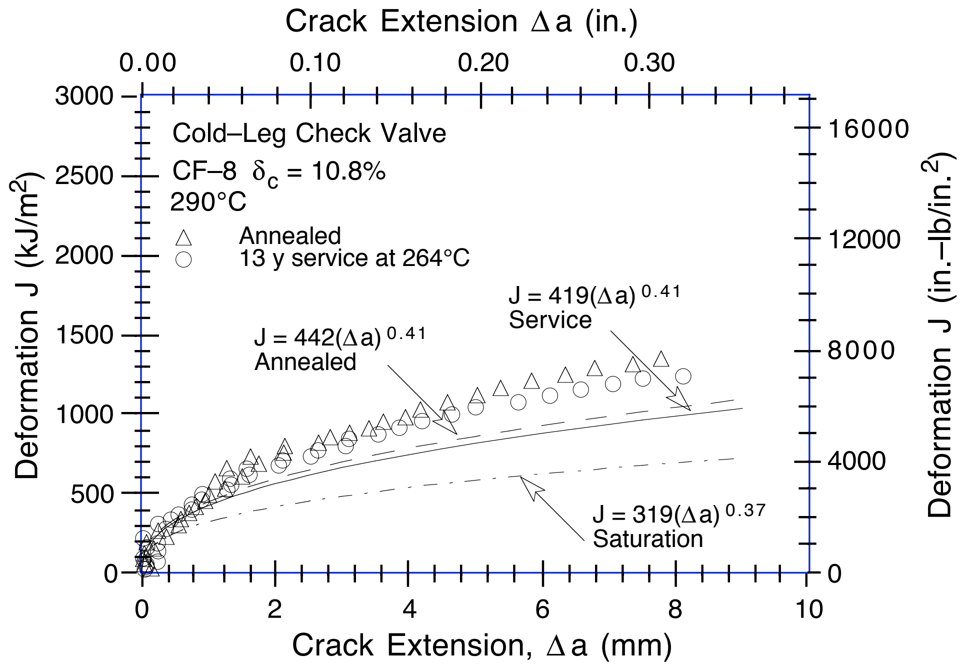

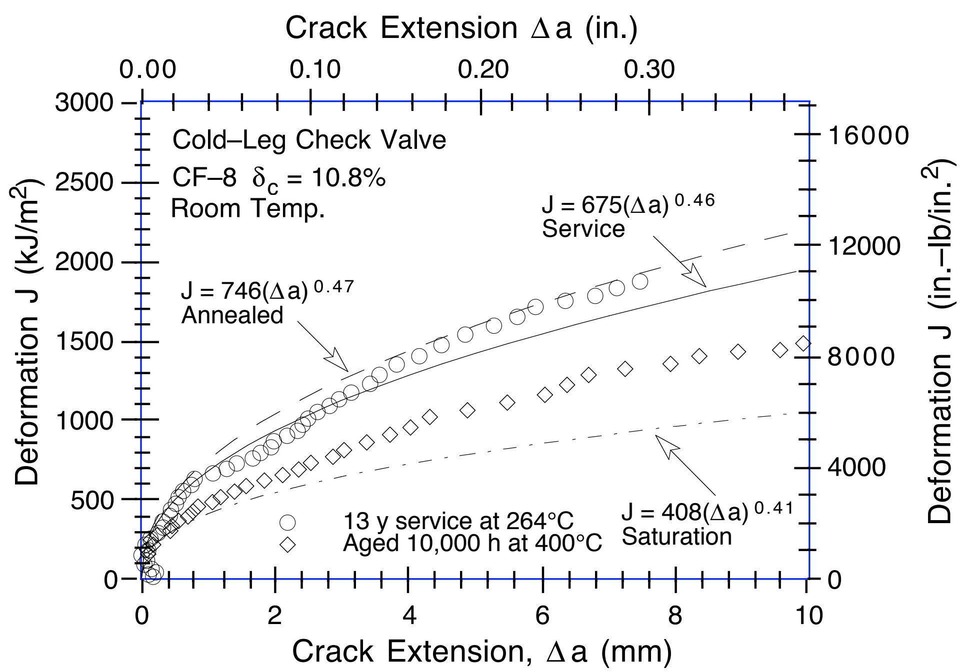

Figure 25. Estimated and measured fracture toughness J–R curves for the cold–leg check valve in the annealed, 13–y service at 264°C, and fully embrittled or saturation condition. (Dashed, solid, and chain–dot lines are the best–fit power–law J–R curves for annealed, service–aged, and laboratory–aged materials, respectively.)

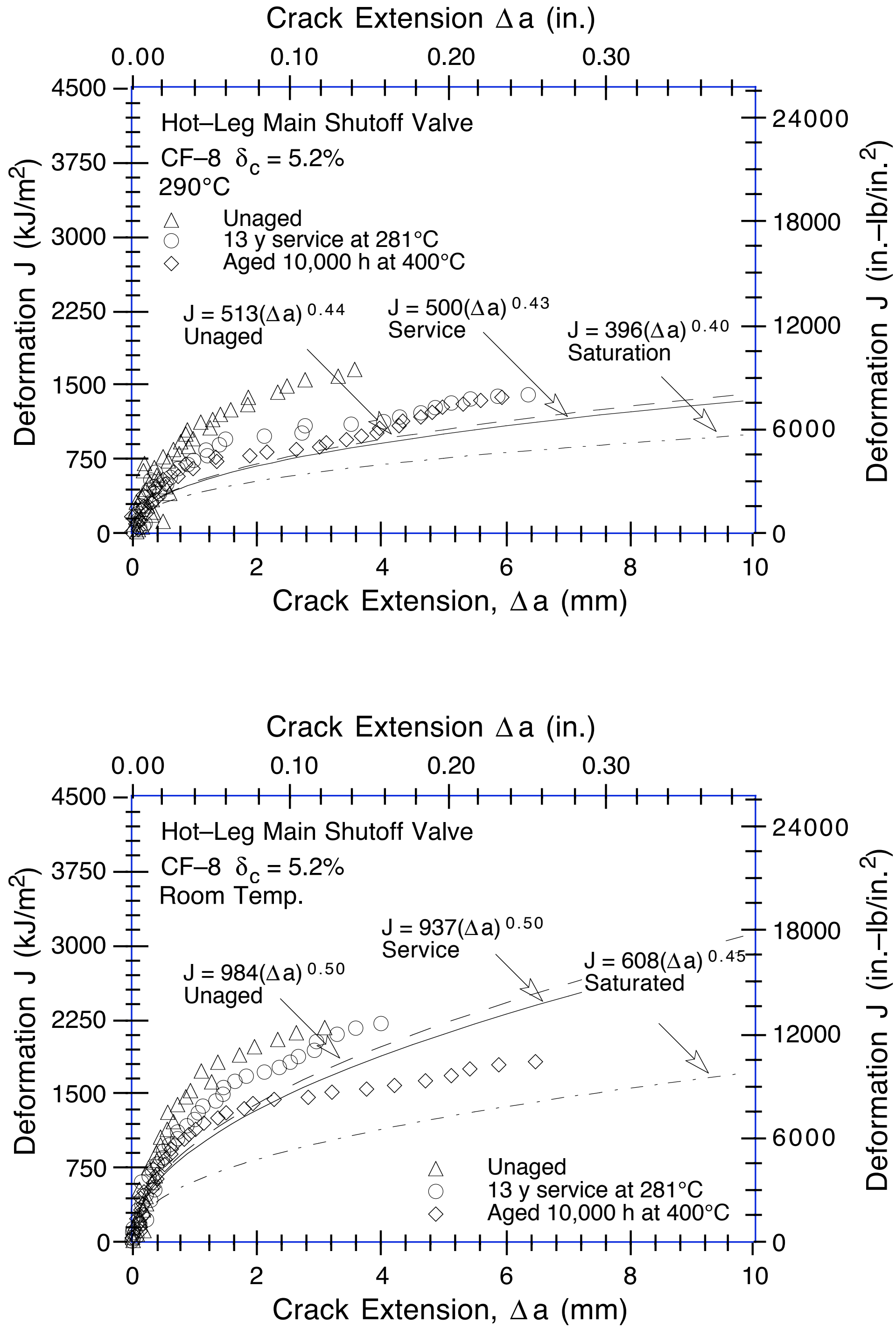

Figure 26. Estimated and measured fracture toughness J–R curves for the hot–leg main shutoff valve in essentially unaged, 13–y service at 281°C, and fully embrittled or saturation condition. (Dashed, solid, and chain–dot lines are the best–fit power–law J–R curves for unaged, service–aged, and laboratory–aged materials, respectively.)

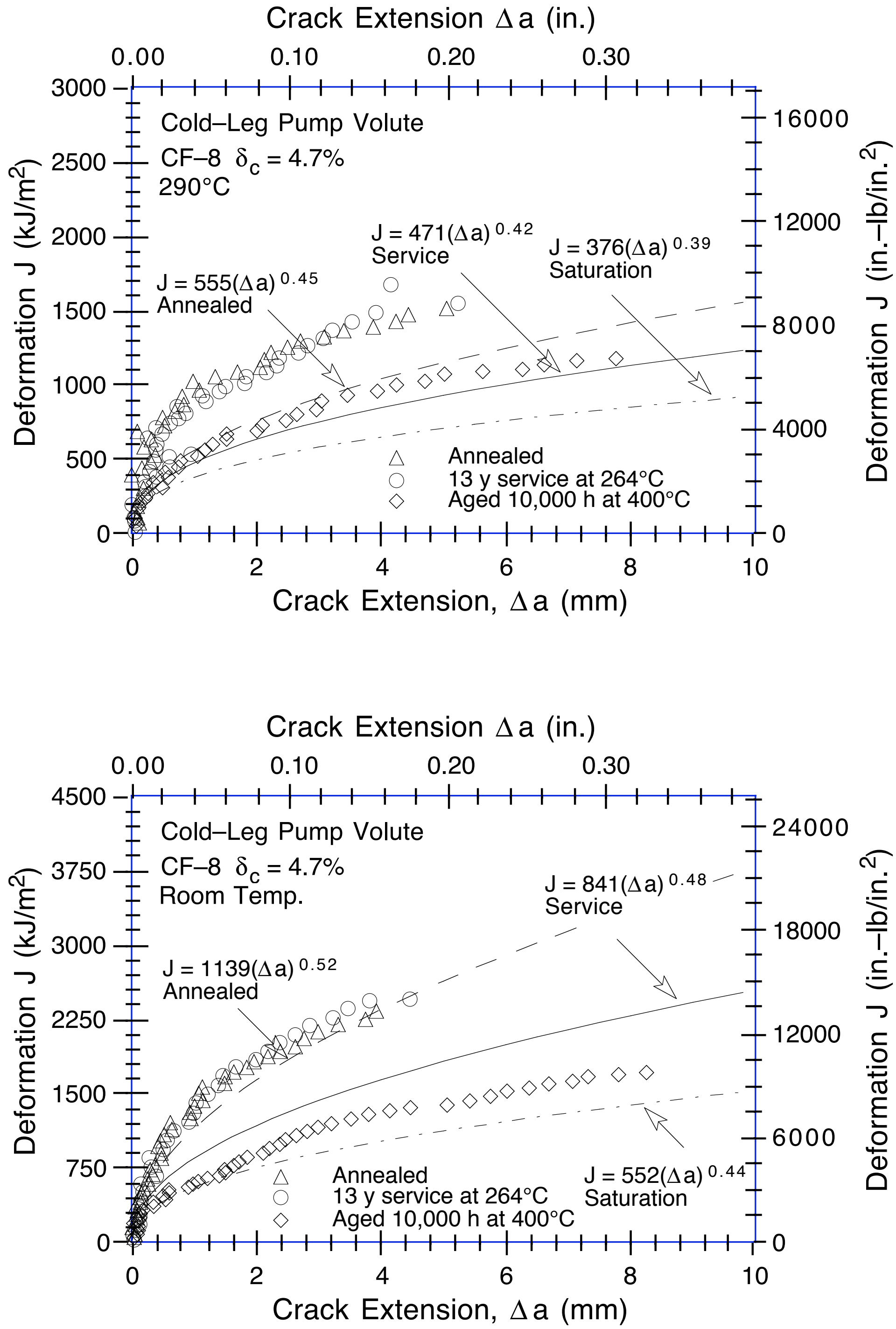

Figure 27. Estimated and measured fracture toughness J–R curves for the cold–leg pump volute in the annealed, 13–y service at 264°C, and fully embrittled or saturation condition. (Dashed, solid, and chain–dot lines are the best–fit power–law J–R curves for annealed, service–aged, and laboratory–aged materials, respectively.)

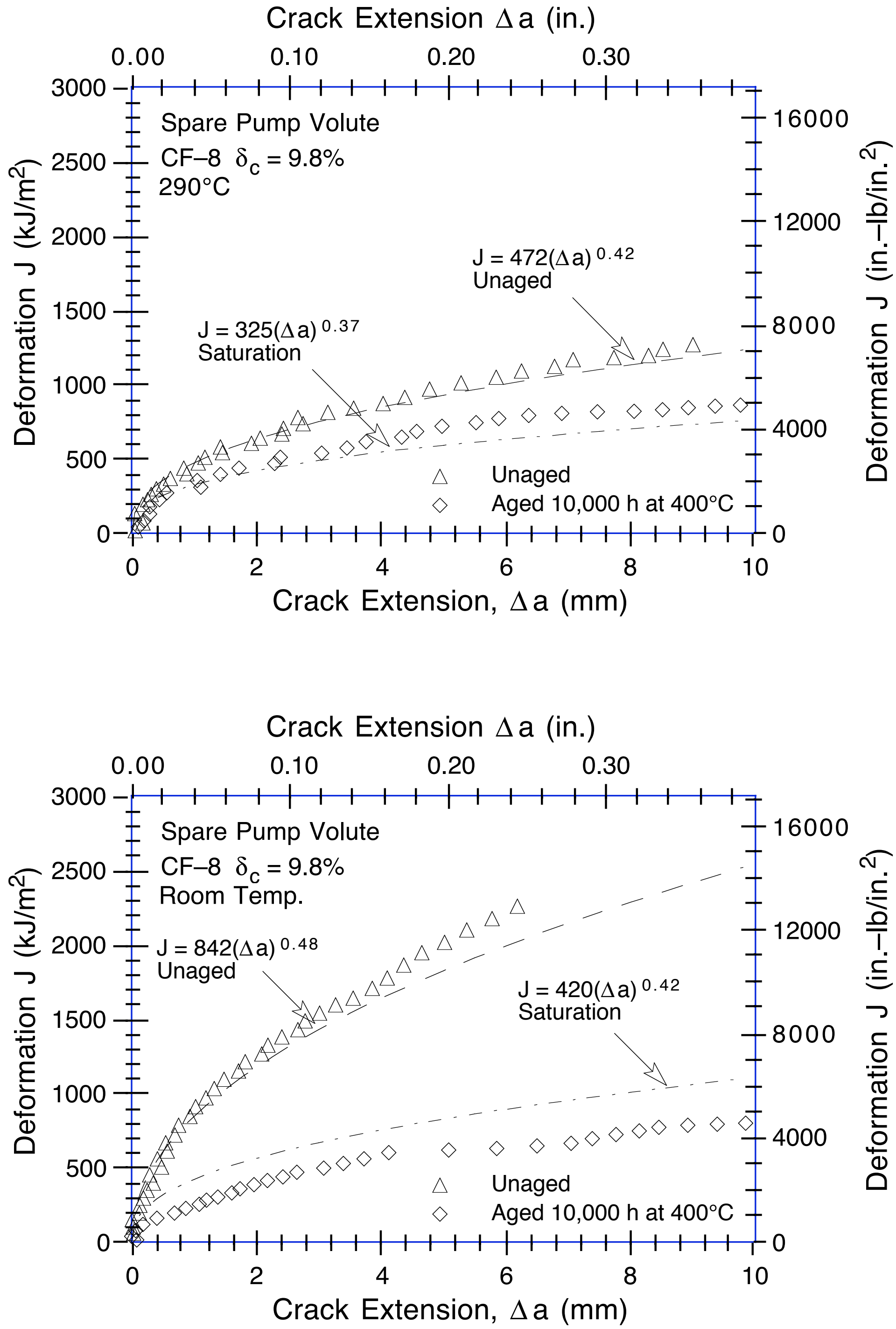

Figure 28. Estimated and measured fracture toughness J–R curves for the spare pump volute in the unaged and fully embrittled or saturation condition. (Dashed and chain–dot lines are the best–fit power–law J–R curves for unaged and laboratory–aged materials, respectively.)

and for CF–8M steel, by

$$R_f = 0.77 + 0.10P \qquad (1.00 \le R_f \le 1.19). \qquad (30)$$

At 290°C (554°F), the tensile–flow–stress ratio for CF–8 steel is given by

$$R_f = 0.83 + 0.09P \qquad (1.00 \le R_f \le 1.14); \qquad (31)$$

and for CF–8M steel, by

$$R_f = 0.69 + 0.14P \qquad (1.00 \le R_f \le 1.24). \qquad (32)$$

The data on tensile properties of cast stainless steels indicate that the increase in yield stress due to thermal aging is much lower than the increase in ultimate stress. At room temperature, the tensile–yield–stress ratio $R_y = (\sigma y_{aged}/\sigma y_{unaged})$ for CF–8 steel is given by

$$R_y = 0.798 + 0.076P \qquad (1.00 \le R_y \le 1.10); \qquad (33)$$

and for CF–8M steel, by

$$R_y = 0.708 + 0.092P \qquad (1.00 \le R_y \le 1.10). \qquad (34)$$

At 290°C (554°F), the tensile–yield–stress ratio for CF–8 steel is given by

$$R_y = 0.788 + 0.086P \qquad (1.00 \le R_y \le 1.09); \qquad (35)$$

and for CF–8M steel, by

$$R_y = 0.635 + 0.129P \qquad (1.00 \le R_y \le 1.14). \qquad (36)$$

The minimum and maximum values of the ratio R_f are given for each grade of steel and temperature, i.e., a minimum or maximum value is assumed, respectively, when the calculated ratio is smaller than the minimum or greater than the maximum. Equations 29–36 are valid for service temperatures between 280 and 330°C (536 and 626°F) and ferrite content >7% for CF–8M steel and >10% for CF–3 and CF–8 steels. Thermal aging has little or no effect on the tensile strength of cast SSs with low ferrite content.

Experimental and estimated tensile yield and flow stress at 290°C (554°F) and at room temperature for the various Shippingport materials are given in Table 4. The materials from the hot–leg main shutoff valve and cold–leg pump volute contain <10% ferrite and, therefore, would show little or no increase in tensile strength. As borne out by experimental data, the tensile strength of these materials remains unchanged after service. Although Eqs. 29–36 are recommended for service temperatures between 280 and 330°C, the increase in tensile yield and flow stress for the cold–leg check valve after service at 264°C and the spare pump volute that was aged at 400°C in the laboratory was obtained from these correlations and Eqs. 17 and 20. A θ value of 3.3 was used for the check valve. The estimated values presented in Table 4 show good agreement with the measured values.

Fracture toughness J_{IC} values for service–aged materials were determined from the estimated J–R curve and flow stress, and are also given in Table 4. The estimated values of J_{IC}

Table 4. Measured and estimated tensile yield and flow stresses and J_{IC} values for service– and laboratory–aged cast stainless steels[a]

Material ID	Test Temp. (°C)	Yield Stress (MPa)[b] Unaged	Yield Stress (MPa)[b] Measured	Yield Stress (MPa)[b] Estimated	Flow Stress (MPa)[b] Unaged	Flow Stress (MPa)[b] Measured	Flow Stress (MPa)[b] Estimated	J_{IC} (kJ/m^2) Measured	J_{IC} (kJ/m^2) Estimated
Service–Aged Material from the Shippingport Reactor									
CA4	25	(208)	228 (222)	208	(363)	377 (382)	381	476	503
	290	(125)	142 (128)	127	(246)	262 (245)	263	361	316
MA1	25	229	231	229	360	350	360	1407	825
	290	160	132	160	260	237	260	739	395
PV	25	(209)	230 (202)	209	(362)	370 (368)	362	1509	699
	290	(131)	157 (126)	131	(269)	266 (237)	269	858	362
Service–Aged Material from the KRB Reactor									
KRB	25	298	296	302	428	428	457	263, 396	323
	290	178	201	184	294	329	320	681	243
Service–Aged Material from the Ringhals 2 Reactor									
Hot–Leg	25	272	267	286	399	424	455	250, 330, 195, 150	169
	290	167	163	186	277	306	335	–	192
Xover–Leg	25	242	256	242	369	392	397	960, 525, 960, 600	252
	290	184	148	190	290	277	325	–	243
Essentially Unaged Material from the Shippingport Reactor Aged for 10,000 h at 400°C in the Laboratory									
MA9	25	229	236	229	360	372	360	1094	442
	290	160	144	160	260	260	260	629	294
VR	25	273	274	300	405	438	470	123	269
	290	159	185	173	267	305	304	214	228

[a] The service conditions for the materials are as follows:
Shippingport Cold–Leg Components: 113,900 h at 264°C.
Shippingport Hot–Leg Components: 113,900 h at 281°C.
KRB Pump Cover Plate: 68,000 h at 284°C.
Ringhals Hot–Leg Elbow: 78,650 h at 325°C (70,000 h at 325°C and 22,000 h at 303°C).
Ringhals Crossover–Leg Elbow: 79,760 h at 291°C (70,000 h at 291°C and 22,000 h at 274°C).

[b] Baseline tensile properties of unaged materials were obtained as follows:
Values in parantheses were determined from instrumented Charpy–impact tests.
Experimental values of MA9 were used for MA1.
Values for KRB pump cover plate were determined from tensile tests on recovery–annealed material.

show very good agreement with the measured value for CA4 and VR materials and are 30–50% lower for MA1, MA9, and PV materials. As mentioned earlier in this section, these correlations do not consider the effect of microstuctural differences and may be conservative for some materials.

The engineering stress–vs.–strain behavior of aged cast stainless steel can also be obtained from the estimated flow stress.[6,8] The engineering stress–vs.–strain curve is expressed by the Ramberg–Osgood equation

$$\frac{\varepsilon}{\varepsilon_o} = \frac{\sigma}{\sigma_o} + \alpha_1 \left(\frac{\sigma}{\sigma_o}\right)^{n_1}, \qquad (37)$$

where σ and ε are engineering stress and strain, respectively; σ_o is an arbitrary reference stress, often assumed to be equal to flow or yield stress; the reference strain $\varepsilon_o = \sigma_o/E$; α_1 and n_1 are Ramberg–Osgood parameters; and E is elastic modulus. The Ramberg–Osgood equation can be rearranged to the form

$$\frac{E\varepsilon - \sigma}{\sigma_f} = \alpha_1 \left(\frac{\sigma}{\sigma_f} \right)^{n_1}. \qquad (38)$$

For all grades of cast stainless steel, the parameter n_1 does not change with thermal aging. The parameter α_1 decreases with aging and shows good correlation with the flow stress σ_f of the material. For engineering stress–vs.–strain curves up to 5% strain, the Ramberg–Osgood parameters at room temperature, for CF–8 steels, are given by

$$\alpha_1 = 157.9 - 0.300\sigma_f \qquad (n_1 = 6.4); \qquad (39)$$

and for CF–8M steel, by

$$\alpha_1 = 50.9 - 0.0724\sigma_f \qquad (n_1 = 5.6). \qquad (40)$$

At 290°C (554°F), the Ramberg–Osgood parameters for engineering stress–vs.–strain curves up to 5% strain, for CF–8 steels, are given by

$$\alpha_1 = 153.3 - 0.373\sigma_f \qquad (n_1 = 7.1); \qquad (41)$$

and for CF–8M steel, by

$$\alpha_1 = 145.9 - 0.314\sigma_f \qquad (n_1 = 6.6). \qquad (42)$$

Estimated and measured tensile stress–vs.–strain curves at room temperature and at 290°C for the various Shippingport materials are shown in Figs. 29–33. Values of 200 GPa at room temperature and 180 GPa at 290°C were used for elastic modulus E in Eq. 38. The estimated curves show excellent agreement with the experimental data.

5 Ringhals Reactor Elbows

Investigation of the hot– and crossover–leg elbows from the Ringhals reactor indicated significant degradation of impact strength and fracture toughness of the hot–leg elbow after 15 y of service at 325°C, whereas the crossover–leg elbow in service at 291°C, showed only moderate degradation.[17] The mechanical properties of the Ringhals elbows were estimated from the correlations presented in Section 4 for CF–8M steel that contained >10% Ni. Information on the chemical composition and initial Charpy–impact energy and tensile strength of the unaged materials was used in the estimations; θ was assumed to be 2.9. The results for Charpy–impact and tensile properties are summarized in Tables 3 and 4, respectively.

The experimental data and estimated decrease in impact energy for hot– and crossover–leg elbows during service at 325 and 291°C, respectively, are shown in Fig. 34. The estimated value of 67 J/cm^2 for the hot–leg elbow is marginally higher than the measured average values of 45 J/cm^2 (equivalent Charpy V–notch impact energy converted from U–notch value) and

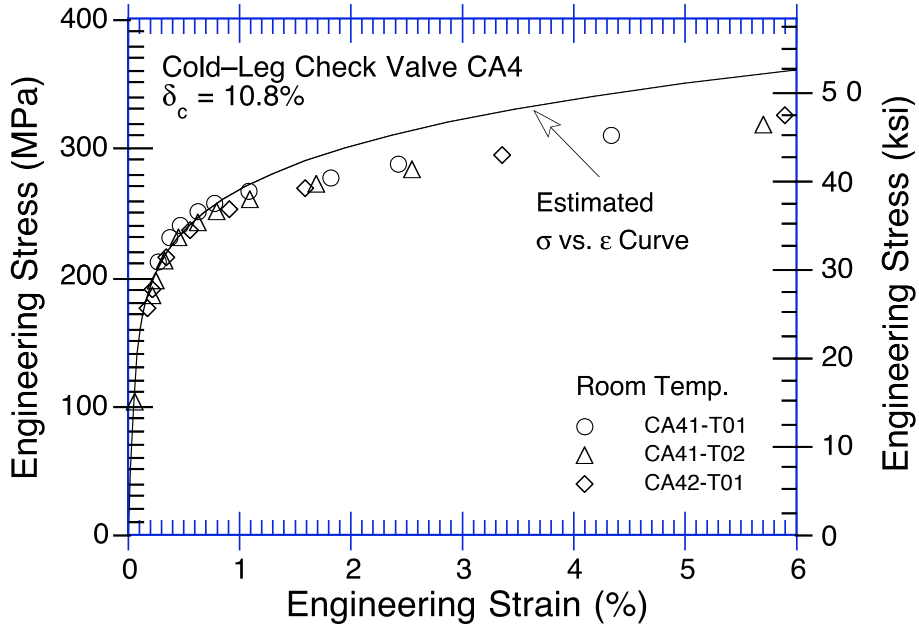

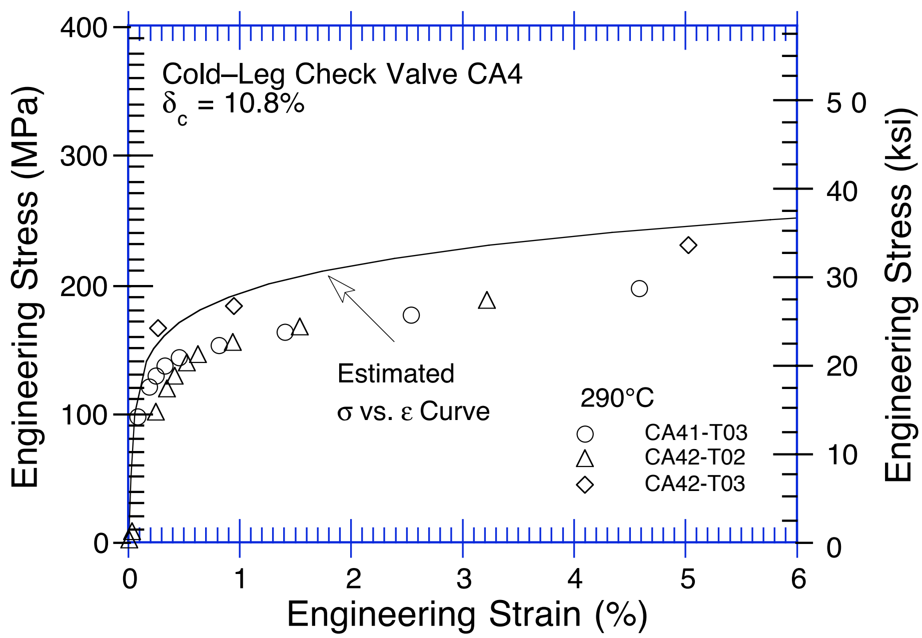

Figure 29. Estimated and measured tensile stress–vs.–strain curves at room temperature and 290°C for the cold–leg check valve after service for ≈13 y at 264°C

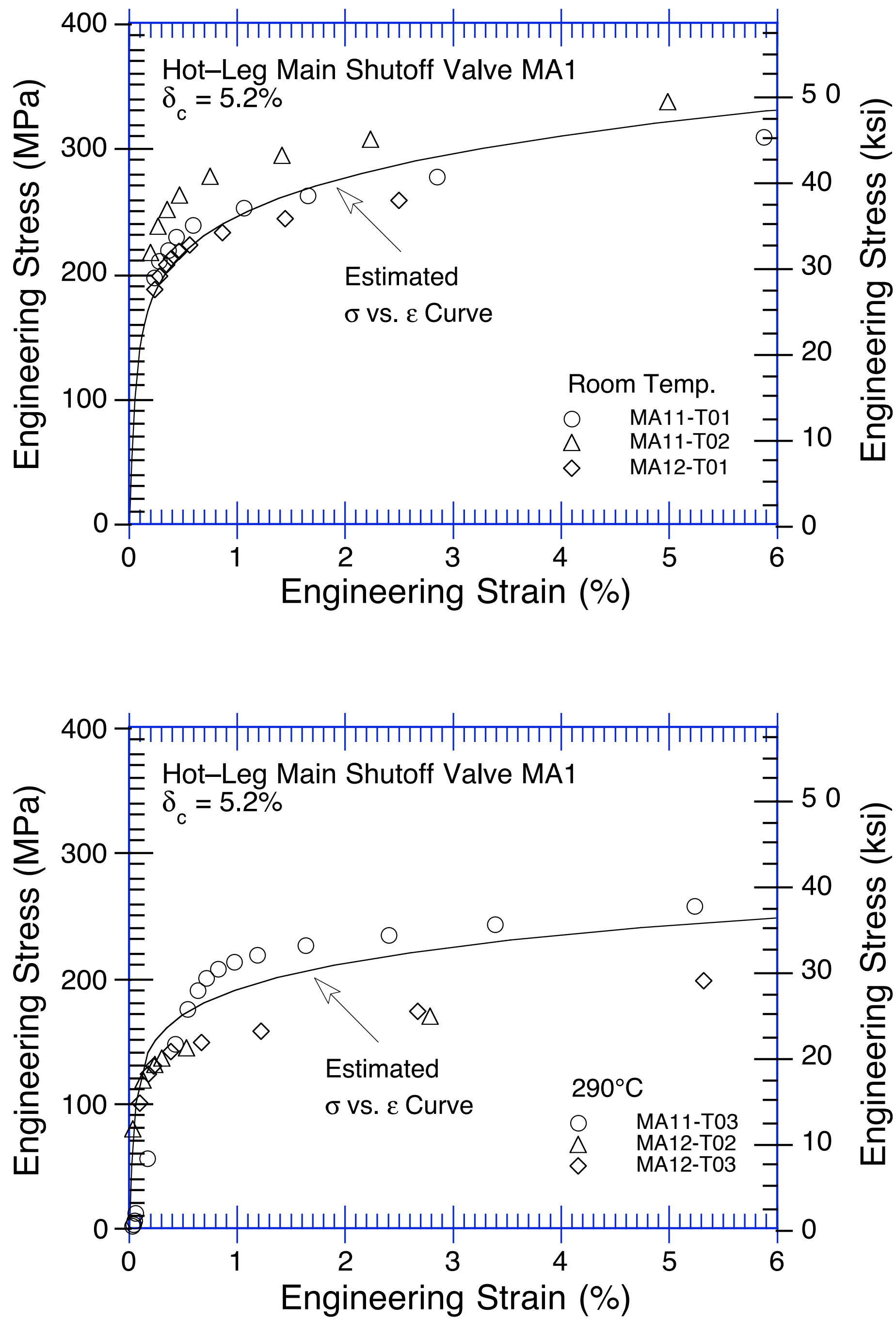

Figure 30. Estimated and measured tensile stress–vs.–strain curves at room temperature and 290°C for the hot–leg main shutoff valve after service for ≈13 y at 281°C

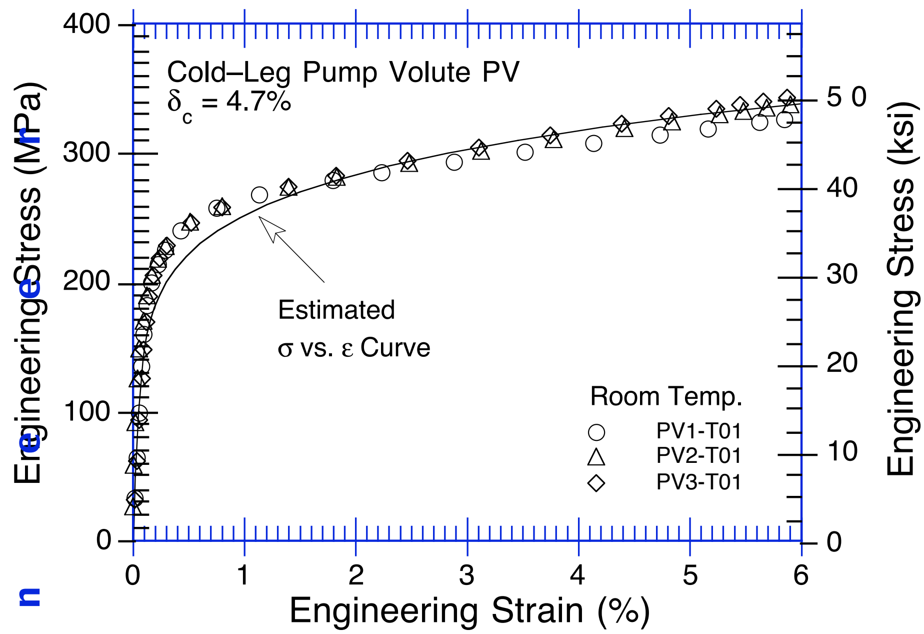

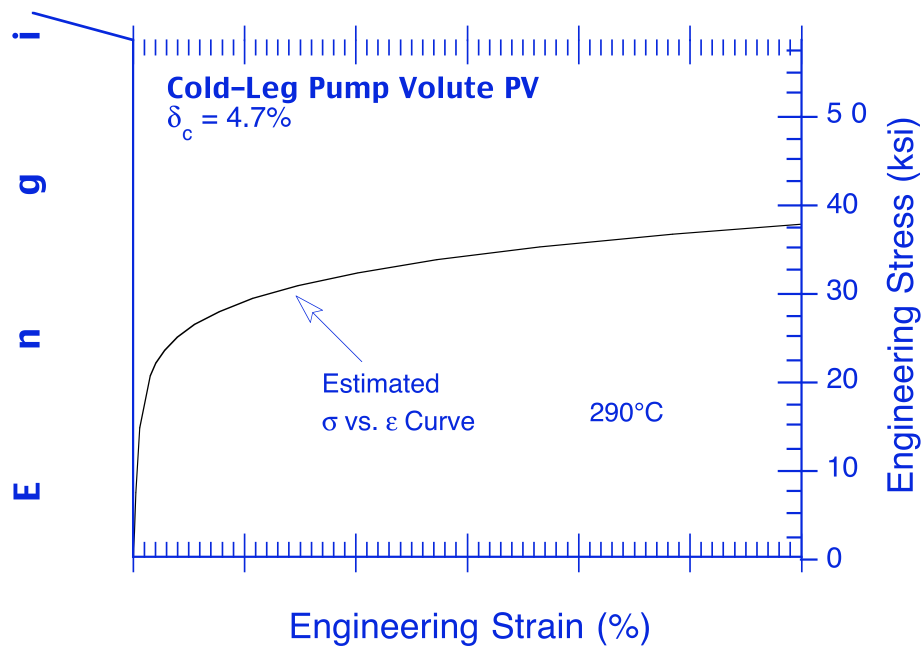

Figure 31. Estimated and measured tensile stress–vs.–strain curves at room temperature and 290°C for the cold–leg pump volute after service for ≈13 y at 264°C

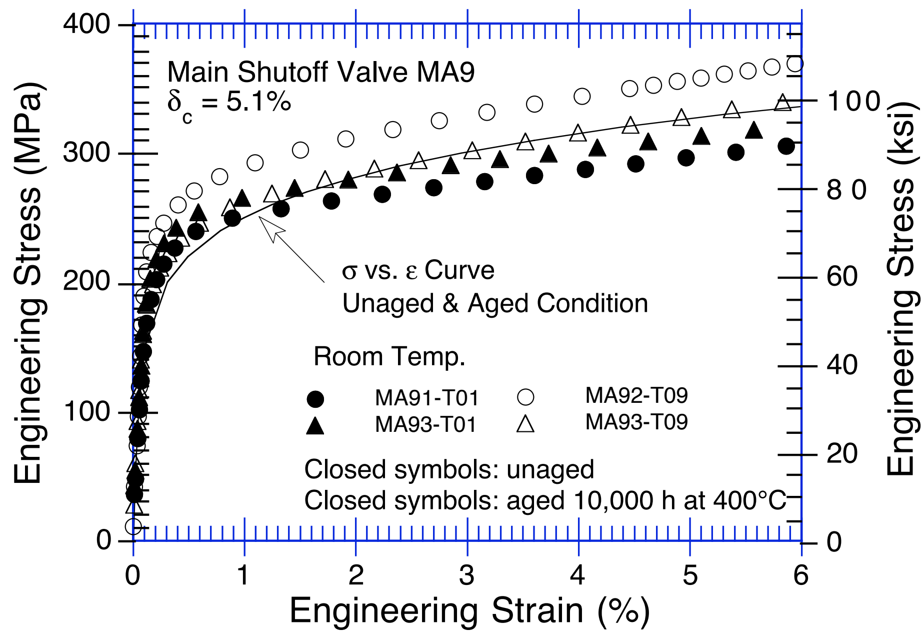

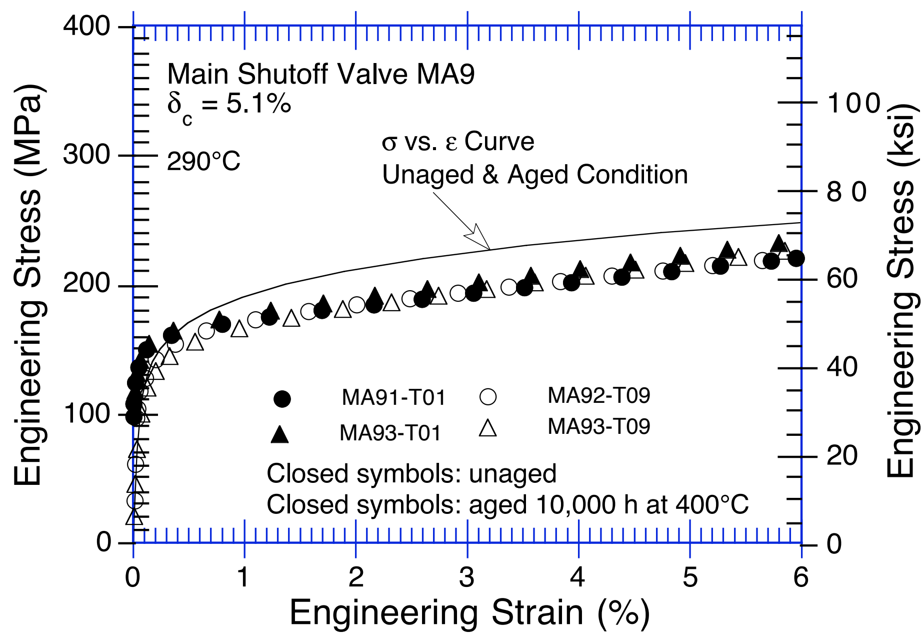

Figure 32. Estimated and measured tensile stress–vs.–strain curves at room temperature and 290°C for material from cooler regions of the hot–leg main shutoff valve in the unaged and fully embrittled or aged condition

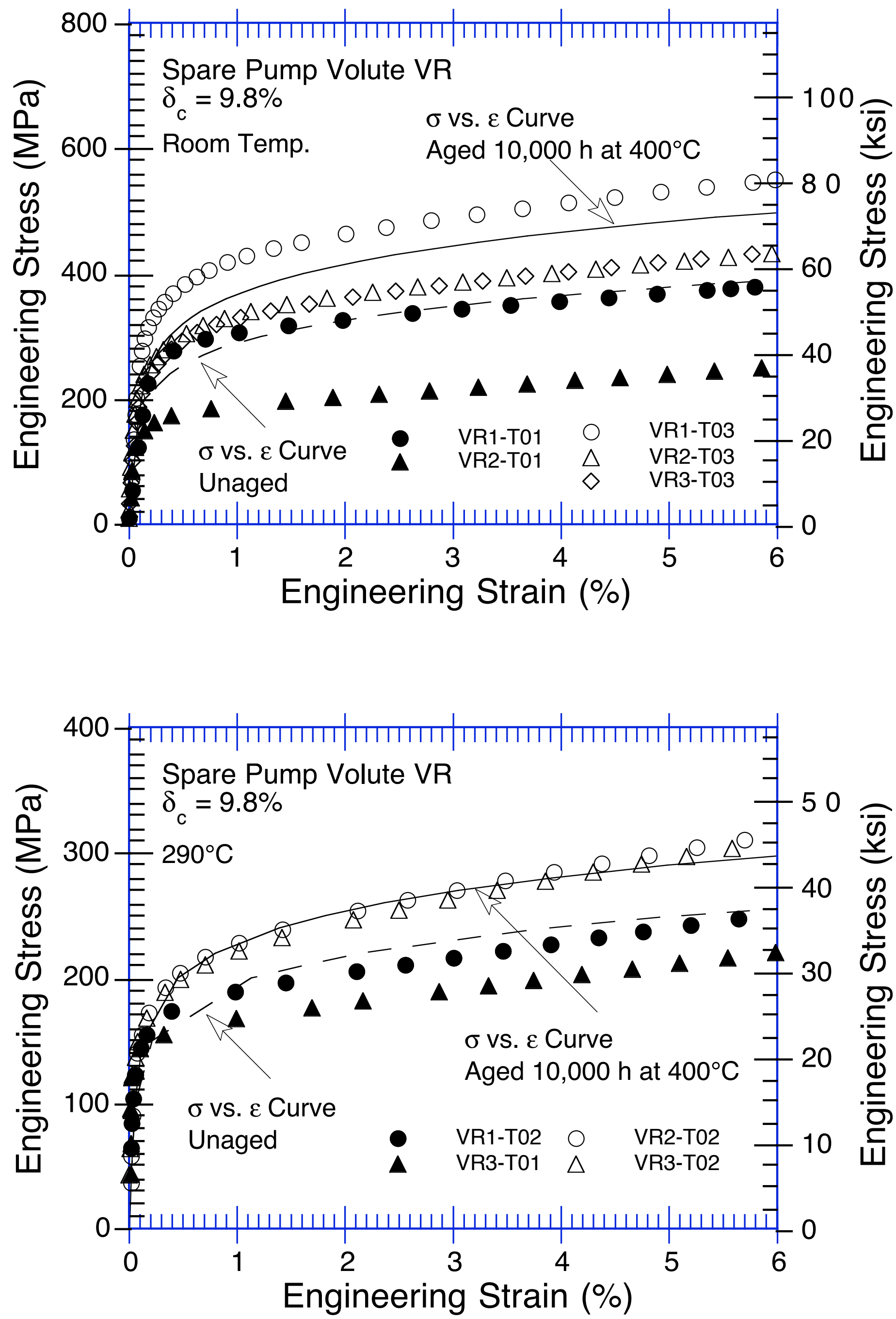

Figure 33. Estimated and measured tensile stress–vs.–strain curves at room temperature and 290°C for the spare pump volute in the unaged and fully embrittled or aged condition

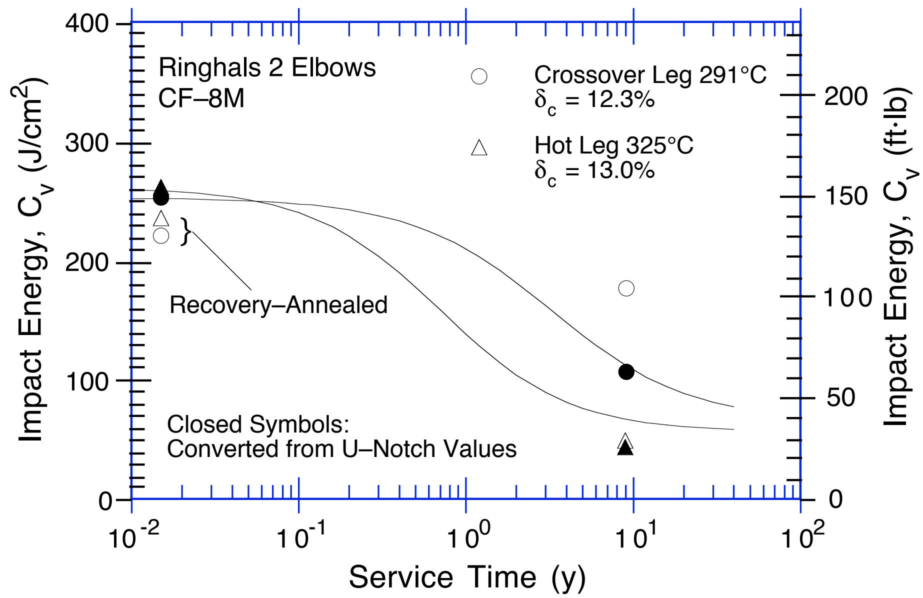

Figure 34. Estimated and experimentally observed room–temperature Charpy–impact energy for the Ringhals hot– and crossover–leg elbows. (Solid lines represent estimated decrease in impact energy.)

50 J/cm^2 (from Charpy V–notch specimens). The estimated 112 J/cm^2 impact energy for the crossover–leg agrees well with the 107 J/cm^2 measured from U–notch specimens and is significantly lower than the 177 J/cm^2 obtained from V–notch specimens. The difference between the V– and U–notch impact energy for the crossover–leg elbow is most likely due to a significant variation in the ferrite content of the material. The saturation impact energies for hot– and crossover–leg elbows are estimated to be 56 and 67 J/cm^2, respectively.

Fracture toughness J–R curves can be estimated from the impact energy. Room–temperature J–R curves for hot– and crossover–leg elbows after ≈15 y of service are shown in Fig. 35. Only the experimental J_{IC} values (not the complete J–R curve) have been reported for these materials.[17] The tensile yield and flow stresses and J_{IC} at room temperature and 290°C for the Ringhals elbows were also estimated by the procedure described in Section 4.3; the results are given in Table 4. The estimated tensile properties are in good agreement with the measured values. The J_{IC} for the hot–leg elbow also is comparable to the measured value, whereas that for the crossover–leg elbow is 50–70% lower. As mentioned above, the ferrite content of the crossover–leg elbow varies significantly. Furthermore, the correlations do not consider the effect of microstuctural differences and may be conservative for some materials.

6 KRB Reactor Pump Cover Plate

The mechanical properties of the pump cover plate assembly from the KRB reactor were also estimated from the correlations presented in Section 4. The material was in service at 284°C for ≈8 y. The results for Charpy–impact and tensile properties are summarized in Tables 3 and 4, respectively. The variation of experimental and estimated RT Charpy–impact energy with service time or after aging at 320, 350, and 400°C in the laboratory, is shown in Fig. 36.

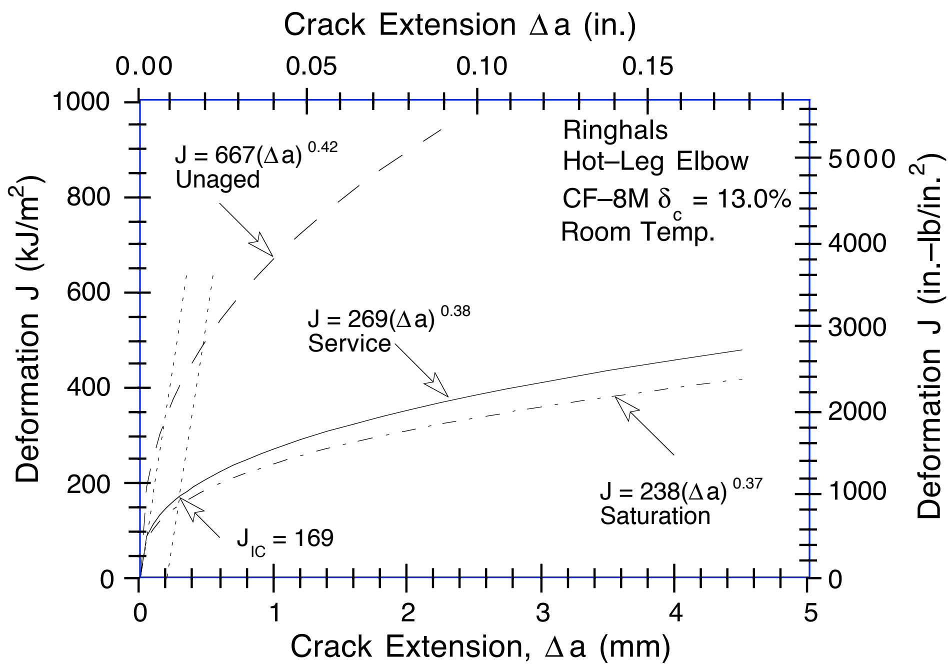

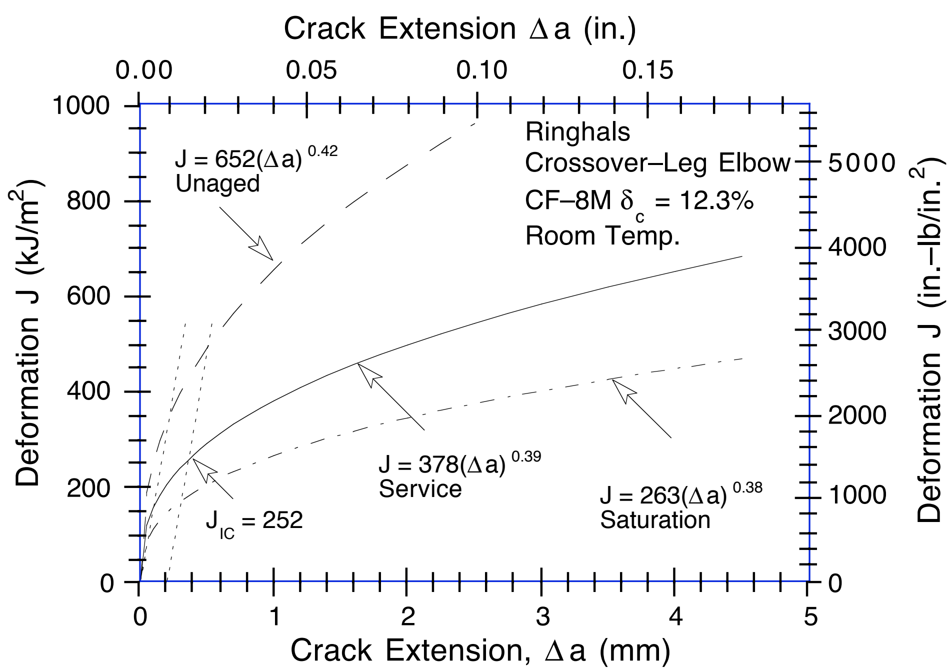

Figure 35. Estimated fracture toughness J–R curves for the Ringhals hot– and crossover–leg elbows in the unaged condition, after service, and at saturation. (Dashed, solid, and chain–dot lines are the estimated power–law J–R curves for unaged, service–aged, and fully embrittled or aged material, respectively.)

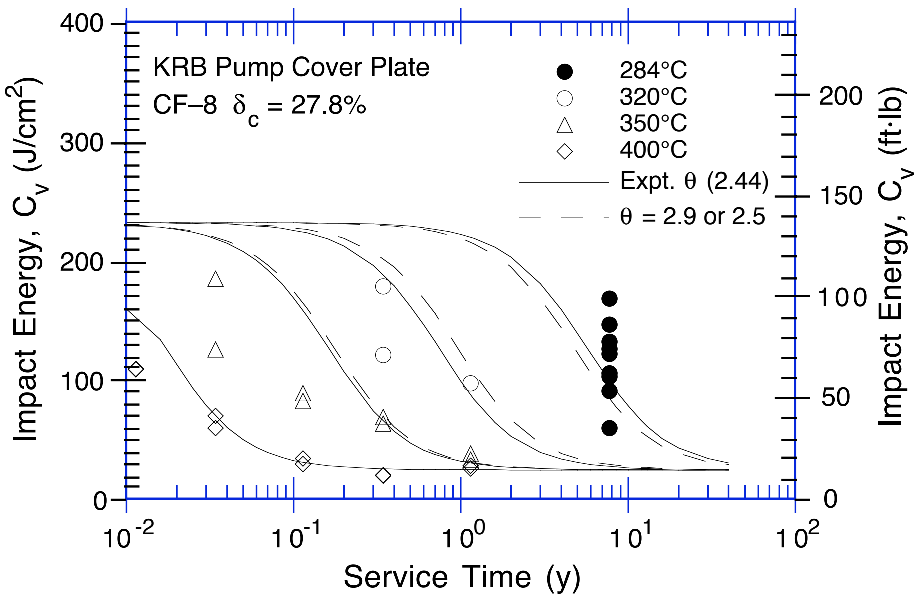

Figure 36. Variation of estimated room–temperature Charpy–impact energy with service time for the KRB pump cover plate

The estimated and measured tensile stress–vs.–strain curves for annealed and service–aged material are presented in Fig. 37. The estimates show very good agreement with the test results. Information on the chemical composition and initial Charpy–impact energy and tensile strength of the unaged materials was used in these estimations.

Fracture toughness J–R curves for the material in the unaged or annealed condition, after service for ≈8 y at 284°C and at saturation, were determined from the estimated impact energies for the specific aging condition and are shown in Fig. 38. The J_{IC} values at room temperature and 290°C were also obtained from the estimated J–R curve and tensile flow stress; results are given in Table 4. The estimated fracture toughness shows good agreement with the measured value at room temperature and is somewhat lower at 290°C.

7 Conclusions

Charpy-impact, tensile, and fracture toughness properties of several cast SS materials from the Shippingport reactor have been characterized. Baseline mechanical properties for the unaged material were determined from tests on either recovery–annealed material, i.e., material that had been annealed for 1 h at 550°C and then water quenched, or on material from a cooler region of the component. The Shippingport materials exhibit modest degradation of mechanical properties because of the relatively low operating temperatures and/or low ferrite content of the materials.

Thermal aging during ≈15 y of reactor service had no effect on yield stress and the increase in ultimate stress is minimal for all materials. The RT Charpy–impact energy decreased from 188 to 145 J/cm^2 (111 to 86 ft·lb) for the check valve CA4, from 320 to 299 J/cm^2 (189 to 176 ft·lb) for the main valve MA1, and from 424 to 322 J/cm^2 (250 to 190 ft·lb) for the pump volute PV. However, the RT Charpy–impact energies of the materials are relatively high and the

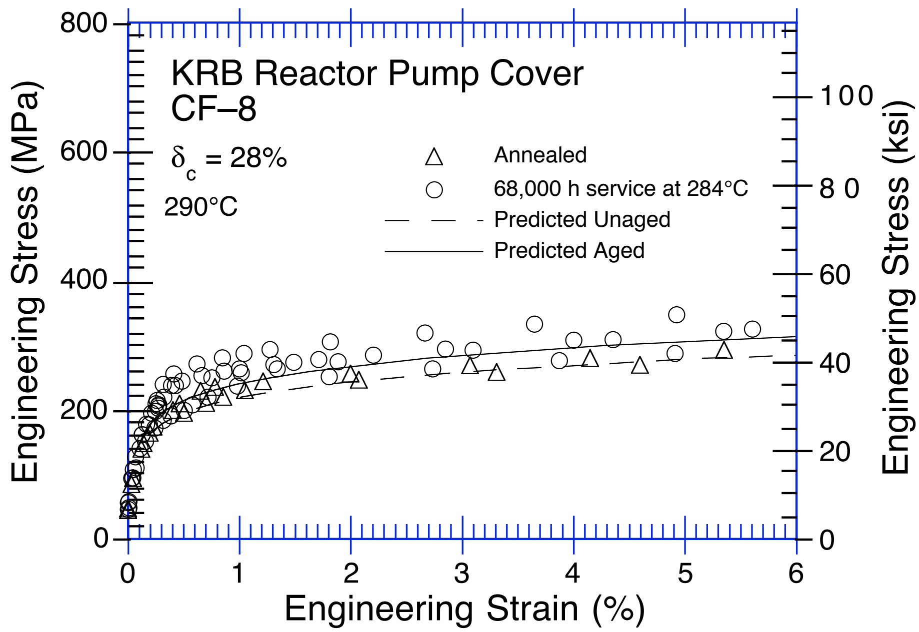

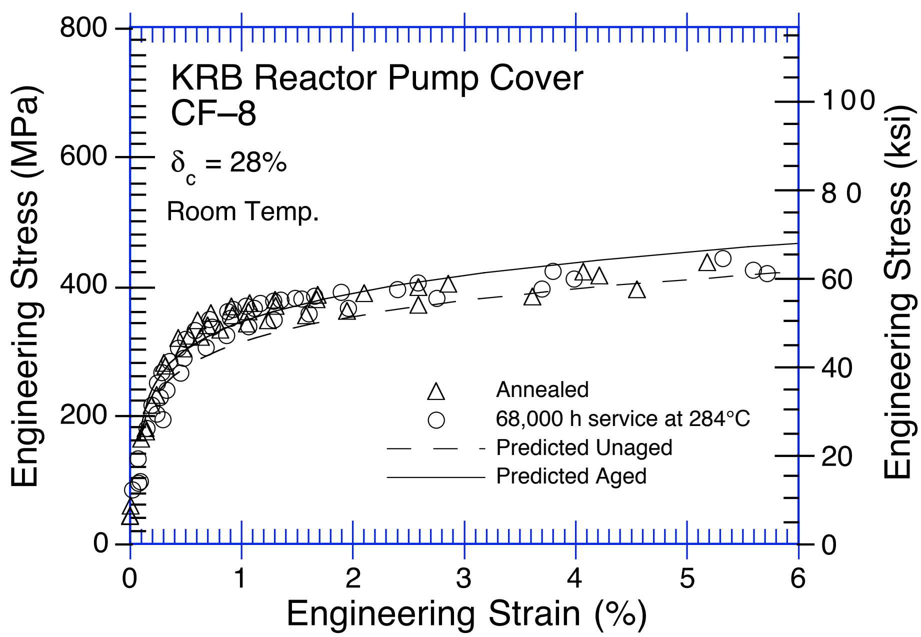

Figure 37. Estimated and measured tensile stress–vs.–strain curves at room temperature and 290°C for the KRB pump cover plate in the annealed condition and after 8 y of service at 284°C

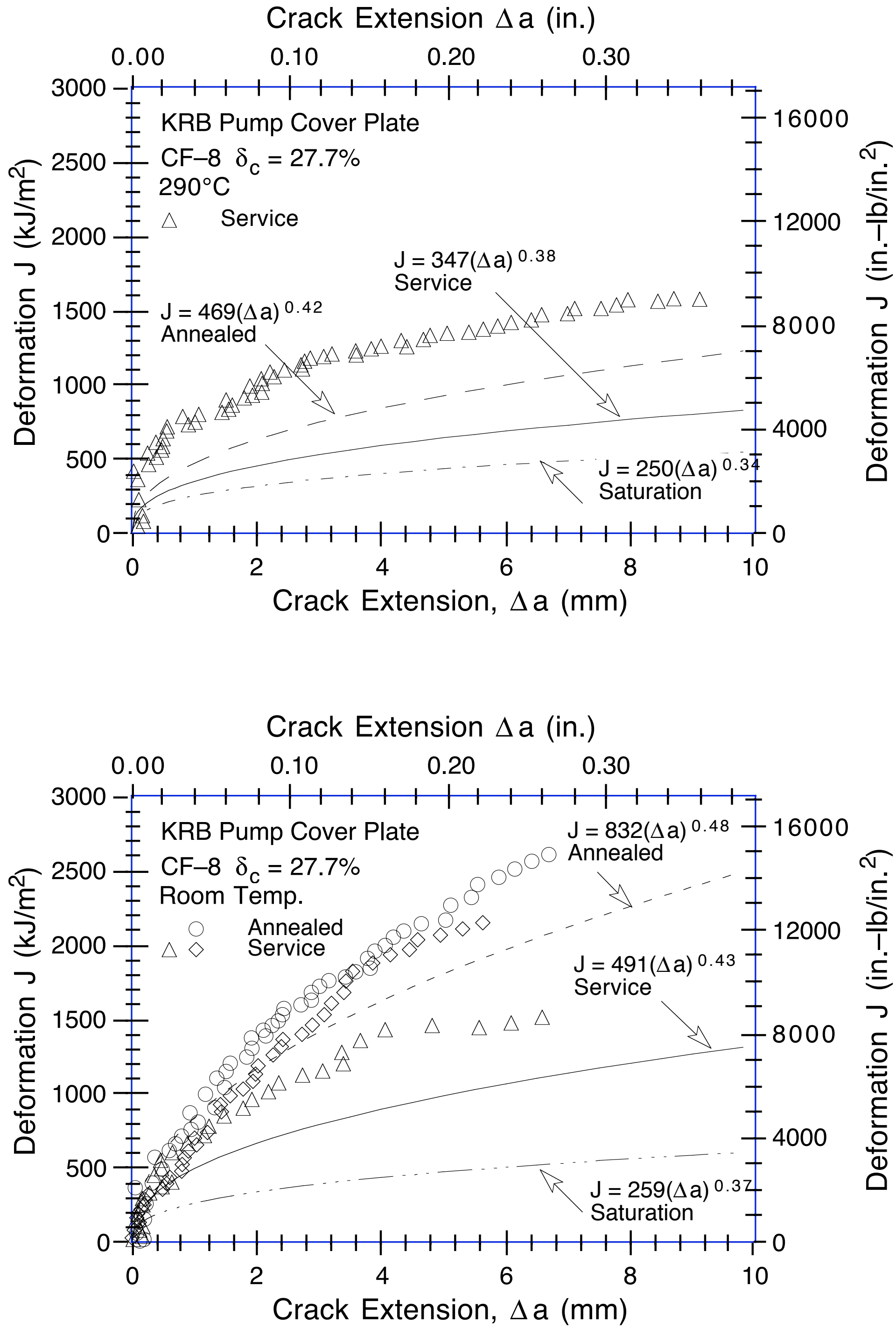

Figure 38. Estimated and measured fracture toughness J–R curve for the KRB pump cover plate in the annealed or unaged condition, after service, and at saturation. (Dashed, solid, and chain–dot lines are the estimated power–law J–R curves for annealed, service–aged, and fully embrittled or aged material, respectively.)

mid–shelf CTTs are very low. The check valve materials CA4 and CB7 are weaker than the material from the main valve MA1 and pump volute PV. Also, the mid–shelf CTT is ≈100°C higher for the check valves because of the presence of phase–boundary carbides that weaken the phase boundaries and thereby promote failure by phase–boundary separation. The results also indicate that the decrease in fracture toughness from reactor service is minimal.

Some materials were aged further in the laboratory to obtain the kinetics of embrittlement and determine the saturation or minimum fracture properties for the specific material. The results indicate that the Shippingport cast SSs are not very susceptible to thermal embrittlement at reactor operating temperatures. Even at saturation or fully embrittled condition, the RT impact energy of the materials is >60 J/cm^2 (>35 ft·lb) and the RT J_d value is >600 kJ/m^2 (>3400 in.–$lb/in.^2$) at 5–mm crack extension.

The results are compared with estimations based on accelerated laboratory aging studies. The procedure and correlations developed at ANL for estimating thermal aging degradation of cast SSs predicted accurate or slightly conservative values for Charpy–impact energy, tensile flow stress, fracture toughness J–R curve, and J_{IC} for the Shippingport materials. For example, the correlations predicted only modest decreases in Charpy–impact energy and fracture toughness of the materials after service. The somewhat conservative estimates are expected for some compositions of cast SSs because the criteria used in developing the estimation scheme ensure that the estimated mechanical properties are adequately conservative for cast SSs as defined by ASTM Specification A–351. The correlations do not consider the effects of metallurgical differences that may arise from differences in production heat treatment or casting processes and, therefore, are somewhat conservative for some steels. The correlations successfully predicted the mechanical properties of the Ringhals reactor hot– and crossover–leg elbows after ≈15 y of service and of the KRB reactor pump cover plate after ≈8 y of service.

References

1. O. K. Chopra and H. M. Chung, “Aging Degradation of Cast Stainless Steels: Effects on Mechanical Properties,” in *Environmental Degradation of Materials in Nuclear Power Systems–Water Reactors*, G. J. Theus and J. R. Weeks, eds., The Metallurgical Society, Warrendale, PA, pp. 737–748 (1988).

2. O. K. Chopra and H. M. Chung, “Effect of Low–Temperature Aging on the Mechanical Properties of Cast Stainless Steels,” in *Properties of Stainless Steels in Elevated–Temperature Service*, M. Prager, ed., MPC Vol. 26, PVP Vol. 132, ASME, New York, pp. 79–105 (1988).

3. O. K. Chopra, “Thermal Aging of Cast Stainless Steels: Mechanisms and Predictions,” in *Fatigue, Degradation, and Fracture – 1990*, W. H. Bamford, C. Becht, S. Bhandari, J. D. Gilman, L. A. James, and M. Prager, eds., MPC Vol. 30, PVP Vol. 195, ASME, New York, pp. 193-214 (1990).

4. O. K. Chopra and A. Sather, *Initial Assessment of the Mechanisms and Significance of Low–Temperature Embrittlement of Cast Stainless Steels in LWR Systems*, NUREG/CR–5385, ANL–89/17 (August 1990).

5. O. K. Chopra, “Thermal Aging of Cast Stainless Steels in LWR Systems: Estimation of Mechanical Properties,” in *Nuclear Plant Systems/Components Aging Management and Life Extension*, I. T. Kisisel, J. Sinnappan, R. W. Carlson, and W. H. Lake, eds., PVP Vol. 228, ASME, New York, pp. 79–92 (1992).

6. O. K. Chopra, Estimation of Fracture Toughness of Cast Stainless Steels during Thermal Aging in LWR Systems – Revision 1, NUREG/CR–4513 Rev. 1, ANL–93/22 (August 1994).

7. O. K. Chopra and W. J. Shack, Assessment of Thermal Embrittlement of Cast Stainless Steels, NUREG/CR–6177, ANL–94/2 (May 1994).

8. W. F. Michaud, P. T. Toben, W. K. Soppet, and O. K. Chopra, Tensile–Property Characterization of Thermally Aged Cast Stainless Steels, NUREG/CR–6142, ANL–93/35 (February 1994).

9. A. Trautwein and W. Gysel, "Influence of Long–Time Aging of CF–8 and CF–8M Cast Steel at Temperatures Between 300 and 500°C on the Impact Toughness and the Structure Properties," in Spectrum, Technische Mitteilungen aus dem+GF+Konzern, No. 5 (May 1981); also in Stainless Steel Castings, V. G. Behal and A. S. Melilli, eds., STP 756, ASTM, Philadelphia, PA, pp. 165–189 (1982).

10. E. I. Landerman and W. H. Bamford, “Fracture Toughness and Fatigue Characteristics of Centrifugally Cast Type 316 Stainless Steel Pipe after Simulated Thermal Service Conditions,” in Ductility and Toughness Considerations in Elevated–Temperature Service, MPC 8, ASME, New York, pp. 99–127 (1978).

11. S. Bonnet, J. Bourgoin, J. Champredonde, D. Guttmann, and M. Guttmann, “Relationship between Evolution of Mechanical Properties of Various Cast Duplex Stainless Steels and Metallurgical and Aging Parameters: An Outline of Current EDF Programmes,” *Mater. Sci. Technol.*, **6**, 221–229 (1990).

12. P. H. Pumphrey and K. N. Akhurst, “Aging Kinetics of CF3 Cast Stainless Steel in Temperature Range 300–400°C,” *Mater. Sci. Technol.*, **6**, 211–219 (1990).

13. G. Slama, P. Petrequin, and T. Mager, “Effect of Aging on Mechanical Properties of Austenitic Stainless Steel Castings and Welds,” presented at *SMIRT Post–Conference Seminar 6, Assuring Structural Integrity of Steel Reactor Pressure Boundary Components*, Aug. 29–30, 1983, Monterey, CA.

14. Y. Meyzaud, P. Ould, P. Balladon, M. Bethmont, and P. Soulat, “Tearing Resistance of Aged Cast Austenitic Stainless Steel,” presented at *Int. Conf. on Thermal Reactor Safety (NUCSAFE 88)*, Oct. 1988, Avignon, France.

15. P. McConnell and J. W. Sheckherd, *Fracture Toughness Characterization of Thermally Embrittled Cast Duplex Stainless Steel*, Report NP–5439, Electric Power Research Institute, Palo Alto, CA (September 1987).

16. G. E. Hale and S. J. Garwood, “The Effect of Aging on the Fracture Behaviour of Cast Stainless Steel and Weldments,” *Mater. Sci. Technol.*, **6**, 230–235 (1990).

17. C. Jansson, "Degradation of Cast Stainless Steel Elbows after 15 Years in Service," presented at *Fontevraud II Int. Symp.,* Sept. 10–14, 1990, Royal Abbey of Fontevraud, France.

18. H. M. Chung, "Thermal Aging of Decommissioned Reactor Cast Stainless Steel Components and Methodology for Life Prediction," in *Life Assessment and Life Extension of Power Plant Components*, T. V. Narayanan, C. B. Bond, J. Sinnappan, A. E. Meligi, M. Prager, T. R. Mager, J. D. Parker, and K. Means, eds., PVP Vol. 171, ASME, New York, pp. 111–125 (1989).

19. H. M. Chung and T. R. Leax, "Embrittlement of Laboratory and Reactor Aged CF3, CF8, and CF8M Duplex Stainless Steels," *Mater. Sci. and Technol.* **6**, 249–262 (1990).

20. W. H. Shack, O. K. Chopra, and H. M. Chung, "Aging Studies on Materials from the Shippingport Reactor," in *Compilation of Contract Research for the Materials Engineering Branch, Division of Engineering: Annual Report for FY 1988*, NUREG–0975, Vol. 7, p. 218 (May 1989).

21. O. K. Chopra, "Studies of Aged Cast Stainless Steel from the Shippingport Reactor," in *Proc. 18th Water Reactor Safety Information Meeting*, U.S. Nuclear Regulatory Commission, NUREG/CP–0114 Vol. 3, p. 369 (April 1991).

22. O. K. Chopra, "Evaluation of Aging Degradation of Structural Components," in *Proc. of the Aging Research Information Conference*, NUREG/CP–0122, Vol. 2, pp. 369–386 (1992).

23. W. L. Server, "Impact Three–Point Bend Testing for Notched and Precracked Specimens," *J. Testing and Eval.* **6**, 29 (1978).

24. L. S. Aubrey, P. F. Wieser, W. J. Pollard, and E. A. Schoefer, "Ferrite Measurement and Control in Cast Duplex Stainless Steel," in *Stainless Steel Castings*, V. G. Behal and A. S. Melilli, eds., ASTM STP 756, pp. 126–164 (1982).

Appendix A

Charpy–Impact Energy

Charpy–impact tests were conducted on Charpy–impact V–notch specimens (Fig. A–1) according to American Society for Testing and Materials (ASTM) Specification E 23. A Dynatup Model 8000A drop–weight impact machine with an instrumented tup and data readout system was used for the Charpy–impact tests. The available energy and impact velocity of the machine can be varied by altering the weight of the crosshead and the drop height; maximum energy and velocity obtainable with the machine were 1.3 kJ and 4 m/s, respectively. Load– and energy–time data were obtained from an instrumented tup and recorded on a dual–beam storage oscilloscope. The instrumented tup consists of a striking head and a strain gauge with a four–arm semiconductor bridge circuit. The strain gauge, which measures the compressive load on the tup during the test, was calibrated by a dynamic loading technique. Initial and final velocities of the tup were measured optically. The load–time traces from each test were digitized and stored on a floppy disk for analysis. Total energy was computed from the load–time trace; the value was corrected for the effects of tup velocity.

The instrumented tup and data readout instrumentation were periodically calibrated by fracturing standard V–notch specimens fabricated from 6061–T6 aluminum and 4340 steel with a hardness of Rockwell R_C 54. Amplifier gain was adjusted from the load– and energy–time traces for the aluminum specimen so that the recorded load limit coincided with the load limit for the material (i.e., 7.74 kN). The linearity of the calibration was established from the results for the 4340 steel specimen, which has a higher limit load. Accuracy of the impact–test

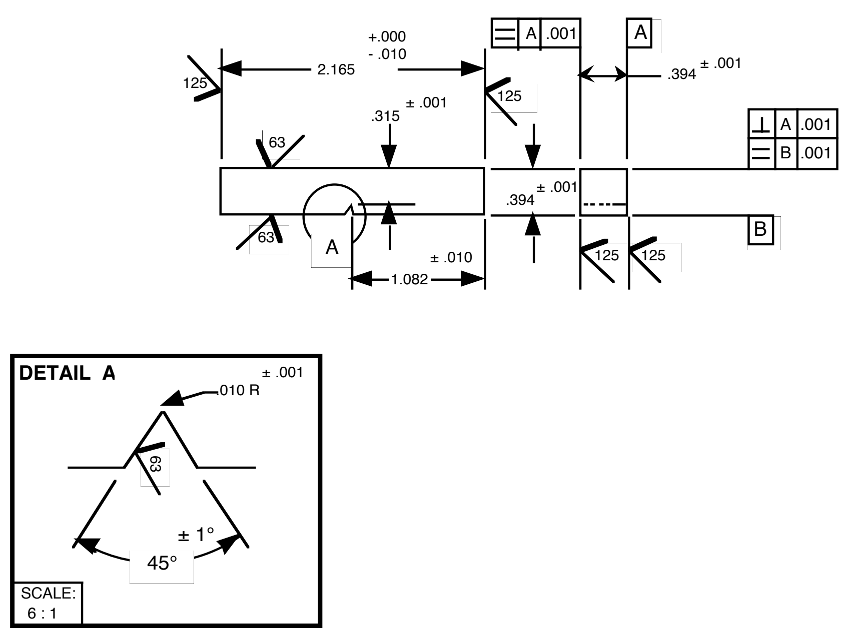

Figure A–1. Configuration of Charpy–impact test specimen: units of measure are inches machine was also checked periodically with Standard Reference Materials 2092 and 2096 (with Charpy–impact energies of 16.41 and 104.12 J, respectively) obtained from the National Institute of Standards and Technology. Tests on the reference materials were performed at –40°C (–40°F) in accordance with the testing procedures of Section 11 of ASTM E 23.

The specimens for high–temperature tests were heated by resistance heating. Pneumatic clamps were used to make electrical connections and hold the specimens in position on the anvils. The anvils were electrically insulated from the base plate. Power to the specimen was interrupted immediately before impact to release the clamps and remove any constraint on the specimen. The temperature was monitored and controlled by a thermocouple attached to the specimen. Specimens for the low–temperature tests were cooled in either a refrigerated bath or liquid nitrogen.

Charpy–impact test specimens were obtained from different locations across the thickness of the various components. Baseline mechanical properties for the unaged materials were obtained from either the material from a cooler region of the component or from recovery–annealed material, i.e., service–aged material that has been annealed for 1 h at 550°C (1022°F) and then water–quenched. Some materials were aged further in the laboratory, at 320, 350, and 400°C (608, 662, and 752°F), to validate the estimates of the saturation impact energy C_{Vsat} and activation energy for embrittlement of the materials. The results are listed in Tables A–1 and A–2.

The values of 0.2% yield and maximum load for each test are also listed in Tables A–1 and A–2, and may be used for estimating tensile properties of the cast materials. For a Charpy specimen, the yield stress is estimated from the expression

$$\sigma_y = C P_y B / W b^2 , \qquad \text{(A–1)}$$

taken from Ref. A–1, where Py is the yield load, W is the specimen width, B is the specimen thickness, b is the uncracked ligament, and C is a constant. The yield load was obtained from the load–time traces of the Charpy tests. Deviation from linearity in the load–time trace occurred at 125–150 μs for the various heats. The load at 200 μs was estimated to represent a 0.2% yield stress. The actual time for 0.2% yield varies with the strain hardening rate of the material; the load at 0.2% yield can be obtained from a power–law fit of the data. The error in the estimated values was <5% for the various tests. The ultimate stress was also obtained from the impact data by means of Eq. A–1 and the maximum load Pm. The constant C was determined by comparing the tensile and Charpy–impact data. The best value of the constant for yield stress was 1.50 for steels of all grades. The constant for ultimate stress was 2.28 for CF–3 and CF–8 steels and 2.54 for CF–8M steel. The estimated values of tensile stress are based on the assumption that strain rate effects are insignificant for the various heats and aging conditions. Equation A–1 should not be used for estimating ultimate stress at temperatures corresponding to the lower–shelf and transition regions.

References

A–1. W. L. Server, "Impact Three–Point Bend Testing for Notched and Precracked Specimens," *J. Test. Eval.*, **6**, 29 (1978).

Table A–1. Charpy–impact test results for cast stainless steel materials from the Shippingport reactor

Specimen ID	Material ID[a]	Temp. (°C)	Impact Energy (J/cm²)	(ft·lb)[b]	Yield Load (kN)	(kip)	Maximum Load (kN)	(kip)
Reactor Service[c]								
CA43–01	CA4	–197	31.1	18.3	13.192	2.966	15.213	3.420
CA41–01	CA4	–100	28.1	16.6	12.391	2.786	12.391	2.786
CA43–03	CA4	–78	33.8	19.9	10.995	2.472	12.420	2.792
CA42–02	CA4	–50	114.1	67.3	11.522	2.590	17.332	3.896
CA42–01	CA4	–20	126.8	74.8	10.946	2.461	16.854	3.789
CA44–01	CA4	0	84.3	49.7	10.145	2.281	14.051	3.159
CA41–02	CA4	25	162.1	95.6	9.354	2.103	15.535	3.492
CA44–02	CA4	25	128.5	75.8	9.589	2.156	14.881	3.345
CA43–04	CA4	50	138.2	81.5	8.427	1.894	13.211	2.970
CA43–02	CA4	75	202.8	119.7	7.948	1.787	13.582	3.053
CA41–03	CA4	125	281.4	166.0	7.118	1.600	13.123	2.950
CA44–03	CA4	200	183.3	108.1	6.142	1.381	11.473	2.579
CA42–03	CA4	290	179.0	105.6	5.546	1.247	9.891	2.224
CA43–05	CA4	290	178.9	105.6	5.390	1.212	10.419	2.342
CB72–01	CB7	–197	73.6	43.4	12.430	2.794	18.601	4.182
CB71–01	CB7	–100	83.8	49.4	11.717	2.634	16.531	3.716
CB72–02	CB7	–50	107.0	63.1	10.956	2.463	15.369	3.455
CB71–02	CB7	–20	142.4	84.0	10.262	2.307	16.922	3.804
CB73–01	CB7	0	211.2	124.6	8.983	2.019	15.428	3.468
CB71–03	CB7	25	162.4	95.8	9.022	2.028	14.012	3.150
CB73–02	CB7	25	203.7	120.2	8.700	1.956	14.666	3.297
CB73–03	CB7	50	269.4	158.9	7.733	1.738	13.592	3.056
CB73–03	CB7	75	295.9	174.6	7.489	1.684	13.592	3.056
CB73–04	CB7	100	304.6	179.7	6.454	1.451	11.317	2.544
CB71–04	CB7	125	241.5	142.5	6.874	1.545	12.313	2.768
CB72–05	CB7	200	339.3	200.2	5.458	1.227	11.464	2.577
CB71–05	CB7	290	292.1	172.3	5.097	1.146	10.712	2.408
CB72–04	CB7	290	256.1	151.1	5.488	1.234	10.302	2.316
CC43–02	CC4	–197	26.5	15.6	12.850	2.878	12.850	2.889
CC44–01	CC4	–120	39.1	23.1	14.022	3.152	14.022	3.152
CC44–03	CC4	0	104.2	61.5	10.458	2.351	14.041	3.157
CC43–03	CC4	25	121.7	71.8	9.686	2.177	14.198	3.192
CC44–02	CC4	125	216.3	127.6	7.079	1.591	12.186	2.740
CC43–01	CC4	290	306.3	180.7	5.605	1.260	11.239	2.527
MA11–05	MA1	–197	49.4	29.1	13.924	3.130	15.115	3.398
MA11–01	MA1	–100	190.6	112.5	13.026	2.928	21.902	4.924
MA11–02	MA1	–20	228.8	135.0	9.764	2.195	16.580	3.727
MA11–03	MA1	25	144.5	85.3	10.106	2.272	14.207	3.194
MA11–06	MA1	25	210.0	123.9	8.524	1.916	14.325	3.220
MA11–04	MA1	125	167.0	98.5	8.671	1.949	12.889	2.898
MA12–01	MA1	–197	96.9	57.2	12.001	2.698	19.148	4.305
MA12–05	MA1	–120	149.3	88.1	11.649	2.619	18.631	4.188
MA13–04	MA1	–100	318.6	188.0	11.561	2.599	22.185	4.987
MA12–02	MA1	–50	281.1	165.8	10.887	2.447	18.025	4.052
MA13–01	MA1	0	293.7	173.3	10.399	2.338	16.346	3.675
MA12–06	MA1	25	279.2	164.7	8.817	1.982	14.959	3.363
MA13–02	MA1	25	337.6	199.2	9.237	2.077	15.877	3.569
MA13–05	MA1	25	280.7	165.6	9.032	2.030	15.174	3.411
MA12–03	MA1	75	249.0	146.9	7.577	1.703	13.143	2.955
MA13–06	MA1	125	269.3	158.9	6.532	1.468	12.284	2.762
MA12–07	MA1	200	227.8	134.4	5.468	1.229	11.063	2.487

Table A–1. (Contd.)

Specimen ID	Material ID[a]	Temp. (°C)	Impact Energy (J/cm^2)	Impact Energy (ft·lb)[b]	Yield Load (kN)	Yield Load (kip)	Maximum Load (kN)	Maximum Load (kip)
MA13–07	MA1	200	231.7	136.7	6.786	1.526	11.551	2.597
MA12–04	MA1	290	197.6	116.6	6.318	1.420	10.594	2.382
MA13–08	MA1	290	175.2	103.4	5.156	1.159	9.940	2.235
MA91–01	MA9	–197	66.8	39.4	14.412	3.240	17.361	3.903
MA93–01	MA9	–197	106.2	62.7	12.625	2.838	19.617	4.410
MA92–01	MA9	–120	252.4	148.9	12.938	2.909	20.720	4.658
MA94–01	MA9	–120	116.2	68.6	11.766	2.645	16.746	3.765
MA91–02	MA9	–100	212.3	125.3	12.069	2.713	19.724	4.434
MA93–02	MA9	–100	210.7	124.3	11.317	2.544	19.168	4.309
MA92–02	MA9	–78	295.5	174.3	11.249	2.529	19.226	4.322
MA94–02	MA9	–78	181.2	106.9	10.184	2.289	18.562	4.173
MA91–03	MA9	–50	299.7	176.8	9.940	2.235	17.322	3.894
MA93–03	MA9	–50	314.7	185.7	10.878	2.445	18.006	4.048
MA92–03	MA9	–20	439.1	259.1	9.208	2.070	16.658	3.745
MA94–03	MA9	–20	411.6	242.8	9.872	2.219	16.805	3.778
MA92–04	MA9	0	332.7	196.3	8.661	1.947	14.910	3.352
MA94–04	MA9	10	370.2	218.4	8.915	2.004	14.852	3.339
MA91–04	MA9	25	350.2	206.6	8.515	1.914	15.233	3.425
MA93–04	MA9	25	408.6	241.1	8.993	2.022	15.223	3.422
MA92–05	MA9	75	316.7	186.9	7.401	1.664	13.465	3.027
MA94–05	MA9	75	312.1	184.1	7.226	1.624	13.270	2.983
MA91–05	MA9	125	338.5	199.7	7.011	1.576	13.192	2.966
MA92–06	MA9	125	259.8	153.3	6.718	1.510	11.971	2.691
MA93–05	MA9	125	314.2	185.4	6.601	1.484	11.522	2.590
MA94–06	MA9	200	251.3	148.3	5.497	1.236	11.444	2.573
MA91–06	MA9	290	246.4	145.4	5.927	1.332	9.852	2.215
MA93–06	MA9	290	235.3	138.8	5.380	1.209	9.901	2.226
PV1–01	PV	–197	96.5	56.9	11.766	2.645	18.748	4.215
PV2–01	PV	–197	136.0	80.2	10.790	2.426	20.730	4.660
PV3–01	PV	–120	192.5	113.6	11.454	2.575	20.544	4.618
PV1–02	PV	–100	256.4	151.3	11.522	2.590	19.841	4.460
PV2–02	PV	–100	295.8	174.5	11.210	2.520	21.023	4.726
PV3–02	PV	–50	277.4	163.7	10.311	2.318	19.099	4.294
PV1–03	PV	–20	338.2	199.5	10.917	2.454	18.025	4.052
PV2–03	PV	–20	374.2	220.8	9.970	2.241	17.781	3.997
PV1–04	PV	25	311.0	183.5	8.856	1.991	15.115	3.398
PV2–04	PV	25	316.9	187.0	8.817	1.982	15.106	3.396
PV3–03	PV	25	337.3	199.0	8.212	1.846	14.666	3.297
PV3–04	PV	75	411.4	242.7	7.851	1.765	14.159	3.183
PV1–05	PV	175	357.6	211.0	5.859	1.317	12.362	2.779
PV2–05	PV	175	342.1	201.8	6.240	1.403	11.229	2.524
PV3–05	PV	200	317.1	187.1	5.654	1.271	11.112	2.498
PV1–06	PV	290	193.5	114.2	5.468	1.229	10.360	2.329
PV2–06	PV	290	282.8	166.9	5.341	1.201	9.345	2.101
PV3–06	PV	290	275.6	162.6	5.322	1.196	9.550	2.147
PV6–01	PV	–197	74.6	44.0	11.317	2.544	16.277	3.659
PV6–02	PV	–100	192.5	113.6	11.454	2.575	20.544	4.618
PV6–03	PV	–20	255.2	150.6	10.936	2.459	16.541	3.719
PV6–04	PV	25	262.4	154.8	9.335	2.099	15.496	3.484
PV6–05	PV	175	235.6	139.0	7.021	1.578	12.284	2.762
PV6–06	PV	290	278.6	164.4	6.327	1.422	10.507	2.362

Table A–1. (Contd.)

Specimen ID	Material ID[a]	Temp. (°C)	Impact Energy (J/cm²)	Impact Energy (ft·lb)[b]	Yield Load (kN)	Yield Load (kip)	Maximum Load (kN)	Maximum Load (kip)
Annealed[d]								
CA42–10	CA4	–197	38.4	22.7	12.235	2.751	14.637	3.291
CA41–12	CA4	–120	72.7	42.9	12.293	2.764	17.478	3.929
CA44–08	CA4	–100	61.2	36.1	12.010	2.700	15.115	3.398
CA42–11	CA4	–50	93.1	54.9	10.770	2.421	16.443	3.697
CA43–11	CA4	–20	144.2	85.1	10.760	2.419	16.385	3.683
CA41–10	CA4	25	196.1	115.7	8.593	1.932	14.373	3.231
CA42–12	CA4	25	179.8	106.1	9.149	2.057	14.705	3.306
CA44–09	CA4	75	191.7	113.1	8.095	1.820	13.397	3.012
CA43–10	CA4	175	216.9	128.0	6.484	1.458	11.551	2.597
CA41–11	CA4	290	225.3	132.9	5.331	1.198	10.321	2.320
MA11–12	MA1	–196	66.9	39.5	12.167	2.735	14.598	3.282
MA11–11	MA1	–120	119.6	70.6	10.966	2.465	14.793	3.326
MA11–10	MA1	–80	186.7	110.2	10.760	2.419	17.752	3.991
MA11–09	MA1	–20	303.2	178.9	9.804	2.204	15.194	3.416
MA11–08	MA1	25	62.2	36.7	10.194	2.292	11.522	2.590
MA12–12	MA1	–196	156.3	92.2	12.235	2.751	21.540	4.842
MA12–11	MA1	–100	218.3	128.8	11.786	2.650	19.431	4.368
MA12–10	MA1	–50	294.7	173.9	10.243	2.303	16.736	3.762
MA13–12	MA1	0	336.1	198.3	9.003	2.024	15.526	3.490
MA12–09	MA1	25	267.1	157.6	8.476	1.905	13.768	3.095
MA13–11	MA1	75	334.9	197.6	8.026	1.804	13.133	2.952
MA12–09	MA1	100	369.3	217.9	6.923	1.556	12.645	2.843
MA13–10	MA1	200	261.6	154.3	6.376	1.433	11.922	2.680
MA13–09	MA1	290	254.0	149.9	4.492	1.010	9.638	2.167
MA91–15	MA9	–197	233.0	137.5	12.645	2.843	24.753	5.565
MA92–15	MA9	–120	290.7	171.5	10.741	2.415	19.695	4.428
MA94–16	MA9	–50	348.9	205.9	10.643	2.393	16.922	3.804
MA95–02	MA9	–20	344.1	203.0	10.956	2.463	16.824	3.782
MA95–01	MA9	25	388.1	229.0	9.286	2.088	14.276	3.209
MA94–17	MA9	175	332.9	196.4	5.976	1.343	12.030	2.704
MA95–12	MA9	290	278.5	164.3	5.781	1.300	9.774	2.197
PV1–09	PV	–197	228.2	134.6	11.356	2.553	22.742	5.113
PV2–09	PV	–197	233.4	137.7	10.995	2.472	22.107	4.970
PV1–10	PV	–120	368.6	217.5	11.298	2.540	21.511	4.836
PV3–09	PV	–120	270.7	159.7	10.887	2.447	18.797	4.226
PV1–11	PV	–100	270.8	159.8	12.508	2.812	22.185	4.987
PV2–10	PV	–100	160.3	94.6	11.063	2.487	16.902	3.800
PV2–11	PV	–80	301.2	177.7	10.555	2.373	19.168	4.309
PV3–10	PV	–80	269.3	158.9	10.262	2.307	18.416	4.140
PV3–11	PV	–50	415.5	245.1	10.331	2.323	19.236	4.324
PV3–12	PV	–20	322.4	190.2	9.999	2.248	15.526	3.490
PV2–12	PV	0	436.7	257.7	8.769	1.971	15.106	3.396
PV1–12	PV	25	404.6	238.7	9.032	2.030	13.885	3.121
PV2–13	PV	25	442.9	261.3	8.827	1.984	15.018	3.376
PV3–13	PV	75	375.9	221.8	7.597	1.708	13.368	3.005
PV1–13	PV	125	353.7	208.7	6.669	1.499	12.128	2.726
PV3–14	PV	290	309.1	182.4	5.576	1.254	11.444	2.573

Table A–1. (Contd.)

Specimen ID	Material ID[a]	Temp. (°C)	Impact Energy (J/cm^2)	Impact Energy (ft·lb)[b]	Yield Load (kN)	Yield Load (kip)	Maximum Load (kN)	Maximum Load (kip)
Unaged Spare Volute[e]								
VR1–02	VR	–197	63.3	37.3	12.500	2.805	16.766	3.769
VR2–02	VR	–120	133.3	78.6	13.534	3.043	21.091	4.741
VR2–04	VR	–80	205.5	121.2	11.659	2.621	19.558	4.397
VR3–02	VR	–50	240.8	142.1	13.172	2.961	20.349	4.575
VR1–03	VR	0	232.3	137.1	11.620	2.612	17.078	3.839
VR1–01	VR	25	200.0	118.0	12.479	2.805	16.766	3.769
VR3–01	VR	25	274.2	161.8	10.839	2.437	16.395	3.686
VR2–03	VR	75	194.2	114.6	9.374	2.107	13.006	2.924
VR2–01	VR	125	197.5	116.5	8.222	1.848	12.831	2.885
VR3–03	VR	125	341.3	201.4	7.851	1.765	13.504	3.036
VR3–04	VR	200	189.9	112.0	6.503	1.462	10.780	2.423
VR1–04	VR	290	263.5	155.5	6.200	1.394	10.341	2.325
Aged 10,000 h at 400°C								
MA91-10	MA9	-197	23.4	13.8	10.321	2.320	10.321	2.320
MA94-09	MA9	-120	36.0	21.2	11.737	2.639	12.372	2.781
MA91-11	MA9	-50	93.6	55.2	11.190	2.516	15.213	3.420
MA94-10	MA9	0	113.0	66.7	9.794	2.202	14.129	3.176
MA92-10	MA9	25	127.6	75.3	8.915	2.004	13.055	2.935
MA94-11	MA9	125	183.0	108.0	7.021	1.578	12.420	2.792
MA95-06	MA9	290	186.7	110.2	5.312	1.194	10.341	2.325
VR1-09	VR	-197	21.3	12.6	13.592	3.056	13.592	3.056
VR2-09	VR	-120	34.9	20.6	12.772	2.871	14.637	3.291
VR1-10	VR	-50	31.4	18.5	11.327	2.546	11.883	2.671
VR2-10	VR	0	73.7	43.5	11.044	2.483	14.582	3.278
VR1-11	VR	25	81.0	47.8	10.253	2.305	14.237	3.201
VR3-09	VR	25	64.0	37.8	10.653	2.395	13.084	2.941
VR2-11	VR	75	90.2	53.2	9.403	2.114	13.299	2.990
VR3-10	VR	175	126.6	74.7	7.382	1.660	12.674	2.849
VR3-11	VR	290	105.7	62.4	5.995	1.348	10.536	2.369

[a] The first letter represents the type of component, C = cold–leg check valve, M = hot–leg main shutoff valve, P = pump volute, and V = spare pump volute.
[b] Impact energy in ft·lb for a standard Charpy impact specimen. To convert J/cm^2 to ft·lb multiply by 0.8 and divide by 1.355818.
[c] The components were at the operating temperature of 281°C for hot leg and 264°C for cold leg for ≈13 y (113,900 h).
[d] Annealed at 550°C for 1 h and water quenched.
[e] In service only during the initial core loading and thus is essentially unaged.

Table A–2. Room–temperature Charpy–impact data for Shippingport cast stainless steels aged further in the laboratory

Specimen ID[a]	Material ID[b]	Aging Condition		Impact Energy		Yield Load		Maximum Load	
		Temp. (°C)	Time (h)	(J/cm^2)	(ft·lb)[c]	(kN)	(kip)	(kN)	(kip)
CA41–10	CA4	Annealed	–	196.1	115.7	8.593	1.932	14.373	3.231
CA42–12	CA4	Annealed	–	179.8	106.1	9.149	2.057	14.705	3.306
CA41–02	CA4	Reactor Aged	–	162.1	95.6	9.354	2.103	15.535	3.492
CA44–02	CA4	Reactor Aged	–	128.5	75.8	9.589	2.156	14.881	3.345
CA41–04	CA4	350	986	114.8	67.7	9.891	2.224	15.067	3.387
CA44–06	CA4	350	986	166.4	98.2	10.253	2.305	15.379	3.457
CA41–07	CA4	350	3000	96.2	56.8	9.618	2.162	14.285	3.211
CA42–07	CA4	350	3000	120.8	71.3	9.227	2.074	14.188	3.190
CA41–08	CA4	350	10000	83.1	49.0	9.755	2.193	14.159	3.183
CA42–08	CA4	350	10000	115.7	68.3	9.569	2.151	15.897	3.574
CA43–09	CA4	350	10000	90.3	53.3	9.188	2.065	13.309	2.992
CA41–09	CA4	400	312	114.1	67.3	9.227	2.074	14.647	3.293
CA44–07	CA4	400	312	102.3	60.4	8.876	1.995	13.905	3.126
CA41–06	CA4	400	986	84.0	49.6	9.852	2.215	13.280	2.985
CA42–06	CA4	400	986	128.1	75.6	9.833	2.211	15.223	3.422
CA41–05	CA4	400	3000	61.9	36.5	10.302	2.316	12.840	2.887
CA42–05	CA4	400	3000	103.2	60.9	9.755	2.193	14.481	3.255
CA42–04	CA4	400	10000	82.8	48.9	9.589	2.156	13.905	3.126
CA43–06	CA4	400	10000	80.2	47.3	9.804	2.204	13.485	3.031
CA44–04	CA4	400	10000	65.3	38.5	9.774	2.197	12.616	2.836
CB71–03	CB7	Reactor Aged	–	162.4	95.8	9.022	2.028	14.012	3.150
CB73–02	CB7	Reactor Aged	–	203.7	120.2	8.700	1.956	14.666	3.297
CB71–07	CB7	400	312	163.8	96.6	9.657	2.171	14.940	3.359
CB73–09	CB7	400	312	263.9	155.7	8.798	1.978	14.988	3.369
CB71–08	CB7	400	986	158.4	93.5	9.120	2.050	13.875	3.119
CB72–08	CB7	400	986	186.4	110.0	9.159	2.059	14.159	3.183
CB71–09	CA4	400	3000	189.1	111.6	9.628	2.164	13.963	3.139
CB72–09	CA4	400	3000	191.4	112.9	9.520	2.140	13.534	3.043
MA11–08	MA1	Annealed	–	62.2	36.7	10.194	2.292	11.522	2.590
MA11–06	MA1	Reactor Aged	–	210.0	123.9	8.524	1.916	14.325	3.220
MA11–04	MA1	Reactor Aged	–	144.5	85.3	10.106	2.272	14.207	3.194
MA11–18	MA1	350	1052	68.1	40.2	9.364	2.105	11.610	2.610
MA11–17	MA1	350	2987	159.2	93.9	9.403	2.114	14.256	3.205
MA11–16	MA1	350	10000	160.4	94.6	9.716	2.184	14.539	3.268
MA11–19	MA1	400	379	56.3	33.2	9.589	2.156	11.092	2.494
MA11–15	MA1	400	1052	47.9	28.3	8.632	1.941	9.833	2.211
MA11–14	MA1	400	2987	96.3	56.8	10.428	2.344	13.885	3.121
MA11–20	MA1	400	2987	58.1	34.3	9.930	2.232	10.321	2.320
MA11–13	MA1	400	10000	123.7	73.0	9.198	2.068	13.758	3.093
MA11–25	MA1	400	10000	138.2	81.5	9.159	2.059	14.022	3.152
MA11–28	MA1	400	10000	159.8	94.3	11.034	2.481	15.930	3.581
MA12–09	MA1	Annealed	–	267.1	157.6	8.476	1.905	13.768	3.095
MA12–06	MA1	Reactor Aged	–	279.2	164.7	8.817	1.982	14.959	3.363
MA13–02	MA1	Reactor Aged	–	337.6	199.2	9.237	2.077	15.877	3.569
MA13–05	MA1	Reactor Aged	–	280.7	165.6	9.032	2.030	15.174	3.411
MA12–18	MA1	350	1052	280.2	165.3	8.524	1.916	14.598	3.282
MA13–18	MA1	350	1052	253.3	149.4	8.612	1.936	14.715	3.308
MA12–17	MA1	350	2987	304.8	179.8	8.739	1.965	14.783	3.323
MA13–17	MA1	350	2987	234.7	138.5	9.794	2.202	15.203	3.418

Table A–2. (Contd.).

Specimen ID[a]	Material ID[b]	Aging Condition Temp. (°C)	Time (h)	Impact Energy (J/cm^2)	(ft·lb)[c]	Yield Load (kN)	(kip)	Maximum Load (kN)	(kip)
MA12–16	MA1	350	10000	219.0	129.2	8.651	1.945	14.139	3.179
MA13–16	MA1	350	10000						
MA12–19	MA1	400	379	263.4	155.4	8.437	1.897	14.852	3.339
MA12–15	MA1	400	1052	236.8	139.7	8.007	1.800	14.012	3.150
MA13–15	MA1	400	1052	236.4	139.5	8.417	1.892	14.998	3.372
MA12–14	MA1	400	2987	193.3	114.0	9.481	2.131	14.334	3.222
MA12–20	MA1	400	2987	230.3	135.9	10.253	2.305	15.545	3.495
MA13–14	MA1	400	2987	216.0	127.4	9.911	2.228	15.682	3.525
MA12–13	MA1	400	10000	194.6	114.8	8.769	1.971	14.676	3.299
MA13–13	MA1	400	10000	117.1	69.1	10.145	2.281	13.700	3.080
MA12–25	MA1	400	10000	164.2	96.9	9.120	2.050	14.246	3.203
MA12–26	MA1	400	10000	189.4	111.7	8.642	1.943	13.983	3.144
MA12–27	MA1	400	10000	239.2	141.1	8.856	1.991	15.067	3.387
MA12–28	MA1	400	10000	211.0	124.5	8.612	1.936	14.862	3.341
MA13–22	MA1	400	10000	142.5	84.1	9.276	2.085	14.520	3.264
MA13–23	MA1	400	10000	183.5	108.3	8.905	2.002	15.067	3.387
MA13–24	MA1	400	10000	205.8	121.4	8.974	2.017	15.281	3.435
MA95–01	MA9	Annealed	–	388.1	229.0	9.286	2.088	14.276	3.209
MA91–04	MA9	Reactor Aged	–	350.2	206.6	8.515	1.914	15.233	3.425
MA93–04	MA9	Reactor Aged	–	408.6	241.1	8.993	2.022	15.223	3.422
MA91–14	MA9	320	2989	287.4	169.6	9.911	2.228	15.340	3.449
MA92–14	MA9	320	2989	262.5	154.9	8.817	1.982	14.325	3.220
MA91–07	MA9	320	10000	279.4	164.8	9.169	2.061	14.705	3.306
MA92–07	MA9	320	10000	294.4	173.7	8.651	1.945	14.744	3.315
MA94–07	MA9	320	29170	312.2	184.2	9.433	2.121	15.936	3.583
MA95–03	MA9	320	29170	299.5	176.7	9.950	2.237	16.404	3.688
MA93–18	MA9	350	311	334.1	197.1	8.788	1.976	14.403	3.238
MA94–18	MA9	350	311	307.9	181.7	8.749	1.967	14.666	3.297
MA95–14	MA9	350	311	416.7	245.9	8.993	2.022	15.028	3.378
MA91–18	MA9	350	986	286.9	169.3	9.882	2.222	14.608	3.284
MA92–18	MA9	350	986	319.0	188.2	8.954	2.013	13.953	3.137
MA91–13	MA9	350	2987	242.3	143.0	9.442	2.123	14.491	3.258
MA92–12	MA9	350	2987	258.3	152.4	9.003	2.024	14.139	3.179
MA92–13	MA9	350	2987	324.7	191.6	9.061	2.037	14.998	3.372
MA91–09	MA9	350	10000	151.7	89.5	9.999	2.248	15.399	3.462
MA94–08	MA9	350	10000	198.2	116.9	8.964	2.015	14.569	3.275
MA91–17	MA9	400	115	303.8	179.2	9.188	2.066	14.471	3.253
MA92–17	MA9	400	115	390.2	230.2	8.192	1.842	14.442	3.247
MA93–15	MA9	400	312	243.1	143.4	8.358	1.879	14.647	3.293
MA95–11	MA9	400	312	222.8	131.5	9.188	2.066	14.471	3.253
MA91–16	MA9	400	986	186.5	110.0	9.520	2.140	15.018	3.376
MA92–16	MA9	400	986	199.7	117.8	9.354	2.103	14.315	3.218
MA93–14	MA9	400	2987	205.4	121.2	9.423	2.118	14.832	3.334
MA94–14	MA9	400	2987	158.4	93.5	9.462	2.127	14.393	3.236
MA95–10	MA9	400	2987	159.8	94.3	10.458	2.351	14.080	3.165
MA92–10	MA9	400	10000	127.6	75.3	8.915	2.004	13.055	2.935
VR1–01	VR	Unaged	–	200.0	118.0	12.479	2.805	16.766	3.769
VR3–01	VR	Unaged	–	274.2	161.8	10.839	2.437	16.395	3.686
VR1–13	VR	320	2989	223.9	132.1	11.434	2.570	15.916	3.578
VR2–13	VR	320	2989	271.9	160.4	10.477	2.355	16.746	3.765

Table A–2. (Contd.).

Specimen ID[a]	Material ID[b]	Aging Condition Temp. (°C)	Aging Condition Time (h)	Impact Energy (J/cm^2)	Impact Energy (ft·lb)[c]	Yield Load (kN)	Yield Load (kip)	Maximum Load (kN)	Maximum Load (kip)
VR1–07	VR	320	10000	187.9	110.9	10.370	2.331	15.672	3.523
VR2–07	VR	320	10000	179.0	105.6	10.272	2.309	15.594	3.506
VR1–05	VR	320	29170	152.5	90.0	10.702	2.406	16.854	3.789
VR2–05	VR	320	29170	108.2	63.8	10.809	2.430	15.799	3.552
VR1–19	VR	350	311	193.5	114.2	10.438	2.347	15.242	3.427
VR2–19	VR	350	311	204.7	120.8	9.081	2.041	15.125	3.400
VR3–19	VR	350	311	242.5	143.1	9.061	2.037	15.194	3.416
VR1–20	VR	350	986	191.7	113.1	11.630	2.615	17.010	3.824
VR2–20	VR	350	986	184.7	109.0	10.887	2.447	16.629	3.738
VR1–14	VR	350	2987	118.9	70.2	11.063	2.487	14.813	3.330
VR2–14	VR	350	2987	124.9	73.7	10.516	2.364	14.481	3.255
VR3–14	VR	350	2987	114.6	67.6	10.214	2.296	14.783	3.323
VR1–08	VR	350	10000	68.1	40.2	10.380	2.334	12.821	2.882
VR2–08	VR	350	10000	77.1	45.5	10.175	2.287	13.329	2.996
VR1–16	VR	400	115	172.5	101.8	9.930	2.232	15.242	3.427
VR4–01	VR	400	115	182.0	107.4	10.233	2.300	16.209	3.644
VR1–17	VR	400	312	106.2	62.7	10.653	2.395	14.754	3.317
VR4–02	VR	400	312	85.3	50.3	10.858	2.441	14.276	3.209
VR1–18	VR	400	986	82.5	48.7	11.727	2.636	14.344	3.225
VR2–18	VR	400	986	104.9	61.9	10.966	2.465	15.145	3.405
VR4–05	VR	400	986	81.2	47.9	11.483	2.581	16.229	3.648
VR1–15	VR	400	2987	100.0	59.0	10.731	2.412	15.252	3.429
VR2–15	VR	400	2987	94.3	55.6	10.946	2.461	15.242	3.427
VR3–15	VR	400	2987	97.0	57.2	10.848	2.439	15.643	3.517
VR1–11	VR	400	10000	81.0	47.8	10.253	2.305	14.237	3.201
VR3–09	VR	400	10000	64.0	37.8	10.653	2.395	13.084	2.941

[a] The first letter represents the type of component, C = cold–leg check valve, M = hot–leg main shutoff valve, P = pump volute, and V = spare pump volute.

[b] Materials MA1 and MA9 are from the same valve except the latter is from a cooler region of the valve. Spare pump volute was in service only during the initial core loading and, thus, is essentially unaged.

[c] Impact energy in ft·lb for a standard Charpy–impact specimen. To convert J/cm^2 to ft·lb multiply by 0.8 and divide by 1.355818.

Appendix B

Tensile Properties

Tensile tests were performed at room temperature and at 290°C (554°F) according to ASTM Specification E 8 and E 21 in an Instron tensile test machine with a maximum loading capacity of 90 kN (20 kips). Cylindrical specimens with a diameter of 5.08 mm (0.2 in.) and a gage length of 20.3 mm (0.8 in.), shown in Fig. B–1, were used for all of the tests. An axial extensometer, with an initial gage length of 20.3 mm (0.8 in.), was used for continuous measurement of strain during RT tests.

Tests at elevated temperatures were conducted in a forced–air recirculating furnace, with a clip gage mounted on the specimen grips. Total strain in the specimen gage length was determined from correlations developed from RT tests conducted with both clip gages attached to the specimen grips and the extensometer mounted on the specimen gage length. Thermocouples were mounted above and below the specimen gage length to monitor and control the temperature within ±2°C. An IBM computer was used to digitize load, crosshead movement, and axial displacement data, and store it on floppy disks. Analog traces of engineering stress–vs.–engineering stain were also obtained for each test. The true fracture stress was obtained from the fracture load and cross–sectional area at fracture. Tensile test data for the various materials are given in Table B–1.

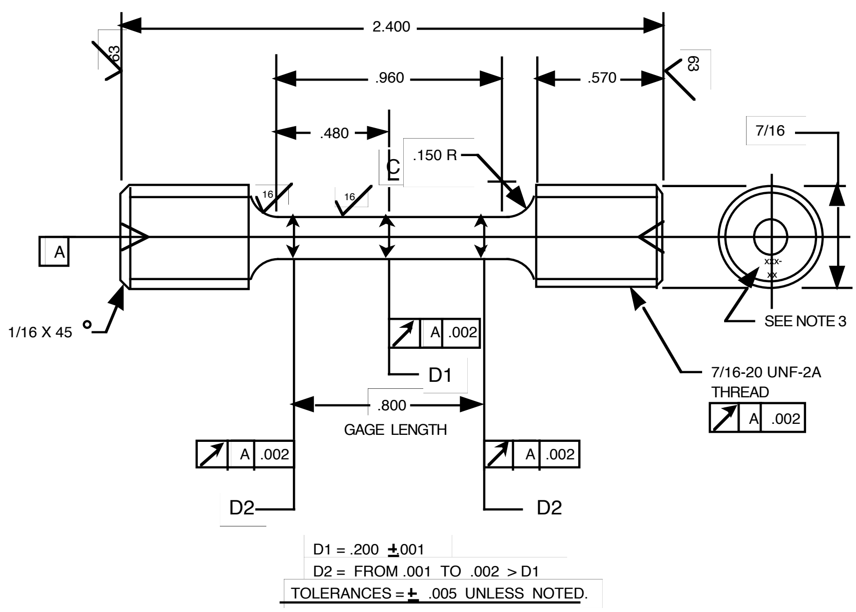

1. THE .800 INCH GAGE LENGTH TO HAVE UNIFORM SLOPE FROM MAX. DIA. D2 TO MIN. DIA. D1. UNIFORM SLOPE MUST NOT EXCEED .004 CHANGE IN DIA. PER 1 INCH CHANGE IN LENGTH.
2. ALL RADII MUST BLEND WITHOUT UNDERCUTS OR STEPS.
3. DIMENSIONS AND SPECIFICATIONS TYPICAL BOTH ENDS.
4. ALL SURFACES TO BE FREE OF BURRS.

Figure B–1. Configuration of tensile test specimen: units of measure are inches

Table B–1. Tensile test results for cast stainless stees from the Shippingport reactor

Specimen ID[a]	Test Temp. (°C)	Engineering Stress 0.2% Yield (MPa)	(ksi)	Ultimate (MPa)	(ksi)	True Fracture Stress (MPa)	(ksi)	Elonga–tion (%)	Red. in Area (%)
Cold Leg Check Valves[b]									
CA41–T01	25	237.1	34.39	528.3	76.62	1268.7	184.01	63.5	66.0
CA41–T02	25	226.8	32.89	519.3	75.32	1404.0	203.63	57.9	73.7
CA42–T01	25	218.7	31.72	532.6	77.25	1466.0	212.63	60.3	68.6
CA41–T03	290	123.2	17.87	378.6	54.91	704.9	102.24	44.1	57.8
CA42–T02	290	132.2	19.17	370.2	53.69	–	–	32.7	35.5
CA42–T03	290	169.9	24.64	396.3	57.48	731.3	106.07	35.9	54.0
PV1-T01	25	230.1	33.37	523.6	75.94	1407.4	204.13	67.8	75.1
PV2-T01	25	226.4	32.84	510.1	73.98	1502.5	217.92	56.6	84.9
PV3-T01	25	233.8	33.91	497.7	72.19	1494.1	216.70	50.0	85.0
PV1–T02	290	143.3	20.78	345.6	50.13	678.4	98.39	29.1	62.1
PV2–T02	290	177.5	25.74	408.8	59.29	515.6	74.78	39.8	37.9
PV3–T02	290	151.4	21.96	368.6	53.46	961.5	139.45	46.6	69.2
Hot Leg Main Shutoff Valves[c]									
MA11–T01	25	226.8	32.89	490.9	71.20	1659.4	240.68	40.2	82.0
MA11–T02	25	252.3	36.59	429.6	62.31	–	–	22.8	30.9
MA12–T01	25	212.6	30.84	486.0	70.49	1374.7	199.38	27.4	73.6
MA11–T03	290	–	–	275.9	40.02	–	–	10.2	13.3
MA12–T02	290	129.6	18.80	330.9	47.99	520.0	75.42	32.6	47.6
MA12–T03	290	134.6	19.52	353.0	51.20	701.4	101.73	31.2	64.3
Unaged[d]									
MA91-T01	25	221.1	32.07	479.9	69.60	1154.7	167.48	67.1	77.2
MA93-T01	25	237.5	34.45	500.8	72.63	1468.2	212.94	65.0	79.1
MA94–T01	290	161.3	23.39	410.4	59.52	646.8	93.81	37.5	46.1
MA92–T01	290	158.5	22.99	308.6	44.76	–	–	24.6	41.7
VR1-T01	25	276.8	40.15	525.2	76.17	1182.1	171.45	42.9	75.8
VR2-T01	25	269.1	39.03	548.7	79.58	822.5	119.29	65.3	58.8
VR1–T02	290	166.3	24.12	388.8	56.39	630.5	91.45	32.1	51.1
VR3–T01	290	151.7	22.00	359.1	52.08	521.0	75.56	32.9	44.9
Aged 10,000 h at 400°C									
MA92-T09	25	251.6	36.49	520.9	75.55	930.5	134.96	25.3	58.1
MA93-T09	25	221.1	32.07	495.0	71.79	1487.8	215.79	39.8	73.7
MA92–T11	290	148.2	21.49	367.9	53.36	603.0	87.46	37.0	50.6
MA93–T11	290	140.0	20.31	382.4	55.46	604.3	87.65	35.3	47.7
VR1-T03	25	–	51.42	678.0	98.34	1249.4	181.21	18.0	50.3
VR2-T03	25	276.9	40.16	611.6	88.71	813.4	117.97	45.0	44.0
VR3-T03	25	271.7	39.41	590.7	85.67	1238.2	179.59	36.4	57.7
VR2–T02	290	186.6	27.06	409.2	59.35	348.1	50.49	18.6	31.0
VR3–T02	290	182.8	26.51	441.8	64.08	604.4	87.66	26.2	35.1

[a] First two letters represent the material identification.
[b] In service for ≈13 y at 264°C.
[c] In service for ≈13 y at 281°C.
[d] Material from cooler region of the component or essentially unaged.

Appendix C

J–R Curve Characterization

The J–R curve tests were performed according to ASTM Specifications E 813–85 (Standard Test Method for J_{IC}, a Measure of Fracture Toughness) and E 1152–87 (Standard Test Method for Determining J–R Curve). Compact–tension (CT) specimens, 25.4 mm (1 in.) thick with 10% side grooves, were used for the tests. The CT specimen design, shown in Fig. C–1, is similar to the specimen of ASTM Specification E 399, the notch region is modified in accordance with E 813 and E 5112, to permit measurement of load–line displacement by axial extensometer. The extensometer was mounted on razor blades that were screwed onto the specimen along the load line.

Prior to testing, the specimens were fatigue–precracked at room temperature and at load levels within the linear elastic range. The final ratio of crack length to width (a/W) after pre–

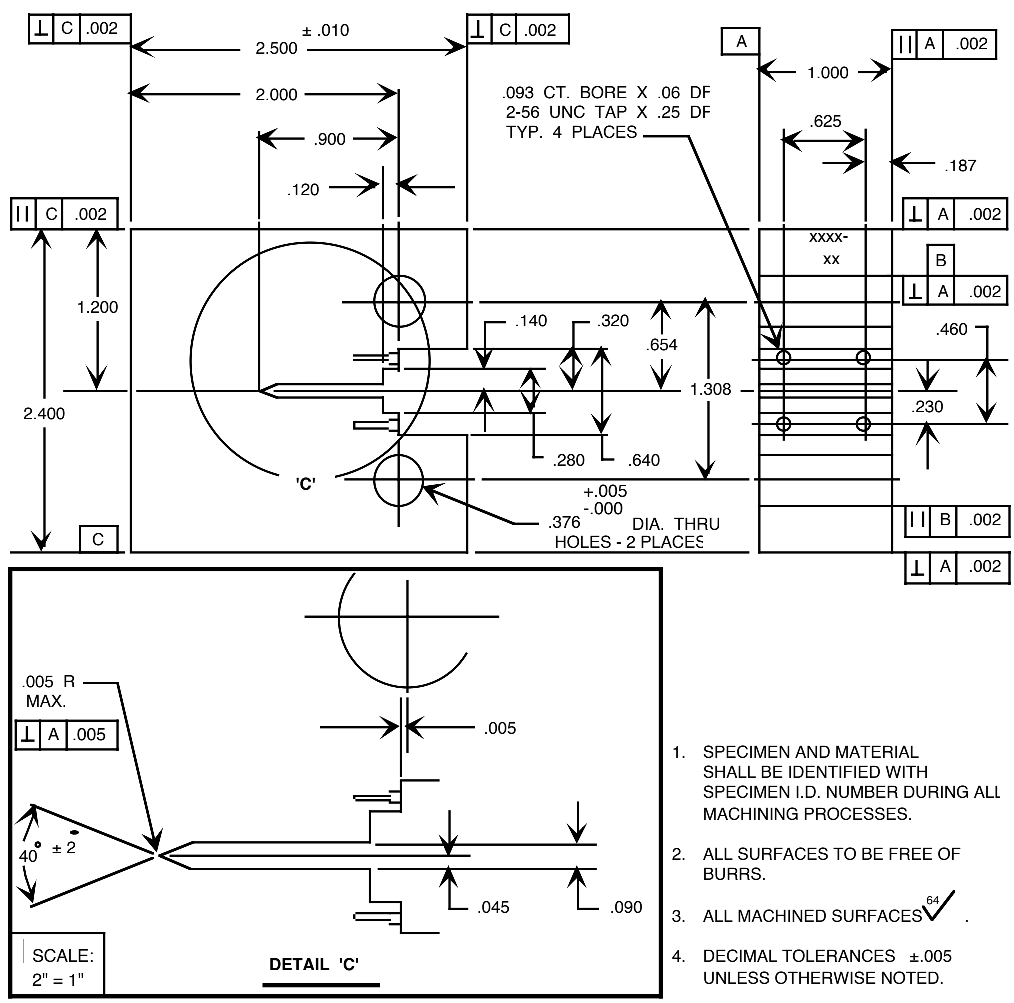

Figure C–1. Configuration of compact–tension test specimen: units of measure are inches cracking was ≈0.55. The final 1–mm (≈0.04–in.) crack extension was carried out at a load range of 13–1.3 kN (2.92–0.292 kip), i.e., during precracking K_{max} was <25 MPa·$m^{1/2}$ (22.6 ksi·$in.^{1/2}$). After precracking, all specimens were side–grooved by 20% of the total specimen thickness, i.e., 10% per side, to ensure uniform crack growth during testing.

The J–R curve tests were performed on an Instron testing machine with 90 kN (20 kip) maximum load capacity. The load and load–line displacement data were digitized with digital voltmeters and stored on a disk for posttest analysis and correction of test data. The single–specimen compliance procedure was used to estimate crack extension. Rotation and modulus corrections were applied to the compliance data. Both deformation theory and modified forms of the J integral were evaluated for each test.

After each test, the specimen was heated to 350°C to heat–tint the exposed fracture surface. The specimen was then fractured at liquid N temperature. The initial (i.e., fatigue precrack) and final (test) crack lengths were measured optically for both halves of the fractured specimen. The crack lengths were determined by the 9/8 averaging technique, i.e., the two near–surface measurements were averaged and the resultant value was averaged with the remaining seven measurements.

The fracture toughness J_{IC} values were determined in accordance with ASTM Specification E 813–81 and E 813–85. For the former, J_{IC} is defined as the intersection of the blunting line given by $J = 2\sigma_f\Delta a$, and the linear fit of the J–vs.–Δa test data between the 0.15– and 1.5–mm exclusion lines. The flow stress σ_f, is the average of the 0.2% yield stress and the ultimate stress. The ASTM Specification E 813–85 procedure defines J_{IC} as the intersection of the 0.2–mm offset line with the power–law fit (of the form $J = C\Delta a^n$) of the test data between the exclusion lines. J–R curve tests on cast stainless steels indicate that a slope of four times the flow stress ($4\sigma_f$) for the blunting line expresses the J–vs.–Δa data better than the slope of $2\sigma_f$ defined in E 813–81 or E 813–85. The fracture toughness J_{IC} values were determined with the $4\sigma_f$ slope.

The tearing modulus was also evaluated for each test. The tearing modulus is given by $T = E(dJ/da)/\sigma_f^2$, where E is the Young's modulus and σ_f is the flow stress. The ASTM E 813–81 value of tearing modulus is determined from the slope dJ/da of the linear fit to the J–vs.–Δa data. For the power–law curve fits, an average value of dJ/da was calculated[C–1] to obtain the average tearing modulus.

The fracture toughness results at room temperature and 290°C for service–aged material from the cold–leg check valve CA4, hot–leg main shutoff valve MA1, and pump volute PV, and relatively unaged material from the spare pump volute VR and cooler regions of the main shutoff valve MA9, are given in Table C–1. The test data, as well as an analysis and qualification of the data, are presented in Tables C–2 to C–61. Photographs of the fracture surface of the test specimens and deformation and modified J–R curves for the various materials are shown in Figs. C–2 to C–61. The blunting, 0.2–mm offset, and 1.5–mm offset lines are shown as dashed lines in the figures.

Data Analysis Procedures

The compliance method was used to determine the crack length during the tests. The Hudak–Saxena calibration equation[C–2] was used to relate the specimen load–line elastic compliance C_i on an unloading/loading sequence with the crack length a_i. The compliance, i.e., slope ($\Delta\delta/\Delta P$) of the load–line displacement–vs.–load record obtained during the unloading/loading sequence, is given by

$$U_{LL} = \frac{1}{\left(B_e E_e C_i\right)^{1/2} + 1} \tag{C–1}$$

and

$$a_i/W = 1.000196 - 4.06319\left(U_{LL}\right) + 11.242\left(U_{LL}\right)^2 - 106.043\left(U_{LL}\right)^3 + 464.335\left(U_{LL}\right)^4 - 650.677\left(U_{LL}\right)^5, \tag{C–2}$$

where E_e is the effective elastic modulus, B_e is the effective specimen thickness expressed as B – $(B – B_N)^2/B$, and W is specimen width.

Both rotation and modulus corrections are applied to the compliance data. The modulus correction[C–2] is used to account for the uncertainties in testing, i.e., in the values of initial crack length determined by compliance and measured optically. The effective modulus E_M is determined from

$$E_e = \frac{1}{C_o B_e}\left(\frac{W + a_o}{W - a_o}\right)^{1/2} f\left(\frac{a_o}{W}\right) \tag{C–3}$$

and

$$f\left(\frac{a_o}{W}\right) = 2.163 + 12.219\left(\frac{a_o}{W}\right) - 20.065\left(\frac{a_o}{W}\right)^2 - 0.9925\left(\frac{a_o}{W}\right)^3 + 20.609\left(\frac{a_o}{W}\right)^4 - 9.9314\left(\frac{a_o}{W}\right)^5, \tag{C–4}$$

where C_o is initial compliance, B_e is effective specimen thickness, and a_o is the initial physical crack size measured optically.

To account for crack–opening displacement in CT specimens, the crack size should be corrected for rotation.[C–3] The corrected compliance is calculated from

$$\theta = \mathrm{Sin}^{-1}\left[\left(\frac{d_m}{2} + D\right) \Big/ \left(D^2 + R^2\right)^{1/2}\right] - \tan^{-1}\left(\frac{D}{R}\right) \tag{C–5}$$

and

$$C_c = C_m \Big/ \left[\left(\frac{H^*}{R}\mathrm{Sin}\theta - \mathrm{Cos}\theta\right)\left(\frac{D}{R}\mathrm{Sin}\theta - \mathrm{Cos}\theta\right)\right], \tag{C–6}$$

where C_c and C_m are the corrected and measured elastic compliance at the load line, H^* is the initial half span of load points, R is the radius of rotation of the crack centerline (= (W+a)/2), a is the updated crack length, D is one–half of the initial distance between the displacement points (i.e., half gage length), d_m is the total measured load–line displacement, and θ is the angle of rotation of a rigid–body element about the unbroken midsection line.

The J value is calculated at any point on the load–vs.–load–line displacement record by means of the relationship

$$\mathbf{J} = \mathbf{J}_{el} + \mathbf{J}_{pl}, \tag{C–7}$$

where J_{el} is the elastic component of J and J_{pl} is the plastic component of J. For a CT specimen, at a point corresponding to the coordinates P_i and δ_i on the specimen load–vs.–load–line displacement record, a_i is $(a_0 + \Delta a_i)$, and the deformation J is given by

$$\mathbf{J}_{d(i)} = \frac{(K_i)^2(1-\upsilon^2)}{E_e} + \mathbf{J}_{pl(i)}, \tag{C–8}$$

where, from ASTM method E 399,

$$K_{(i)} = \left[\frac{P_i}{(BB_N W_e)^{1/2}}\right] f\left(\frac{a_i}{W}\right), \tag{C–9}$$

with

$$f\left(\frac{a_i}{W}\right) = \left[2+\left(\frac{a_i}{W}\right)\right]\left[0.886+4.64\left(\frac{a_i}{W}\right)-13.32\left(\frac{a_i}{W}\right)^2+14.72\left(\frac{a_i}{W}\right)^3 -5.6\left(\frac{a_i}{W}\right)^4\right] \Big/ \left[1-\left(\frac{a_i}{W}\right)\right]^{3/2} \tag{C–10}$$

and

$$\mathbf{J}_{pl(i)} = \left[\mathbf{J}_{pl(i-1)} + \left(\frac{\eta_i}{b_i}\right)\frac{A_{pl(i)} - A_{pl(i-1)}}{B_N}\right]\left[1-\left(\frac{\gamma_i}{b_i}\right)(a_i - a_{i-1})\right], \tag{C–11}$$

where υ is Poisson's ratio, b is the uncracked ligament, A_{pl} is the plastic component of the area under the load–vs.–load–line displacement record, and η ισ a factor that accounts for the tensile component of the load as given by

$$\eta_i = 2 + 0.522\, b_i/W, \tag{C–12}$$

and γ, a factor that accounts for limited crack growth as given by

$$\gamma_i = 1 + 0.76\, b_i/W. \tag{C–13}$$

The modified J values (J_M) are calculated from the relationship (from Ref. C–4)

$$\mathbf{J}_{M(i)} = \mathbf{J}_{d(i)} + \Delta\mathbf{J}_i, \tag{C–14}$$

where

$$\Delta\mathbf{J}_i = \Delta\mathbf{J}_{i-1} + \left(\frac{\gamma_i}{b_i}\right)\mathbf{J}_{pl(i)}(a_i - a_{i-1}). \tag{C–15}$$

According to ASTM Specification E 1152–87, the J_D–R curves are valid only for crack growth up to 10% of the initial uncracked ligament. Also, they show a dependence on specimen size. The

J_M–R curves have been demonstrated to be independent of specimen size and yield valid results for larger crack growth.

Data Qualification

The various validity criteria specified in ASTM Specification E 813–85 for J_{IC} and in ASTM Specification E 1152–87 for J–R curves, were used to qualify the results from each test. The various criteria include maximum values of crack extension and J–integrals; limits for initial uncracked ligaments, effective elastic modulus, and optically measured physical crack lengths; and spacing of J–Δa data points. The ω criterion (from Ref. C–5) was also used to ensure that a region of J dominance exists.

For the present investigation, most of the unaged or service–aged specimens yielded invalid J_{IC} values because of the relatively high toughness of the material. The reasons for the discrepancies are data–point spacing, shape of the final crack front, or size of the uncracked ligament. In general, the size of the uncracked ligament or the specimen thickness was inadequate because of the relatively high toughness of the material. The J_{max} limit for the J–vs.–Δa data was ignored in most tests to obtain a good power–law fit of the test data.

All tests showed significant load relaxation during the unloading/reloading cycle for estimating the crack length by elastic compliance. All unloadings were 25% of the load. The load at the end of the unloading/reloading cycle was always lower than it was at the start of the unloading cycle. The difference was appreciable for the RT tests. Therefore, the initial 20–30% of the unloading curve was ignored in estimating crack length.

References

C–1. A. L. Hiser, F. J. Loss, and B. H. Menke, *J–R Curve Characterization of Irradiated Low Upper Shelf Welds*, NUREG/CR–3506, MEA–2028, Materials Engineering Associates, Inc., Lanham, MD (April 1984).

C–2. A. Saxena and S. J. Hudak, Jr., "Review and Extention of Compliance Information for Common Crack Growth Specimen," *Int. J. Fracture*, **5**, Vol. 14, 453–468 (1978).

C–3. F. J. Loss, B. H. Menke, and R. A. Gray, Jr., "Development of J–R Curve Procedures," in *NRL–EPRI Research Program (RP 886–2), Evaluation and Prediction of Neutron Embrittlement in Reactor Pressure Vessel Materials Annual Progress Report for FY 1978*, J. R. Hawthorn, ed., NRL Report 8327, Naval Research Laboratory, Annapolis, MD (August 1979).

C–4. H. A. Ernst, "Material Resistance and Instability Beyond J–Controlled Crack Growth," *Elastic–Plastic Fracture: Second Sym., Vol. I: Inelastic Crack Analysis*, ASTM STP 803, American Society for Testing and Materials, Philadelphia (1983).

C–5. J. W. Hutchinson and P. C. Paris, "The Theory of Stability Analysis of J–Controlled Crack Growth," *Elastic Plastic Fracture*, ASTM STP 668, American Society for Testing and Materials, Philadelphia, pp. 37–64 (1983).

Table C–1. Fracture toughness test results for cast stainless steels from the Shippingport reactor components

Specimen Number	Heat	Test No.	Test Temp. (°C)	a/W	Δa Final[a] Comp. (mm)	Δa Final[a] Opt. (mm)	Deformation J^b J_{IC} (kJ/m²)	Deformation J^b T_{av}	Deformation J^b C (kJ/m²)	Deformation J^b n	Modified J^b J_{IC} (kJ/m²)	Modified J^b T_{av}	Modified J^b C (kJ/m²)	Modified J^b n	Flow Stress (MPa)	Impact Energy[c] (J/cm²)	Condition Time (h)	Condition Temp. (°C)
CA4–01T	CA4	68	25	0.585	7.46	7.94	476.3	342	631.8	0.427	487.4	395	662.0	0.473	377.1	145	113,900	264
CA4–02T	CA4	118	25	0.563	10.39	12.14	301.9	264	469.9	0.473	306.2	296	491.6	0.510	391.5	64	10,000	400
CA4–01B	CA4	64	290	0.561	7.78	9.12	291.7	790	475.9	0.698	312.3	846	500.4	0.715	246.3	225	Annealed	–
CA4–02B	CA4	65	290	0.573	8.11	8.98	361.2	568	484.0	0.504	370.8	649	506.1	0.552	251.1	180	113,900	264
MA1–01T	MA1	69	25	0.581	4.00	5.52	1407.0	456	1306.4	0.374	1509.3	591	1340.2	0.462	345.1	299	113,900	281
MA1–01B	MA1	67	290	0.591	6.36	7.88	739.1	618	745.7	0.429	810.5	654	791.7	0.438	237.0	186	113,900	281
MA9–01I	MA9	83	25	0.523	3.10	6.07	1677.1	375	1504.1	0.367	1938.9	364	1678.3	0.342	359.8	357	Unaged	–
MA9–02O	MA9	116	25	0.575	6.47	7.47	1093.5	382	1117.9	0.326	1163.4	464	1171.7	0.379	372.0	128	10,000	400
MA9–01O	MA9	97	290	0.558	3.58	4.74	1120.6	690	1010.6	0.420	1245.8	805	1064.1	0.469	259.7	253	Unaged	–
MA9–02I	MA9	121	290	0.568	5.84	6.67	629.2	354	668.0	0.277	689.4	376	718.4	0.282	259.6	185	10,000	400
PVC–01	PV	78	25	0.570	3.92	4.83	1545.7	466	1422.8	0.350	1648.9	637	1443.9	0.455	362.0	424	Annealed	–
PVI–02	PV	81	25	0.553	4.46	5.02	1508.8	600	1386.5	0.428	1623.9	748	1423.2	0.508	370.3	322	113,900	264
PVO–01	PV	119	25	0.576	8.25	9.56	424.6	289	603.0	0.450	432.4	328	630.5	0.491	410.0	–	10,000	400
PVI–01	PV	80	290	0.556	5.05	6.29	978.6	406	951.0	0.277	912.4	746	892.0	0.487	269.2	330	Annealed	–
PVC–02	PV	79	290	0.561	5.23	5.56	857.6	437	855.7	0.327	889.3	613	875.5	0.436	265.8	279	113,900	264
PVO–02	PV	120	290	0.584	7.76	9.03	388.4	424	517.4	0.465	368.3	538	532.1	0.566	286.0	–	10,000	400
VRI–01	VR	82	25	0.568	6.18	7.75	699.6	462	884.1	0.510	716.3	533	919.6	0.564	405.0	237	Unaged	–
VRO–02	VR	117	25	0.580	10.56	11.24	122.6	129	248.9	0.541	122.8	141	259.3	0.571	437.7	64	10,000	400
VRO–01	VR	96	290	0.561	8.99	9.88	332.4	460	457.6	0.477	340.1	524	478.9	0.521	266.8	264	Unaged	–
VRI–02	VR	122	290	0.558	12.23	13.28	213.8	271	331.6	0.448	215.1	305	345.8	0.486	305.1	106	10,000	400

[a]Final crack extension: Comp. = determined from compliance and Opt. = measured optically.
[b]J_{IC} determined with a slope of four times the flow stress for the blunting line.
[c]Charpy–impact energy at the test temperature.

Table C–2. Test data for specimen CA4–01T

Test Number	: 0068	Test Temp.	: 25°C
Material Type	: CF–8	Heat Number	: CA
Aging Temp.	: 264°C	Aging Time	: 113,900 h
Spec. Thickness	: 25.35 mm	Net Thickness	: 20.34 mm
Spec. Width	: 50.82 mm	Flow Stress	: 377.10 MPa

Unload Number	J_d (kJ/m^2)	J_m (kJ/m^2)	Δa (mm)	Load (kN)	Deflection (mm)
1	11.57	11.61	0.1818	17.005	0.225
2	25.72	25.70	0.1164	20.151	0.376
3	42.36	42.53	0.2230	21.725	0.526
4	63.25	63.22	0.1595	22.992	0.708
5	88.31	87.80	0.0505	24.043	0.910
6	114.75	114.49	0.0914	24.859	1.115
7	147.16	146.23	0.0078	25.658	1.360
8	180.85	180.93	0.1083	26.322	1.610
9	215.68	215.26	0.0667	27.047	1.860
10	251.41	252.09	0.1440	27.680	2.114
11	285.83	288.39	0.2580	28.212	2.361
12	321.41	325.33	0.3304	28.698	2.610
13	359.53	363.24	0.3203	29.035	2.861
14	396.49	402.78	0.4305	29.381	3.112
15	434.71	441.37	0.4449	29.892	3.361
16	472.62	481.47	0.5224	30.197	3.610
17	511.96	522.14	0.5655	30.593	3.863
18	551.50	563.82	0.6300	30.734	4.117
19	588.38	605.10	0.7528	30.762	4.366
20	626.24	644.92	0.8042	30.766	4.609
21	661.23	690.99	1.0754	30.709	4.879
22	689.96	728.52	1.2798	30.486	5.109
23	724.47	770.15	1.4362	30.247	5.360
24	755.21	812.21	1.6725	30.278	5.609
25	790.56	853.49	1.7900	30.251	5.859
26	825.10	896.29	1.9458	30.198	6.110
27	864.69	938.04	1.9845	30.318	6.359
28	898.54	983.65	2.1855	29.997	6.618
29	930.48	1025.20	2.3431	29.926	6.864
30	968.85	1068.14	2.4147	29.891	7.117
31	1005.35	1110.42	2.5017	29.852	7.361
32	1047.91	1162.83	2.6430	29.947	7.660
33	1087.29	1215.67	2.8272	29.816	7.961
34	1128.79	1267.78	2.9664	29.710	8.261
35	1168.16	1321.31	3.1442	29.350	8.564
36	1223.55	1400.79	3.4291	28.998	9.011
37	1280.04	1469.89	3.5707	28.841	9.412
38	1345.43	1559.06	3.8215	28.325	9.912
39	1399.58	1647.93	4.1677	28.008	10.414
40	1469.38	1752.88	4.4962	27.516	11.012
41	1534.86	1858.68	4.8504	26.742	11.612
42	1587.69	1963.10	5.2789	25.823	12.214
43	1644.41	2064.12	5.6274	24.956	12.812
44	1708.70	2165.24	5.9021	24.432	13.413
45	1746.72	2266.44	6.3516	23.345	14.010
46	1778.46	2363.29	6.7955	22.583	14.606
47	1826.17	2460.15	7.1156	21.905	15.209
48	1866.97	2556.83	7.4643	21.336	15.803

Table C–3. Deformation J_{IC} and J–R curve results for specimen CA4–01T

Test Number	: 0068	Test Temp.	: 25°C
Material Type	: CF–8	Heat Number	: CA
Aging Temp.	: 264°C	Aging Time	: 113,900 h
Spec. Thickness	: 25.35 mm	Net Thickness	: 20.34 mm
Spec. Width	: 50.82 mm	Flow Stress	: 377.10 MPa
Modulus E	: 201.66 GPa	(Effective)	
Modulus E	: 193.10 GPa	(Nominal)	
Init. Crack	: 29.7156 mm	Init. a/w	: 0.5848 (Measured)
Final Crack	: 37.6594 mm	Final a/w	: 0.7411 (Measured)
Final Crack	: 37.1799 mm	Final a/w	: 0.7317 (Compliance)

Linear Fit	**$J = B+M(\Delta a)$**		
Intercept B	: 362.721 kJ/m^2	Slope M	: 248.79 kJ/m^2mm
Fit Coeff. R	: 0.9711	(14 Data Points)	
J_{IC}	: 434.4 kJ/m^2	(2480.3 $in.–lb/in.^2$)	
Δa (J_{IC})	: 0.288 mm	(0.0113 in.)	
T Average	: 352.8	(J_{IC} at 0.15)	

Power–Law Fit	**$J = C(\Delta a)^n$**		
Coeff. C	: 631.76 kJ/m^2	Exponent n	: 0.4267
Fit Coeff. R	: 0.9803	(14 Data Points)	
J_{IC} (0.20)	: 476.3 kJ/m^2	(2719.6 $in.–lb/in.^2$)	
Δa (J_{IC})	: 0.516 mm	(0.0203 in.)	
T Average	: 342.1	(J_{IC} at 0.20)	
J_{IC} (0.15)	: 448.1 kJ/m^2	(2558.7 $in.–lb/in.^2$)	
Δa (J_{IC})	: 0.447 mm	(0.0176 in.)	
T Average	: 349.7	(J_{IC} at 0.15)	
K_{jc}	: 416.9 $MPa–m^{0.5}$		

J_{IC} Validity & Data Qualification (E 813–85)		
J_{max} Allowed	: 530.44 kJ/m^2	($J_{max}=b_o\sigma_f/15$)
Data Limit	: J_{max} Ignored	
Δa (max) Allowed	: 2.071 mm	(at 1.5 Exclusion Line)
Data Limit	: 1.5 Exclusion Line	
Data Points	: Zone A = 7	Zone B = 4
Data Point Spacing	: OK	
b_{net} or b_o Size	: Inadequate	
dJ/da at J_{IC}	: OK	
a_o Measurement	: 9 Outside Limit	
a_o Measurement	: 1 Outside Limit	
a_f Measurement	: Near–surface	Outside Limit
Crack Size Estimate	: Inadequate	(by Compliance)
E Effective	: OK	
J_{IC} Estimate	: Invalid	

J–R Curve Validity & Data Qualification (E 1152–86)		
J_{max} Allowed	: 383.47 kJ/m^2	($J_{max}=b_{net}\sigma_f/20$)
Δa (max) Allowed	: 2.110 mm	($\Delta a=0.1b_o$)
Δa (max) Allowed	: 3.995 mm	($\omega=5$)
Data Points	: Zone A = 19	Zone B = 8
Data Point Spacing	: OK	
J–R Curve Data	: Invalid	

Table C–4. Modified J_{IC} and J–R curve results for specimen CA4–01T

Linear Fit	**$J = B+M(\Delta a)$**		
Intercept B	: 348.207 kJ/m^2	Slope M	: 291.92 kJ/m^2mm
Fit Coeff. R	: 0.9800	(14 Data Points)	
J_{IC}	: 431.8 kJ/m^2	(2465.5 $in.–lb/in.^2$)	
Δa (J_{IC})	: 0.286 mm	(0.0113 in.)	
T Average	: 414.0	(J_{IC} at 0.15)	
Power–Law Fit	**$J = C(\Delta a)^n$**		
Coeff. C	: 661.98 kJ/m^2	Exponent n	: 0.4726
Fit Coeff. R	: 0.9861	(14 Data Points)	
J_{IC} (0.20)	: 487.4 kJ/m^2	(2783.0 $in.–lb/in.^2$)	
Δa (J_{IC})	: 0.523 mm	(0.0206 in.)	
T Average	: 395.3	(J_{IC} at 0.20)	
J_{IC} (0.15)	: 454.5 kJ/m^2	(2595.5 $in.–lb/in.^2$)	
Δa (J_{IC})	: 0.451 mm	(0.0178 in.)	
T Average	: 403.5	(J_{IC} at 0.15)	
K_{jc}	: 436.7 $MPa–m^{0.5}$		

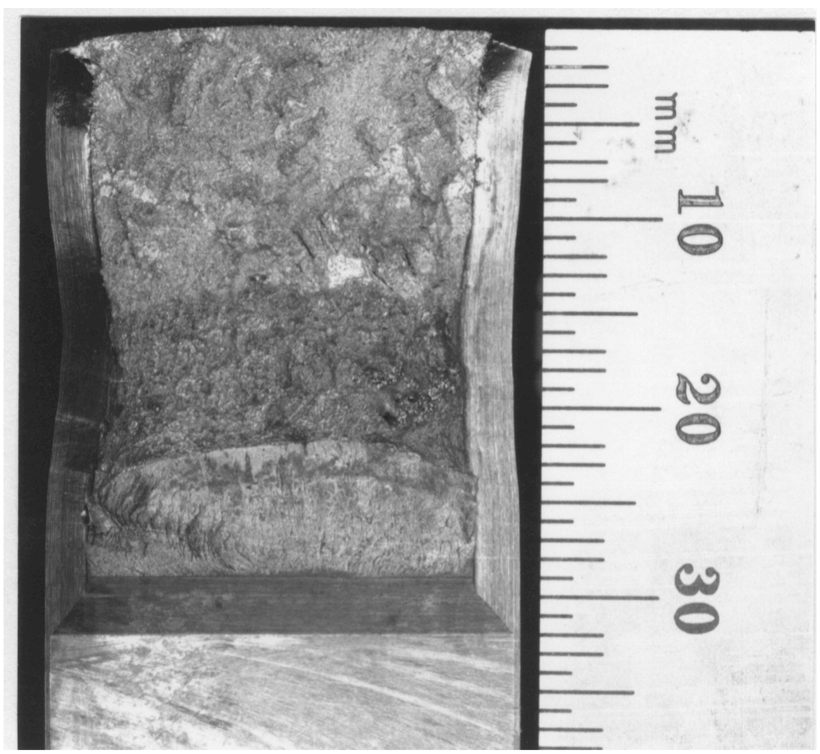

Figure C–2. Fracture surface of the cold–leg check valve CA4 tested at room temperature after 13 y of service at 264°C

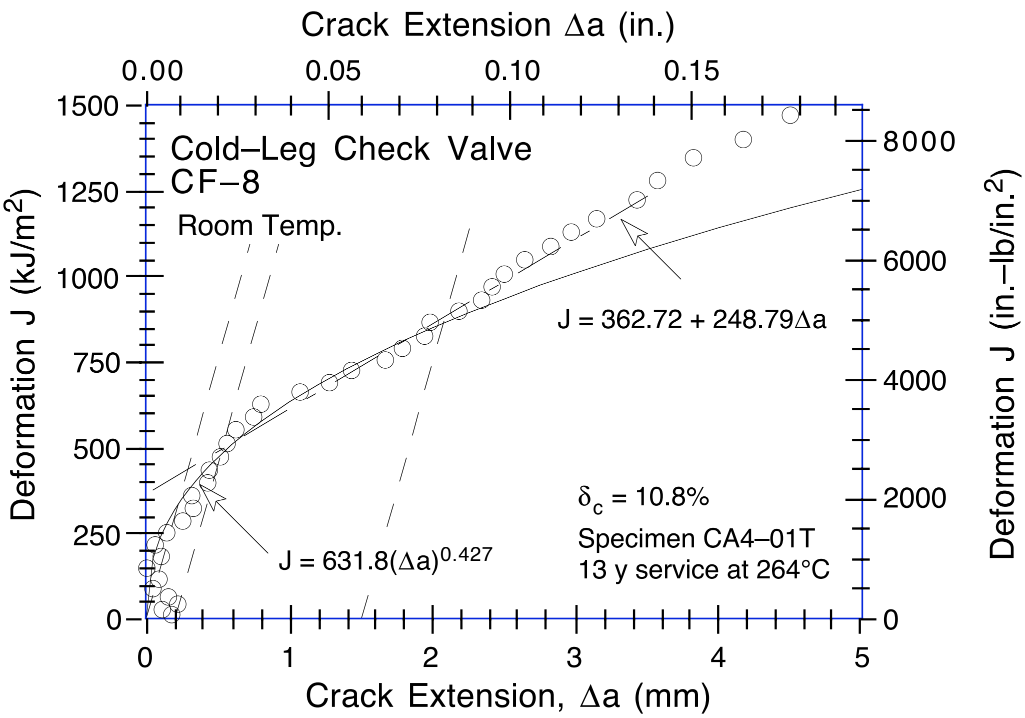

Figure C–3. Deformation J–R Curve at room temperature for the cold–leg check valve CA4 after 13 y of service at 264°C

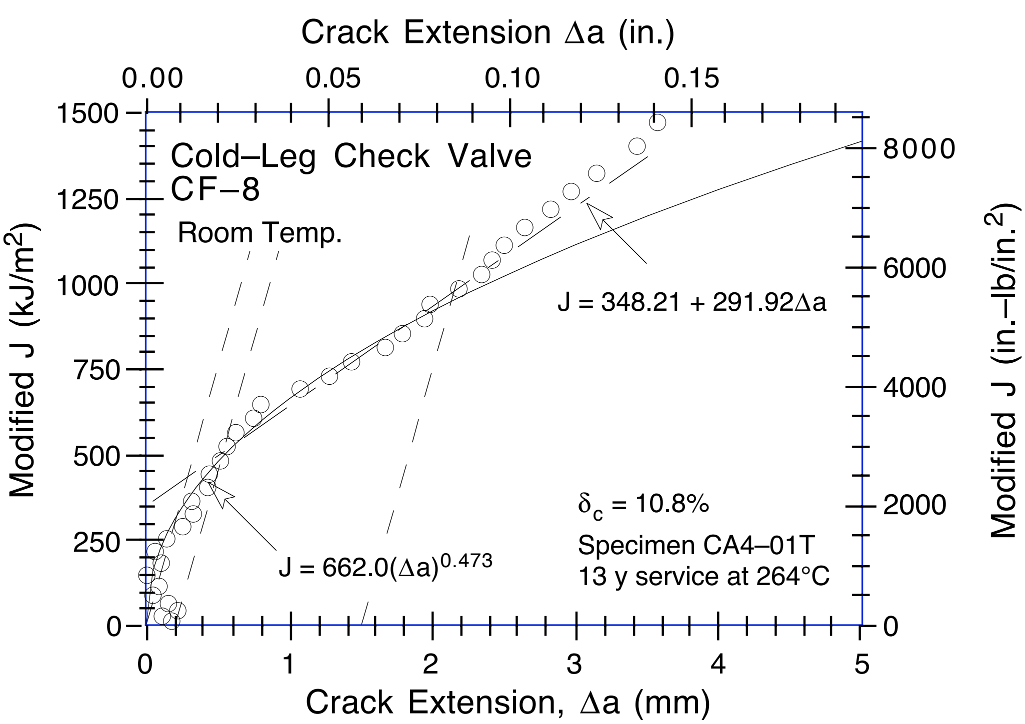

Figure C–4. Modified J-R Curve at room temperature for the cold–leg check valve CA4 after 13 y of service at 264°C

Table C–5. Test data for specimen CA4–02T

Test Number	: 0118	Test Temp.	: 25°C
Material Type	: CF–8	Heat Number	: CA4
Aging Temp.	: 400°C	Aging Time	: 10,000 h
Spec. Thickness	: 25.37 mm	Net Thickness	: 20.21 mm
Spec. Width	: 50.83 mm	Flow Stress	: 391.50 MPa

Unload Number	J_d (kJ/m^2)	J_m (kJ/m^2)	Δa (mm)	Load (kN)	Deflection (mm)
1	13.15	13.15	-0.0142	18.339	0.253
2	39.06	39.05	-0.0175	22.886	0.504
3	75.24	75.14	-0.0447	25.528	0.805
4	114.89	114.70	-0.0593	27.161	1.106
5	156.29	157.49	0.1113	28.486	1.407
6	184.78	185.81	0.0939	29.332	1.609
7	214.05	216.10	0.1835	29.737	1.810
8	243.88	245.52	0.1525	30.389	2.008
9	274.46	277.47	0.2433	30.793	2.212
10	302.51	308.83	0.4407	31.337	2.409
11	333.02	339.75	0.4629	31.406	2.610
12	363.61	372.47	0.5667	31.636	2.810
13	393.01	404.98	0.7060	31.815	3.009
14	423.98	437.68	0.7772	31.964	3.211
15	454.88	470.54	0.8522	32.270	3.410
16	482.98	504.73	1.0688	31.907	3.611
17	511.76	537.12	1.1891	32.315	3.809
18	547.47	579.68	1.4006	32.199	4.059
19	583.81	622.16	1.5766	31.789	4.311
20	615.76	664.29	1.8499	31.382	4.559
21	653.80	713.02	2.1166	31.167	4.849
22	686.96	756.62	2.3618	30.899	5.109
23	729.27	807.05	2.5402	30.611	5.410
24	765.04	858.88	2.8714	30.468	5.710
25	806.57	908.89	3.0358	30.199	6.012
26	857.20	978.52	3.3770	29.744	6.411
27	904.82	1046.75	3.7220	29.074	6.813
28	950.91	1112.52	4.0310	28.497	7.206
29	1015.46	1197.04	4.3200	27.904	7.707
30	1058.96	1282.45	4.8867	26.693	8.208
31	1107.87	1378.94	5.4831	25.041	8.807
32	1154.52	1473.53	6.0447	24.472	9.407
33	1217.98	1567.02	6.3724	23.992	10.005
34	1281.94	1662.96	6.6979	23.301	10.606
35	1320.15	1758.46	7.2468	21.823	11.209
36	1350.21	1863.14	7.9197	20.353	11.911
37	1398.62	1962.83	8.3544	19.481	12.609
38	1427.55	2063.56	8.9290	17.744	13.310
39	1437.16	2155.22	9.5555	16.562	14.004
40	1478.57	2245.44	9.9090	15.873	14.706
41	1499.98	2337.17	10.3935	14.633	15.406

Table C–6. Deformation J_{IC} and J–R curve results for specimen CA4-02T

Test Number	: 0118	Test Temp	: 25 °C
Material Type	: CF-8	Heat Number	: CA4
Aging Temp	: 400 °C	Aging Time	: 10,000 h
Spec. Thickness	: 25.37 mm	Net Thickness	: 20.21 mm
Spec. Width	: 50.83 mm	Flow Stress	: 391.50 MPa
Modulus E	: 188.37 GPa	(Effective)	
Modulus E	: 200.00 GPa	(Nominal)	
Init. Crack	: 28.6094 mm	Init. a/w	: 0.5629 (Measured)
Final Crack	: 40.7469 mm	Final a/w	: 0.8017 (Measured)
Final Crack	: 39.0028 mm	Final a/w	: 0.7673 (Compliance)
Linear Fit	**$J = B+M(\Delta a)$**		
Intercept B	: 241.553 kJ/m^2	Slope M	: 216.31 kJ/m^{2}mm
Fit Coeff. R	: 0.9845	(11 Data Points)	
J_{IC}	: 280.3 kJ/m^2	(1600.4 in.–lb/in.^{2})	
Δa (J_{IC})	: 0.179 mm	(0.0070 in.)	
T Average	: 265.8	(J_{IC} at 0.15)	
Power–Law Fit	**$J = C(\Delta a)^n$**		
Coeff. C	: 469.87 kJ/m^2	Exponent n	: 0.4734
Fit Coeff. R	: 0.9943	(11 Data Points)	
$J_{IC}(0.20)$	: 301.9 kJ/m^2	(1724.0 in.–lb/in.^{2})	
Δa (J_{IC})	: 0.393 mm	(0.0155 in.)	
T Average	: 264.3	(J_{IC} at 0.20)	
$J_{IC}(0.15)$	: 276.7 kJ/m^2	(1580.0 in.–lb/in.^{2})	
Δa (J_{IC})	: 0.327 mm	(0.0129 in.)	
T Average	: 270.4	(J_{IC} at 0.15)	
K_{jc}	: 346.6 MPa–m$^{0.5}$		
J_{IC} Validity & Data Qualification (E 813–85)			
J_{max} Allowed	: 579.91 kJ/m^2	($J_{max}=b_o\sigma_f/15$)	
Data Limit	: J_{max} Ignored		
Δa (max) Allowed	: 1.907 mm	(at 1.5 Exclusion Line)	
Data Limit	: 1.5 Exclusion Line		
Data Points	: Zone A = 4	Zone B = 3	
Data Point Spacing	: OK		
$b_{net.}$ or b_o Size	: OK		
dJ/da at J_{IC}	: OK		
a_o Measurement	: 1 Outside Limit		
Final Crack Shape	: OK		
Crack size estimate	: Inadequate	(by Compliance)	
E Effective	: OK		
J_{IC} Estimate	: Invalid		
J–R Curve Validity & Data Qualification (E 1152–86)			
J_{max} Allowed	: 395.57 kJ/m^2	($J_{max}=b_{net}\sigma_f/20$)	
Δa (max) Allowed	: 2.222 mm	($\Delta a=0.1b_o$)	
Δa (max) Allowed	: 4.396 mm	($\omega=5$)	
Data Points	: Zone A = 11	Zone B = 6	
Data Point Spacing	: Inadequate		
J-R Curve Data	: Invalid		

Table C–7. Modified J_{IC} and J–R curve results for specimen CA4–02T

Linear Fit	**J = B+M(Δa)**		
Intercept B	: 233.201 kJ/m^2	Slope M	: 245.81 kJ/m^{2}mm
Fit Coeff. R	: 0.9894	(11 Data Points)	
J_{IC}	: 276.6 kJ/m^2	(1579.6 in.–lb/in.^{2})	
Δa (J_{IC})	: 0.177 mm	(0.0070 in.)	
T Average	: 302.1	(J1c at 0.15)	
Power–Law Fit	**J = C(Δa)^n**		
Coeff. C	: 491.57 kJ/m^2	Exponent n	: 0.5103
Fit Coeff. R	: 0.9960	(11 Data Points)	
J_{IC} (0.20)	: 306.2 kJ/m^2	(1748.5 in.–lb/in.^{2})	
Δa (J_{IC})	: 0.396 mm	(0.0156 in.)	
T Average	: 296.4	(J_{IC} at 0.20)	
J_{IC} (0.15)	: 278.1 kJ/m^2	(1588.2 in.–lb/in.^{2})	
Δa (Jic)	: 0.328 mm	(0.0129 in.)	
T Average	: 302.8	(J_{IC} at 0.15)	
K_{jc}	: 360.4 MPa–m$^{0.5}$		

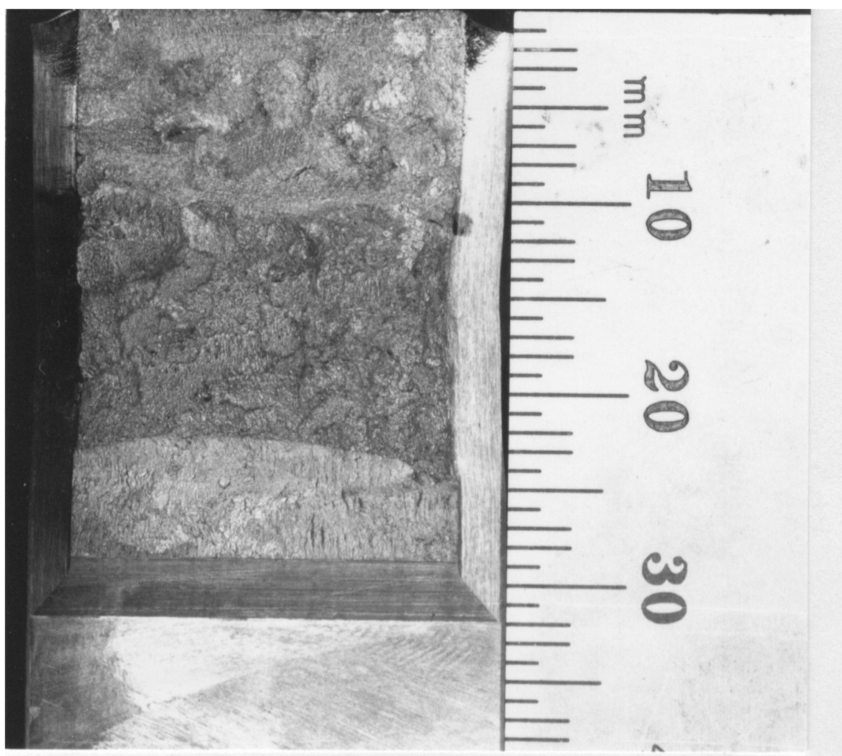

Figure C–5. Fracture surface of service–aged CA4 material from the cold–leg check valve aged further for 10,000 h at 400°C and tested at 25°C

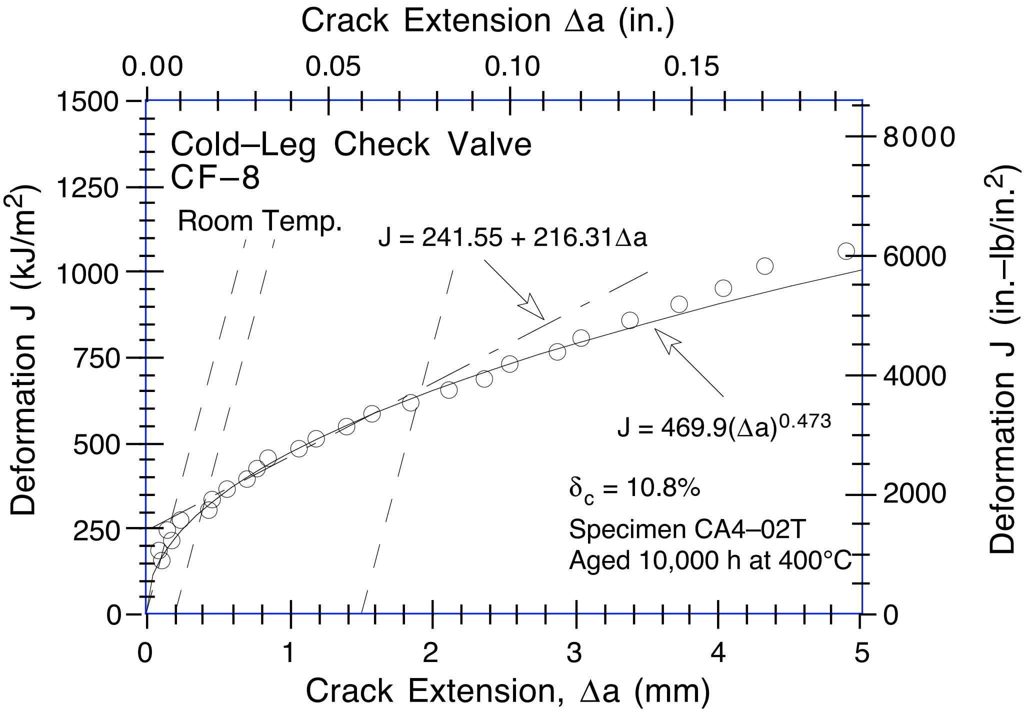

Figure C–6. Deformation J–R Curve at room temperature for material from the cold–leg check valve CA4 aged for 10,000 h at 400°C after service

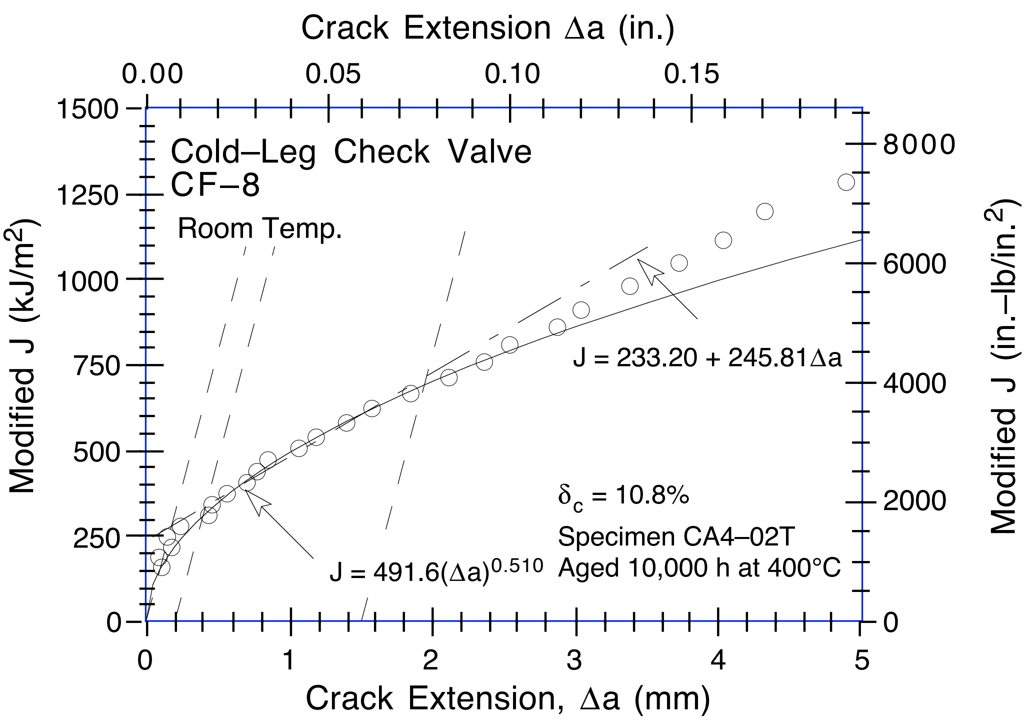

Figure C–7. Modified J–R Curve at room temperature for material from the cold–leg check valve CA4 aged for 10,000 h at 400°C after service

Table C–8. Test data for specimen CA4–01B

Test Number	: 0064	Test Temp.	: 290°C
Material Type	: CF–8	Heat Number	: CA
Aging Temp.	: 550°C	Aging Time	: 1 h
Spec. Thickness	: 25.37 mm	Net. Thickness	: 20.33 mm
Spec. Width	: 50.80 mm	Flow Stress	: 246.30 MPa

Unload Number	J_d (kJ/m^2)	J_m (kJ/m^2)	Δa (mm)	Load (kN)	Deflection (mm)
1	9.44	9.43	-0.0234	13.753	0.257
2	28.57	28.79	0.1610	16.375	0.510
3	53.58	53.51	0.0511	17.611	0.808
4	85.38	85.24	0.0348	18.721	1.157
5	118.76	118.73	0.0526	19.594	1.509
6	152.93	154.06	0.1895	20.222	1.862
7	188.91	188.90	0.0826	20.774	2.209
8	223.44	227.19	0.3793	21.401	2.561
9	261.94	263.82	0.2537	21.868	2.910
10	296.86	304.08	0.5658	22.248	3.261
11	336.25	344.01	0.5938	22.561	3.621
12	373.62	384.12	0.7191	22.867	3.964
13	411.74	424.77	0.8239	23.125	4.311
14	450.03	466.73	0.9613	23.239	4.662
15	490.03	508.44	1.0200	23.496	5.010
16	526.04	552.08	1.2618	23.708	5.360
17	572.89	593.63	1.1071	23.992	5.710
18	604.21	640.04	1.5180	23.954	6.063
19	654.38	680.99	1.2850	24.163	6.412
20	681.38	727.98	1.7625	24.236	6.759
21	728.53	769.83	1.6439	24.212	7.107
22	753.16	817.57	2.1348	24.017	7.458
23	794.97	860.11	2.1494	23.780	7.808
24	815.57	907.21	2.6585	23.500	8.159
25	849.30	950.25	2.8289	23.323	8.506
26	878.69	996.38	3.1216	23.125	8.857
27	906.39	1041.60	3.4148	22.837	9.207
28	945.98	1094.52	3.6264	22.364	9.619
29	975.27	1145.75	3.9596	22.079	10.012
30	1023.90	1209.84	4.1807	21.582	10.516
31	1070.69	1287.07	4.5895	21.269	11.110
32	1112.58	1364.25	5.0364	20.635	11.714
33	1158.09	1438.41	5.3790	19.982	12.310
34	1205.31	1526.53	5.8386	19.287	13.012
35	1242.99	1612.18	6.3479	18.539	13.710
36	1283.47	1696.59	6.7892	17.753	14.413
37	1307.39	1779.99	7.3584	17.086	15.112
38	1342.81	1861.46	7.7776	16.502	15.811

Table C–9. Deformation J_{IC} and J–R curve results for specimen CA4–01B

Test Number	: 0064	Test Temp.	: 290°C
Material Type	: CF–8	Heat Number	: CA
Aging Temp.	: 550°C	Aging Time	: 1 h
Spec. Thickness	: 25.37 mm	Net. Thickness	: 20.33 mm
Spec. Width	: 50.80 mm	Flow Stress	: 246.30 MPa
Modulus E	: 158.60 GPa	(Effective)	
Modulus E	: 180.00 GPa	(Nominal)	
Init. Crack	: 28.5063 mm	Init. a/w	: 0.5611 (Measured)
Final Crack	: 37.6250 mm	Final a/w	: 0.7406 (Measured)
Final Crack	: 36.2839 mm	Final a/w	: 0.7142 (Compliance)
Linear Fit	**$J = B+M(\Delta a)$**		
Intercept B	: 178.882 kJ/m^2	Slope M	: 294.64 kJ/m^{2}mm
Fit Coeff. R	: 0.9605	(14 Data Points)	
J_{IC}	: 255.2 kJ/m^2	(1457.3 in.–lb/in.^{2})	
Δa (J_{IC})	: 0.259 mm	(0.0102 in.)	
T Average	: 767.4	(J_{IC} at 0.15)	
Power–Law Fit	**$J = C(\Delta a)^n$**		
Coeff. C	: 475.94 kJ/m^2	Exponent n	: 0.6984
Fit Coeff. R	: 0.9762	(14 Data Points)	
J_{IC} (0.20)	: 291.7 kJ/m^2	(1665.6 in.–lb/in.^{2})	
Δa (J_{IC})	: 0.496 mm	(0.0195 in.)	
T Average	: 790.3	(J_{IC} at 0.20)	
J_{IC} (0.15)	: 254.7 kJ/m^2	(1454.4 in.–lb/in.^{2})	
Δa (J_{IC})	: 0.409 mm	(0.0161 in.)	
T Average	: 800.6	(J_{IC} at 0.15)	
K_{jc}	: 371.6 MPa–m$^{0.5}$		
J_{IC} Validity & Data Qualification (E 813–85)			
J_{max} Allowed	: 366.10 kJ/m^2	($J_{max}=b_o\sigma_f/15$)	
Data Limit	: J_{max} Ignored		
Δa (max) Allowed	: 2.387 mm	(at 1.5 Exclusion Line)	
Data Limit	: 1.5 Exclusion Line		
Data Points	: Zone A = 4	Zone B = 3	
Data Point Spacing	: OK		
$b_{net.}$ or b_o Size	: Inadequate		
dJ/da at J_{IC}	: OK		
a_f Measurement	: Near–surface	Outside Limit	
Initial Crack Shape	: OK		
Crack Size Estimate	: Inadequate	(by Compliance)	
E Effective	: Inadequate		
J_{IC} Estimate	: Invalid		
J–R Curve Validity & Data Qualification (E 1152–86)			
J_{max} Allowed	: 250.40 kJ/m^2	($J_{max}=b_{net}\sigma_f/20$)	
Δa (max) Allowed	: 2.230 mm	($\Delta a=0.1b_o$)	
Δa (max) Allowed	: 6.226 mm	($\omega=5$)	
Data Points	: Zone A = 21	Zone B = 1	
Data Point Spacing	: Inadequate		
J–R Curve Data	: Invalid		

Table C–10. Modified J_{IC} and J–R curve results for specimen CA4–01B

Linear Fit	**J = B+M(Δa)**		
Intercept B	: 179.004 kJ/m^2	Slope M	: 320.56 kJ/m^2mm
Fit Coeff. R	: 0.9673	(14 Data Points)	
J_{IC}	: 265.3 kJ/m^2	(1515.1 in.–lb/in.^{2})	
Δa (J_{IC})	: 0.269 mm	(0.0106 in.)	
T Average	: 834.9	(J_{IC} at 0.15)	
Power–Law Fit	**J = C(Δa)^n**		
Coeff. C	: 500.42 kJ/m^2	Exponent n	: 0.7145
Fit Coeff. R	: 0.9778	(14 Data Points)	
J_{IC} (0.20)	: 312.3 kJ/m^2	(1783.6 in.–lb/in.^{2})	
Δa (J_{IC})	: 0.517 mm	(0.0204 in.)	
T Average	: 845.5	(J_{IC} at 0.20)	
J_{IC} (0.15)	: 272.0 kJ/m^2	(1553.4 in.–lb/in.^{2})	
Δa (J_{IC})	: 0.426 mm	(0.0168 in.)	
T Average	: 855.9	(J_{IC} at 0.15)	
K_{jc}	: 388.3 MPa–m$^{0.5}$		

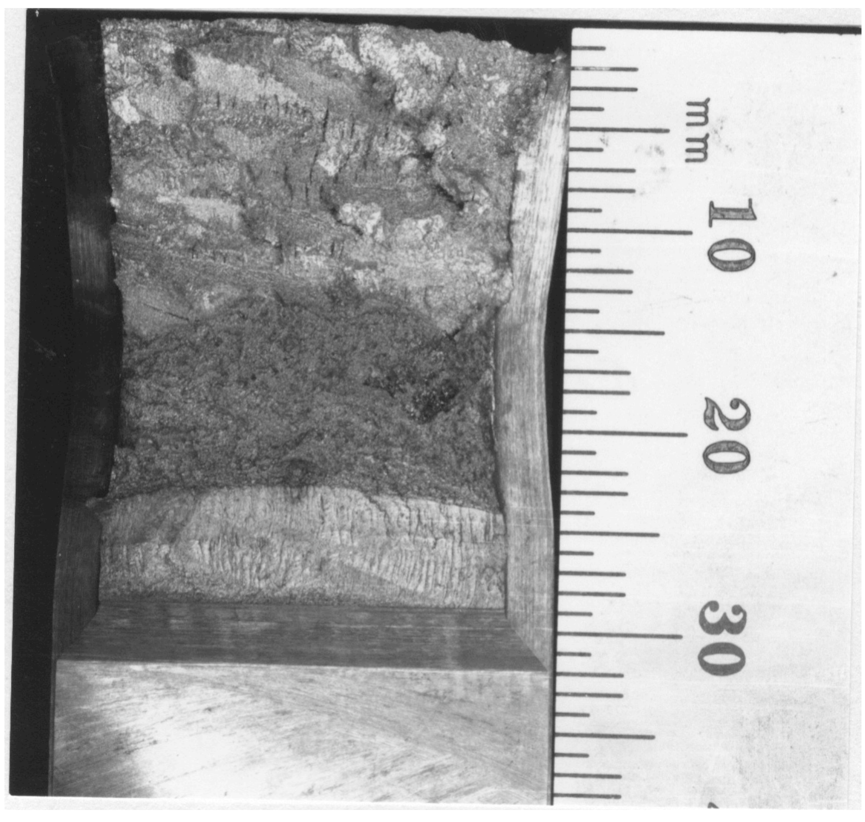

Figure C–8. Fracture surface of recovery–annealed material from the cold–leg check valve CA4 tested at 290°C

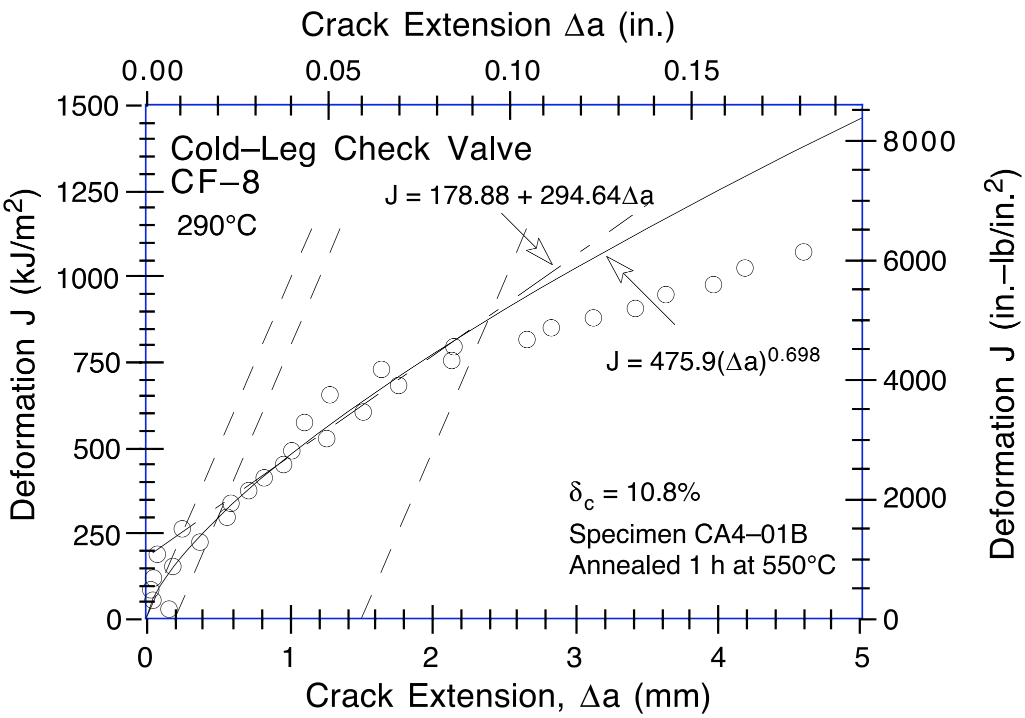

Figure C–9. Deformation J–R Curve at 290°C for material from the cold–leg check valve CA4 annealed for 1 h at 550°C and water quenched

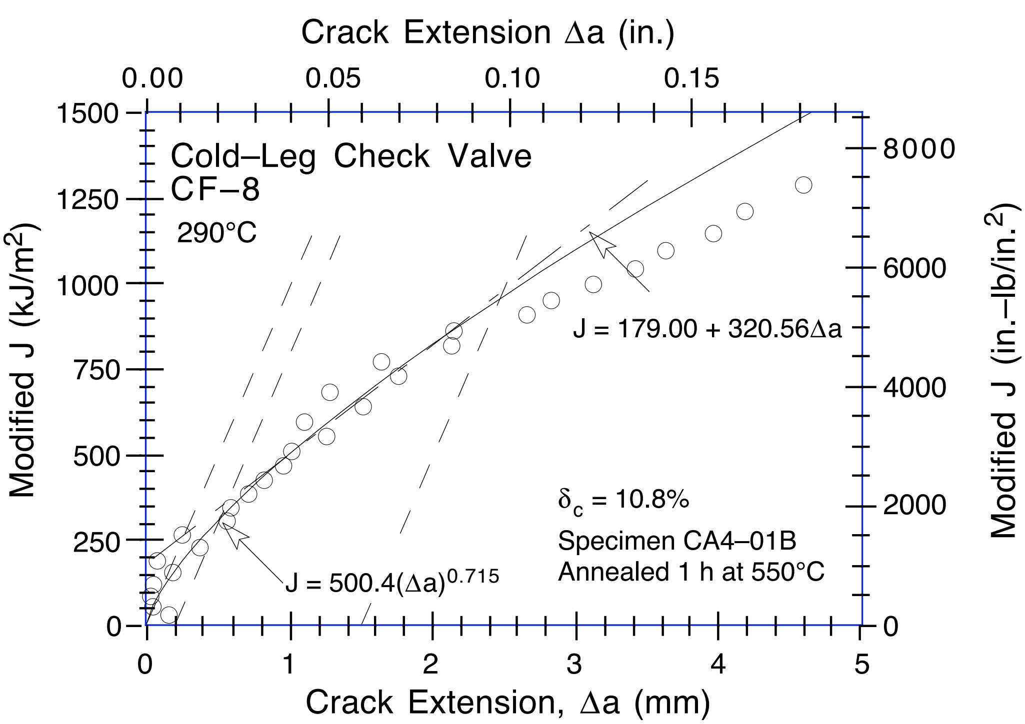

Figure C–10. Modified J–R Curve at 290°C for material from the cold–leg check valve CA4 annealed for 1 h at 550°C and water quenched

Table C–11. Test data for specimen CA4–02B

Test Number	: 0065	Test Temp.	: 290°C
Material Type	: CF–8	Heat Number	: CA
Aging Temp.	: 264°C	Aging Time	: 113,900 h
Spec. Thickness	: 25.37 mm	Net. Thickness	: 20.30 mm
Spec. Width	: 50.80 mm	Flow Stress	: 251.10 MPa

Unload Number	J_d (kJ/m^2)	J_m (kJ/m^2)	Δa (mm)	Load (kN)	Deflection (mm)
1	7.42	7.41	–0.0503	12.495	0.262
2	20.60	20.69	0.0554	14.193	0.455
3	35.74	35.87	0.0819	15.220	0.659
4	51.63	51.75	0.0796	15.950	0.859
5	67.90	68.64	0.2515	16.622	1.058
6	90.30	89.97	0.0347	17.224	1.312
7	113.18	111.91	–0.1169	17.849	1.556
8	134.80	136.39	0.2590	18.354	1.809
9	158.95	159.04	0.0942	18.834	2.060
10	181.67	183.38	0.2480	19.247	2.301
11	213.90	212.98	0.0345	19.769	2.606
12	247.31	243.83	–0.1444	20.089	2.909
13	271.94	276.75	0.3755	20.562	3.209
14	304.30	306.96	0.2552	20.905	3.510
15	334.11	340.63	0.4496	21.247	3.810
16	364.73	373.69	0.5622	21.480	4.110
17	394.08	407.87	0.7661	21.729	4.410
18	427.80	441.49	0.7621	21.974	4.709
19	458.89	476.77	0.9131	22.197	5.008
20	493.65	511.76	0.9205	22.433	5.309
21	519.37	549.26	1.2886	22.535	5.613
22	551.92	583.92	1.3506	22.572	5.910
23	588.73	620.22	1.3366	22.609	6.211
24	615.36	657.90	1.6233	22.593	6.510
25	652.20	692.91	1.5784	22.670	6.806
26	671.68	733.07	2.0614	22.533	7.116
27	703.54	767.60	2.1208	22.499	7.409
28	728.66	812.71	2.5423	22.278	7.757
29	765.72	855.11	2.6491	22.009	8.107
30	794.90	906.37	3.0662	21.676	8.507
31	840.26	954.39	3.1137	21.610	8.905
32	867.30	1007.21	3.5503	21.239	9.311
33	909.20	1068.70	3.8622	20.760	9.807
34	949.05	1131.46	4.2061	20.246	10.311
35	991.94	1205.99	4.6509	19.737	10.909
36	1037.69	1278.64	5.0059	18.917	11.511
37	1070.75	1363.07	5.6427	18.110	12.210
38	1110.87	1444.01	6.1182	17.203	12.910
39	1148.95	1524.53	6.5846	16.654	13.607
40	1183.54	1604.70	7.0582	16.074	14.307
41	1217.87	1684.53	7.5061	15.465	15.011
42	1231.04	1762.46	8.1139	14.286	15.716

Table C-12. Deformation J_{IC} and J–R curve results for specimen CA4–02B

Test Number	: 0065	Test Temp.	: 290°C
Material Type	: CF–8	Heat Number	: CA
Aging Temp.	: 264°C	Aging Time	: 113,900 h
Spec. Thickness	: 25.37 mm	Net. Thickness	: 20.30 mm
Spec. Width	: 50.80 mm	Flow Stress	: 251.10 MPa
Modulus E	: 167.75 GPa	(Effective)	
Modulus E	: 180.00 GPa	(Nominal)	
Init. Crack	: 29.1094 mm	Init. a/w	: 0.5730 (Measured)
Final Crack	: 38.0859 mm	Final a/w	: 0.7497 (Measured)
Final Crack	: 37.2233 mm	Final a/w	: 0.7327 (Compliance)
Linear Fit	**J = B+M(Δa)**		
Intercept B	: 264.390 kJ/m^2	Slope M	: 213.91 kJ/m^{2}mm
Fit Coeff. R	: 0.9692	(12 Data Points)	
J_{IC}	: 335.9 kJ/m^2	(1918.2 in.–lb/in.^{2})	
Δa (J_{IC})	: 0.334 mm	(0.0132 in.)	
T Average	: 569.1	(J_{IC} at 0.15)	
Power–Law Fit	**J = C(Δa)^n**		
Coeff. C	: 483.95 kJ/m^2	Exponent n	: 0.5038
Fit Coeff. R	: 0.9790	(12 Data Points)	
J_{IC} (0.20)	: 361.2 kJ/m^2	(2062.8 in.–lb/in.^{2})	
Δa (J_{IC})	: 0.560 mm	(0.0220 in.)	
T Average	: 567.5	(J_{IC} at 0.20)	
J_{IC} (0.15)	: 335.9 kJ/m^2	(1918.1 in.–lb/in.^{2})	
Δa (J_{IC})	: 0.484 mm	(0.0191 in.)	
T Average	: 578.3	(J_{IC} at 0.15)	
K_{jc}	: 348.3 MPa–m$^{0.5}$		
J_{IC} Validity & Data Qualification (E 813–85)			
J_{max} Allowed	: 363.13 kJ/m^2	($J_{max}=b_o\sigma_f/15$)	
Data Limit	: J_{max} Ignored		
Δa (max) Allowed	: 2.220 mm	(at 1.5 Exclusion Line)	
Data Limit	: 1.5 Exclusion Line		
Data Points	: Zone A = 5	Zone B = 3	
Data Point Spacing	: OK		
$b_{net.}$ or b_o Size	: Inadequate		
dJ/da at J_{IC}	: OK		
a_f Measurement	: Near–surface	Outside Limit	
Initial Crack Shape	: OK		
Crack Size Estimate	: Inadequate	(by Compliance)	
E Effective	: OK		
J_{IC} Estimate	: Invalid		
J–R Curve Validity & Data Qualification (E 1152–86)			
J_{max} Allowed	: 254.89 kJ/m^2	($J_{max}=b_{net}\sigma_f/20$)	
Δa (max) Allowed	: 2.169 mm	($\Delta a=0.1b_o$)	
Δa (max) Allowed	: 4.650 mm	($\omega=5$)	
Data Points	: Zone A = 21	Zone B = 3	
Data Point Spacing	: Inadequate		
J–R Curve Data	: Invalid		

Table C-13. Modified J_{IC} and J–R curve results for specimen CA4–02B

Linear Fit	**$J = B+M(\Delta a)$**		
Intercept B	: 250.099 kJ/m^2	Slope M	: 249.63 kJ/m^{2}mm
Fit Coeff. R	: 0.9787	(12 Data Points)	
J_{IC}	: 332.8 kJ/m^2	(1900.4 in.–lb/in.^{2})	
Δa (J_{IC})	: 0.331 mm	(0.0130 in.)	
T Average	: 664.2	(J_{IC} at 0.15)	
Power–Law Fit	**$J = C(\Delta a)^n$**		
Coeff. C	: 506.05 kJ/m^2	Exponent n	: 0.5519
Fit Coeff. R	: 0.9843	(12 Data Points)	
J_{IC} (0.20)	: 370.8 kJ/m^2	(2117.1 in.–lb/in.^{2})	
Δa (J_{IC})	: 0.569 mm	(0.0224 in.)	
T Average	: 649.3	(J_{IC} at 0.20)	
J_{IC} (0.15)	: 341.3 kJ/m^2	(1948.7 in.–lb/in.^{2})	
Δa (J_{IC})	: 0.490 mm	(0.0193 in.)	
T Average	: 660.6	(J_{IC} at 0.15)	
K_{jc}	: 366.5 MPa–m$^{0.5}$		

Figure C–11. Fracture surface of the cold–leg check valve CA4 tested at 290°C after 13 y of service at 264°C

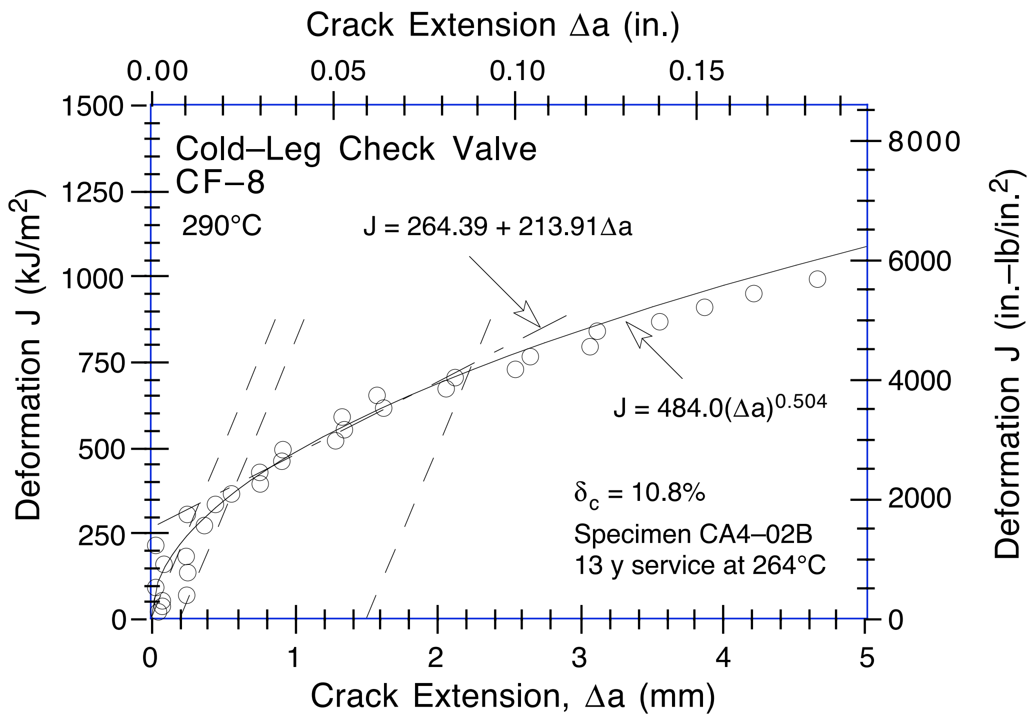

Figure C–12. Deformation J–R Curve at 290°C for the cold–leg check valve CA4 after 13 y of service at 264°C

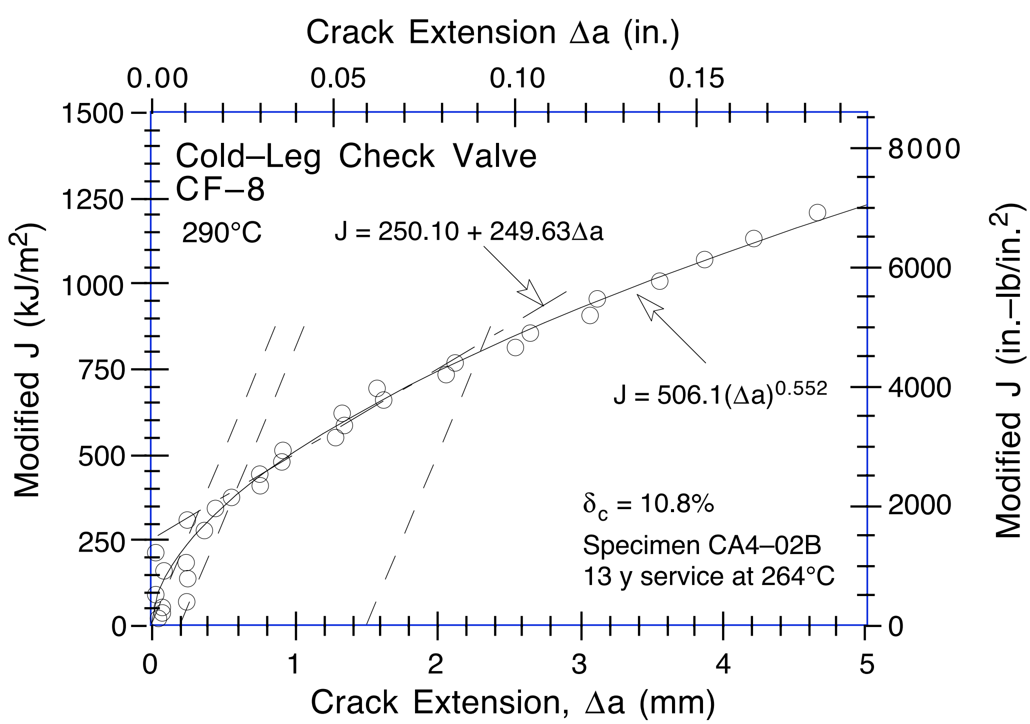

Figure C–13. Modified J–R Curve at 290°C for the cold–leg check valve CA4 after 13 y of service at 264°C

Table C–14. Test data for specimen MA1–01T

Test Number	: 0069	Test Temp.	: 25°C
Material Type	: CF–8	Heat Number	: MA1
Aging Temp.	: 281°C	Aging Time	: 113,000 h
Spec. Thickness	: 25.37 mm	Net Thickness	: 20.35 mm
Spec. Width	: 50.79 mm	Flow Stress	: 345.10 MPa

Unload Number	J_d (kJ/m^2)	J_m (kJ/m^2)	Δa (mm)	Load (kN)	Deflection (mm)
1	11.84	11.85	0.0128	16.366	0.252
2	30.78	30.80	0.0281	19.915	0.455
3	57.67	57.85	0.0881	21.696	0.705
4	92.85	92.53	–0.0170	23.015	1.008
5	137.27	136.91	–0.0232	24.195	1.369
6	179.84	180.98	0.1295	25.167	1.709
7	224.69	227.23	0.2399	25.867	2.060
8	272.46	273.87	0.1670	26.653	2.408
9	322.98	323.34	0.1101	27.361	2.760
10	372.52	374.12	0.1676	27.868	3.111
11	420.96	425.89	0.3026	28.473	3.461
12	473.76	476.84	0.2362	29.060	3.809
13	524.39	531.80	0.3755	29.563	4.160
14	601.71	601.56	0.1634	30.241	4.624
15	660.17	664.56	0.2786	30.627	5.006
16	723.89	730.60	0.3323	31.034	5.418
17	784.04	794.83	0.4188	31.560	5.808
18	846.69	861.36	0.4945	31.986	6.207
19	913.52	929.49	0.5182	32.232	6.611
20	976.92	998.26	0.6084	32.650	7.008
21	1039.11	1068.69	0.7378	33.060	7.410
22	1109.17	1138.75	0.7378	33.359	7.814
23	1170.34	1210.82	0.8887	33.456	8.211
24	1232.78	1282.49	1.0091	33.459	8.612
25	1300.03	1354.35	1.0660	33.766	9.012
26	1367.20	1427.95	1.1412	33.958	9.413
27	1423.26	1502.51	1.3473	33.789	9.811
28	1486.29	1576.52	1.4638	34.092	10.214
29	1558.63	1649.70	1.4724	34.080	10.610
30	1617.17	1727.00	1.6535	33.926	11.013
31	1673.27	1802.79	1.8362	33.766	11.419
32	1715.21	1877.10	2.1254	33.221	11.813
33	1761.51	1951.61	2.3682	32.666	12.218
34	1813.34	2023.95	2.5385	32.677	12.611
35	1870.65	2098.52	2.6765	32.558	13.011
36	1933.07	2193.93	2.9293	32.435	13.510
37	2021.26	2286.51	2.9613	32.257	14.011
38	2091.92	2405.15	3.2949	31.685	14.619
39	2157.06	2514.90	3.5917	30.825	15.209
40	2204.51	2625.72	3.9963	29.938	15.807

Table C-15. Deformation J_{IC} and J–R curve results for specimen MA1–01T

Test Number	: 0069	Test Temp.	: 25°C
Material Type	: CF–8	Heat Number	: MA1
Aging Temp.	: 281°C	Aging Time	: 113,000 h
Spec. Thickness	: 25.37 mm	Net Thickness	: 20.35 mm
Spec. Width	: 50.79 mm	Flow Stress	: 345.10 MPa
Modulus E	: 171.88 GPa	(Effective)	
Modulus E	: 193.10 GPa	(Nominal)	
Init. Crack	: 29.5250 mm	Init. a/w	: 0.5813 (Measured)
Final Crack	: 35.0469 mm	Final a/w	: 0.6901 (Measured)
Final Crack	: 33.5213 mm	Final a/w	: 0.6600 (Compliance)
Linear Fit	**$J = B+M(\Delta a)$**		
Intercept B	: 1033.794 kJ/m^2	Slope M	: 321.35 kJ/m^2mm
Fit Coeff. R	: 0.9804	(11 Data Points)	
J_{IC}	: 1347.5 kJ/m^2	(7694.4 in.–lb/in.^{2})	
Δa (J_{IC})	: 0.976 mm	(0.0384 in.)	
T Average	: 463.8	(J_{IC} at 0.15)	
Power–Law Fit	**$J = C(\Delta a)^n$**		
Coeff. C	: 1306.41 kJ/m^2	Exponent n	: 0.3742
Fit Coeff. R	: 0.9824	(11 Data Points)	
J_{IC} (0.20)	: 1407.0 kJ/m^2	(8034.4 in.–lb/in.^{2})	
Δa (J_{IC})	: 1.219 mm	(0.0480 in.)	
T Average	: 456.3	(J_{IC} at 0.20)	
J_{IC} (0.15)	: 1374.7 kJ/m^2	(7849.9 in.–lb/in.^{2})	
Δa (J_{IC})	: 1.146 mm	(0.0451 in.)	
T Average	: 462.5	(J_{IC} at 0.15)	
K_{jc}	: 578.8 MPa–$m^{0.5}$		
J_{IC} Validity & Data Qualification (E 813–85)			
J_{max} Allowed	: 489.17 kJ/m^2	($J_{max}=b_o\sigma_f/15$)	
Data Limit	: J_{max} Ignored		
Δa (max) Allowed	: 2.912 mm	(at 1.5 Exclusion Line)	
Data Limit	: 1.5 Exclusion Line		
Data Points	: Zone A = 5	Zone B = 4	
Data Point Spacing	: OK		
b_{net} or b_o Size	: Inadequate		
dJ/da at J_{IC}	: OK		
a_o Measurement	: 6 Outside Limit		
a_f Measurement	: Near–surface	Outside Limit	
Crack Size Estimate	: Inadequate	(by Compliance)	
E Effective	: Inadequate		
J_{IC} Estimate	: Invalid		
J–R Curve Validity & Data Qualification (E 1152–86)			
J_{max} Allowed	: 351.05 kJ/m^2	($J_{max}=b_{net}\sigma_f/20$)	
Δa (max) Allowed	: 2.126 mm	($\Delta a=0.1b_o$)	
Δa (max) Allowed	: 3.536 mm	($\omega=5$)	
Data Points	: Zone A = 38	Zone B = 0	
Data Point Spacing	: Inadequate		
J–R Curve Data	: Invalid		

Table C-16. Modified J_{IC} and J–R curve results for specimen MA1–01T

Linear Fit	**$J = B+M(\Delta a)$**		
Intercept B	: 991.938 kJ/m^2	Slope M	: 418.39 kJ/m^{2}mm
Fit Coeff. R	: 0.9887	(11 Data Points)	
J_{IC}	: 1423.3 kJ/m^2	(8127.6 in.–lb/in.^{2})	
Δa (J_{IC})	: 1.031 mm	(0.0406 in.)	
T Average	: 603.8	(J_{IC} at 0.15)	
Power–Law Fit	**$J = C(\Delta a)^n$**		
Coeff. C	: 1340.18 kJ/m^2	Exponent n	: 0.4620
Fit Coeff. R	: 0.9883	(11 Data Points)	
J_{IC} (0.20)	: 1509.3 kJ/m^2	(8618.4 in.–lb/in.^{2})	
Δa (J_{IC})	: 1.293 mm	(0.0509 in.)	
T Average	: 590.5	(J_{IC} at 0.20)	
J_{IC} (0.15)	: 1463.8 kJ/m^2	(8358.4 in.–lb/in.^{2})	
Δa (J_{IC})	: 1.210 mm	(0.0477 in.)	
T Average	: 597.8	(J_{IC} at 0.15)	
K_{jc}	: 625.6 MPa–m$^{0.5}$		

Figure C–14. Fracture surface of the hot–leg main shutoff valve MA1 tested at room temperature after 13 y of service at 281°C

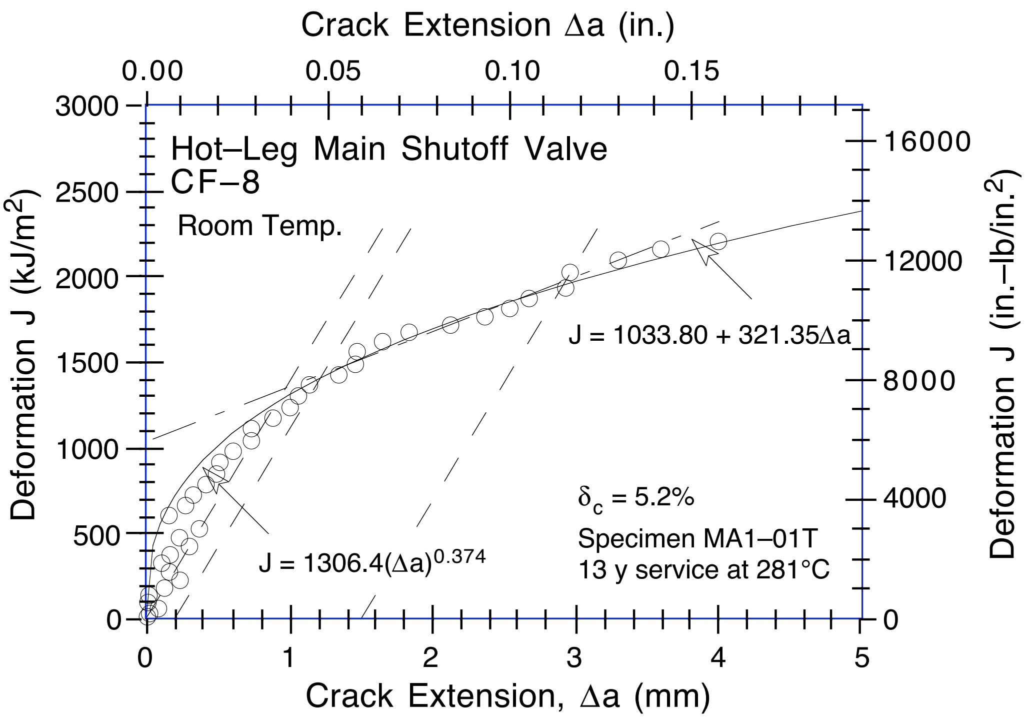

Figure C–15. Deformation J–R Curve at room temperature for hot–leg main shutoff valve MA1 after 13 y of service at 281°C

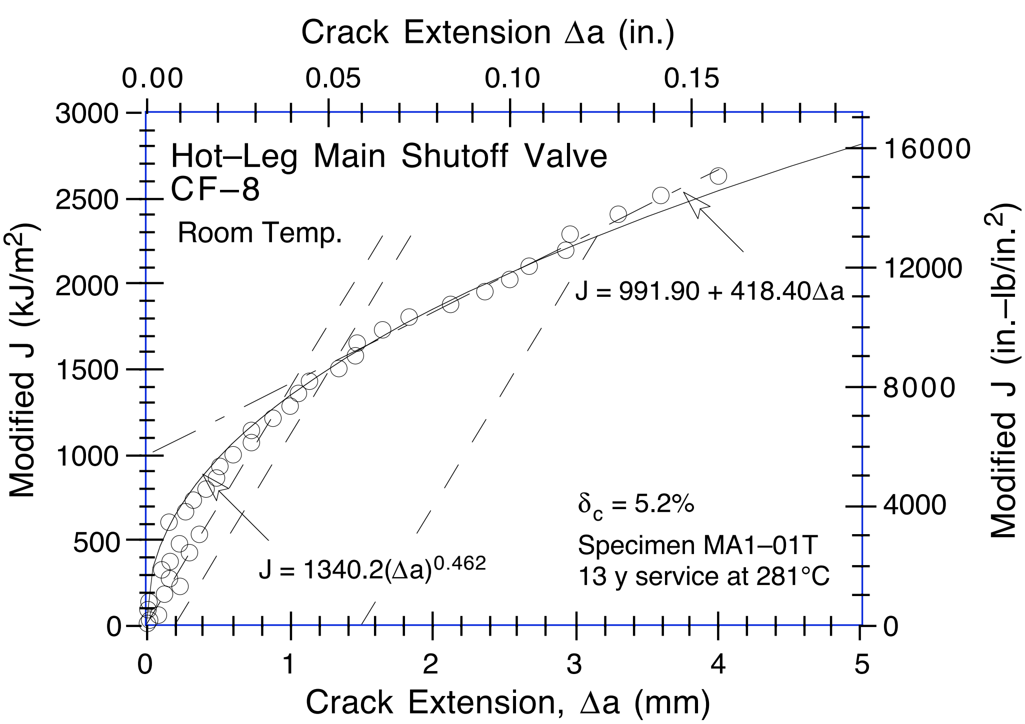

Figure C–16. Modified J–R Curve at room temperature for hot–leg main shutoff valve MA1 after 13 y of service at 281°C

Table C–17. Test data for specimen MA1–01B

Test Number	: 0067	Test Temp.	: 290°C
Material Type	: CF–8	Heat Number	: MA1
Aging Temp.	: 281°C	Aging Time	: 113,900 h
Spec. Thickness	: 25.37 mm	Net. Thickness	: 20.38 mm
Spec. Width	: 50.80 mm	Flow Stress	: 237.00 MPa

Unload Number	J_d (kJ/m^2)	J_m (kJ/m^2)	Δa (mm)	Load (kN)	Deflection (mm)
1	9.39	9.38	–0.0214	11.823	0.254
2	26.52	26.36	–0.1457	13.772	0.508
3	49.22	49.79	0.1382	14.947	0.808
4	72.96	73.75	0.1933	15.643	1.109
5	98.15	99.05	0.2142	16.339	1.409
6	129.56	129.63	0.1026	16.977	1.759
7	161.91	161.65	0.0677	17.485	2.109
8	199.41	199.61	0.1067	18.030	2.510
9	236.99	238.51	0.1997	18.655	2.909
10	277.42	278.16	0.1535	19.138	3.309
11	316.18	320.03	0.3158	19.646	3.710
12	359.11	361.24	0.2369	20.093	4.108
13	398.27	405.57	0.4489	20.452	4.508
14	433.97	436.72	0.2768	20.754	4.805
15	466.85	471.89	0.3568	21.003	5.111
16	495.41	506.75	0.5626	21.339	5.414
17	535.57	538.65	0.3118	21.508	5.709
18	562.16	576.16	0.6243	21.654	6.013
19	615.62	620.49	0.3843	21.970	6.413
20	650.45	670.24	0.7502	22.151	6.809
21	690.95	717.47	0.9047	22.282	7.209
22	735.36	765.99	0.9930	22.500	7.608
23	780.98	822.66	1.2140	22.620	8.059
24	838.06	878.38	1.1886	22.737	8.513
25	889.51	942.46	1.4082	22.542	9.010
26	944.76	1004.02	1.5108	21.984	9.508
27	980.62	1080.44	2.1305	21.605	10.112
28	1012.14	1153.63	2.7324	21.232	10.709
29	1079.84	1224.93	2.7809	20.460	11.309
30	1096.91	1299.61	3.5203	19.713	11.907
31	1124.54	1369.97	4.0426	19.155	12.510
32	1173.30	1440.84	4.2982	18.779	13.111
33	1215.49	1513.82	4.6361	18.569	13.710
34	1265.56	1586.37	4.8704	18.530	14.310
35	1313.76	1660.67	5.1287	18.154	14.912
36	1355.27	1733.76	5.4269	17.716	15.511
37	1379.60	1806.70	5.8673	17.041	16.113
38	1393.61	1877.15	6.3600	16.503	16.714

Table C–18. Deformation J_{IC} and J–R curve results for specimen MA1–01B

Test Number	: 0067	Test Temp.	: 290°C
Material Type	: CF–8	Heat Number	: MA1
Aging Temp.	: 281°C	Aging Time	: 113,900 h
Spec. Thickness	: 25.37 mm	Net. Thickness	: 20.38 mm
Spec. Width	: 50.80 mm	Flow Stress	: 237.00 MPa
Modulus E	: 150.48 GPa	(Effective)	
Modulus E	: 180.00 GPa	(Nominal)	
Init. Crack	: 30.0063 mm	Init. a/w	: 0.5907 (Measured)
Final Crack	: 37.8844 mm	Final a/w	: 0.7458 (Measured)
Final Crack	: 36.3663 mm	Final a/w	: 0.7159 (Compliance)

Linear Fit	**$J = B+M(\Delta a)$**		
Intercept B	: 517.242 kJ/m^2	Slope M	: 239.53 kJ/m^2mm
Fit Coeff. R	: 0.9099	(7 Data Points)	
J_{IC}	: 692.1 kJ/m^2	(3952.1 in.–lb/in.^{2})	
Δa (J_{IC})	: 0.730 mm	(0.0287 in.)	
T Average	: 641.7	(J_{IC} at 0.15)	

Power–Law Fit	**$J = C(\Delta a)^n$**		
Coeff. C	: 745.68 kJ/m^2	Exponent n	: 0.4291
Fit Coeff. R	: 0.9422	(7 Data Points)	
J_{IC} (0.20)	: 739.1 kJ/m^2	(4220.6 in.–lb/in.^{2})	
Δa (J_{IC})	: 0.980 mm	(0.0386 in.)	
T Average	: 617.5	(J_{IC} at 0.20)	
J_{IC} (0.15)	: 713.7 kJ/m^2	(4075.2 in.–lb/in.^{2})	
Δa (J_{IC})	: 0.903 mm	(0.0355 in.)	
T Average	: 627.0	(J_{IC} at 0.15)	
K_{jc}	: 414.7 MPa–$m^{0.5}$		

J_{IC} Validity & Data Qualification (E 813–85)

J_{max} Allowed	: 328.46 kJ/m^2	($J_{max}=b_o\sigma_f/15$)
Data Limit	: J_{max} Ignored	
Δa (max) Allowed	: 2.706 mm	(at 1.5 Exclusion Line)
Data Limit	: 1.5 Exclusion Line	
Data Points	: Zone A = 5	Zone B = 1
Data Point Spacing	: OK	
$b_{net.}$ or b_o Size	: Inadequate	
dJ/da at J_{IC}	: OK	
a_o Measurement	: 9 Outside Limit	
Final Crack Shape	: OK	
Crack Size Estimate	: Inadequate	(by Compliance)
E Effective	: Inadequate	
J_{IC} Estimate	: Invalid	

J–R Curve Validity & Data Qualification (E 1152–86)

J_{max} Allowed	: 241.48 kJ/m^2	($J_{max}=b_{net}\sigma_f/20$)
Δa (max) Allowed	: 2.079 mm	($\Delta a=0.1b_o$)
Δa (max) Allowed	: 4.014 mm	($\omega=5$)
Data Points	: Zone A = 27	Zone B = 0
Data Point Spacing	: Inadequate	
J–R Curve Data	: Invalid	

Table C–19. Modified J_{IC} and J–R curve results for specimen MA–01B

Linear Fit	**J = B+M(Δa)**		
Intercept B	: 573.082 kJ/m^2	Slope M	: 241.16 kJ/m^2mm
Fit Coeff. R	: 0.9658	(7 Data Points)	
J_{IC}	: 768.6 kJ/m^2	(4388.9 $in.–lb/in.^2$)	
Δa (J_{IC})	: 0.811 mm	(0.0319 in.)	
T Average	: 646.1	(J_{IC} at 0.15)	
Power–Law Fit	**$J = C(\Delta a)^n$**		
Coeff. C	: 791.71 kJ/m^2	Exponent n	: 0.4383
Fit Coeff. R	: 0.9735	(7 Data Points)	
J_{IC} (0.20)	: 810.5 kJ/m^2	(4628.1 $in.–lb/in.^2$)	
Δa (J_{IC})	: 1.055 mm	(0.0415 in.)	
T Average	: 654.3	(J_{IC} at 0.20)	
J_{IC} (0.15)	: 783.5 kJ/m^2	(4473.9 $in.–lb/in.^2$)	
Δa (J_{IC})	: 0.976 mm	(0.0384 in.)	
T Average	: 663.7	(J_{IC} at 0.15)	
K_{jc}	: 433.0 $MPa–m^{0.5}$		

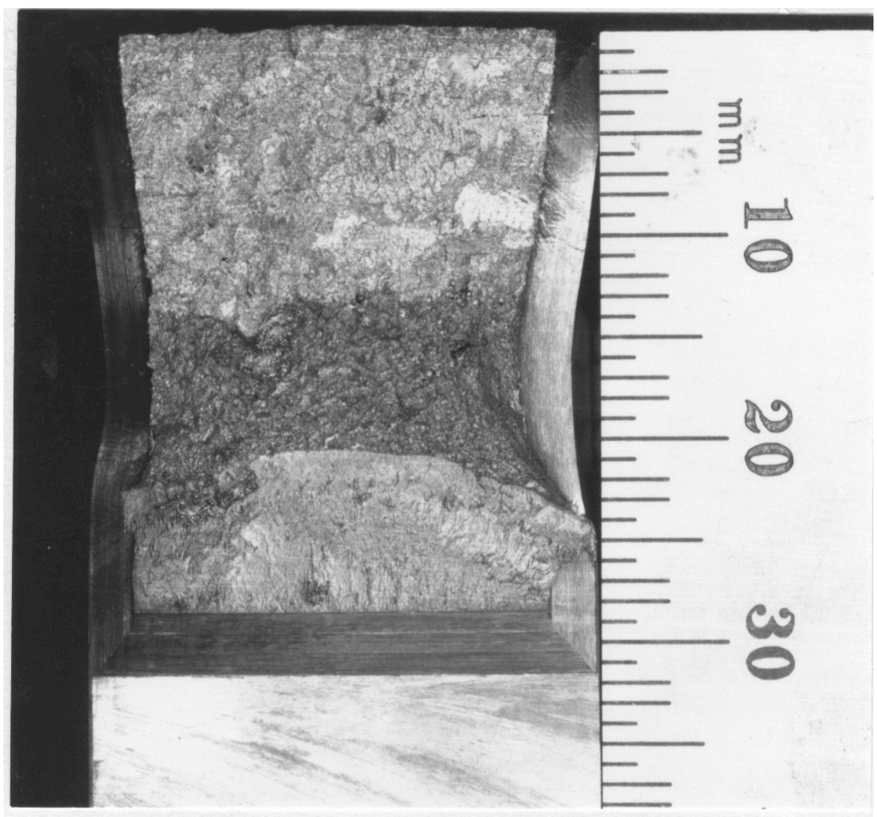

Figure C–17. Fracture surface of the hot–leg main shutoff valve MA1 tested at 290°C after 13 y of service at 281°C

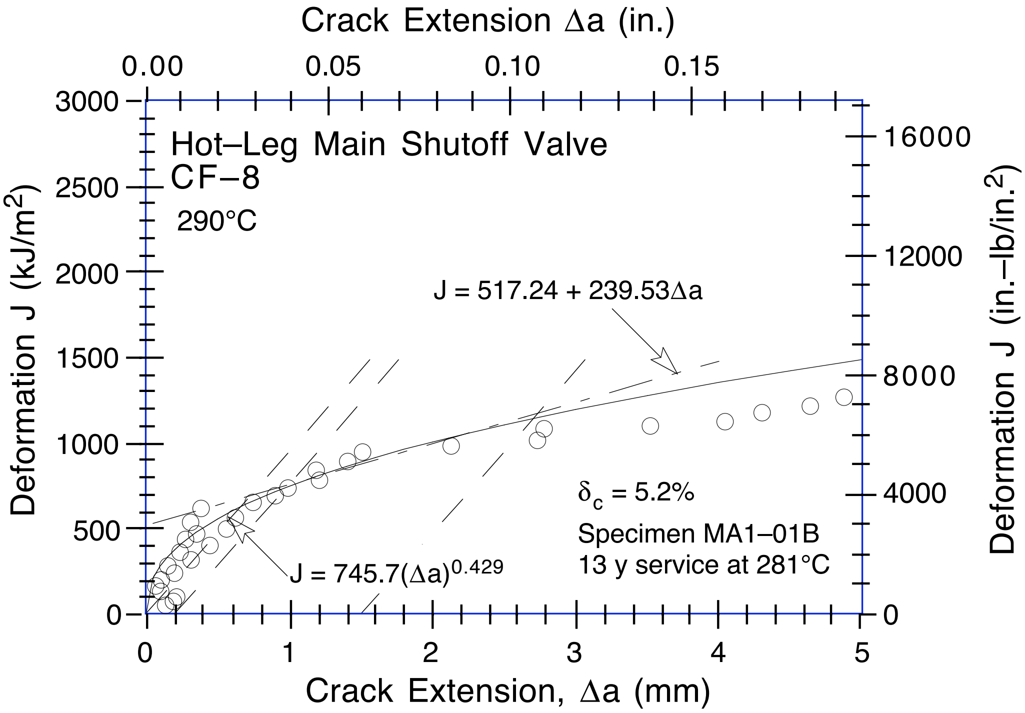

Figure C–18. Deformation J–R Curve at 290°C for hot–leg main shutoff valve MA1 after 13 y of service at 281°C

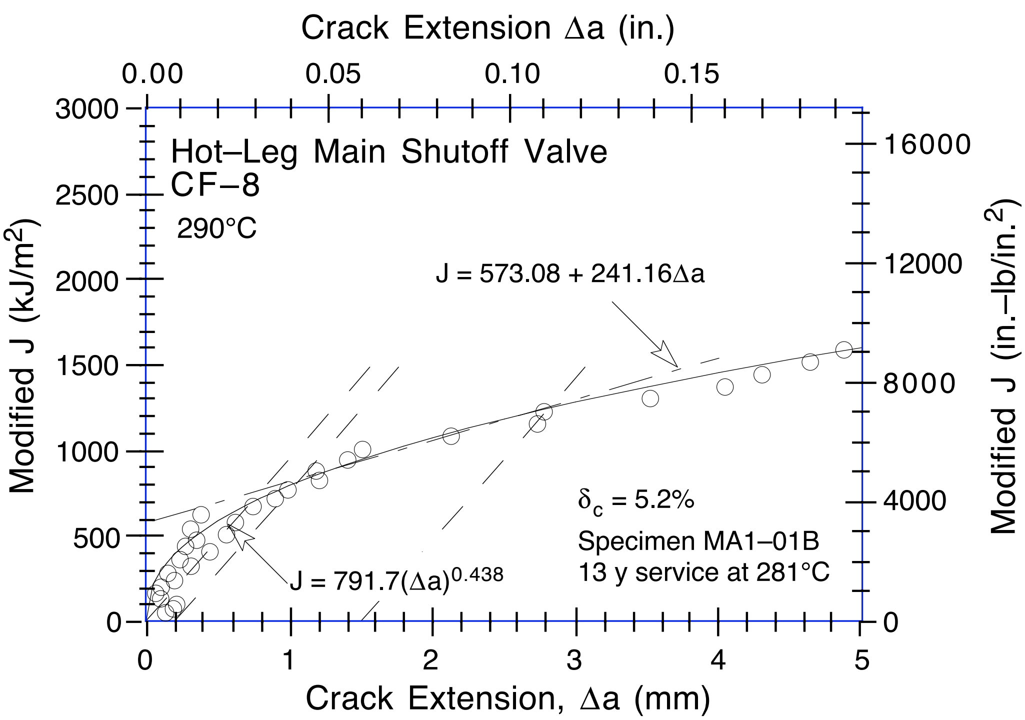

Figure C–19. Modified J–R Curve at 290°C for hot–leg main shutoff valve MA1 after 13 y of service at 281°C

Table C–20. Test data for specimen MA9–01I

Test Number	: 0083	Test Temp.	: 25°C
Material Type	: CF–8	Heat Number	: MA9
Aging Temp.	: 25°C	Aging Time	: 0 h
Spec. Thickness	: 25.34 mm	Net Thickness	: 20.27 mm
Spec. Width	: 50.81 mm	Flow Stress	: 366.00 MPa

Unload Number	J_d (kJ/m^2)	J_m (kJ/m^2)	Δa (mm)	Load (kN)	Deflection (mm)
1	16.82	16.83	0.0255	19.187	0.304
2	46.22	46.21	0.0167	22.320	0.607
3	78.35	78.63	0.0964	23.812	0.908
4	112.35	113.19	0.1986	24.799	1.214
5	147.36	147.02	0.0393	25.494	1.510
6	184.39	184.23	0.0571	26.045	1.816
7	219.75	220.54	0.1414	26.670	2.110
8	270.35	270.76	0.1141	27.718	2.510
9	321.69	323.39	0.1902	28.289	2.913
10	386.89	389.70	0.2442	29.109	3.409
11	455.87	458.36	0.2312	29.822	3.909
12	529.20	528.65	0.1244	30.726	4.410
13	596.68	602.53	0.3218	31.378	4.910
14	668.64	676.56	0.3786	32.067	5.413
15	748.51	752.16	0.2739	32.792	5.916
16	820.70	830.46	0.4098	33.497	6.412
17	899.51	908.72	0.3985	34.290	6.911
18	977.70	990.46	0.4645	34.755	7.414
19	1059.12	1071.90	0.4647	35.147	7.911
20	1137.47	1157.32	0.5769	35.540	8.418
21	1214.16	1240.75	0.6763	36.110	8.910
22	1307.18	1326.67	0.5789	36.579	9.418
23	1382.19	1413.97	0.7377	36.800	9.909
24	1459.66	1501.96	0.8660	37.299	10.410
25	1523.38	1572.78	0.9487	37.677	10.809
26	1612.05	1692.10	1.2824	37.832	11.459
27	1724.81	1788.62	1.1166	38.341	12.009
28	1813.65	1905.24	1.3840	38.224	12.619
29	1886.33	2015.73	1.7299	38.100	13.212
30	1969.53	2127.08	1.9742	37.492	13.815
31	2041.85	2243.89	2.3420	36.888	14.440
32	2110.11	2349.54	2.6381	36.658	15.014
33	2161.14	2460.99	3.0974	35.475	15.614

Table C–21. Deformation J_{IC} and J–R curve results for specimen MA9–01I

Test Number	: 0083	Test Temp.	: 25°C
Material Type	: CF–8	Heat Number	: MA9
Aging Temp.	: 25°C	Aging Time	: 0 h
Spec. Thickness	: 25.34 mm	Net Thickness	: 20.27 mm
Spec. Width	: 50.81 mm	Flow Stress	: 366.00 MPa
Modulus E	: 147.60 GPa	(Effective)	
Modulus E	: 193.10 GPa	(Nominal)	
Init. Crack	: 26.5500 mm	Init. a/w	: 0.5226 (Measured)
Final Crack	: 32.6188 mm	Final a/w	: 0.6420 (Measured)
Final Crack	: 29.6474 mm	Final a/w	: 0.5835 (Compliance)

Linear Fit	**$J = B+M(\Delta a)$**		
Intercept B	: 1221.790 kJ/m^2	Slope M	: 352.27 kJ/m^{2}mm
Fit Coeff. R	: 0.9616	(5 Data Points)	
J_{IC}	: 1608.9 kJ/m^2	(9187.3 in.–lb/in.^{2})	
Δa (J_{IC})	: 1.099 mm	(0.0433 in.)	
T Average	: 388.1	(J_{IC} at 0.15)	

Power–Law Fit	**$J = C(\Delta a)^n$**		
Coeff. C	: 1504.13 kJ/m^2	Exponent n	: 0.3667
Fit Coeff. R	: 0.9786	(5 Data Points)	
J_{IC} (0.20)	: 1677.1 kJ/m^2	(9576.5 in.–lb/in.^{2})	
Δa (J_{IC})	: 1.346 mm	(0.0530 in.)	
T Average	: 375.4	(J_{IC} at 0.20)	
J_{IC} (0.15)	: 1643.0 kJ/m^2	(9381.9 in.–lb/in.^{2})	
Δa (J_{IC})	: 1.272 mm	(0.0501 in.)	
T Average	: 380.2	(J_{IC} at 0.15)	
Kjc	: 577.9 MPa–m$^{0.5}$		

J_{IC} Validity & Data Qualification (E 813–85)

J_{max} Allowed	: 591.90 kJ/m^2	($J_{max}=b_o\sigma_f/15$)
Data Limit	: J_{max} Ignored	
Δa (max) Allowed	: 3.046 mm	(at 1.5 Exclusion Line)
Data Limit	: 1.5 Exclusion Line	
Data Points	: Zone A = 2	Zone B = 1
Data Point Spacing	: OK	
b_{net} or b_o Size	: Inadequate	
dJ/da at J_{IC}	: OK	
a_o Measurement	: 2 Outside Limit	
a_o Measurement	: 8 Outside Limit	
a_f Measurement	: Near–surface	Outside Limit
Crack Size Estimate	: Inadequate	(by Compliance)
E Effective	: Inadequate	
J_{IC} Estimate	: Invalid	

J–R Curve Validity & Data Qualification (E 1152–86)

J_{max} Allowed	: 370.92 kJ/m^2	($J_{max}=b_{net}\sigma_f//20$)
Δa (max) Allowed	: 2.426 mm	($\Delta a=0.1b_o$)
Δa (max) Allowed	: 3.472 mm	($\omega=5$)
Data Points	: Zone A = 33	Zone B = 0
Data Point Spacing	: Inadequate	
J–R Curve Data	*: Invalid*	

Table C–22. Modified J_{IC} and J–R curve results for specimen MA9–01I

Linear Fit	**$J = B+M(\Delta a)$**		
Intercept B	: 1475.937 kJ/m^2	Slope M	: 324.02 kJ/m^{2}mm
Fit Coeff. R	: 0.9946	(5 Data Points)	
J_{IC}	: 1895.5 kJ/m^2	(10823.4 in.–lb/in.^{2})	
Δa (J_{IC})	: 1.295 mm	(0.0510 in.)	
T Average	: 357.0	(J_{IC} at 0.15)	
Power–Law Fit	**$J = C(\Delta a)^n$**		
Coeff. C	: 1678.28 kJ/m^2	Exponent n	: 0.3421
Fit Coeff. R	: 0.9985	(5 Data Points)	
J_{IC} (0.20)	: 1938.5 kJ/m^2	(11069.5 in.–lb/in.^{2})	
Δa (J_{IC})	: 1.524 mm	(0.0600 in.)	
T Average	: 364.1	(J_{IC} at 0.20)	
J_{IC} (0.15)	: 1906.9 kJ/m^2	(10888.7 in.–lb/in.^{2})	
Δa (J_{IC})	: 1.453 mm	(0.0572 in.)	
T Average	: 368.5	(J_{IC} at 0.15)	
Kjc	: 607.5 MPa–m$^{0.5}$		

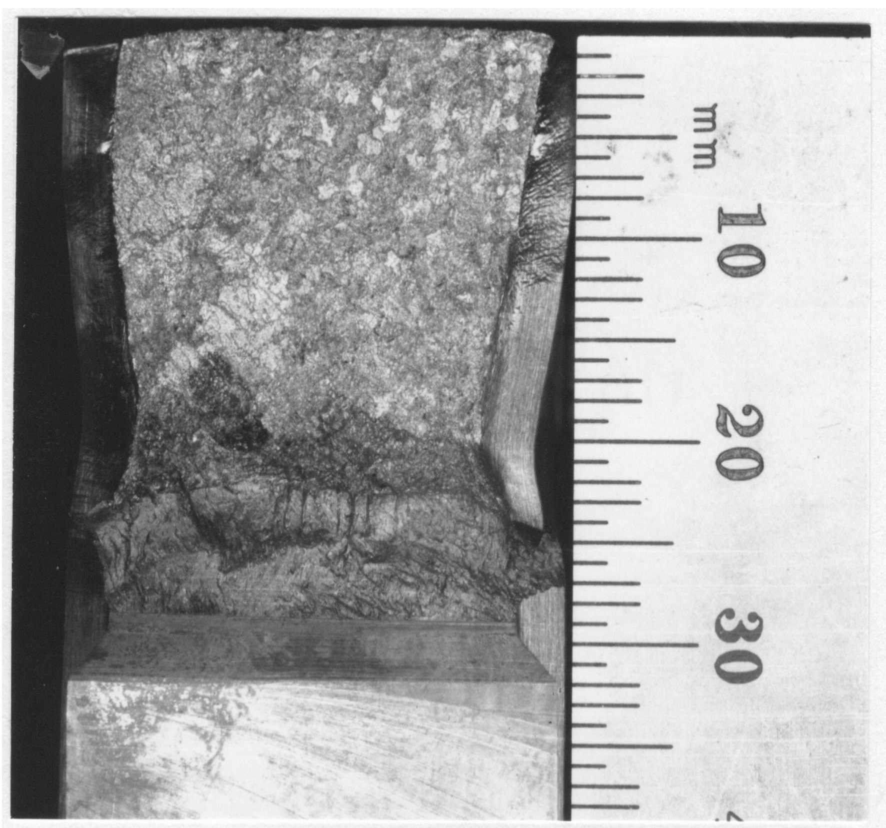

Figure C–20. Fracture surface of essentially unaged material MA9 from the hot–leg main shutoff valve tested at room temperature

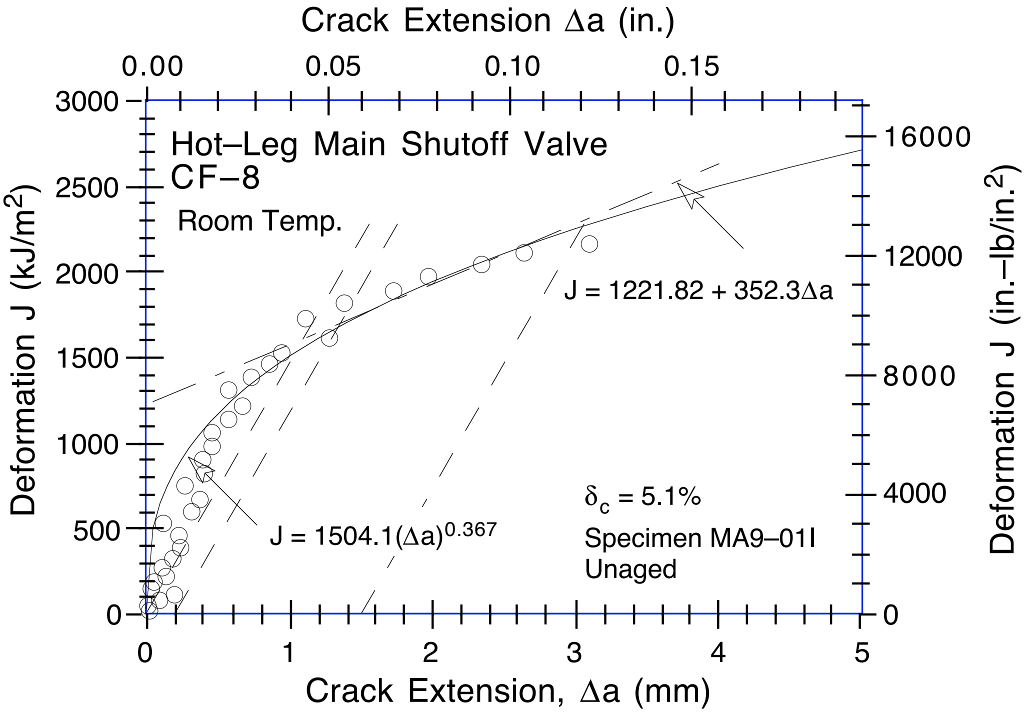

Figure C–21. Deformation J–R Curve at room temperature for essentially unaged material MA9 from the hot–leg main shutoff valve

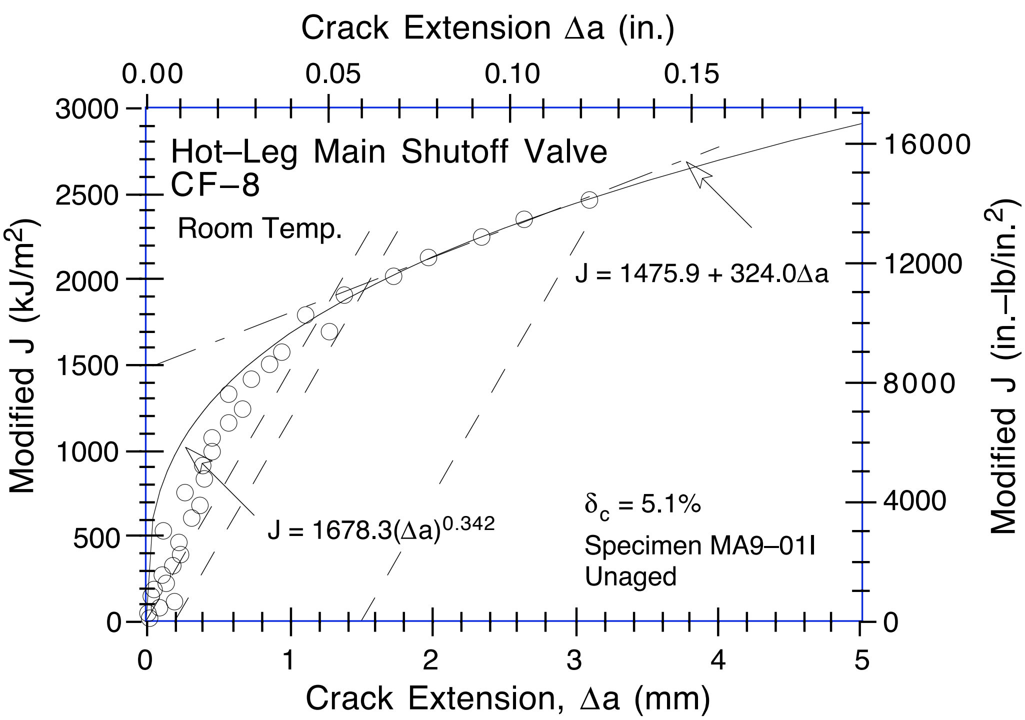

Figure C–22. Modified J–R Curve at room temperature for essentially unaged material MA9 from the hot–leg main shutoff valve

Table C–23. Test data for specimen MA9–02O

Test Number	: 0116	Test Temp	: 25 °C
Material Type	: CF-8	Heat Number	: MA9
Aging Temp	: 400 °C	Aging Time	: 10,000 h
Spec. Thickness	: 25.37 mm	Net Thickness	: 20.24 mm
Spec. Width	: 50.55 mm	Flow Stress	: 372.20 MPa

Unload Number	J_d (kJ/m^2)	J_m (kJ/m^2)	Δa (mm)	Load (kN)	Deflection (mm)
1	13.83	13.80	-0.0745	17.787	0.255
2	39.18	39.29	0.0088	21.269	0.505
3	73.62	73.81	0.0298	23.272	0.807
4	110.41	111.27	0.1450	24.780	1.107
5	149.59	150.41	0.1396	25.768	1.410
6	190.24	190.92	0.1266	26.590	1.708
7	232.68	232.80	0.0843	27.510	2.008
8	275.00	276.98	0.2024	28.108	2.309
9	319.73	320.70	0.1477	29.001	2.610
10	379.67	381.60	0.1907	29.732	3.007
11	443.28	443.94	0.1421	30.345	3.409
12	505.85	508.32	0.2028	31.312	3.808
13	550.62	557.78	0.3468	31.698	4.109
14	591.13	598.31	0.3474	32.044	4.358
15	631.50	640.92	0.4071	32.440	4.609
16	683.02	692.50	0.4084	32.890	4.913
17	736.11	743.00	0.3495	33.057	5.207
18	781.88	797.52	0.5354	33.372	5.511
19	833.29	849.02	0.5370	33.819	5.809
20	882.81	903.43	0.6285	34.209	6.110
21	936.42	957.81	0.6420	34.352	6.414
22	987.50	1012.30	0.6988	34.354	6.710
23	1033.67	1067.99	0.8490	34.790	7.010
24	1084.35	1123.10	0.9154	34.969	7.311
25	1133.63	1180.03	1.0247	34.952	7.614
26	1197.48	1254.08	1.1614	34.913	8.007
27	1247.27	1321.00	1.3803	34.590	8.359
28	1301.39	1386.13	1.5143	34.438	8.709
29	1343.73	1453.15	1.8017	33.969	9.059
30	1395.16	1517.71	1.9480	33.420	9.412
31	1437.91	1591.83	2.2820	32.406	9.807
32	1457.73	1665.33	2.8338	31.699	10.209
33	1507.88	1754.23	3.2127	30.890	10.707
34	1541.95	1847.34	3.7634	29.700	11.220
35	1577.40	1933.30	4.2147	28.848	11.712
36	1624.78	2039.47	4.7128	27.776	12.310
37	1677.20	2143.42	5.1273	27.082	12.908
38	1743.35	2247.97	5.4200	26.519	13.510
39	1784.66	2353.15	5.8843	25.486	14.109
40	1817.31	2470.93	6.4732	24.078	14.806

Table C–24. Deformation J_{IC} and J–R curve results for specimen MA9–02O

Test Number	: 0116	Test Temp	: 25 °C
Material Type	: CF-8	Heat Number	: MA9
Aging Temp	: 400 °C	Aging Time	: 10,000 h
Spec. Thickness	: 25.37 mm	Net Thickness	: 20.24 mm
Spec. Width	: 50.55 mm	Flow Stress	: 372.20 MPa
Modulus E	: 204.49 GPa	(Effective)	
Modulus E	: 200.00 GPa	(Nominal)	
Init. Crack	: 29.0781 mm	Init. a/w	: 0.5752 (Measured)
Final Crack	: 36.5438 mm	Final a/w	: 0.7229 (Measured)
Final Crack	: 35.5513 mm	Final a/w	: 0.7033 (Compliance)
Linear Fit	**$J = B+M(\Delta a)$**		
Intercept B	: 846.616 kJ/m^2	Slope M	: 276.08 kJ/m^2mm
Fit Coeff. R	: 0.9784	(9 Data Points)	
J_{IC}	: 1039.4 kJ/m^2	(5934.9 in.–lb/in.^{2})	
Δa (J_{IC})	: 0.698 mm	(0.0275 in.)	
T Average	: 407.5	(J_{IC} at 0.15)	
Power–Law Fit	**$J = C(\Delta a)^n$**		
Coeff. C	: 1117.93 kJ/m^2	Exponent n	: 0.3258
Fit Coeff. R	: 0.9917	(9 Data Points)	
J_{IC} (0.20)	: 1093.5 kJ/m^2	(6244.2 in.–lb/in.^{2})	
Δa (J_{IC})	: 0.935 mm	(0.0368 in.)	
T Average	: 381.9	(J_{IC} at 0.20)	
J_{IC} (0.15)	: 1067.0 kJ/m^2	(6092.9 in.–lb/in.^{2})	
Δa (J_{IC})	: 0.867 mm	(0.0341 in.)	
T Average	: 388.4	(J_{IC} at 0.15)	
Kjc	: 555.6 MPa–$m^{0.5}$		
J_{IC} Validity & Data Qualification (E 813–85)			
J_{max} Allowed	: 532.81 kJ/m^2	($J_{max}=b_o\sigma_f/15$)	
Data Limit	: J_{max} Ignored		
Δa (max) Allowed	: 2.514 mm	(at 1.5 Exclusion Line)	
Data Limit	: 1.5 Exclusion Line		
Data Points	: Zone A = 4	Zone B = 2	
Data Point Spacing	: OK		
b_{net} or b_o Size	: Inadequate		
dJ/da at J_{IC}	: OK		
a_o Measurement	: 4, 8,9,& 1 Outside Limit		
Final Crack Shape	: OK		
Crack size estimate	: Inadequate	(by Compliance)	
E Effective	: OK		
J_{IC} Estimate	: Invalid		
J–R Curve Validity & Data Qualification (E 1152–86)			
J_{max} Allowed	: 376.74 kJ/m^2	($J_{max}=b_{net}\sigma_f/20$)	
Δa (max) Allowed	: 2.147 mm	($\Delta a=0.1b_o$)	
Δa (max) Allowed	: 3.092 mm	($\omega=5$)	
Data Points	: Zone A = 31	Zone B = 0	
Data Point Spacing	: Inadequate		
J-R Curve Data	: Invalid		

Table C–25. Modified J_{IC} and J–R curve results for specimen MA9–02O

Linear Fit	**J = B+M(Δa)**		
Intercept B	: 841.109 kJ/m^2	Slope M	: 340.72 kJ/m^{2}mm
Fit Coeff. R	: 0.9917	(8 Data Points)	
J_{IC}	: 1090.7 kJ/m^2	(6228.3 in.–lb/in.^{2})	
Δa (J_{IC})	: 0.733 mm	(0.0288 in.)	
T Average	: 502.9	(J_{IC} at 0.15)	
Power–Law Fit	**J = C(Δa)^n**		
Coeff. C	: 1171.72 kJ/m^2	Exponent n	: 0.3792
Fit Coeff. R	: 0.9978	(8 Data Points)	
J_{IC} (0.20)	: 1163.4 kJ/m^2	(6643.4 in.–lb/in.^{2})	
Δa (J_{IC})	: 0.981 mm	(0.0386 in.)	
T Average	: 464.2	(J_{IC} at 0.20)	
J_{IC} (0.15)	: 1130.1 kJ/m^2	(6453.2 in.–lb/in.^{2})	
Δa (J_{IC})	: 0.909 mm	(0.0358 in.)	
T Average	: 471.6	(J_{IC} at 0.15)	
Kjc	: 588.3 MPa–m$^{0.5}$		

Figure C–23. Fracture surface of MA9 material from cooler region of the hot–leg main shutoff valve aged 10,000 h at 400°C and tested at 25°C

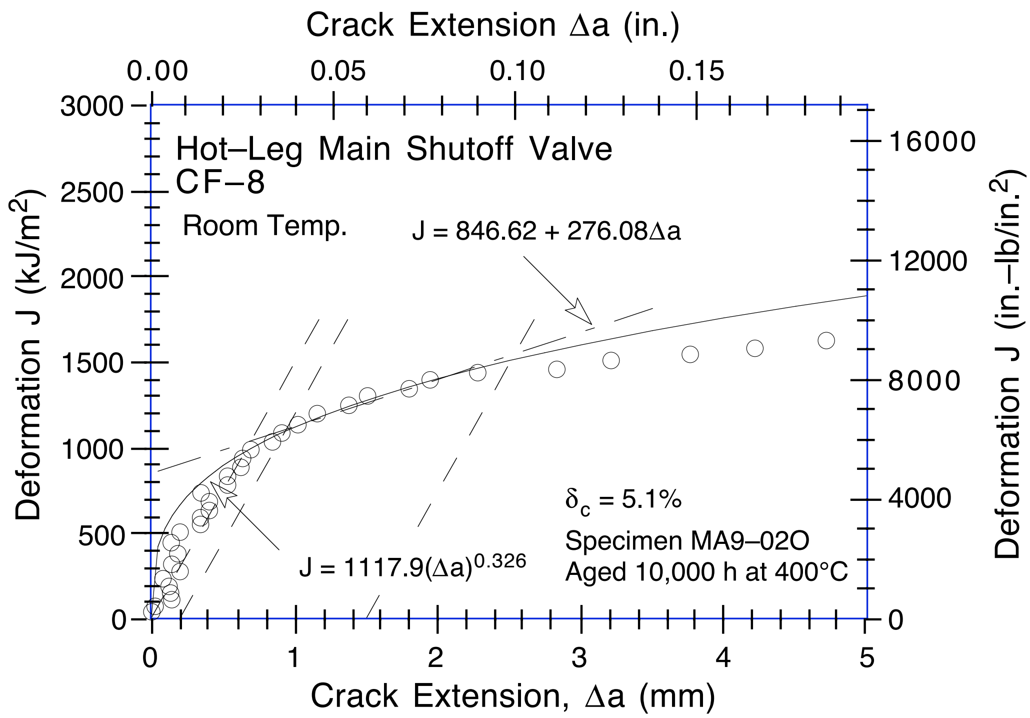

Figure C–24. Deformation J–R Curve at room temperature for material from cooler region of the hot–leg main shutoff valve aged 10,000 h at 400°C

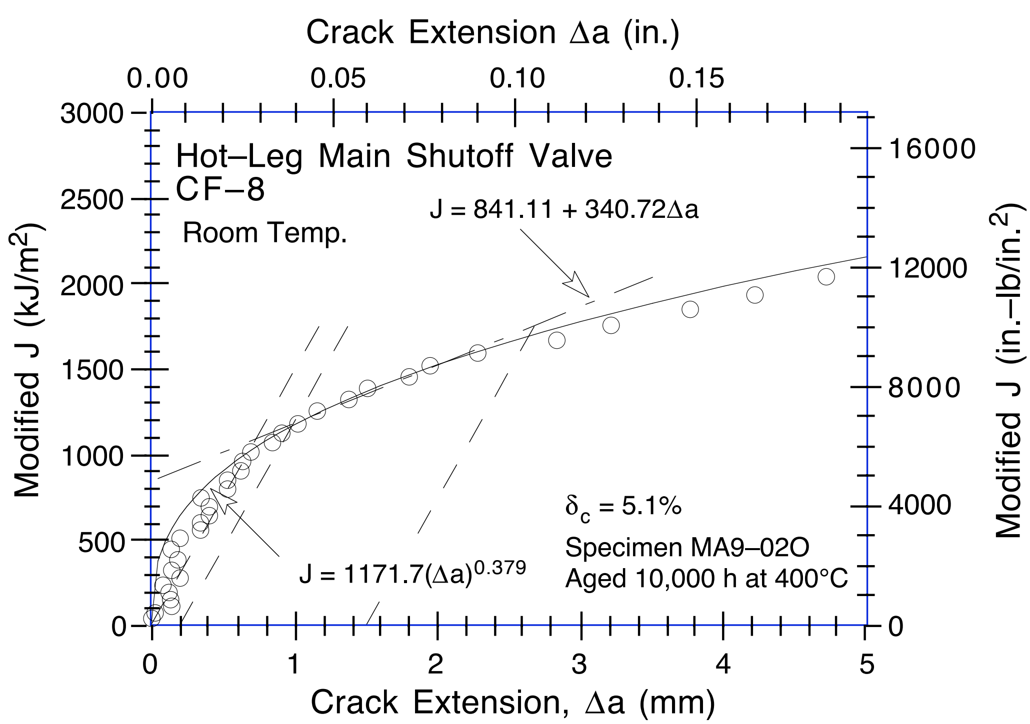

Figure C–25. Modified J–R Curve at room temperature for material from cooler region of the hot–leg main shutoff valve aged 10,000 h at 400°C

Table C–26. Test data for specimen MA9–01O

Test Number	: 0097	Test Temp.	: 290°C
Material Type	: CF–8	Heat Number	: MA9
Aging Temp.	: 25°C	Aging Time	: 0 h
Spec. Thickness	: 25.37 mm	Net Thickness	: 20.32 mm
Spec. Width	: 50.78 mm	Flow Stress	: 259.70 MPa

Unload Number	J_d (kJ/m^2)	J_m (kJ/m^2)	Δa (mm)	Load (kN)	Deflection (mm)
1	14.34	14.39	0.0797	13.618	0.306
2	36.13	35.84	–0.1083	15.415	0.610
3	59.55	60.13	0.1718	16.498	0.910
4	88.64	88.56	0.0326	17.400	1.258
5	117.70	120.72	0.5089	18.201	1.609
6	151.18	150.68	0.0908	18.899	1.955
7	184.01	185.95	0.3256	19.483	2.309
8	213.44	215.63	0.3463	20.120	2.614
9	246.50	244.92	0.0763	20.559	2.911
10	275.82	277.06	0.2551	21.138	3.210
11	309.73	307.74	0.0726	21.611	3.510
12	338.24	341.35	0.3343	21.986	3.809
13	373.67	373.27	0.1710	22.447	4.109
14	399.18	409.10	0.6142	23.003	4.410
15	440.83	441.06	0.2341	23.332	4.711
16	469.52	478.37	0.5486	23.739	5.008
17	511.52	512.78	0.2930	24.220	5.312
18	545.17	550.78	0.4299	24.574	5.612
19	582.42	587.26	0.4070	25.003	5.911
20	626.87	623.98	0.1951	25.254	6.209
21	659.80	663.50	0.3657	25.569	6.510
22	703.80	701.05	0.2083	25.913	6.813
23	727.97	741.42	0.5862	26.266	7.109
24	770.82	780.64	0.5060	26.537	7.420
25	799.04	821.18	0.7657	26.620	7.713
26	842.07	859.53	0.6720	26.770	8.008
27	872.30	902.33	0.9133	27.041	8.311
28	919.19	942.32	0.7872	27.323	8.613
29	950.89	985.43	0.9874	27.388	8.911
30	998.48	1025.99	0.8697	27.745	9.209
31	1040.91	1069.79	0.8915	28.078	9.511
32	1061.78	1114.35	1.2600	28.238	9.812
33	1116.21	1158.71	1.1105	28.386	10.136
34	1145.87	1201.40	1.2977	28.407	10.415
35	1193.94	1258.49	1.4215	28.343	10.805
36	1241.06	1318.76	1.5939	28.498	11.209
37	1295.22	1394.46	1.8621	28.731	11.709
38	1369.53	1469.59	1.8716	28.726	12.213
39	1419.72	1561.74	2.3395	28.616	12.801
40	1482.36	1638.97	2.4941	28.132	13.316
41	1545.77	1731.18	2.7835	27.830	13.912
42	1583.78	1823.95	3.3095	27.206	14.511
43	1649.60	1919.46	3.5801	26.376	15.152

Table C–27. Deformation J_{IC} and J–R curve results for specimen MA9–01O

Test Number	: 0097	Test Temp.	: 290°C
Material Type	: CF–8	Heat Number	: MA9
Aging Temp.	: 25°C	Aging Time	: 0 h
Spec. Thickness	: 25.37 mm	Net Thickness	: 20.32 mm
Spec. Width	: 50.78 mm	σ_f	: 259.70 MPa
Modulus E	: 169.85 GPa	(Effective)	
Modulus E	: 180.00 GPa	(Nominal)	
Init. Crack	: 28.3156 mm	Init. a/w	: 0.5576 (Measured)
Final Crack	: 33.0531 mm	Final a/w	: 0.6509 (Measured)
Final Crack	: 31.8957 mm	Final a/w	: 0.6281 (Compliance)
Linear Fit	**J = B+M(Δa)**		
Intercept B	: 768.962 kJ/m^2	Slope M	: 285.67 kJ/m^{2}mm
Fit Coeff. R	: 0.9751	(9 Data Points)	
J_{IC}	: 1060.6 kJ/m^2	(6056.4 in.–lb/in.^{2})	
Δa (J_{IC})	: 1.021 mm	(0.02402 in.)	
T Average	: 714.3	(J_{IC} at 0.15)	
Power–Law Fit	**J = C(Δa)^n**		
Coeff. C	: 1010.57 kJ/m^2	Exponent n	: 0.4204
Fit Coeff. R	: 0.9791	(9 Data Points)	
J_{IC} (0.20)	: 1120.6 kJ/m^2	(6399.1 in.–lb/in.^{2})	
Δa (J_{IC})	: 1.279 mm	(0.0503 in.)	
T Average	: 689.6	(J_{IC} at 0.20)	
J_{IC} (0.15)	: 1091.3 kJ/m^2	(6231.4 in.–lb/in.^{2})	
Δa (J_{IC})	: 1.201 mm	(0.0473 in.)	
T Average	: 698.5	(J_{IC} at 0.15)	
Kjc	: 522.1 MPa–m$^{0.5}$		
J_{IC} Validity & Data Qualification (E 813–85)			
J_{max} Allowed	: 388.97 kJ/m^2	(J_{max}=$b_o\sigma_f$/15)	
Data Limit	: J_{max} Ignored		
Δa (max) Allowed	: 3.056 mm	(at 1.5 Exclusion Line)	
Data Limit	: 1.5 Exclusion Line		
Data Points	: Zone A = 4	Zone B = 2	
Data Point Spacing	: OK		
b_{net} or b_o Size	: Inadequate		
dJ/da at J_{IC}	: OK		
a_f Measurement	: Near–Surface	Outside Limit	
Initial Crack Shape	: OK		
Crack Size Estimate	: Inadequate	(by Compliance)	
E Effective	: OK		
J_{IC} Estimate	: Invalid		
J–R Curve Validity & Data Qualification (E 1152–86)			
J_{max} Allowed	: 263.86 kJ/m^2	(J_{max}=$b_{net}\sigma_f$/20)	
Δa (max) Allowed	: 2.247 mm	(Δa=0.1b_o)	
Δa (max) Allowed	: 3.939 mm	(ω=5)	
Data Points	: Zone A = 40	Zone B = 2	
Data Point Spacing	: Inadequate		
J–R Curve Data	: Invalid		

Table C–28. Modified J_{IC} and J–R curve results for specimen MA9–01O

Linear Fit	**J = B+M(Δa)**		
Intercept B	: 780.191 kJ/m^2	Slope M	: 341.90 kJ/m^{2}mm
Fit Coeff. R	: 0.9903	(11 Data Points)	
J_{IC}	: 1163.0 kJ/m^2	(6640.7 in.–lb/in.^{2})	
Δa (J_{IC})	: 1.120 mm	(0.0441 in.)	
T Average	: 854.9	(J_{IC} at 0.15)	
Power–Law Fit	**J = C(Δa)^n**		
Coeff. C	: 10.64.09 kJ/m^2	Exponent n	: 0.4693
Fit Coeff. R	: 0.9902	(7 Data Points)	
J_{IC} (0.20)	: 1245.8 kJ/m^2	(7113.8 in.–lb/in.^{2})	
Δa (J_{IC})	: 1.399 mm	(0.0551 in.)	
T Average	: 805.3	(J_{IC} at 0.20)	
J_{IC} (0.15)	: 1209.9 kJ/m^2	(6908.6 in.–lb/in.^{2})	
Δa (J_{IC})	: 1.315 mm	(0.0518 in.)	
T Average	: 814.7	(J_{IC} at 0.15)	
Kjc	: 560.2 MPa–m$^{0.5}$		

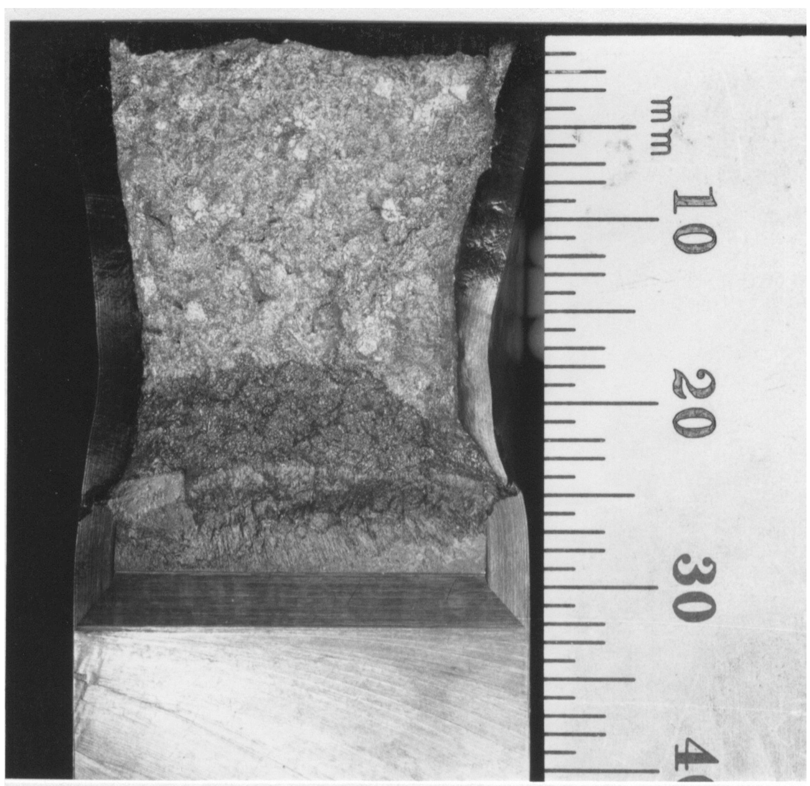

Figure C–26. Fracture surface of essentially unaged material MA9 from the hot–leg main shutoff valve tested at 290°C

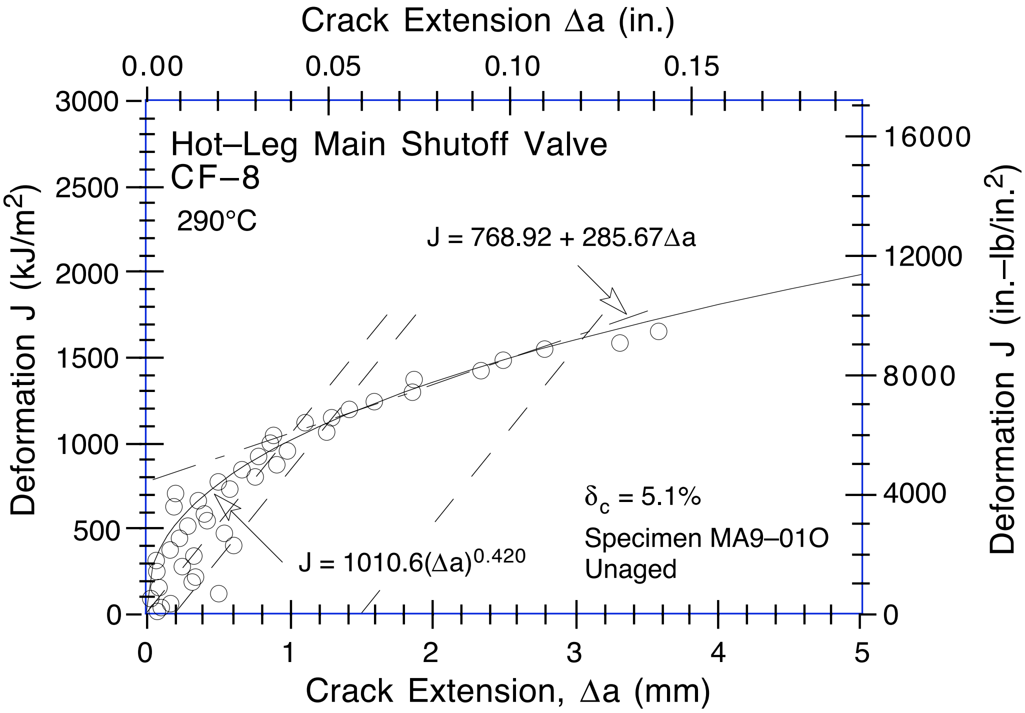

Figure C–27. Deformation J–R Curve at 290°C for essentially unaged material MA9 from the hot–leg main shutoff valve

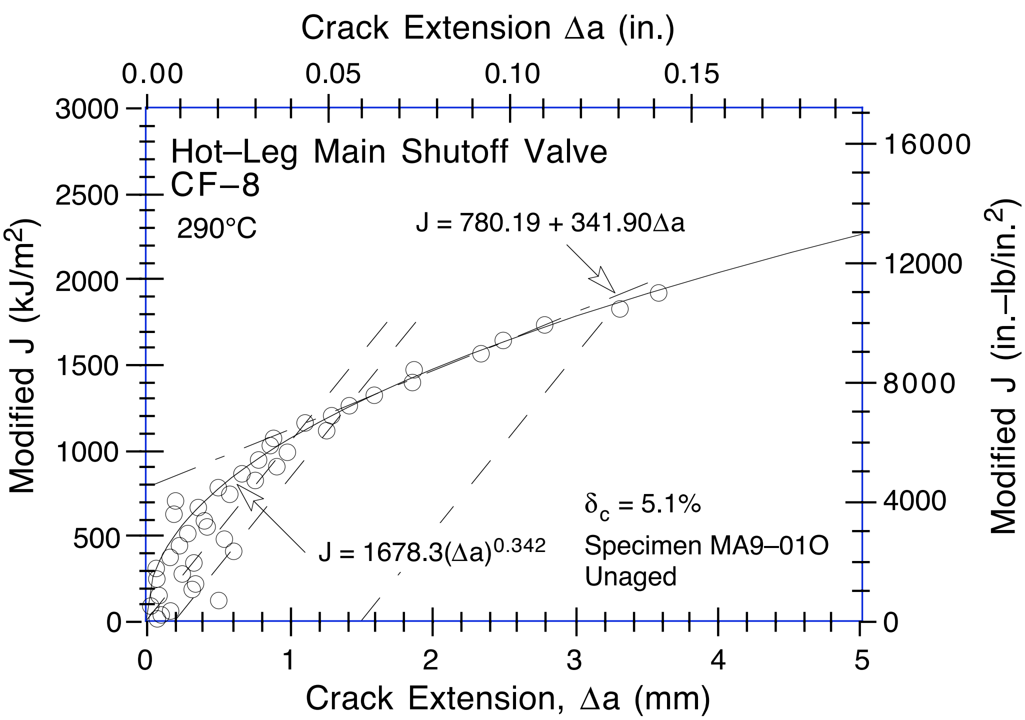

Figure C–28. Modified J–R Curve at 290°C for essentially unaged material MA9 from the hot–leg main shutoff valve

Table C–29. Test data for specimen MA9–02I

Test Number	: 0121	Test Temp	: 290°C
Material Type	: CF-8	Heat Number	: MA9
Aging Temp	: 400°C	Aging Time	: 10,000 h
Spec. Thickness	: 25.39 mm	Net Thickness	: 20.30 mm
Spec. Width	: 50.77 mm	Flow Stress	: 259.60 MPa

Unload Number	J_d (kJ/m^2)	J_m (kJ/m^2)	Δa (mm)	Load (kN)	Deflection (mm)
1	11.29	11.29	0.0048	12.723	0.267
2	34.92	35.10	0.1119	14.782	0.606
3	58.53	57.85	-0.1696	15.879	0.909
4	90.89	91.42	0.0716	16.894	1.305
5	125.38	126.41	0.1432	17.788	1.707
6	163.05	162.74	-0.0012	18.559	2.107
7	199.40	201.72	0.2282	19.273	2.504
8	234.52	235.90	0.1584	19.900	2.856
9	270.30	272.20	0.1913	20.446	3.208
10	304.93	309.37	0.3337	20.948	3.558
11	341.19	346.79	0.3916	21.462	3.906
12	383.96	385.10	0.1938	21.931	4.260
13	419.86	425.25	0.3647	22.303	4.606
14	459.33	465.23	0.3837	22.673	4.957
15	495.92	506.57	0.5442	23.000	5.306
16	538.57	547.97	0.5053	23.346	5.659
17	573.17	590.75	0.7425	23.628	6.004
18	617.87	633.02	0.6773	23.809	6.357
19	650.48	677.92	0.9875	24.035	6.707
20	697.52	719.89	0.8679	23.944	7.056
21	721.82	766.35	1.3648	23.945	7.409
22	764.83	808.65	1.3499	23.660	7.761
23	782.74	853.74	1.8994	23.116	8.107
24	816.95	901.99	2.1682	22.590	8.504
25	841.26	952.29	2.6426	22.137	8.908
26	868.38	1000.78	3.0149	21.822	9.306
27	910.93	1049.86	3.1227	21.765	9.708
28	941.53	1100.81	3.4435	21.601	10.107
29	975.57	1150.65	3.6813	21.400	10.507
30	1008.74	1201.34	3.9336	21.202	10.908
31	1055.22	1250.88	3.9756	21.174	11.307
32	1083.67	1303.17	4.2901	21.112	11.706
33	1129.19	1353.09	4.3455	21.056	12.107
34	1171.15	1419.08	4.6341	20.977	12.606
35	1219.03	1483.11	4.8187	20.794	13.105
36	1269.25	1548.46	4.9834	20.540	13.608
37	1302.58	1613.73	5.3168	20.136	14.105
38	1339.25	1678.06	5.5939	19.935	14.607
39	1369.48	1743.84	5.9364	19.606	15.113

Table C–30. Deformation J_{IC} and J–R curve results for specimen MA9–02I

Test Number	: 0121	Test Temp	: 290°C
Material Type	: CF-8	Heat Number	: MA9
Aging Temp	: 400°C	Aging Time	: 10,000 h
Spec. Thickness	: 25.39 mm	Net Thickness	: 20.30 mm
Spec. Width	: 50.77 mm	Flow Stress	: 259.60 MPa
Modulus E	: 172.28 GPa	(Effective)	
Modulus E	: 180.00 GPa	(Nominal)	
Init. Crack	: 28.8406 mm	Init. a/w	: 0.5681 (Measured)
Final Crack	: 35.5125 mm	Final a/w	: 0.6995 (Measured)
Final Crack	: 34.7770 mm	Final a/w	: 0.6850 (Compliance)
Linear Fit	**J = B+M(Δa)**		
Intercept B	: 527.587 kJ/m^2	Slope M	: 140.12 kJ/m^{2}mm
Fit Coeff. R	: 0.8914	(7 Data Points)	
J_{IC}	: 609.9 kJ/m^2	(3482.6 in.–lb/in.^{2})	
Δa (J_{IC})	: 0.587 mm	(0.0231 in.)	
T Average	: 358.2	(J_{IC} at 0.15)	
Power–Law Fit	**J = C(Δa)^n**		
Coeff. C	: 667.98 kJ/m^2	Exponent N	: 0.2772
Fit Coeff. R	: 0.9075	(7 Data Points)	
J_{IC} (0.20)	: 629.2 kJ/m^2	(3592.9 in.–lb/in.^{2})	
Δa (J_{IC})	: 0.806 mm	(0.0317 in.)	
T Average	: 354.3	(J_{IC} at 0.20)	
J_{IC} (0.15)	: 615.0 kJ/m^2	(3511.9 in.–lb/in.^{2})	
Δa (J_{IC})	: 0.742 mm	(0.0292 in.)	
T Average	: 361.3	(J_{IC} at 0.15)	
Kjc	: 381.0 MPa–m$^{0.5}$		
J_{IC} Validity & Data Qualification (E 813–85)			
J_{max} Allowed	: 379.47 kJ/m^2	($J_{max}=b_o\sigma_f/15$)	
Data Limit	: J_{max} Ignored		
Δa (max) Allowed	: 2.311 mm	(at 1.5 Exclusion Line)	
Data Limit	: 1.5 Exclusion Line		
Data Points	: Zone A = 3	Zone B = 2	
Data Point Spacing	: OK		
b_{net} or b_o Size	: Inadequate		
dJ/da at J_{IC}	: OK		
a_o Measurement	: 1 Outside Limit		
Final Crack Shape	: OK		
Crack size estimate	: Inadequate	(by Compliance)	
E Effective	: OK		
J_{IC} Estimate	: Invalid		
J–R Curve Validity & Data Qualification (E 1152–86)			
J_{max} Allowed	: 263.52 kJ/m^2	($J_{max}=b_{net}\sigma_f/20$)	
Δa (max) Allowed	: 2.193 mm	(Δa=0.1b_o)	
Δa (max) Allowed	: 2.666 mm	(ω=5)	
Data Points	: Zone A = 21	Zone B = 1	
Data Point Spacing	: Inadequate		
J-R Curve Data	: Invalid		

Table C–31. Modified J_{IC} and J–R curve results for specimen MA9–02I

Linear Fit	**$J = B+M(\Delta a)$**		
Intercept B	: 562.439 kJ/m^2	Slope M	: 156.74 kJ/m^{2}mm
Fit Coeff. R	: 0.9510	(6 Data Points)	
J_{IC}	: 662.4 kJ/m^2	(3782.6 in.–lb/in.^{2})	
Δa (J_{IC})	: 0.638 mm	(0.0251 in.)	
T Average	: 400.7	(J_{IC} at 0.15)	
Power–Law Fit	**$J = C(\Delta a)^n$**		
Coeff. C	: 718.38 kJ/m^2	Exponent N	: 0.2817
Fit Coeff. R	: 0.9405	(6 Data Points)	
J_{IC} (0.20)	: 689.4 kJ/m^2	(3936.4 in.–lb/in.^{2})	
Δa (J_{IC})	: 0.864 mm	(0.0340 in.)	
T Average	: 375.9	(J_{IC} at 0.20)	
J_{IC} (0.15)	: 674.5 kJ/m^2	(3851.6 in.–lb/in.^{2})	
Δa (J_{IC})	: 0.800 mm	(0.0315 in.)	
T Average	: 383.0	(J_{IC} at 0.15)	
Kjc	: 397.6 MPa–m$^{0.5}$		

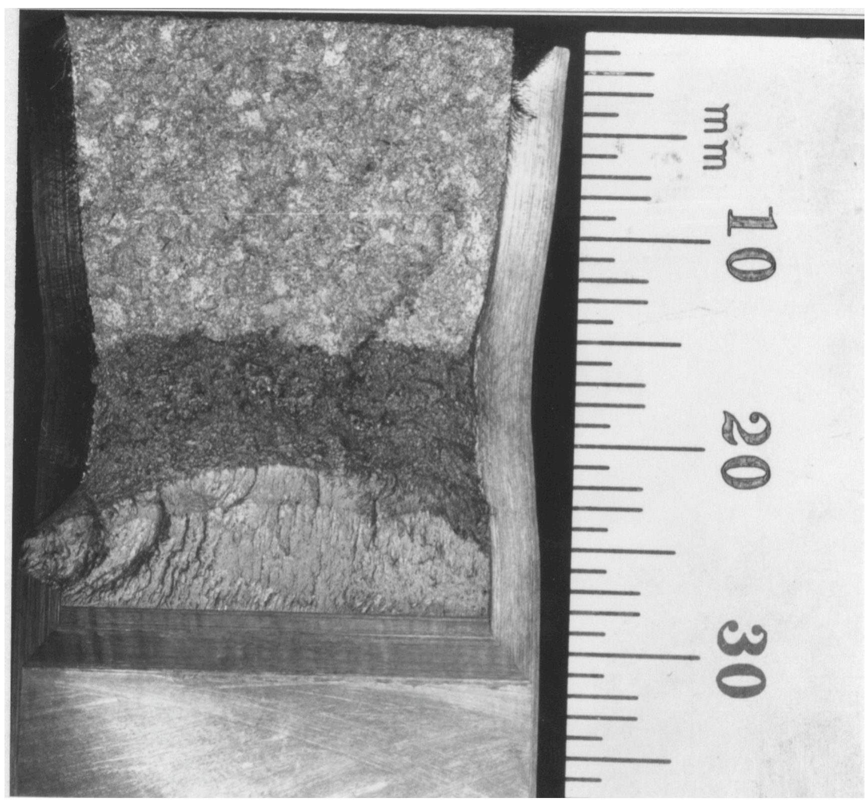

Figure C–29. Fracture surface of MA9 material from cooler region of the hot–leg main shutoff valve aged 10,000 h at 400°C and tested at 290°C

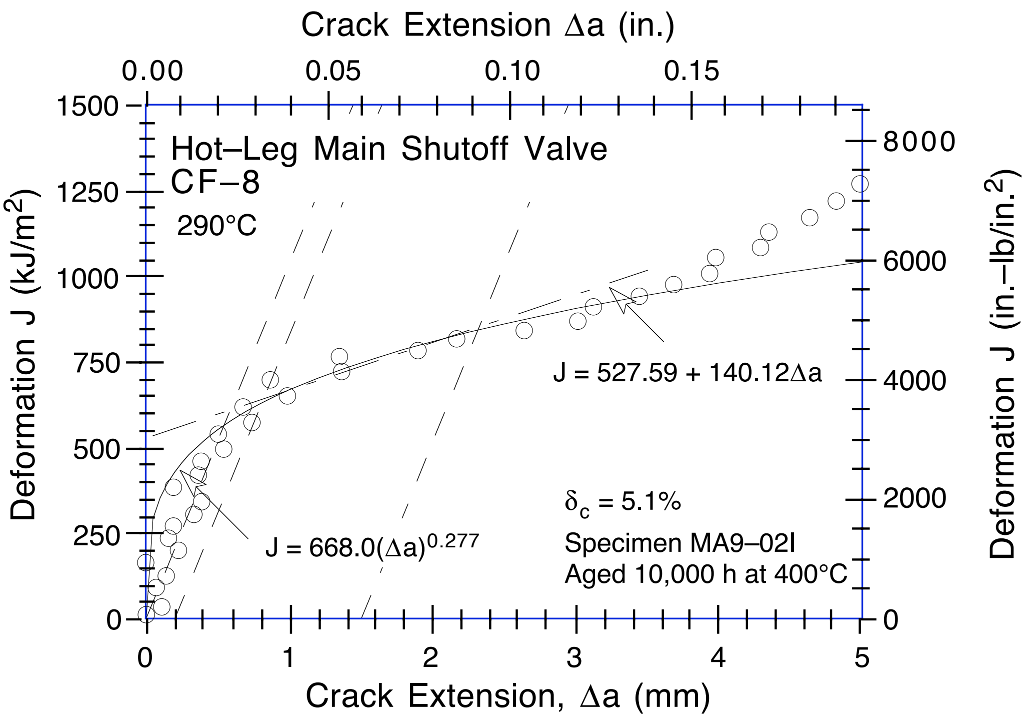

Figure C–30. Deformation J–R Curve at 290°C for material from cooler region of the hot–leg main shutoff valve aged 10,000 h at 400°C

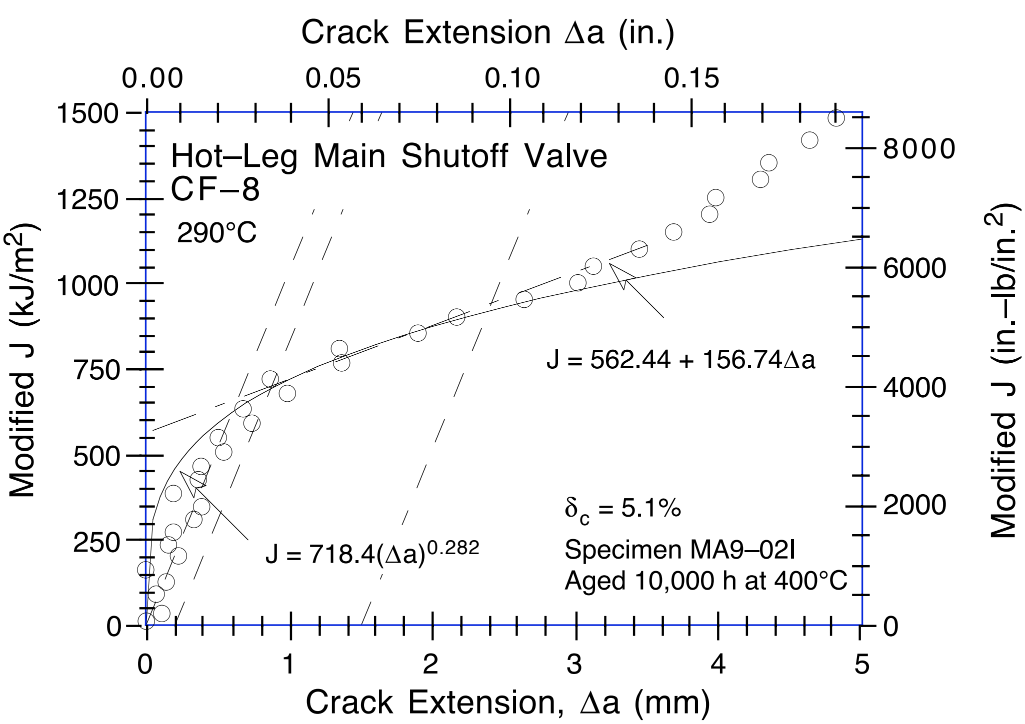

Figure C–31. Modified J–R Curve at 290°C for material from cooler region of the hot–leg main shutoff valve aged 10,000 h at 400°C

Table C–32. Test data for specimen PVC–01

Test Number	: 0078	Test Temp.	: 25°C
Material Type	: CF–8	Heat Number	: PV
Aging Temp.	: 550°C	Aging Time	: 1 h
Spec. Thickness	: 25.39 mm	Net Thickness	: 20.33 mm
Spec. Width	: 50.81 mm	Flow Stress	: 362.04 MPa

Unload Number	J_d (kJ/m^2)	J_m (kJ/m^2)	Δa (mm)	Load (kN)	Deflection (mm)
1	9.28	9.27	−0.0854	18.185	0.202
2	24.89	24.94	−0.0138	21.480	0.356
3	47.63	47.80	0.0450	23.169	0.560
4	77.34	77.54	0.0552	24.533	0.808
5	109.64	109.41	−0.0229	25.452	1.062
6	144.04	144.04	0.0082	26.186	1.324
7	175.27	175.80	0.0630	26.771	1.560
8	210.19	209.31	−0.0596	27.477	1.809
9	244.72	245.95	0.0958	28.039	2.062
10	279.75	280.67	0.0757	28.443	2.310
11	316.30	317.49	0.0910	29.015	2.561
12	353.59	354.20	0.0618	29.373	2.810
13	398.57	400.96	0.1399	29.795	3.116
14	443.95	446.34	0.1400	30.445	3.414
15	494.98	498.00	0.1620	30.980	3.743
16	536.35	540.62	0.2020	31.261	4.011
17	582.66	589.33	0.2725	31.857	4.311
18	631.89	638.07	0.2594	32.119	4.612
19	679.11	688.60	0.3423	32.506	4.913
20	730.57	738.16	0.2979	32.856	5.212
21	777.56	789.11	0.3839	33.246	5.507
22	840.67	856.98	0.4793	33.677	5.900
23	894.93	910.87	0.4725	34.245	6.212
24	959.64	972.74	0.4226	34.482	6.563
25	1020.71	1036.20	0.4620	35.002	6.914
26	1080.32	1099.92	0.5256	35.231	7.266
27	1135.99	1163.66	0.6435	35.391	7.612
28	1201.69	1227.79	0.6219	35.663	7.965
29	1244.56	1295.83	0.9541	35.957	8.318
30	1308.68	1358.72	0.9388	36.011	8.666
31	1369.48	1425.85	1.0143	36.093	9.014
32	1426.25	1494.19	1.1463	36.546	9.369
33	1498.09	1559.43	1.0746	36.678	9.716
34	1561.29	1628.31	1.1336	36.620	10.065
35	1595.84	1698.70	1.4938	36.583	10.418
36	1663.56	1767.02	1.4996	36.327	10.784
37	1714.56	1833.57	1.6440	36.272	11.117
38	1761.24	1903.25	1.8501	35.884	11.470
39	1814.33	1969.51	1.9641	35.715	11.813
40	1867.58	2049.72	2.1889	35.750	12.217
41	1921.93	2128.47	2.3851	35.493	12.618
42	1969.85	2207.06	2.6234	35.527	13.014
43	2050.46	2306.55	2.7635	35.392	13.515
44	2120.58	2407.98	2.9860	35.065	14.015
45	2192.55	2528.27	3.3132	33.902	14.616
46	2243.34	2645.66	3.7457	32.919	15.215
47	2329.05	2759.57	3.9208	32.872	15.812

Table C–33. Deformation J_{IC} and J–R curve results for specimen PVC–01

Test Number	: 0078	Test Temp.	: 25°C
Material Type	: CF–8	Heat Number	: PV
Aging Temp.	: 550°C	Aging Time	: 1 h
Spec. Thickness	: 25.39 mm	Net Thickness	: 20.33 mm
Spec. Width	: 50.81 mm	Flow Stress	: 362.04 MPa
Modulus E	: 195.28 GPa	(Effective)	
Modulus E	: 193.10 GPa	(Nominal)	
Init. Crack	: 28.9750 mm	Init. a/w	: 0.5703 (Measured)
Final Crack	: 33.8031 mm	Final a/w	: 0.6654 (Measured)
Final Crack	: 32.8958 mm	Final a/w	: 0.6475 (Compliance)
Linear Fit	**$J = B+M(\Delta a)$**		
Intercept B	: 1182.587 kJ/m^2	Slope M	: 310.44 kJ/m^{2}mm
Fit Coeff. R	: 0.9869	(9 Data Points)	
J_{IC}	: 1505.3 kJ/m^2	(8595.4 in.–lb/in.^{2})	
Δa (J_{IC})	: 1.039 mm	(0.0409 in.)	
T Average	: 462.5	(J_{IC} at 0.15)	
Power–Law Fit	**$J = C(\Delta a)^n$**		
Coeff. C	: 1422.76 kJ/m^2	Exponent n	: 0.3497
Fit Coeff. R	: 0.9875	(9 Data Points)	
J_{IC} (0.20)	: 1545.7 kJ/m^2	(8826.0 in.–lb/in.^{2})	
Δa (J_{IC})	: 1.267 mm	(0.0499 in.)	
T Average	: 465.8	(J_{IC} at 0.20)	
J_{IC} (0.15)	: 1514.6 kJ/m^2	(8648.8 in.–lb/in.^{2})	
Δa (J_{IC})	: 1.196 mm	(0.0471 in.)	
T Average	: 472.2	(J_{IC} at 0.15)	
Kjc	: 636.1 MPa–m$^{0.5}$		
J_{IC} Validity & Data Qualification (E 813–85)			
J_{max} Allowed	: 526.89 kJ/m^2	($J_{max}=b_o\sigma_f/15$)	
Data Limit	: J_{max} Ignored		
Δa (max) Allowed	: 2.931 mm	(at 1.5 Exclusion Line)	
Data Limit	: 1.5 Exclusion Line		
Data Points	: Zone A = 3	Zone B = 3	
Data Point Spacing	: OK		
b_{net} or b_o Size	: Inadequate		
dJ/da at J_{IC}	: OK		
a_f Measurement	: Near–surface	Outside Limit	
Initial Crack Shape	: OK		
Crack Size Estimate	: Inadequate	(by Compliance)	
E Effective	: OK		
J_{IC} Estimate	: Invalid		
J–R Curve Validity & Data Qualification (E 1152–86)			
J_{max} Allowed	: 367.98 kJ/m^2	($J_{max}=b_{net}\sigma_f//20$)	
Δa (max) Allowed	: 2.183 mm	($\Delta a=0.1b_o$)	
Δa (max) Allowed	: 3.321 mm	($\omega=5$)	
Data Points	: Zone A = 43	Zone B = 0	
Data Point Spacing	: Inadequate		
J–R Curve Data	: Invalid		

Table C–34. Modified J_{IC} and J–R curve results for specimen PVC–01

Linear Fit	**$J = B+M(\Delta a)$**		
Intercept B	: 1093.141 kJ/m^2	Slope M	: 436.50 kJ/m^{2}mm
Fit Coeff. R	: 0.9954	(10 Data Points)	
J_{IC}	: 1564.8 kJ/m^2	(8935.3 in.–lb/in.^{2})	
Δa (J_{IC})	: 1.081 mm	(0.0425 in.)	
T Average	: 650.3	(J_{IC} at 0.15)	
Power–Law Fit	**$J = C(\Delta a)^n$**		
Coeff. C	: 1443.94 kJ/m^2	Exponent n	: 0.4551
Fit Coeff. R	: 0.9941	(10 Data Points)	
J_{IC} (0.20)	: 1648.9 kJ/m^2	(9415.6 in.–lb/in.^{2})	
Δa (J_{IC})	: 1.339 mm	(0.0527 in.)	
T Average	: 636.6	(J_{IC} at 0.20)	
J_{IC} (0.15)	: 1601.9 kJ/m^2	(9146.9 in.–lb/in.^{2})	
Δa (J_{IC})	: 1.256 mm	(0.0495 in.)	
T Average	: 644.3	(J_{IC} at 0.15)	
Kjc	: 691.5 MPa–m$^{0.5}$		

Figure C–32. Fracture surface of recovery–annealed material from the pump volute PV tested at room temperature

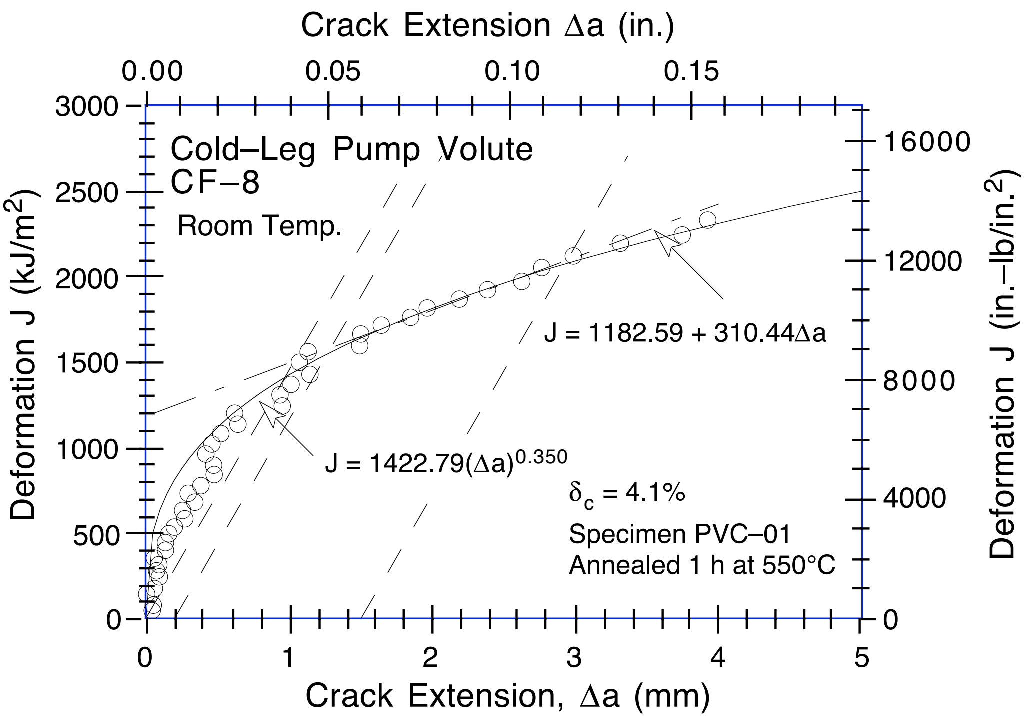

Figure C–33. Deformation J–R Curve at room temperature for recovery–annealed material PV from the cold–leg pump volute

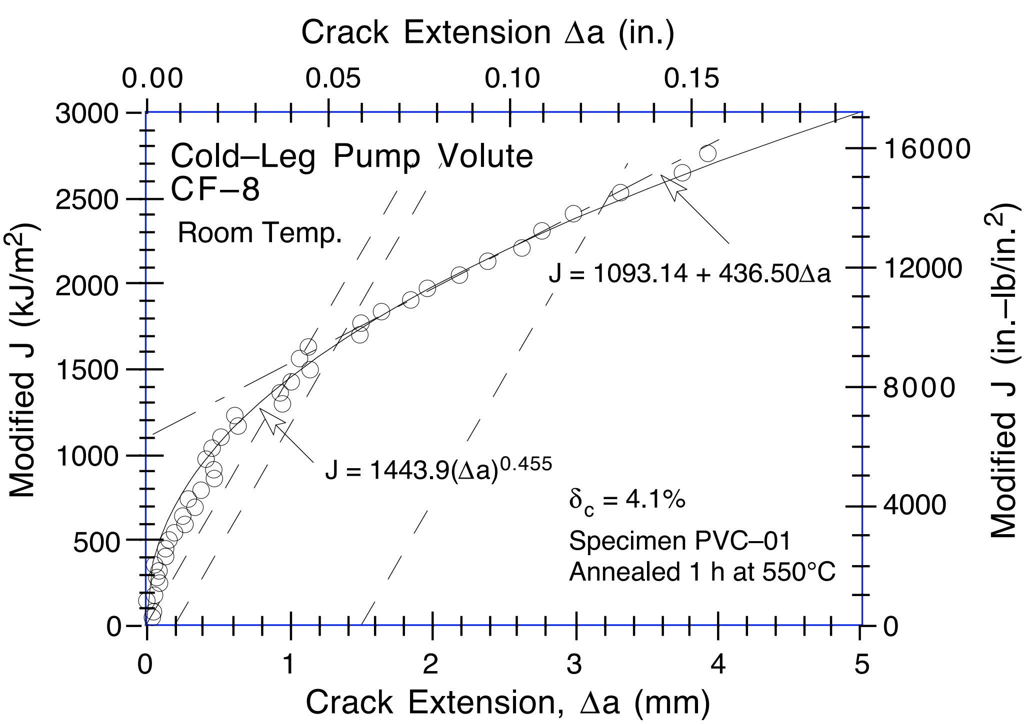

Figure C–34. Modified J–R Curve at room temperature for recovery–annealed material PV from the cold–leg pump volute

Table C–35. Test data for specimen PVI–02

Test Number	: 0081	Test Temp.	: 25°C
Material Type	: CF–8	Heat Number	: PV
Aging Temp.	: 264°C	Aging Time	: 113,900 h
Spec. Thickness	: 25.33 mm	Net Thickness	: 20.23 mm
Spec. Width	: 50.79 mm	Flow Stress	: 370.30 MPa

Unload Number	J_d (kJ/m^2)	J_m (kJ/m^2)	Δa (mm)	Load (kN)	Deflection (mm)
1	19.97	20.00	0.0421	21.619	0.304
2	67.85	67.83	0.0285	26.041	0.709
3	121.31	121.58	0.0767	28.076	1.110
4	177.33	178.10	0.1294	29.502	1.508
5	252.03	252.83	0.1316	30.969	2.010
6	330.74	331.08	0.1059	32.142	2.512
7	410.63	412.00	0.1514	33.355	3.010
8	502.26	504.42	0.1792	34.233	3.561
9	580.69	581.91	0.1507	35.162	4.012
10	661.33	671.97	0.4002	36.040	4.511
11	753.77	760.82	0.3170	36.963	5.010
12	849.14	854.47	0.2815	37.779	5.511
13	933.72	951.38	0.5102	38.475	6.012
14	1027.05	1048.38	0.5717	39.173	6.516
15	1118.30	1146.63	0.6791	39.605	7.011
16	1205.51	1251.28	0.9250	40.000	7.525
17	1298.08	1349.06	0.9929	40.498	8.009
18	1401.51	1456.23	1.0380	40.880	8.526
19	1487.90	1559.14	1.2240	41.053	9.009
20	1579.49	1666.58	1.3910	41.207	9.515
21	1676.72	1771.80	1.4700	41.424	10.010
22	1765.23	1881.96	1.6717	41.220	10.515
23	1837.73	1990.80	1.9930	41.089	11.013
24	1922.11	2098.61	2.1895	40.747	11.514
25	2007.88	2207.92	2.3771	40.524	12.014
26	2085.34	2317.87	2.6238	40.060	12.515
27	2183.06	2447.87	2.8558	39.802	13.111
28	2261.72	2581.30	3.2302	39.530	13.715
29	2354.79	2711.14	3.4692	38.755	14.314
30	2430.05	2842.67	3.8180	37.349	14.917
31	2449.81	2970.31	4.4642	36.075	15.517

Table C–36. Deformation J_{IC} and J–R curve results for specimen PVI–02

Test Number	: 0081	Test Temp.	: 25°C
Material Type	: CF–8	Heat Number	: PV
Aging Temp.	: 264°C	Aging Time	: 113,900 h
Spec. Thickness	: 25.33 mm	Net Thickness	: 20.23 mm
Spec. Width	: 50.79 mm	Flow Stress	: 370.30 MPa
Modulus E	: 209.17 GPa	(Effective)	
Modulus E	: 193.10 GPa	(Nominal)	
Init. Crack	: 28.0813 mm	Init. a/w	: 0.5529 (Measured)
Final Crack	: 33.1031 mm	Final a/w	: 0.6518 (Measured)
Final Crack	: 32.5454 mm	Final a/w	: 0.6408 (Compliance)

Linear Fit	**$J = B+M(\Delta a)$**		
Intercept B	: 1043.409 kJ/m^2	Slope M	: 402.05 kJ/m^2mm
Fit Coeff. R	: 0.9915	(9 Data Points)	
J_{IC}	: 1432.1 kJ/m^2	(8177.8 in.–lb/in.^{2})	
Δa (J_{IC})	: 0.967 mm	(0.0381 in.)	
T Average	: 613.3	(J_{IC} at 0.15)	

Power–Law Fit	**$J = C(\Delta a)^n$**		
Coeff. C	: 1386.51 kJ/m^2	Exponent n	: 0.4276
Fit Coeff. R	: 0.9933	(9 Data Points)	
J_{IC} (0.20)	: 1508.8 kJ/m^2	(8615.8 in.–lb/in.^{2})	
Δa (J_{IC})	: 1.219 mm	(0.0480 in.)	
T Average	: 600.2	(J_{IC} at 0.20)	
J_{IC} (0.15)	: 1466.4 kJ/m^2	(8373.5 in.–lb/in.^{2})	
Δa (J_{IC})	: 1.140 mm	(0.0449 in.)	
T Average	: 608.2	(J_{IC} at 0.15)	
Kjc	: 680.9 MPa–$m^{0.5}$		

J_{IC} Validity & Data Qualification (E 813–85)

J_{max} Allowed	: 560.60 kJ/m^2	($J_{max}=b_o\sigma_f/15$)
Data Limit	: J_{max} Ignored	
Δa (max) Allowed	: 2.997 mm	(at 1.5 Exclusion Line)
Data Limit	: 1.5 Exclusion Line	
Data Points	: Zone A = 4	Zone B = 3
Data Point Spacing	: OK	
b_{net} or b_o Size	: Inadequate	
dJ/da at J_{IC}	: OK	
a_f Measurement	: Near–surface	Outside Limit
Initial Crack Shape	: OK	
Crack Size Estimate	: Inadequate	(by Compliance)
E Effective	: OK	
J_{IC} Estimate	: Invalid	

J–R Curve Validity & Data Qualification (E 1152–86)

J_{max} Allowed	: 374.58 kJ/m^2	($J_{max}=b_{net}\sigma_f//20$)
Δa (max) Allowed	: 2.271 mm	($\Delta a=0.1b_o$)
Δa (max) Allowed	: 4.001 mm	($\omega=5$)
Data Points	: Zone A = 30	Zone B = 1
Data Point Spacing	: Inadequate	
J–R Curve Data	: Invalid	

Table C–37. Modified J_{IC} and J–R curve results for specimen PVI–02

Linear Fit	**$J = B+M(\Delta a)$**		
Intercept B	: 995.819 kJ/m^2	Slope M	: 502.51 kJ/m^2mm
Fit Coeff. R	: 0.9956	(10 Data Points)	
J_{IC}	: 1507.1 kJ/m^2	(8606.0 in.–lb/in.^{2})	
Δa (J_{IC})	: 1.017 mm	(0.0401 in.)	
T Average	: 766.5	(J_{IC} at 0.15)	
Power–Law Fit	**$J = C(\Delta a)^n$**		
Coeff. C	: 1423.22 kJ/m^2	Exponent n	: 0.5083
Fit Coeff. R	: 0.9970	(10 Data Points)	
J_{IC} (0.20)	: 1623.9 kJ/m^2	(9273.0 in.–lb/in.^{2})	
Δa (J_{IC})	: 1.296 mm	(0.0510 in.)	
T Average	: 747.6	(J_{IC} at 0.20)	
J_{IC} (0.15)	: 1566.4 kJ/m^2	(8944.3 in.–lb/in.^{2})	
Δa (J_{IC})	: 1.207 mm	(0.0475 in.)	
T Average	: 756.4	(J_{IC} at 0.15)	
Kjc	: 736.1 MPa–$m^{0.5}$		

Figure C–35. Fracture surface of pump volute PV tested at room temperature after 13 y of service at 264°C

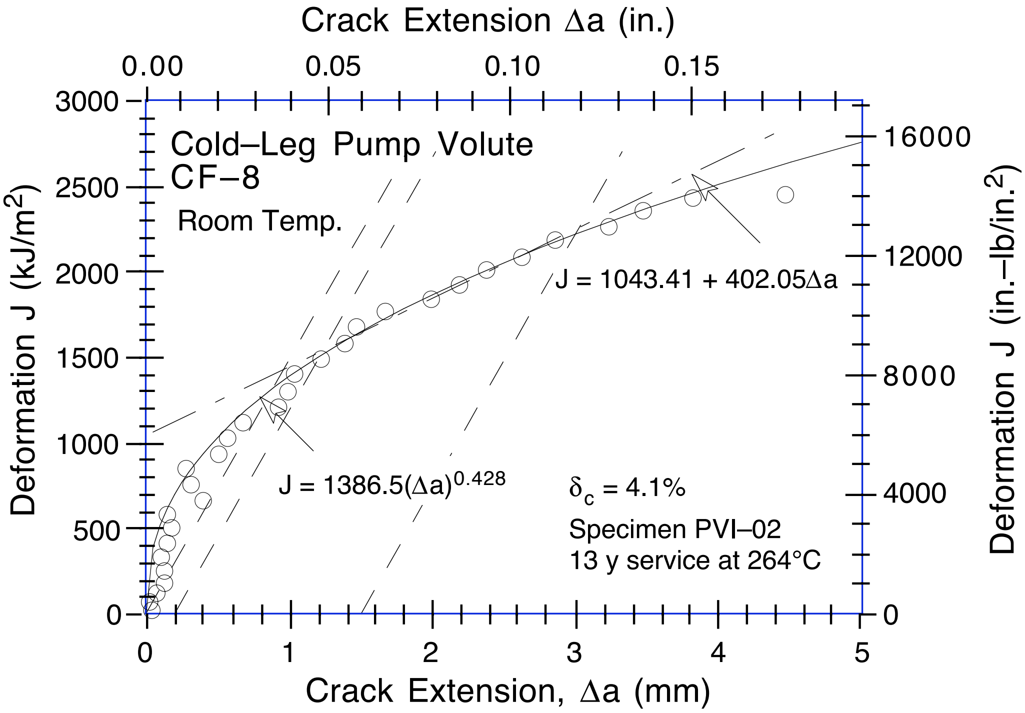

Figure C–36. Deformation J–R Curve at room temperature for the cold–leg pump volute PV after 13 y of service at 264°C

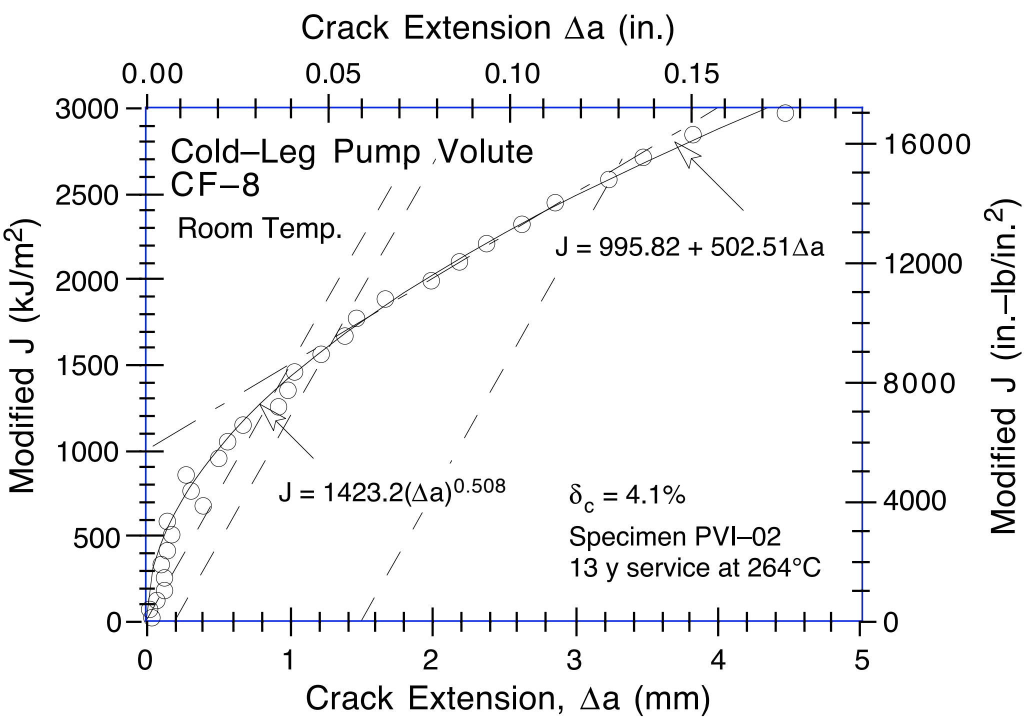

Figure C–37. Modified J–R Curve at room temperature for the cold–leg pump volute PV after 13 y of service at 264°C

Table C–38. Test data for specimen PVO–01

Test Number	: 0119	Test Temp.	: 25°C
Material Type	: CF–8	Heat Number	: PV
Aging Temp.	: 400°C	Aging Time	: 10,000 h
Spec. Thickness	: 25.39 mm	Net Thickness	: 20.26 mm
Spec. Width	: 50.75 mm	Flow Stress	: 410.00 MPa

Unload Number	J_d (kJ/m^2)	J_m (kJ/m^2)	Δa (mm)	Load (kN)	Deflection (mm)
1	12.90	12.87	-0.0989	17.899	0.252
2	39.22	39.41	0.0427	22.306	0.504
3	75.34	75.72	0.0944	24.909	0.806
4	114.73	115.18	0.1053	26.449	1.106
5	156.49	157.00	0.1127	27.668	1.405
6	185.85	185.59	0.0364	28.496	1.606
7	215.26	215.90	0.1130	29.112	1.807
8	244.80	245.72	0.1334	29.675	2.006
9	282.97	284.09	0.1460	30.255	2.256
10	321.88	323.68	0.1833	30.650	2.507
11	360.32	365.70	0.3568	31.105	2.765
12	398.53	403.77	0.3509	31.496	3.006
13	427.96	438.15	0.5490	31.531	3.208
14	461.09	470.07	0.5042	31.725	3.410
15	491.93	503.91	0.6079	31.979	3.607
16	525.08	536.65	0.5951	31.767	3.807
17	550.18	572.22	0.9135	31.846	4.008
18	579.72	604.27	0.9856	31.684	4.209
19	610.51	638.06	1.0669	31.878	4.408
20	639.14	672.70	1.2216	31.634	4.609
21	666.00	707.15	1.4077	31.866	4.810
22	695.24	740.67	1.5076	31.969	5.008
23	730.38	775.11	1.4919	31.982	5.211
24	767.73	819.40	1.6374	32.137	5.457
25	807.18	863.21	1.7238	32.029	5.708
26	853.48	916.72	1.8585	32.165	6.008
27	892.89	970.58	2.1130	31.968	6.306
28	939.47	1023.04	2.2110	31.896	6.608
29	983.12	1077.41	2.3800	31.585	6.908
30	1030.26	1130.42	2.4681	31.705	7.207
31	1072.87	1185.44	2.6452	31.472	7.508
32	1114.38	1239.67	2.8187	31.236	7.809
33	1155.01	1293.66	2.9930	31.021	8.108
34	1192.22	1347.81	3.2048	30.361	8.409
35	1237.58	1419.77	3.5206	29.834	8.809
36	1283.48	1490.15	3.7970	28.670	9.212
37	1320.09	1558.41	4.1389	27.991	9.607
38	1355.90	1626.03	4.4678	26.883	10.007
39	1380.18	1710.38	5.0614	25.863	10.507
40	1421.27	1789.79	5.4222	24.859	11.007
41	1466.12	1871.65	5.7544	24.462	11.510
42	1517.84	1954.33	6.0188	23.795	12.027
43	1552.82	2032.65	6.3740	23.278	12.506
44	1592.69	2112.30	6.6861	22.484	13.007
45	1621.37	2191.77	7.0693	21.625	13.510
46	1663.40	2267.60	7.3142	21.101	14.007
47	1686.55	2361.42	7.8046	19.948	14.607
48	1707.56	2449.31	8.2506	19.101	15.207

Table C–39. Deformation J_{IC} and J–R curve results for specimen PVO–01

Test Number	: 0119	Test Temp	: 25 °C
Material Type	: CF-8	Heat Number	: PV
Aging Temp	: 400 °C	Aging Time	: 10,000 h
Spec. Thickness:	: 25.39 mm	Net Thickness	: 20.26 mm
Spec. Width	: 50.75 mm	Flow Stress	: 410.00 MPa
Modulus E	: 193.04 GPa	(Effective)	
Modulus E	: 200.00 GPa	(Nominal)	
Init. Crack	: 29.2250 mm	Init. a/w	: 0.5758 (Measured)
Final Crack	: 38.7813 mm	Final a/w	: 0.7641 (Measured)
Final Crack	: 37.4756 mm	Final a/w	: 0.7384 (Compliance)
Linear Fit	**$J = B+M(\Delta a)$**		
Intercept B	: 312.535 kJ/m^2	Slope M	: 275.67 kJ/m^2mm
Fit Coeff. R	: 0.9826	(14 Data Points)	
J_{IC}	: 375.7 kJ/m^2	(2145.2 in.–lb/in.^{2})	
Δa (J_{IC})	: 0.229 mm	(0.0090 in.)	
T Average	: 316.6	(J_{IC} at 0.15)	
Power–Law Fit	**$J = C(\Delta a)^n$**		
Coeff. C	: 602.97 kJ/m^2	Exponent n	: 0.4503
Fit Coeff. R	: 0.9711	(14 Data Points)	
J_{IC} (0.20)	: 424.6 kJ/m^2	(2424.6 in.–lb/in.^{2})	
Δa (J_{IC})	: 0.459 mm	(0.0181 in.)	
T Average	: 288.9	(J_{IC} at .20)	
J_{IC} (0.15)	: 395.0 kJ/m^2	(2255.5 in.–lb/in.^{2})	
Δa (J_{IC})	: 0.391 mm	(0.0154 in.)	
T Average	: 295.4	(J_{IC} at 0.15)	
Kjc	: 398.9 MPa–$m^{0.5}$		
J_{IC} Validity & Data Qualification (E 813–85)			
J_{max} Allowed	: 588.40 kJ/m^2	($J_{max}=b_o\sigma_f/15$)	
Data Limit	: J_{max} Ignored		
Δa (max) Allowed	: 2.003 mm	(at 1.5 Exclusion Line)	
Data Limit	: 1.5 Exclusion Line		
Data Points	: Zone A = 4	Zone B = 6	
Data Point Spacing	: OK		
b_{net} or b_o Size	: Inadequate		
dJ/da at J_{IC}	: OK		
a_f Measurement	: Near-surface	outside limit	
Initial Crack Shape	: OK		
Crack size estimate	: Inadequate	(by Compliance)	
E Effective	: OK		
J_{IC} Estimate	: Invalid		
J–R Curve Validity & Data Qualification (E 1152–86)			
J_{max} Allowed	: 415.37 kJ/m^2	($J_{max}=b_{net}\sigma_f/20$)	
Δa (max) Allowed	: 2.153 mm	($\Delta a=0.1b_o$)	
Δa (max) Allowed	: 4.193 mm	($\omega=5$)	
Data Points	: Zone A = 18	Zone B = 8	
Data Point Spacing	: OK		
J-R Curve Data	: Invalid		

Table C–40. Modified J_{IC} and J–R curve results for specimen PVO–01

Linear Fit	**$J = B+M(\Delta a)$**		
Intercept B	: 300.136 kJ/m^2	Slope M	: 314.63 kJ/m^2mm
Fit Coeff. R	: 0.9857	(14 Data Points)	
J_{IC}	: 371.4 kJ/m^2	(2120.7 $in.–lb/in.^2$)	
Δa (J_{IC})	: 0.226 mm	(0.0089 in.)	
T Average	: 361.3	(J_{IC} at 0.15)	
Power–Law Fit	**$J = C(\Delta a)^n$**		
Coeff. C	: 630.46 kJ/m^2	Exponent n	: 0.4906
Fit Coeff. R	: 0.9756	(14 Data Points)	
J_{IC} (0.20)	: 432.4 kJ/m^2	(2469.0 $in.–lb/in.^2$)	
Δa (J_{IC})	: 0.464 mm	(0.0183 in.)	
T Average	: 327.6	(J_{IC} at 0.20)	
J_{IC} (0.15)	: 398.8 kJ/m^2	(2277.1 $in.–lb/in.^2$)	
Δa (J_{IC})	: 0.393 mm	(0.0155 in.)	
T Average	: 334.5	(J_{IC} at 0.15)	
Kjc	: 415.8 $MPa–m^{0.5}$		

Figure C–38. Fracture surface of service–aged PV material from the pump volute aged further for 10,000 h at 400°C and tested at room temperature

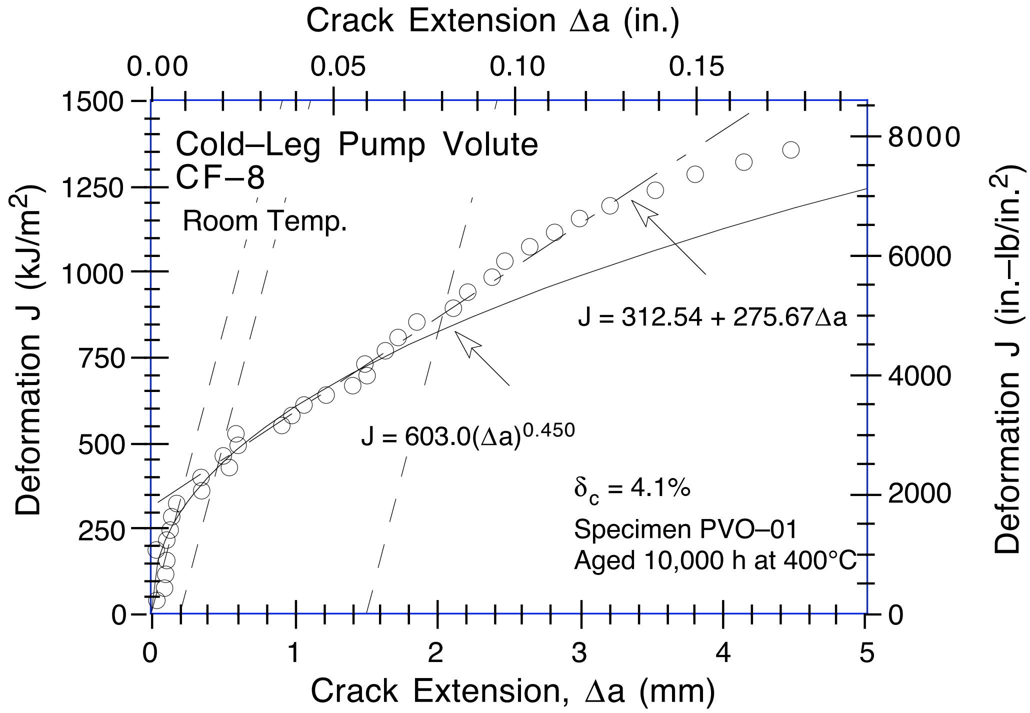

Figure C–39. Deformation J–R Curve at room temperature for service–aged PV material from the pump volute aged further for 10,000 h at 400°C

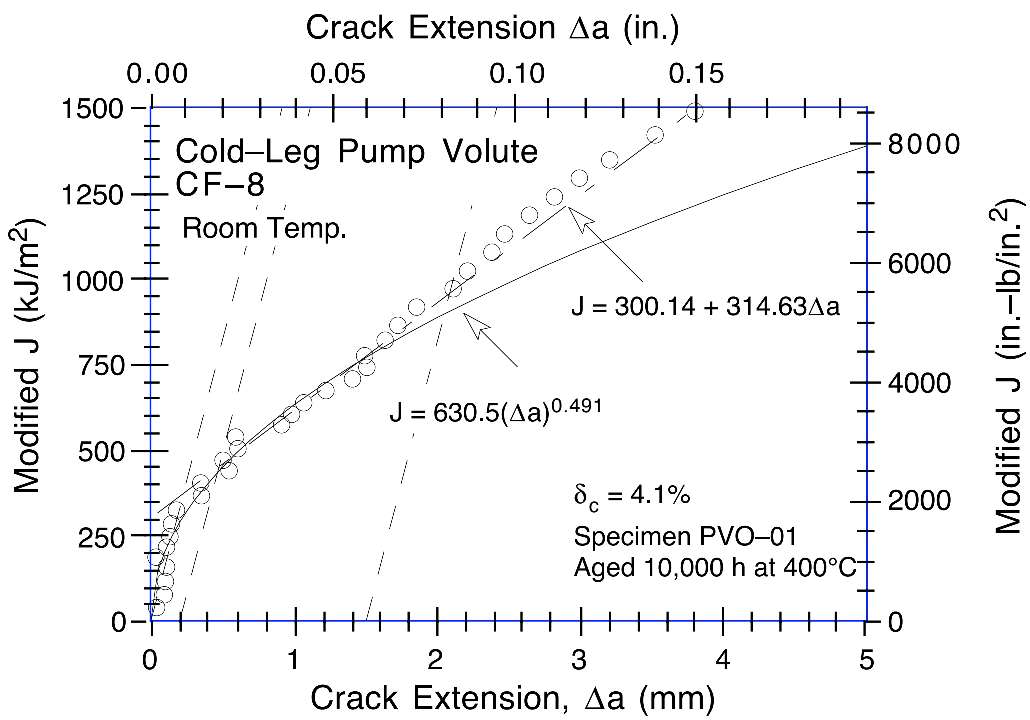

Figure C–40. Modified J–R Curve at room temperature for service–aged PV material from the pump volute aged further for 10,000 h at 400°C

Table C–41. Test data for specimen PVI–01

Test Number	: 0080	Test Temp.	: 290°C
Material Type	: CF–8	Heat Number	: PV
Aging Temp.	: 550°C	Aging Time	: 1 h
Spec. Thickness	: 25.35 mm	Net Thickness	: 20.22 mm
Spec. Width	: 50.79 mm	Flow Stress	: 269.19 MPa

Unload Number	J_d (kJ/m^2)	J_m (kJ/m^2)	Δa (mm)	Load (kN)	Deflection (mm)
1	15.13	15.02	–0.1850	14.314	0.306
2	37.74	37.88	–0.0500	15.935	0.608
3	69.98	70.75	0.1227	17.206	1.009
4	104.73	105.39	0.1030	18.188	1.408
5	142.15	142.29	0.0368	19.000	1.810
6	180.34	181.06	0.0940	19.869	2.210
7	220.16	221.18	0.1174	20.497	2.612
8	265.35	262.07	–0.1695	21.162	3.018
9	302.31	305.23	0.1897	21.718	3.409
10	352.24	346.59	–0.2397	22.365	3.810
11	393.18	393.03	0.0049	23.001	4.209
12	436.99	441.00	0.1703	23.573	4.627
13	478.10	485.89	0.3071	24.043	5.007
14	524.44	534.54	0.3825	24.485	5.409
15	579.19	583.11	0.1983	24.917	5.809
16	626.43	634.64	0.3160	25.434	6.210
17	684.65	684.13	0.0959	25.788	6.608
18	719.86	737.89	0.5346	26.053	7.006
19	775.72	792.29	0.5027	26.282	7.434
20	817.41	843.41	0.6975	26.491	7.810
21	863.97	897.17	0.8375	26.653	8.210
22	919.98	951.72	0.8109	26.756	8.616
23	960.19	1007.64	1.0830	26.747	9.015
24	1019.29	1060.82	0.9862	26.689	9.414
25	1053.10	1117.58	1.3446	26.552	9.814
26	1084.02	1172.26	1.7008	26.434	10.212
27	1114.29	1227.84	2.0652	26.360	10.611
28	1167.17	1285.15	2.1258	26.401	11.027
29	1214.41	1340.92	2.2375	26.461	11.415
30	1250.69	1398.35	2.5039	26.296	11.810
31	1290.75	1454.92	2.7038	26.127	12.207
32	1317.13	1513.99	3.0860	25.739	12.615
33	1360.55	1585.48	3.3995	25.196	13.118
34	1385.96	1655.34	3.8776	24.546	13.610
35	1421.19	1725.39	4.2371	24.081	14.114
36	1469.72	1794.16	4.4373	23.480	14.610
37	1510.08	1899.77	5.0487	22.738	15.358

Table C–42. Deformation J_{IC} and J–R curve results for specimen PVI–01

Test Number	: 0080	Test Temp.	: 290°C
Material Type	: CF–8	Heat Number	: PV
Aging Temp.	: 550°C	Aging Time	: 1 h
Spec. Thickness	: 25.35 mm	Net Thickness	: 20.22 mm
Spec. Width	: 50.79 mm	Flow Stress	: 269.19 MPa
Modulus E	: 172.73 GPa	(Effective)	
Modulus E	: 180.00 GPa	(Nominal)	
Init. Crack	: 28.2531 mm	Init. a/w	: 0.5563 (Measured)
Final Crack	: 34.5469 mm	Final a/w	: 0.6803 (Measured)
Final Crack	: 33.3018 mm	Final a/w	: 0.6557 (Compliance)
Linear Fit	**J = B+M(Δa)**		
Intercept B	: 796.938 kJ/m^2	Slope M	: 175.50 kJ/m^{2}mm
Fit Coeff. R	: 0.9408	(6 Data Points)	
J_{IC}	: 952.1 kJ/m^2	(5436.8 in.–lb/in.^{2})	
Δa (J_{IC})	: 0.884 mm	(0.0348 in.)	
T Average	: 418.3	(J_{IC} at 0.15)	
Power–Law Fit	**J = C(Δa)^n**		
Coeff. C	: 951.03 kJ/m^2	Exponent n	: 0.2765
Fit Coeff. R	: 0.9227	(6 Data Points)	
J_{IC} (0.20)	: 978.6 kJ/m^2	(5588.0 in.–lb/in.^{2})	
Δa (J_{IC})	: 1.109 mm	(0.0437 in.)	
T Average	: 405.5	(J_{IC} at 0.20)	
J_{IC} (0.15)	: 962.4 kJ/m^2	(5495.3 in.–lb/in.^{2})	
Δa (J_{IC})	: 1.044 mm	(0.0411 in.)	
T Average	: 411.9	(J_{IC} at 0.15)	
Kjc	: 463.9 MPa–m$^{0.5}$		
J_{IC} Validity & Data Qualification (E 813–85)			
J_{max} Allowed	: 404.36 kJ/m^2	($J_{max}=b_o\sigma_f/15$)	
Data Limit	: J_{max} Ignored		
Δa (max) Allowed	: 2.657 mm	(at 1.5 Exclusion Line)	
Data Limit	: 1.5 Exclusion Line		
Data Points	: Zone A = 1	Zone B = 4	
Data Point Spacing	: OK		
b_{net} or b_o Size	: Inadequate		
dJ/da at J_{IC}	: OK		
a_f Measurement	: Near–surface	Outside Limit	
Initial Crack Shape	: OK		
Crack Size Estimate	: Inadequate	(by Compliance)	
E Effective	: OK		
J_{IC} Estimate	: Invalid		
J–R Curve Validity & Data Qualification (E 1152–86)			
J_{max} Allowed	: 272.19 kJ/m^2	($J_{max}=b_{net}\sigma_f//20$)	
Δa (max) Allowed	: 2.253 mm	(Δa=0.1b_o)	
Δa (max) Allowed	: 2.662 mm	(ω=5)	
Data Points	: Zone A = 29	Zone B = 0	
Data Point Spacing	: Inadequate		
J–R Curve Data	: Invalid		

Table C–43. Modified J_{IC} and J–R curve results for specimen PVI–01

Linear Fit	**$J = B+M(\Delta a)$**		
Intercept B	: 657.014 kJ/m^2	Slope M	: 295.22 kJ/m^{2}mm
Fit Coeff. R	: 0.9799	(6 Data Points)	
J_{IC}	: 905.2 kJ/m^2	(5168.9 in.–lb/in.^{2})	
Δa (J_{IC})	: 0.841 mm	(0.0331 in.)	
T Average	: 703.7	(J_{IC} at 0.15)	
Power–Law Fit	**$J = C(\Delta a)^n$**		
Coeff. C	: 892.04 kJ/m^2	Exponent n	: 0.4873
Fit Coeff. R	: 0.9750	(6 Data Points)	
J_{IC} (0.20)	: 912.4 kJ/m^2	(5209.8 in.–lb/in.^{2})	
Δa (J_{IC})	: 1.047 mm	(0.0412 in.)	
T Average	: 745.6	(J_{IC} at 0.20)	
J_{IC} (0.15)	: 876.1 kJ/m^2	(5002.6 in.–lb/in.^{2})	
Δa (J_{IC})	: 0.964 mm	(0.0379 in.)	
T Average	: 756.0	(J_{IC} at 0.15)	
Kjc	: 508.3 MPa–m$^{0.5}$		

Figure C–41. Fracture surface of recovery–annealed material from the pump volute PV tested at 290°C

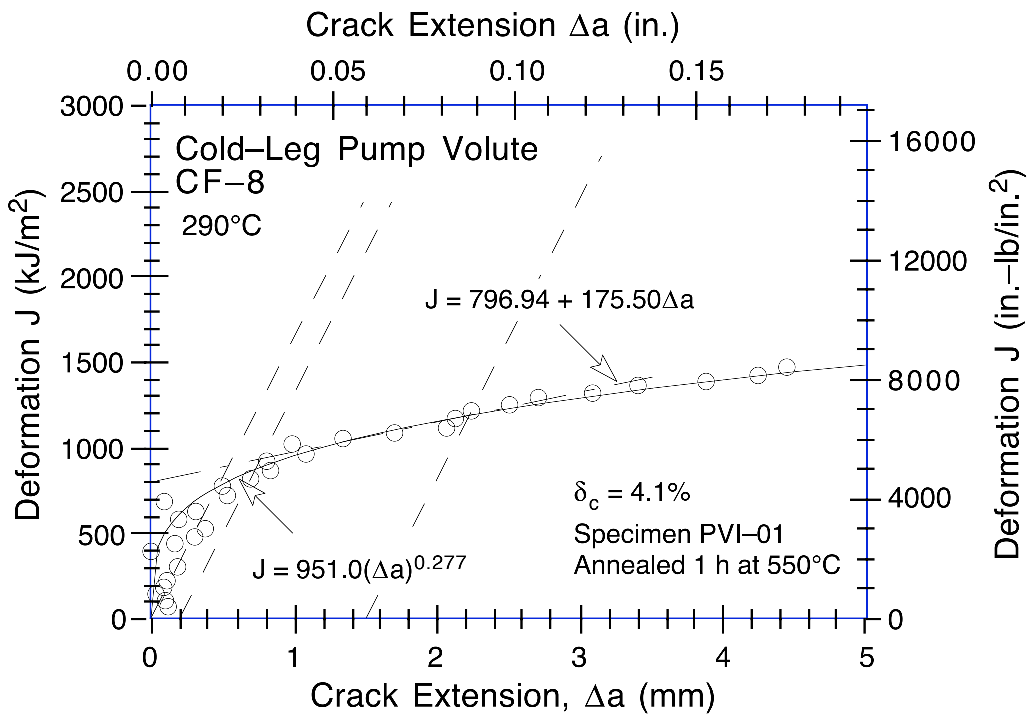

Figure C–42. Deformation J–R Curve at 290°C for recovery–annealed material PV from the pump volute

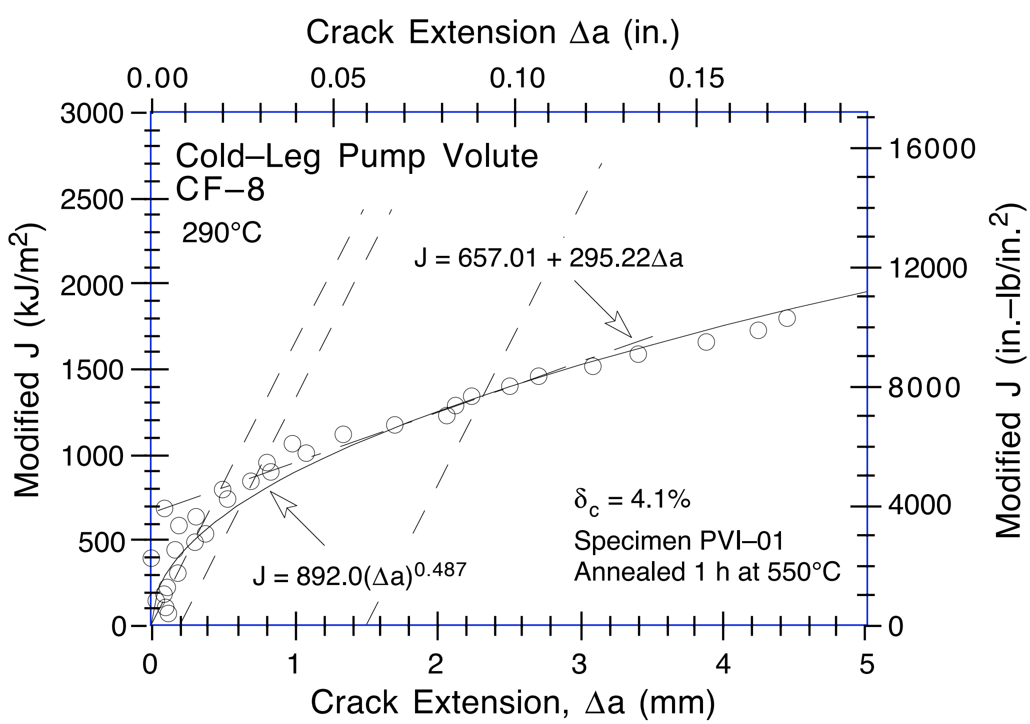

Figure C–43. Modified J–R Curve at 290°C for recovery–annealed material PV from the pump volute

Table C–44. Test data for specimen PVC–02

Test Number	: 0079	Test Temp.	: 290°C
Material Type	: CF–8	Heat Number	: PV
Aging Temp.	: 264°C	Aging Time	: 113,900 h
Spec. Thickness	: 25.37 mm	Net Thickness	: 20.28 mm
Spec. Width	: 50.82 mm	Flow Stress	: 265.80 MPa

Unload Number	J_d (kJ/m^2)	J_m (kJ/m^2)	Δa (mm)	Load (kN)	Deflection (mm)
1	7.34	7.35	0.0605	12.915	0.206
2	21.31	21.11	−0.1789	14.980	0.408
3	41.06	40.63	−0.2924	16.156	0.659
4	61.28	61.75	−0.0075	16.988	0.907
5	82.20	82.91	0.0480	17.639	1.156
6	104.55	105.26	0.0465	18.274	1.406
7	132.98	132.79	−0.0759	18.976	1.705
8	162.34	161.84	−0.1100	19.458	2.007
9	191.01	191.79	0.0083	20.019	2.308
10	223.01	221.28	−0.1910	20.474	2.608
11	249.49	253.70	0.2263	21.015	2.906
12	283.77	284.08	−0.0148	21.540	3.209
13	313.53	318.22	0.2280	21.968	3.510
14	346.31	350.61	0.2085	22.201	3.809
15	376.93	385.42	0.3999	22.775	4.109
16	413.69	419.62	0.2932	23.046	4.413
17	442.03	456.30	0.6145	23.461	4.712
18	483.08	489.98	0.3536	23.714	5.012
19	514.28	528.75	0.6032	24.135	5.315
20	531.56	557.24	0.9573	24.475	5.544
21	557.79	565.04	0.3931	25.176	5.641
22	596.19	603.86	0.4053	24.655	5.928
23	636.90	638.98	0.2554	24.971	6.212
24	666.85	678.24	0.4918	25.252	6.509
25	708.92	716.16	0.3925	25.527	6.815
26	738.92	756.19	0.6206	25.756	7.112
27	771.85	795.27	0.7543	25.877	7.413
28	805.95	834.99	0.8703	25.929	7.712
29	851.09	873.18	0.7339	25.913	8.006
30	884.78	931.32	1.1884	25.997	8.421
31	924.15	967.63	1.1339	25.891	8.708
32	950.05	1009.62	1.4098	25.833	9.007
33	984.01	1049.74	1.5116	25.821	9.308
34	1006.89	1091.81	1.8173	25.786	9.608
35	1052.24	1138.54	1.8383	25.881	9.957
36	1081.24	1189.51	2.1601	25.795	10.312
37	1124.38	1244.68	2.3284	25.931	10.711
38	1177.20	1300.38	2.3668	25.854	11.108
39	1211.86	1358.83	2.6712	25.814	11.508
40	1260.20	1419.88	2.8265	25.672	11.940
41	1306.84	1487.79	3.0747	25.366	12.410
42	1364.55	1558.32	3.2169	24.874	12.909
43	1419.98	1644.08	3.5357	24.436	13.506
44	1482.64	1744.65	3.9114	24.168	14.215
45	1668.41	1958.27	4.1535	24.025	15.706
46	1543.72	1953.07	5.2297	23.802	15.708

Table C–45. Deformation J_{IC} and J–R curve results for specimen PVC–02

Test Number	: 0079	Test Temp.	: 290°C
Material Type	: CF–8	Heat Number	: PV
Aging Temp.	: 264°C	Aging Time	: 113,900 h
Spec. Thickness	: 25.37 mm	Net Thickness	: 20.28 mm
Spec. Width	: 50.82 mm	Flow Stress	: 265.80 MPa
Modulus E	: 160.39 GPa	(Effective)	
Modulus E	: 180.00 GPa	(Nominal)	
Init. Crack	: 28.5063 mm	Init. a/w	: 0.5610 (Measured)
Final Crack	: 34.0688 mm	Final a/w	: 0.6704 (Measured)
Final Crack	: 33.7359 mm	Final a/w	: 0.6639 (Compliance)

Linear Fit	**$J = B+M(\Delta a)$**		
Intercept B	: 671.267 kJ/m^2	Slope M	: 199.53 kJ/m^2mm
Fit Coeff. R	: 0.9724	(9 Data Points)	
J_{IC}	: 826.3 kJ/m^2	(4718.6 $in.–lb/in.^2$)	
Δa (J_{IC})	: 0.777 mm	(0.0306 in.)	
T Average	: 453.0	(J_{IC} at 0.15)	

Power–Law Fit	**$J = C(\Delta a)^n$**		
Coeff. C	: 855.74 kJ/m^2	Exponent n	: 0.3271
Fit Coeff. R	: 0.9659	(9 Data Points)	
J_{IC} (0.20)	: 857.6 kJ/m^2	(4897.0 $in.–lb/in.^2$)	
Δa (J_{IC})	: 1.007 mm	(0.0396 in.)	
T Average	: 437.4	(J_{IC} at 0.20)	
J_{IC} (0.15)	: 838.1 kJ/m^2	(4785.6 $in.–lb/in.^2$)	
Δa (J_{IC})	: 0.938 mm	(0.0369 in.)	
T Average	: 444.5	(J_{IC} at 0.15)	
Kjc	: 433.1 $MPa–m^{0.5}$		

J_{IC} Validity & Data Qualification (E 813–85)			
J_{max} Allowed	: 395.31 kJ/m^2	($J_{max}=b_o\sigma_f/15$)	
Data Limit	: J_{max} Ignored		
Δa (max) Allowed	: 2.600 mm	(at 1.5 Exclusion Line)	
Data Limit	: 1.5 Exclusion Line		
Data Points	: Zone A = 2	Zone B = 3	
Data Point Spacing	: OK		
b_{net} or b_o Size	: Inadequate		
dJ/da at J_{IC}	: OK		
ao Measurement	: 9 Outside Limit		
ao Measurement	: 1 Outside Limit		
a_f Measurement	: Near–surface	Outside Limit	
Crack Size Estimate	: OK	(by Compliance)	
E Effective	: Inadequate		
J_{IC} Estimate	: Invalid		

J–R Curve Validity & Data Qualification (E 1152–86)			
J_{max} Allowed	: 269.51 kJ/m^2	($J_{max}=b_{net}\sigma_f//20$)	
Δa (max) Allowed	: 2.231 mm	($\Delta a=0.1b_o$)	
Δa (max) Allowed	: 3.120 mm	($\omega=5$)	
Data Points	: Zone A = 37	Zone B = 1	
Data Point Spacing	: Inadequate		
J–R Curve Data	: Invalid		

Table C–46. Modified J_{IC} and J–R curve results for specimen PVC–02

Linear Fit	**J = B+M(Δa)**		
Intercept B	: 622.039 kJ/m^2	Slope M	: 275.71 kJ/m^{2}mm
Fit Coeff. R	: 0.9909	(11 Data Points)	
J_{IC}	: 839.8 kJ/m^2	(4795.5 in.–lb/in.^{2})	
Δa (J_{IC})	: 0.790 mm	(0.0311 in.)	
T Average	: 625.9	(J_{IC} at 0.15)	
Power–Law Fit	**J = C(Δa)^n**		
Coeff. C	: 875.54 kJ/m^2	Exponent n	: 0.4358
Fit Coeff. R	: 0.9835	(11 Data Points)	
J_{IC} (0.20)	: 889.3 kJ/m^2	(5078.1 in.–lb/in.^{2})	
Δa (J_{IC})	: 1.036 mm	(0.0408 in.)	
T Average	: 612.9	(J_{IC} at 0.20)	
J_{IC} (0.15)	: 859.5 kJ/m^2	(4907.8 in.–lb/in.^{2})	
Δa (J_{IC})	: 0.958 mm	(0.0377 in.)	
T Average	: 621.9	(J_{IC} at 0.15)	
Kjc	: 468.5 MPa–m$^{0.5}$		

Figure C–44. Fracture surface of pump volute PV tested at 290°C after 13 y of service at 264°C

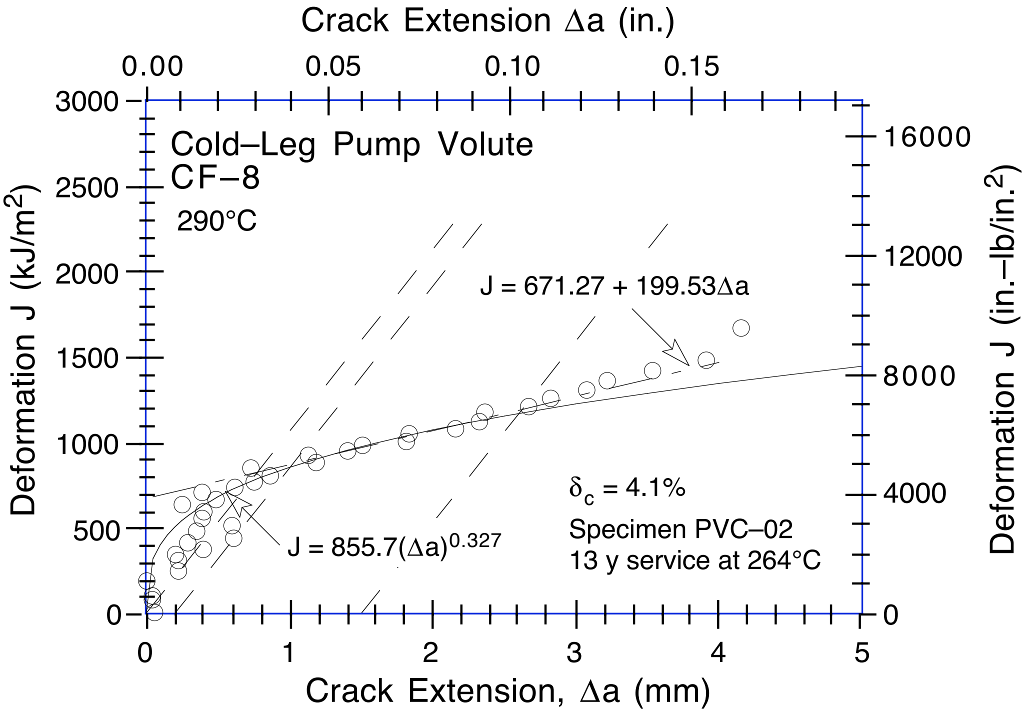

Figure C–45. Deformation J–R Curve at 290°C for the cold–leg pump volute PV after 13 y of service at 264°C

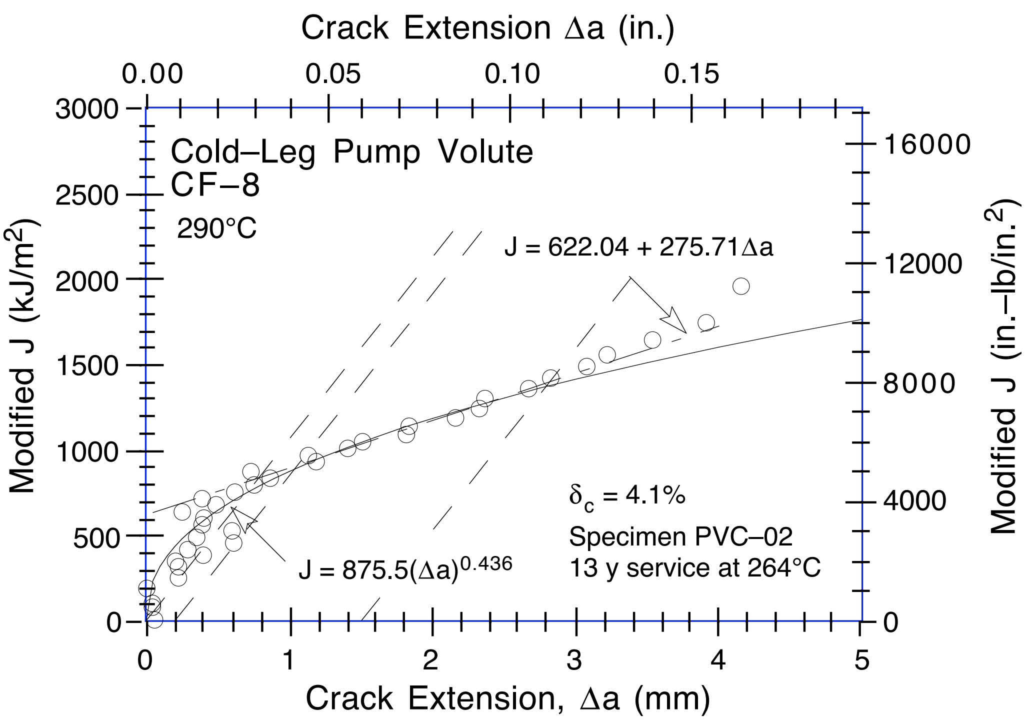

Figure C–46. Modified J–R Curve at 290°C for the cold–leg pump volute PV after 13 y of service at 264°C

Table C–47. Test data for specimen PVO–02

Test Number	: 0120	Test Temp	: 290°C
Material Type	: CF-8	Heat Number	: PV
Aging Temp	: 400°C	Aging Time	: 10,000 h
Spec. Thickness	: 25.39 mm	Net Thickness	: 20.27 mm
Spec. Width	: 50.80 mm	Flow Stress	: 286.00 MPa

Unload Number	J_d (kJ/m^2)	J_m (kJ/m^2)	Δa (mm)	Load (kN)	Deflection (mm)
1	9.65	9.65	-0.0211	11.793	0.254
2	26.63	26.61	-0.0263	14.058	0.506
3	49.80	50.05	0.0754	15.516	0.807
4	75.02	74.46	-0.1237	16.533	1.107
5	101.31	101.80	0.0618	17.441	1.407
6	133.83	133.67	-0.0241	18.200	1.757
7	167.14	168.30	0.1129	18.885	2.108
8	201.82	203.33	0.1436	19.569	2.459
9	237.09	239.73	0.2240	20.118	2.808
10	268.38	271.71	0.2670	20.538	3.108
11	303.26	310.80	0.4992	20.967	3.460
12	339.54	344.02	0.3486	21.230	3.769
13	373.63	383.53	0.5879	21.499	4.105
14	408.35	417.04	0.5393	21.673	4.406
15	444.46	458.99	0.7536	21.928	4.757
16	484.28	499.75	0.7850	22.139	5.108
17	518.33	542.67	1.0605	22.287	5.457
18	556.68	585.12	1.1780	22.261	5.813
19	597.37	630.46	1.3015	22.382	6.183
20	629.19	671.05	1.5208	22.287	6.509
21	664.65	706.61	1.5230	22.054	6.806
22	687.68	751.58	2.0140	21.948	7.155
23	725.25	792.97	2.0947	21.881	7.505
24	757.67	844.59	2.4766	21.721	7.908
25	797.34	893.47	2.6493	21.394	8.308
26	830.09	943.99	2.9652	21.281	8.706
27	886.92	1005.91	3.0492	21.230	9.207
28	925.48	1070.79	3.4585	20.766	9.707
29	955.32	1133.33	3.9406	20.072	10.207
30	994.01	1193.79	4.2443	19.421	10.707
31	1021.46	1255.40	4.6979	18.855	11.208
32	1066.99	1326.34	5.0153	18.014	11.807
33	1087.20	1398.25	5.6300	17.358	12.411
34	1098.20	1465.26	6.2669	16.209	13.006
35	1131.54	1530.84	6.6157	15.680	13.606
36	1160.38	1610.16	7.1327	14.998	14.307
37	1172.75	1686.67	7.7587	14.220	15.007

Table C–48. Deformation J_{IC} and J–R curve results for specimen PVO–02

Test Number	: 0120	Test Temp	: 290°C
Material Type	: CF-8	Heat Number	: PV
Aging Temp	: 400°C	Aging Time	: 10,000 h
Spec. Thickness	: 25.39 mm	Net Thickness	: 20.27 mm
Spec. Width	: 50.80 mm	Flow Stress	: 286.00 MPa
Modulus E	: 163.50 GPa	(Effective)	
Modulus E	: 180.00 GPa	(Nominal)	
Init. Crack	: 29.6531 mm	Init. a/w	: 0.5838 (Measured)
Final Crack	: 38.6813 mm	Final a/w	: 0.7615 (Measured)
Final Crack	: 37.4119 mm	Final a/w	: 0.7365 (Compliance)

Linear Fit	**$J = B+M(\Delta a)$**		
Intercept B	: 294.072 kJ/m^2	Slope M	: 213.73 kJ/m^{2}mm
Fit Coeff. R	: 0.9735	(11 Data Points)	
J_{IC}	: 361.6 kJ/m^2	(2065.0 in.–lb/in.^{2})	
Δa (J_{IC})	: 0.316 mm	(0.0124 in.)	
T Average	: 427.2	(J_{IC} at 0.15)	

Power–Law Fit	**$J = C(\Delta a)^n$**		
Coeff. C	: 517.37 kJ/m^2	Exponent N	: 0.4645
Fit Coeff. R	: 0.9823	(11 Data Points)	
J_{IC} (0.20)	: 388.4 kJ/m^2	(2218.1 in.–lb/in.^{2})	
Δa (J_{IC})	: 0.540 mm	(0.0212 in.)	
T Average	: 424.1	(J_{IC} at 0.20)	
J_{IC} (0.15)	: 363.5 kJ/m^2	(2075.8 in.–lb/in.^{2})	
Δa (J_{IC})	: 0.468 mm	(0.0184 in.)	
T Average	: 432.8	(J_{IC} at 0.15)	
Kjc	: 347.2 MPa–m$^{0.5}$		

J_{IC} Validity & Data Qualification (E 813–85)

J_{max} Allowed	: 403.11 kJ/m^2	($J_{max}=b_o\sigma_f/15$)
Data Limit	: J_{max} Ignored	
Δa (max) Allowed	: 2.145 mm	(at 1.5 Exclusion Line)
Data Limit	: 1.5 Exclusion Line	
Data Points	: Zone A = 4	Zone B = 2
Data Point Spacing	: OK	
b_{net} or b_o Size	: Inadequate	
dJ/da at J_{IC}	: OK	
a_f Measurement	: Near-surface	outside limit
Initial Crack Shape	: OK	
Crack size estimate	: Inadequate	(by Compliance)
E Effective	: OK	
J_{IC} Estimate	: Invalid	

J–R Curve Validity & Data Qualification (E 1152–86)

J_{max} Allowed	: 289.85 kJ/m^2	($J_{max}=b_{net}\sigma_f/20$)
Δa (max) Allowed	: 2.114 mm	($\Delta a=0.1b_o$)
Δa (max) Allowed	: 4.318 mm	($\omega=5$)
Data Points	: Zone A = 17	Zone B = 2
Data Point Spacing	: Inadequate	
J-R Curve Data	: Invalid	

Table C–49. Modified J_{IC} and J–R curve results for specimen PVO–02

Linear Fit	**J = B+M(Δa)**		
Intercept B	: 250.572 kJ/m^2	Slope M	: 270.16 kJ/m^{2}mm
Fit Coeff. R	: 0.9732	(12 Data Points)	
J_{IC}	: 328.0 kJ/m^2	(1873.2 in.–lb/in.^{2})	
Δa (J_{IC})	: 0.287 mm	(0.0113 in.)	
T Average	: 540.0	(J_{IC} at 0.15)	
Power–Law Fit	**J = C(Δa)^n**		
Coeff. C	: 532.11 kJ/m^2	Exponent N	: 0.5658
Fit Coeff. R	: 0.9759	(12 Data Points)	
J_{IC} (0.20)	: 368.3 kJ/m^2	(2103.2 in.–lb/in.^{2})	
Δa (J_{IC})	: 0.522 mm	(0.0205 in.)	
T Average	: 538.1	(J_{IC} at 0.20)	
J_{IC} (0.15)	: 336.0 kJ/m^2	(1918.4 in.–lb/in.^{2})	
Δa (J_{IC})	: 0.444 mm	(0.0175 in.)	
T Average	: 547.6	(J_{IC} at 0.15)	
Kjc	: 370.2 MPa–m$^{0.5}$		

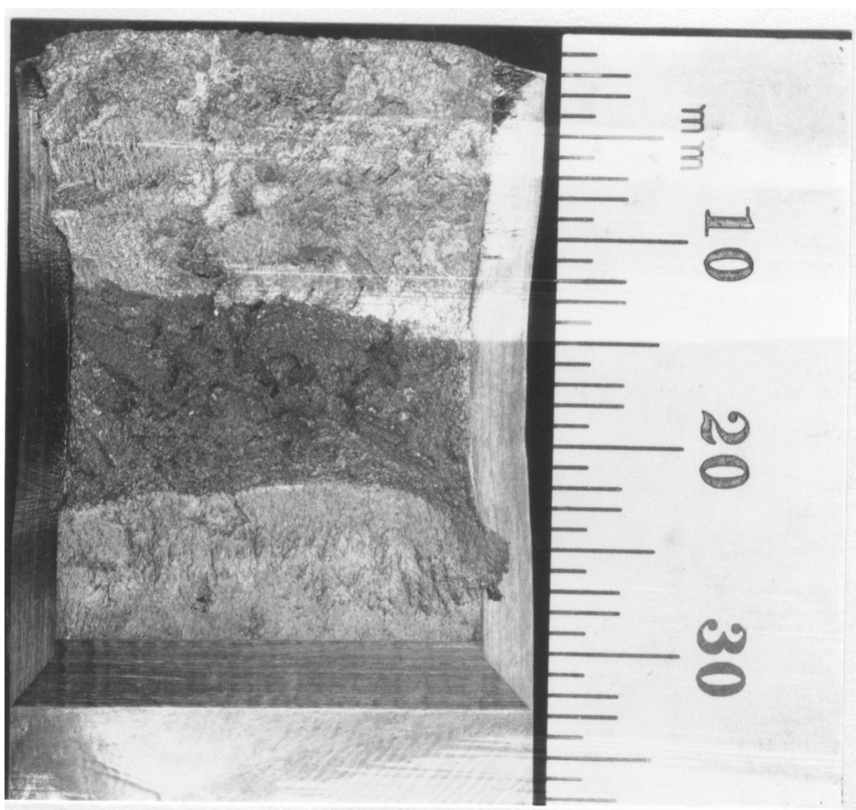

Figure C–47. Fracture surface of service–aged material PV from the pump volute aged further for 10,000 h at 400°C and tested at 290°C

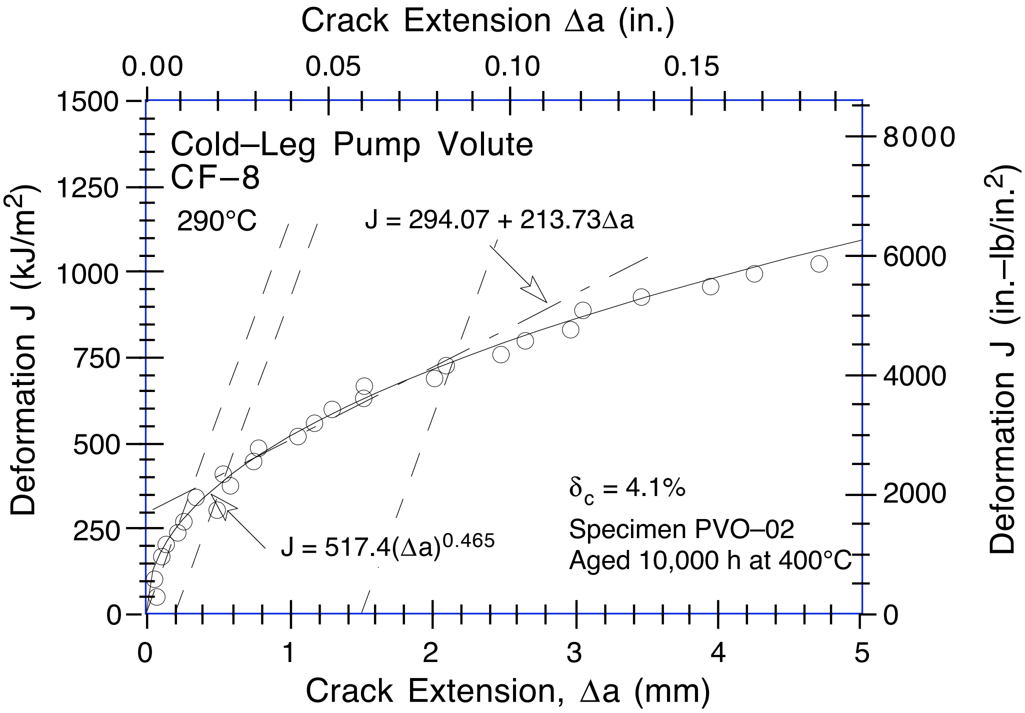

Figure C–48. Deformation J–R Curve at 290°C of service–aged material PV from the pump volute aged further for 10,000 h at 400°C

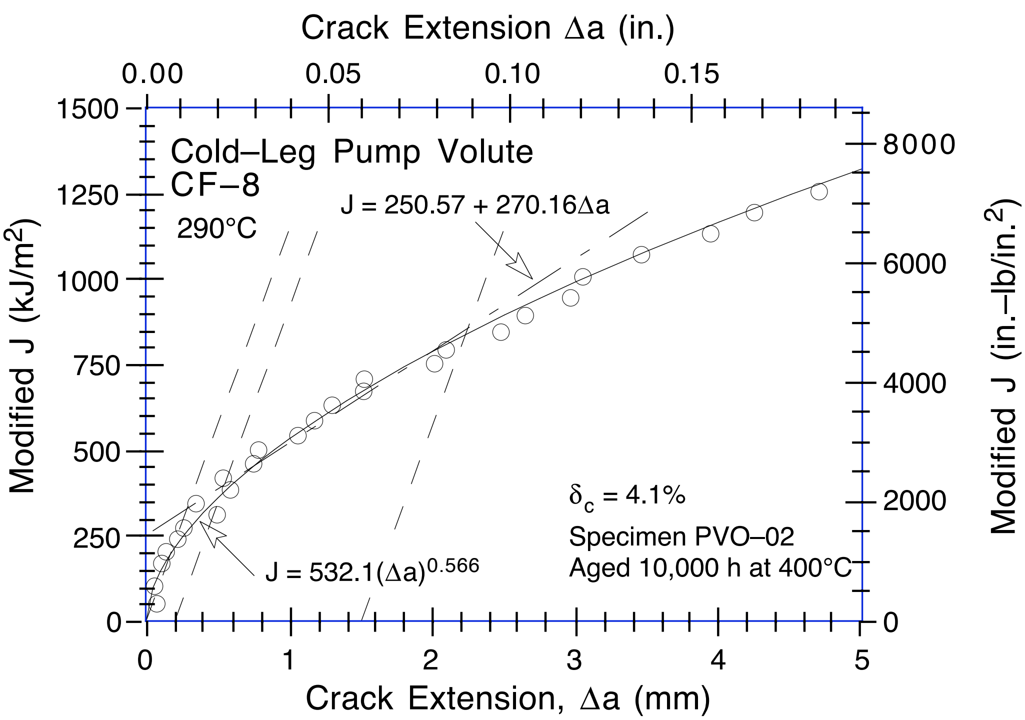

Figure C–49. Modified J–R Curve at 290°C of service–aged material PV from the pump volute aged further for 10,000 h at 400°C

Table C–50. Test data for specimen VRI–01

Test Number	: 0082	Test Temp.	: 25°C
Material Type	: CF–8	Heat Number	: VR
Aging Temp.	: 25°C	Aging Time	: 0 h
Spec. Thickness	: 25.40 mm	Net Thickness	: 20.25 mm
Spec. Width	: 50.81 mm	Flow Stress	: 405.00 MPa

Unload Number	J_d (kJ/m^2)	J_m (kJ/m^2)	Δa (mm)	Load (kN)	Deflection (mm)
1	19.34	19.27	–0.1614	22.264	0.302
2	58.57	58.95	0.0300	27.614	0.606
3	101.65	102.00	0.0232	29.814	0.909
4	147.89	148.17	0.0143	31.023	1.209
5	195.51	196.95	0.1266	32.047	1.510
6	245.20	246.76	0.1358	33.050	1.815
7	295.06	297.52	0.1912	33.482	2.113
8	345.61	349.13	0.2466	34.298	2.411
9	396.55	402.32	0.3482	34.958	2.711
10	450.70	455.00	0.2905	35.236	3.010
11	502.46	512.32	0.4838	35.824	3.315
12	558.59	566.22	0.4143	36.405	3.616
13	611.42	624.64	0.5722	36.713	3.918
14	666.75	679.11	0.5499	36.914	4.211
15	719.31	737.93	0.6985	37.203	4.511
16	783.71	805.12	0.7588	37.403	4.861
17	844.04	874.43	0.9380	37.655	5.209
18	908.45	943.89	1.0309	37.929	5.562
19	969.29	1014.34	1.1956	38.031	5.911
20	1031.37	1084.51	1.3249	37.927	6.260
21	1092.61	1156.11	1.4802	37.829	6.612
22	1148.04	1227.94	1.7118	38.055	6.962
23	1209.98	1298.12	1.8217	37.915	7.310
24	1262.02	1370.89	2.0836	37.444	7.659
25	1323.68	1441.14	2.1865	37.159	8.009
26	1376.92	1513.83	2.4082	36.709	8.359
27	1425.81	1585.97	2.6616	36.588	8.711
28	1484.79	1656.33	2.7800	36.324	9.061
29	1535.56	1730.44	3.0124	35.787	9.417
30	1591.70	1813.86	3.2712	34.856	9.826
31	1638.26	1891.19	3.5514	34.379	10.210
32	1703.85	1991.91	3.8548	33.798	10.711
33	1773.59	2091.68	4.1012	33.567	11.210
34	1862.18	2214.43	4.3649	33.290	11.815
35	1944.39	2336.18	4.6532	32.851	12.412
36	2013.03	2457.60	5.0183	31.687	13.012
37	2097.03	2596.29	5.3753	31.043	13.710
38	2171.49	2735.73	5.7766	30.129	14.412
39	2255.15	2889.73	6.1849	27.685	15.212

Table C–51. Deformation J_{IC} and J–R curve results for specimen VRI–01

Test Number	: 0082	Test Temp.	: 25°C
Material Type	: CF–8	Heat Number	: VR
Aging Temp.	: 25°C	Aging Time	: 0 h
Spec. Thickness	: 25.40 mm	Net Thickness	: 20.25 mm
Spec. Width	: 50.81 mm	Flow Stress	: 405.00 MPa
Modulus E	: 198.61 GPa	(Effective)	
Modulus E	: 193.10 GPa	(Nominal)	
Init. Crack	: 28.8406 mm	Init. a/w	: 0.5676 (Measured)
Final Crack	: 36.5938 mm	Final a/w	: 0.7202 (Measured)
Final Crack	: 35.0255 mm	Final a/w	: 0.6894 (Compliance)
Linear Fit	**$J = B+M(\Delta a)$**		
Intercept B	: 493.721 kJ/m^2	Slope M	: 384.86 kJ/m^2mm
Fit Coeff. R	: 0.9929	(11 Data Points)	
J_{IC}	: 647.6 kJ/m^2	(3697.7 $in.–lb/in.^2$)	
Δa (J_{IC})	: 0.400mm	(0.0157 in.)	
T Average	: 466.0	(J_{IC} at 0.15)	
Power–Law Fit	**$J = C(\Delta a)^n$**		
Coeff. C	: 884.08 kJ/m^2	Exponent n	: 0.5098
Fit Coeff. R	: 0.9974	(13 Data Points)	
J_{IC} (0.20)	: 699.6 kJ/m^2	(3994.6 $in.–lb/in.^2$)	
Δa (J_{IC})	: 0.632 mm	(0.0249 in.)	
T Average	: 461.5	(J_{IC} at 0.20)	
J_{IC} (0.15)	: 654.1 kJ/m^2	(3734.8 $in.–lb/in.^2$)	
Δa (J_{IC})	: 0.554 mm	(0.0218 in.)	
T Average	: 469.7	(J_{IC} at 0.15)	
Kjc	: 520.6 $MPa–m^{0.5}$		
J_{IC} Validity & Data Qualification (E 813–85)			
J_{max} Allowed	: 593.12 kJ/m^2	($J_{max}=b_o\sigma_f/15$)	
Data Limit	: J_{max} Ignored		
Δa (max) Allowed	: 2.342 mm	(at 1.5 Exclusion Line)	
Data Limit	: 1.5 Exclusion Line		
Data Points	: Zone A = 4	Zone B = 4	
Data Point Spacing	: OK		
b_{net} or b_o Size	: Inadequate		
dJ/da at J_{IC}	: OK		
a_f Measurement	: Near–surface	Outside Limit	
Initial Crack Shape	: OK		
Crack Size Estimate	: Inadequate	(by Compliance)	
E Effective	: OK		
J_{IC} Estimate	: Invalid		
J–R Curve Validity & Data Qualification (E 1152–86)			
J_{max} Allowed	: 409.98 kJ/m^2	($J_{max}=b_{net}\sigma_f//20$)	
Δa (max) Allowed	: 2.197 mm	($\Delta a=0.1b_o$)	
Δa (max) Allowed	: 4.701 mm	($\omega=5$)	
Data Points	: Zone A = 25	Zone B = 0	
Data Point Spacing	: Inadequate		
J–R Curve Data	: Invalid		

Table C–52. Modified J_{IC} and J–R curve results for specimen VRI–01

Linear Fit	**J = B+M(Δa)**		
Intercept B	: 472.274 kJ/m^2	Slope M	: 442.26 kJ/m^{2}mm
Fit Coeff. R	: 0.9961	(12 Data Points)	
J_{IC}	: 649.6 kJ/m^2	(3709.5 in.–lb/in.^{2})	
Δa (J_{IC})	: 0.401 mm	(0.0158 in.)	
T Average	: 535.5	(J_{IC} at 0.15)	
Power–Law Fit	**J = C(Δa)^n**		
Coeff. C	: 919.57 kJ/m^2	Exponent n	: 0.5640
Fit Coeff. R	: 0.9986	(12 Data Points)	
J_{IC} (0.20)	: 716.3 kJ/m^2	(4090.3 in.–lb/in.^{2})	
Δa (J_{IC})	: 0.642 mm	(0.0253 in.)	
T Average	: 532.6	(J_{IC} at 0.20)	
J_{IC} (0.15)	: 662.3 kJ/m^2	(3781.9 in.–lb/in.^{2})	
Δa (J_{IC})	: 0.559 mm	(0.0220 in.)	
T Average	: 541.2	(J_{IC} at 0.15)	
Kjc	: 549.5 MPa–m$^{0.5}$		

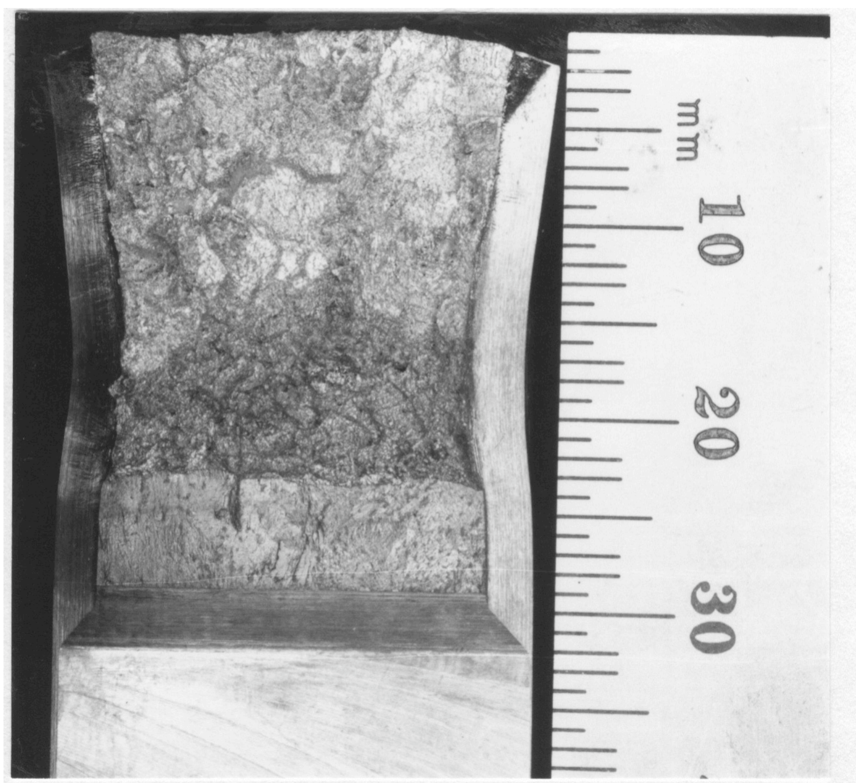

Figure C–50. Fracture surface of the unaged spare pump volute VR tested at room temperature

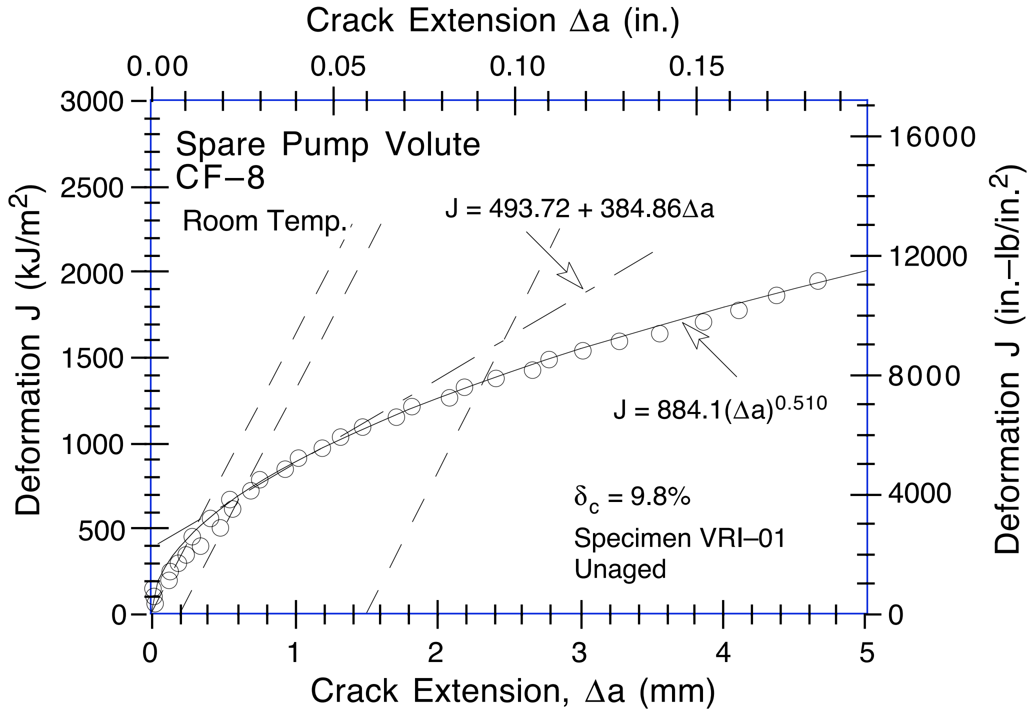

Figure C–51. Deformation J–R Curve at room temperature for unaged spare pump volute VR

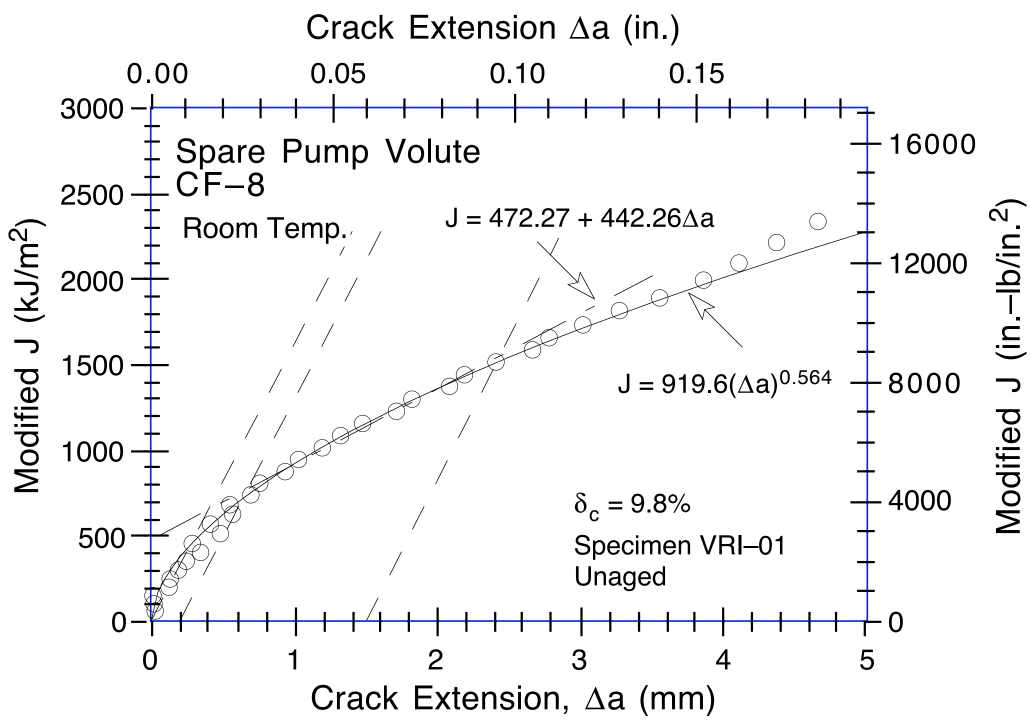

Figure C–52. Modified J–R Curve at room temperature for unaged spare pump volute VR

Table C–53. Test data for specimen VRO–02

Test Number	: 0117	Test Temp	: 25 °C
Material Type	: CF-8	Heat Number	: VR
Aging Temp	: 400 °C	Aging Time	: 10,000 h
Spec. Thickness	: 25.40 mm	Net Thickness	: 20.24 mm
Spec. Width	: 50.75 mm	Flow Stress	: 437.70 MPa

Unload Number	J_d (kJ/m^2)	J_m (kJ/m^2)	Δa (mm)	Load (kN)	Deflection (mm)
1	11.71	11.72	0.0824	16.974	0.252
2	37.61	37.52	0.0027	22.855	0.505
3	75.93	76.06	0.0696	26.076	0.806
4	117.73	118.52	0.1846	27.881	1.108
5	160.39	163.06	0.4102	28.574	1.406
6	195.50	201.08	0.6870	28.901	1.656
7	223.36	231.23	0.8728	29.088	1.856
8	251.47	262.29	1.0814	29.221	2.054
9	280.77	293.57	1.2051	29.278	2.256
10	301.72	317.64	1.3832	29.044	2.406
11	329.59	349.76	1.6029	29.128	2.607
12	358.15	381.18	1.7368	28.709	2.808
13	385.10	413.50	1.9663	28.432	3.007
14	412.88	446.73	2.1806	27.822	3.219
15	435.95	476.59	2.4297	27.199	3.410
16	467.42	514.55	2.6480	26.492	3.658
17	494.29	555.16	3.0767	25.896	3.917
18	526.02	597.91	3.3931	25.029	4.207
19	558.13	642.36	3.7214	24.471	4.506
20	601.66	702.35	4.1184	23.480	4.908
21	616.29	760.01	5.0796	20.622	5.308
22	628.69	809.10	5.8525	19.370	5.706
23	645.64	858.48	6.4941	18.121	6.106
24	664.54	907.11	7.0482	17.298	6.504
25	694.00	955.71	7.3821	16.616	6.909
26	720.25	1005.26	7.7647	16.115	7.307
27	744.67	1053.69	8.1364	15.256	7.707
28	769.85	1100.16	8.4480	14.594	8.105
29	783.76	1147.27	8.9104	13.680	8.506
30	791.64	1190.59	9.3822	12.573	8.907
31	796.72	1231.66	9.8425	11.849	9.305
32	803.54	1271.72	10.2509	11.172	9.706
33	817.11	1311.83	10.5631	10.467	10.116

Table C–54. Deformation J_{IC} and J–R curve results for specimen VRO–02

Test Number	: 0117	Test Temp	: 25 °C
Material Type	: CF-8	Heat Number	: VR
Aging Temp	: 400 °C	Aging Time	: 10,000 h
Spec. Thickness	: 25.40 mm	Net Thickness	: 20.24 mm
Spec. Width	: 50.75 mm	Flow Stress	: 437.70 MPa
Modulus E	: 174.15 GPa	(Effective)	
Modulus E	: 200.00 GPa	(Nominal)	
Init. Crack	: 29.4563 mm	Init. a/w	: 0.5804 (Measured)
Final Crack	: 40.6969 mm	Final a/w	: 0.8019 (Measured)
Final Crack	: 40.0194 mm	Final a/w	: 0.7885 (Compliance)
Linear Fit	**$J = B+M(\Delta a)$**		
Intercept B	: 97.983 kJ/m^2	Slope M	: 145.93 kJ/m^2mm
Fit Coeff. R	: 0.9978	(7 Data Points)	
J_{IC}	: 106.9 kJ/m^2	(610.4 in.–lb/in.^{2})	
Δa (J_{IC})	: 0.061 mm	(0.0024 in.)	
T Average	: 132.7	(J1c at 0.15)	
Power–Law Fit	**$J = C(\Delta a)^n$**		
Coeff. C	: 248.89 kJ/m^2	Exponent n	: 0.5408
Fit Coeff. R	: 0.9912	(7 Data Points)	
J_{IC} (0.20)	: 122.6 kJ/m^2	(700.1 in.–lb/in.^{2})	
Δa (Jic)	: 0.270 mm	(0.0106 in.)	
T Average	: 128.8	(J_{IC} at 0.20)	
J_{IC} (0.15)	: 107.4 kJ/m^2	(613.2 in.–lb/in.^{2})	
Δa (J_{IC})	: 0.211 mm	(0.0083 in.)	
T Average	: 131.7	(J_{IC} at 0.15)	
Kjc	: 239.9 MPa–$m^{0.5}$		
J_{IC} Validity & Data Qualification (E 813–85)			
J_{max} Allowed	: 621.41 kJ/m^2	($J_{max}=b_o\sigma_f/15$)	
Data Limit	: J_{max} Ignored		
Δa (max) Allowed	: 1.689 mm	(at 1.5 Exclusion Line)	
Data Limit	: 1.5 Exclusion Line		
Data Points	: Zone A = 1 Zone B = 3		
Data Point Spacing	: OK		
b_{net} or b_o Size	: OK		
dJ/da at J_{IC}	: OK		
af Measurement	: Near-surface	outside limit	
Initial Crack Shape	: OK		
Crack size estimate	: Inadequate	(by Compliance)	
E Effective	: Inadequate		
J_{IC} Estimate	: Invalid		
J–R Curve Validity & Data Qualification (E 1152–86)			
J_{max} Allowed	: 442.86 kJ/m^2	($J_{max}=b_{net}\sigma_f/20$)	
Δa (max) Allowed	: 2.130 mm	($\Delta a=0.1b_o$)	
Δa (max) Allowed	: 4.953 mm	($\omega=5$)	
Data Points	: Zone A = 3 Zone B = 10		
Data Point Spacing	: OK		
J-R Curve Data	: Invalid		

Table C–55. Modified J_{IC} and J–R curve results for specimen VRO–02

Linear Fit	**J = B+M(Δa)**		
Intercept B	: 93.678 kJ/m^2	Slope M	: 160.56 kJ/m^{2}mm
Fit Coeff. R	: 0.9981	(7 Data Points)	
J_{IC}	: 103.1 kJ/m^2	(588.9 in.–lb/in.^{2})	
Δa (J_{IC})	: 0.059 mm	(0.0023 in.)	
T Average	: 146.0	(J_{IC} at 0.15)	
Power–Law Fit	**J = C(Δa)^n**		
Coeff. C	: 259.31 kJ/m^2	Exponent n	: 0.5713
Fit Coeff. R	: 0.9912	(7 Data Points)	
J_{IC} (0.20)	: 122.8 kJ/m^2	(701.0 in.–lb/in.^{2})	
Δa (J_{IC})	: 0.270 mm	(0.0106 in.)	
T Average	: 140.8	(J_{IC} at 0.20)	
J_{IC} (0.15)	: 106.6 kJ/m^2	(608.5 in.–lb/in.^{2})	
Δa (J_{IC})	: 0.211 mm	(0.0083 in.)	
T Average	: 143.7	(J_{IC} at 0.15)	
Kjc	: 247.3 MPa–m$^{0.5}$		

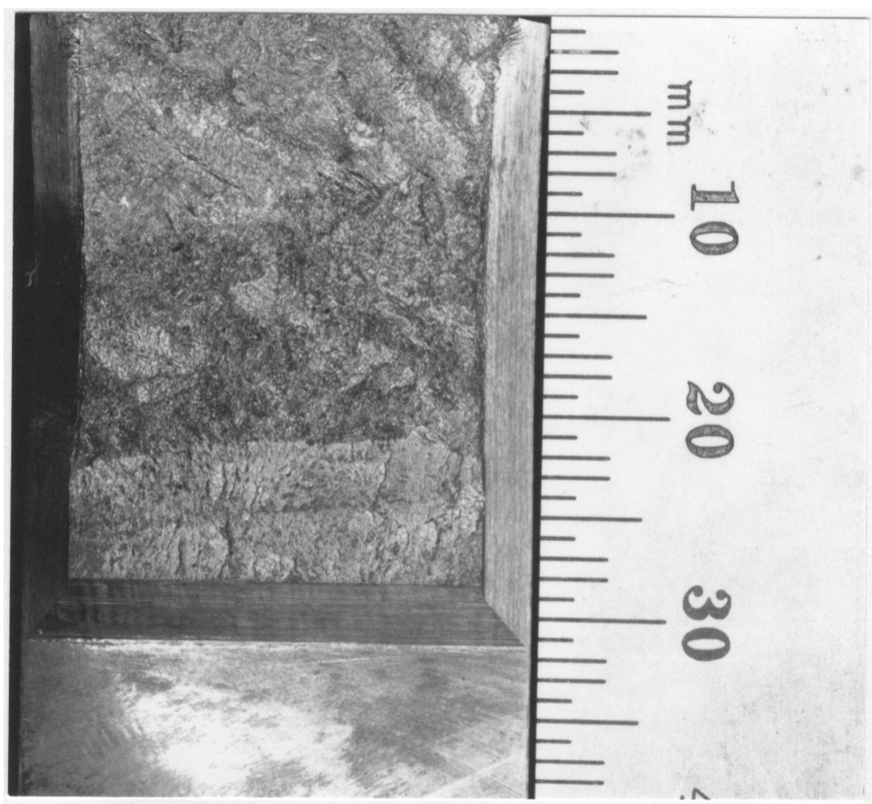

Figure C–53. Fracture surface of material from the spare pump volute VR aged 10,000 h at 400°C and tested at room temperature

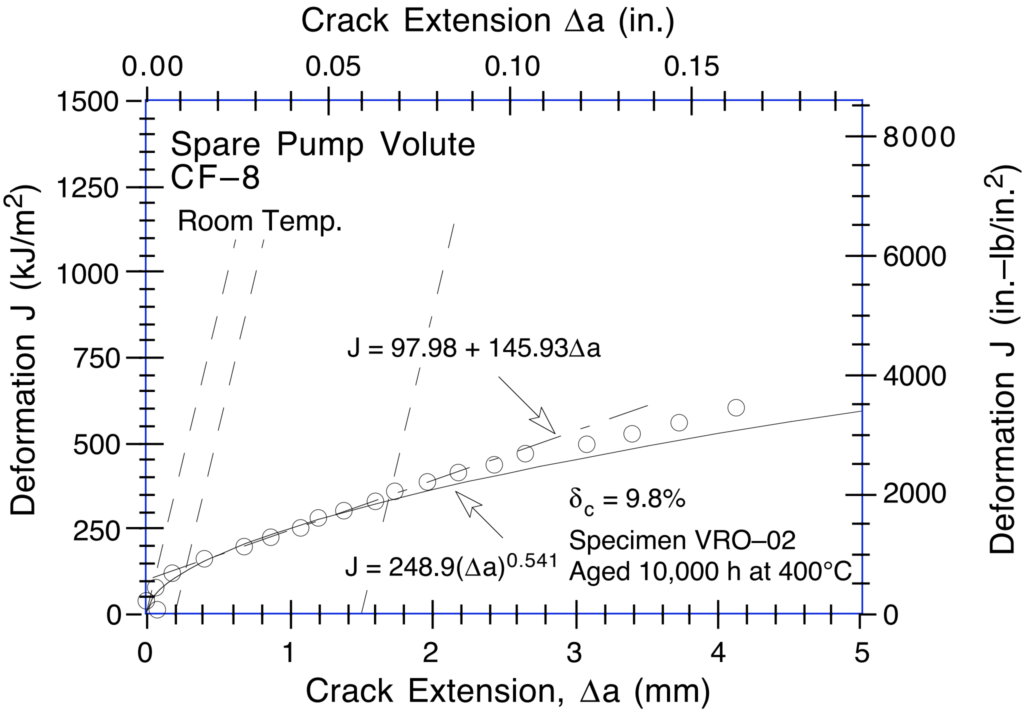

Figure C–54. Deformation J–R Curve at room temperature for material from the spare pump volute VR aged 10,000 h at 400°C

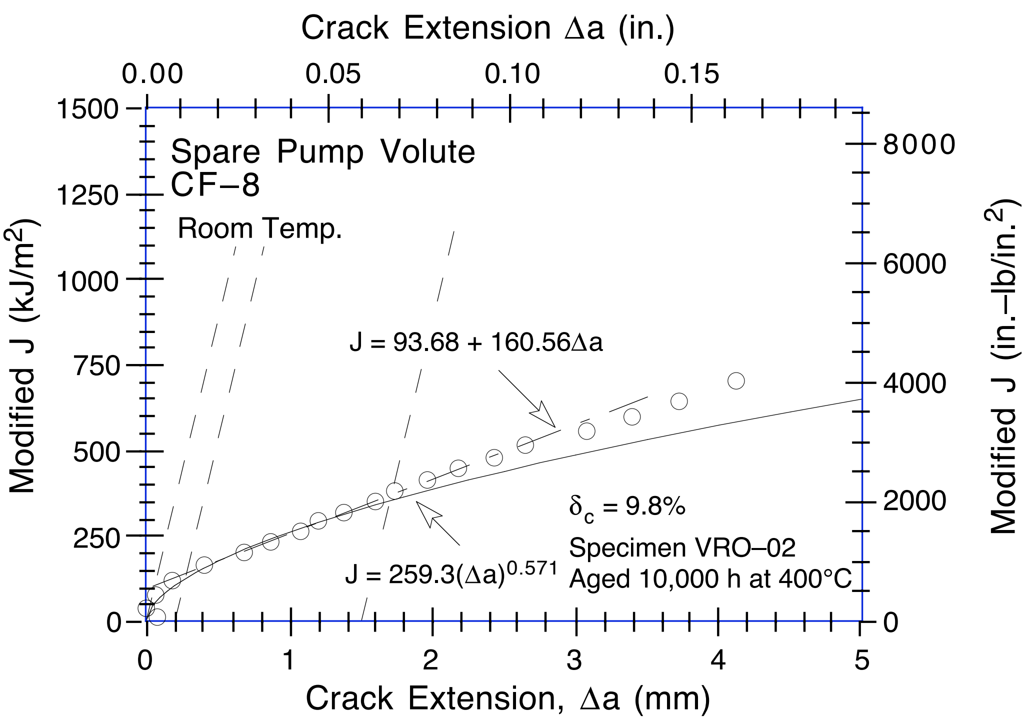

Figure C–55. Modified J–R Curve at room temperature for material from the spare pump volute VR aged 10,000 h at 400°C

Table C–56. Test data for specimen VRO–01

Test Number	: 0096	Test Temp.	: 290°C
Material Type	: CF–8	Heat Number	: VR
Aging Temp.	: 25°C	Aging Time	: 0 h
Spec. Thickness	: 25.33 mm	Net Thickness	: 20.27 mm
Spec. Width	: 50.84 mm	Flow Stress	: 266.83 MPa

Unload Number	J_d (kJ/m^2)	J_m (kJ/m^2)	Δa (mm)	Load (kN)	Deflection (mm)
1	15.91	15.94	0.0553	15.547	0.318
2	40.17	39.93	−0.0958	18.143	0.607
3	68.59	69.31	0.1872	19.553	0.910
4	98.60	97.45	−0.1773	20.520	1.208
5	129.73	130.19	0.0539	21.327	1.509
6	162.87	161.37	−0.1671	22.037	1.810
7	193.74	196.05	0.1871	22.609	2.108
8	226.69	229.86	0.2548	23.250	2.410
9	261.18	265.22	0.3138	23.786	2.709
10	296.36	301.80	0.3974	24.242	3.011
11	331.10	338.77	0.5145	24.632	3.309
12	366.68	376.62	0.6214	24.952	3.611
13	399.35	415.54	0.8895	25.091	3.910
14	438.27	453.20	0.8404	25.289	4.212
15	472.16	493.45	1.0679	25.427	4.510
16	508.57	533.16	1.1768	25.644	4.815
17	540.05	573.63	1.4538	25.769	5.111
18	580.24	612.70	1.4219	25.784	5.411
19	605.19	656.27	1.9235	25.686	5.714
20	638.55	695.00	2.0597	25.552	6.011
21	666.08	737.24	2.4119	25.304	6.310
22	705.14	777.44	2.4377	25.372	6.613
23	733.88	820.84	2.7522	25.347	6.912
24	778.46	861.36	2.6700	25.205	7.217
25	811.71	919.46	3.1426	24.670	7.611
26	841.39	972.55	3.5635	23.580	8.003
27	868.95	1027.34	4.0288	23.107	8.410
28	913.08	1093.48	4.3809	22.634	8.905
29	967.92	1175.21	4.7788	21.890	9.508
30	1011.39	1255.24	5.2839	20.890	10.110
31	1046.09	1332.69	5.8400	20.106	10.711
32	1088.61	1408.41	6.2462	19.386	11.311
33	1119.11	1484.76	6.7773	18.701	11.910
34	1165.44	1558.48	7.0769	18.096	12.509
35	1178.81	1634.68	7.7320	16.843	13.122
36	1192.05	1703.24	8.2852	16.274	13.711
37	1237.26	1772.48	8.5133	15.821	14.310
38	1268.42	1857.21	8.9943	14.816	15.012

Table C–57. Deformation J_{IC} and J–R curve results for specimen VRO–01

Test Number	: 0096	Test Temp.	: 290°C
Material Type	: CF–8	Heat Number	: VR
Aging Temp.	: 25°C	Aging Time	: 0 h
Spec. Thickness	: 25.33 mm	Net Thickness	: 20.27 mm
Spec. Width	: 50.84 mm	Flow Stress	: 266.83 MPa
Modulus E	: 167.27 GPa	(Effective)	
Modulus E	: 180.00 GPa	(Nominal)	
Init. Crack	: 28.5406 mm	Init. a/w	: 0.5614 (Measured)
Final Crack	: 38.4188 mm	Final a/w	: 0.7557 (Measured)
Final Crack	: 37.5349 mm	Final a/w	: 0.7383 (Compliance)
Linear Fit	**$J = B+M(\Delta a)$**		
Intercept B	: 254.657 kJ/m^2	Slope M	: 194.97 kJ/m^2mm
Fit Coeff. R	: 0.9699	(10 Data Points)	
J_{IC}	: 311.6 kJ/m^2	(1779.1 $in.–lb/in.^2$)	
Δa (J_{IC})	: 0.292 mm	(0.0115 in.)	
T Average	: 458.0	(J_{IC} at 0.15)	
Power–Law Fit	**$J = C(\Delta a)^n$**		
Coeff. C	: 457.58 kJ/m^2	Exponent n	: 0.4765
Fit Coeff. R	: 0.9828	(10 Data Points)	
J_{IC} (0.20)	: 332.4 kJ/m^2	(1898.3 $in.–lb/in.^2$)	
Δa (J_{IC})	: 0.511 mm	(0.0201 in.)	
T Average	: 459.5	(J_{IC} at 0.20)	
J_{IC} (0.15)	: 309.4 kJ/m^2	(1766.7 $in.–lb/in.^2$)	
Δa (J_{IC})	: 0.440 mm	(0.0173 in.)	
T Average	: 469.0	(J_{IC} at 0.15)	
K_{jc}	: 330.6 $MPa–m^{0.5}$		
J_{IC} Validity & Data Qualification (E 813–85)			
J_{max} Allowed	: 396.64 kJ/m^2	($J_{max}=b_o\sigma_f/15$)	
Data Limit	: J_{max} Ignored		
Δa (max) Allowed	: 2.112 mm	(at 1.5 Exclusion Line)	
Data Limit	: 1.5 Exclusion Line		
Data Points	: Zone A = 3	Zone B = 2	
Data Point Spacing	: OK		
b_{net} or b_o Size	: Inadequate		
dJ/da at J_{IC}	: OK		
a_o Measurement	: 9 Outside Limit		
a_o Measurement	: 1 Outside Limit		
a_f Measurement	: Near–Surface	Outside Limit	
Crack Size Estimate	: Inadequate	(by Compliance)	
E Effective	: OK		
J_{IC} Estimate	: Invalid		
J–R Curve Validity & Data Qualification (E 1152–86)			
J_{max} Allowed	: 270.42 kJ/m^2	($J_{max}=b_{net}\sigma_f/20$)	
Δa (max) Allowed	: 2.230 mm	($\Delta a=0.1b_o$)	
Δa (max) Allowed	: 4.423 mm	($\omega=5$)	
Data Points	: Zone A = 14	Zone B = 3	
Data Point Spacing	: Inadequate		
J–R Curve Data	: Invalid		

Table C–58. Modified J_{IC} and J–R curve results for specimen VRO–01

Linear Fit	**$J = B+M(\Delta a)$**		
Intercept B	: 243.338 kJ/m^2	Slope M	: 226.83 kJ/m^{2}mm
Fit Coeff. R	: 0.9793	(10 Data Points)	
J_{IC}	: 309.0 kJ/m^2	(1764.5 in.–lb/in.^{2})	
Δa (J_{IC})	: 0.290 mm	(0.0114 in.)	
T Average	: 532.9	(J_{IC} at 0.15)	
Power–Law Fit	**$J = C(\Delta a)^n$**		
Coeff. C	: 478.86 kJ/m^2	Exponent n	: 0.5211
Fit Coeff. R	: 0.9872	(10 Data Points)	
J_{IC} (0.20)	: 340.1 kJ/m^2	(1942.2 in.–lb/in.^{2})	
Δa (J_{IC})	: 0.519 mm	(0.0204 in.)	
T Average	: 524.1	(J_{IC} at 0.20)	
J_{IC} (0.15)	: 313.6 kJ/m^2	(1790.7 in.–lb/in.^{2})	
Δa (J_{IC})	: 0.444 mm	(0.0175 in.)	
T Average	: 534.1	(J_{IC} at 0.15)	
K_{jc}	: 346.4 MPa–m$^{0.5}$		

Figure C–56. Fracture surface of the unaged spare pump volute VR tested at 290°C

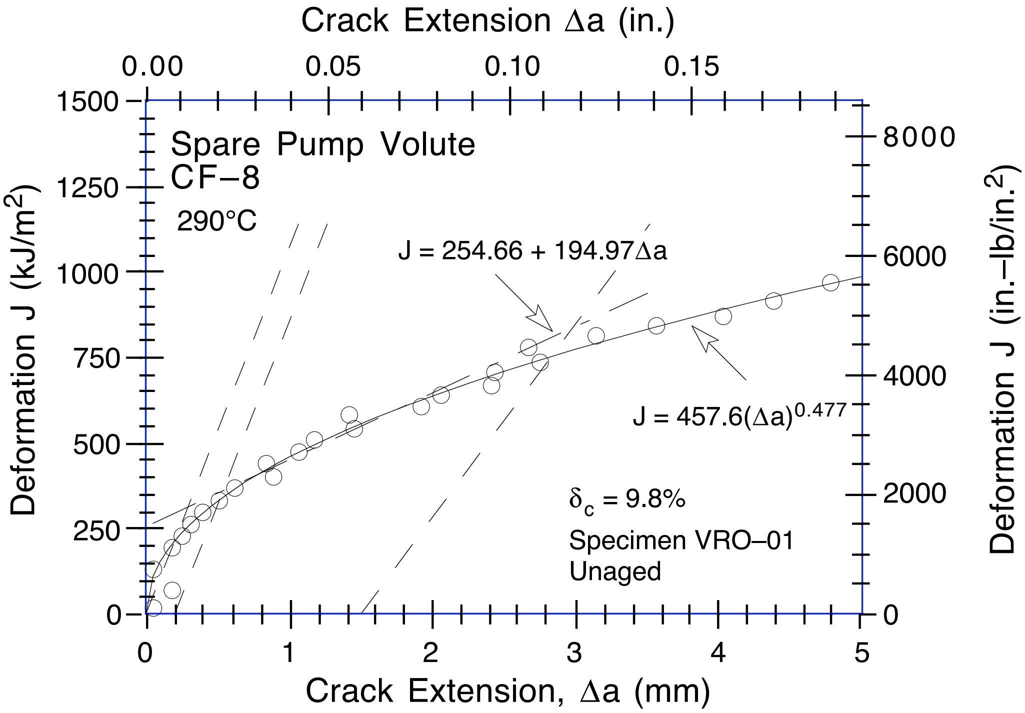

Figure C–57. Deformation J–R Curve at 290°C for unaged spare pump volute VR

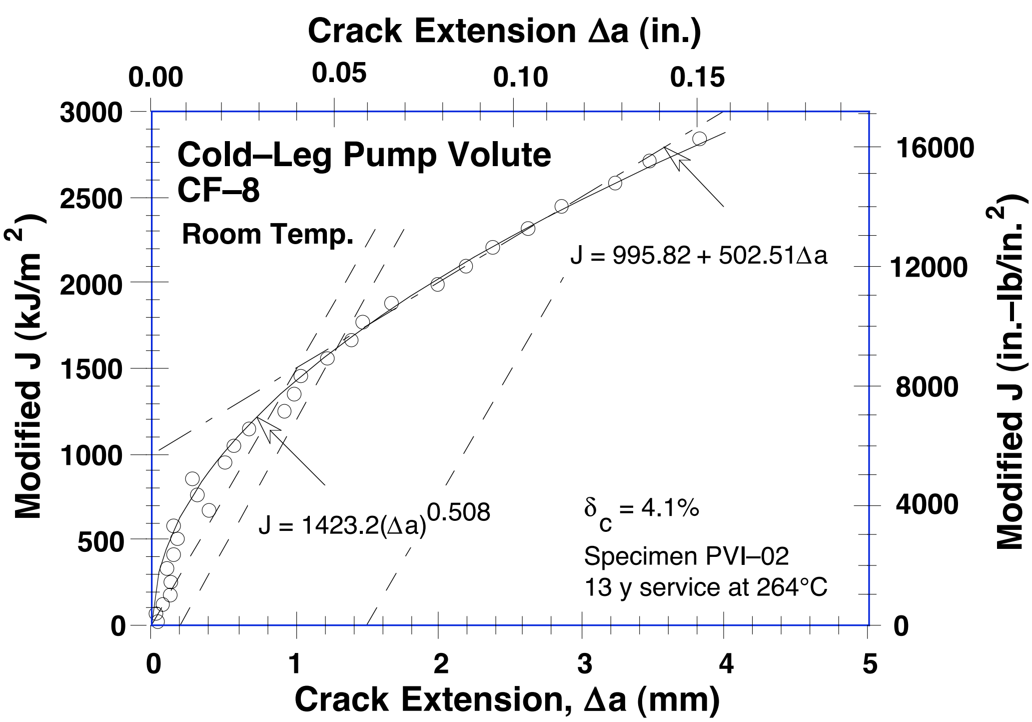

Figure C–58. Modified J–R Curve at 290°C for unaged spare pump volute VR

Table C–59. Test data for specimen VRI–02

Test Number	: 0122	Test Temp	: 290°C
Material Type	: CF-8	Heat Number	: VR
Aging Temp	: 400°C	Aging Time	: 10,000 h
Spec. Thickness	: 25.33 mm	Net Thickness	: 20.32 mm
Spec. Width	: 50.80 mm	Flow Stress	: 305.10 MPa

Unload Number	J_d (kJ/m^2)	J_m (kJ/m^2)	Δa (mm)	Load (kN)	Deflection (mm)
1	11.27	11.24	–0.1042	15.270	0.255
2	42.07	42.43	0.1060	19.718	0.605
3	83.39	84.12	0.1964	22.275	1.008
4	128.46	129.82	0.2891	23.877	1.407
5	176.68	178.04	0.2892	25.022	1.806
6	226.20	229.51	0.4454	25.791	2.207
7	269.61	274.71	0.5638	26.235	2.555
8	308.23	322.96	1.1097	26.463	2.905
9	354.48	368.06	1.0535	26.560	3.257
10	395.79	418.07	1.4272	26.516	3.607
11	435.67	465.67	1.7243	26.010	3.958
12	468.49	514.77	2.2933	25.524	4.311
13	509.83	559.04	2.3866	24.998	4.654
14	537.28	608.90	3.0450	24.085	5.009
15	573.52	660.29	3.4548	23.687	5.406
16	614.33	713.45	3.7620	23.452	5.807
17	644.42	767.96	4.3276	22.947	6.205
18	684.87	819.78	4.5718	22.254	6.607
19	718.15	873.02	4.9726	21.339	7.006
20	741.44	925.13	5.5188	20.523	7.409
21	769.53	973.63	5.8844	19.589	7.805
22	790.96	1023.56	6.3686	18.622	8.209
23	805.95	1071.10	6.8969	17.850	8.606
24	815.67	1117.20	7.4624	16.585	9.005
25	819.79	1160.81	8.0527	15.335	9.405
26	830.33	1203.09	8.5090	14.748	9.807
27	843.13	1245.59	8.9191	14.074	10.207
28	852.34	1287.52	9.3540	13.460	10.606
29	861.93	1328.39	9.7548	12.958	11.005
30	888.45	1379.39	10.0524	12.220	11.505
31	887.35	1429.21	10.6458	10.897	12.008
32	879.58	1472.71	11.2237	10.133	12.505
33	874.98	1514.85	11.7323	9.284	13.005
34	868.79	1555.74	12.2275	8.555	13.505

Table C–60. Deformation J_{IC} and J–R curve results for specimen VRI–02

Test Number	: 0122	Test Temp	: 290°C
Material Type	: CF-8	Heat Number	: VR
Aging Temp	: 400°C	Aging Time	: 10,000 h
Spec. Thickness	: 25.33 mm	Net Thickness	: 20.32 mm
Spec. Width	: 50.80 mm	Flow Stress	: 305.10 MPa
Modulus E	: 172.77 GPa	(Effective)	
Modulus E	: 180.00 GPa	(Nominal)	
Init. Crack	: 28.3219 mm	Init. a/w	: 0.5575 (Measured)
Final Crack	: 41.6063 mm	Final a/w	: 0.8190 (Measured)
Final Crack	: 40.5494 mm	Final a/w	: 0.7982 (Compliance)
Linear Fit	**J = B+M(Δa)**		
Intercept B	: 167.80 kJ/m^2	Slope M	: 155.48 kJ/m^{2}mm
Fit Coeff. R	: 0.9687	(6 Data Points)	
J_{IC}	: 192.3 kJ/m^2	(1098.0 in.–lb/in.^{2})	
Δa (J_{IC})	: 0.158 mm	(0.0062 in.)	
T Average	: 288.6	(J_{IC} at 0.15)	
Power–Law Fit	**J = C(Δa)^n**		
Coeff. C	: 331.58 kJ/m^2	Exponent N	: 0.4477
Fit Coeff. R	: 0.9658	(6 Data Points)	
J_{IC} (0.20)	: 213.8 kJ/m^2	(1220.7 in.–lb/in.^{2})	
Δa (J_{IC})	: 0.375 mm	(0.0148 in.)	
T Average	: 270.8	(J_{IC} at 0.20)	
J_{IC} (0.15)	: 196.6 kJ/m^2	(1122.5 in.–lb/in.^{2})	
Δa (J_{IC})	: 0.311 mm	(0.0122 in.)	
T Average	: 277.4	(J_{IC} at 0.15)	
Kjc	: 275.0 MPa–m$^{0.5}$		
J_{IC} Validity & Data Qualification (E 813–85)			
J_{max} Allowed	: 457.25 kJ/m^2	($J_{max}=b_o\sigma_f/15$)	
Data Limit	: J_{max} Ignored		
Δa (max) Allowed	: 1.859 mm	(at 1.5 Exclusion Line)	
Data Limit	: 1.5 Exclusion Line		
Data Points	: Zone A = 2	Zone B = 2	
Data Point Spacing	: OK		
b_{net} or b_o Size	: OK		
dJ/da at J_{IC}	: OK		
a_f Measurement	: Near-surface	outside limit	
Initial Crack Shape	: OK		
Crack size estimate	: Inadequate	(by Compliance)	
E Effective	: OK		
J_{IC} Estimate	: Invalid		
J–R Curve Validity & Data Qualification (E 1152–86)			
J_{max} Allowed	: 310.01 kJ/m^2	($J_{max}=b_{net}\sigma_f/20$)	
Δa (max) Allowed	: 2.248 mm	($\Delta a=0.1b_o$)	
Δa (max) Allowed	: 4.175 mm	($\omega=5$)	
Data Points	: Zone A = 5	Zone B = 5	
Data Point Spacing	: Inadequate		
J-R Curve Data	: Invalid		

Table C–61. Modified J_{IC} and J–R curve results for specimen VRI–02

Linear Fit	**$J = B+M(\Delta a)$**		
Intercept B	: 160.956 kJ/m^2	Slope M	: 176.04 kJ/m^2mm
Fit Coeff. R	: 0.9751	(6 Data Points)	
J_{IC}	: 188.1 kJ/m^2	(1074.0 in.–lb/in.^{2})	
Δa (J_{IC})	: 0.154 mm	(0.0061 in.)	
T Average	: 326.7	(J_{IC} at 0.15)	
Power–Law Fit	**$J = C(\Delta a)^n$**		
Coeff. C	: 345.76 kJ/m^2	Exponent N	: 0.4855
Fit Coeff. R	: 0.9717	(6 Data Points)	
J_{IC} (0.20)	: 215.1 kJ/m^2	(128.3 in.–lb/in.^{2})	
Δa (J_{IC})	: 0.376 mm	(0.0148 in.)	
T Average	: 304.5	(J_{IC} at 0.20)	
J_{IC} (0.15)	: 196.0 kJ/m^2	(1119.1 in.–lb/in.^{2})	
Δa (J_{IC})	: 0.311 mm	(0.0122 in.)	
T Average	: 311.4	(J_{IC} at 0.15)	
K_{jc}	: 285.1 MPa–$m^{0.5}$		

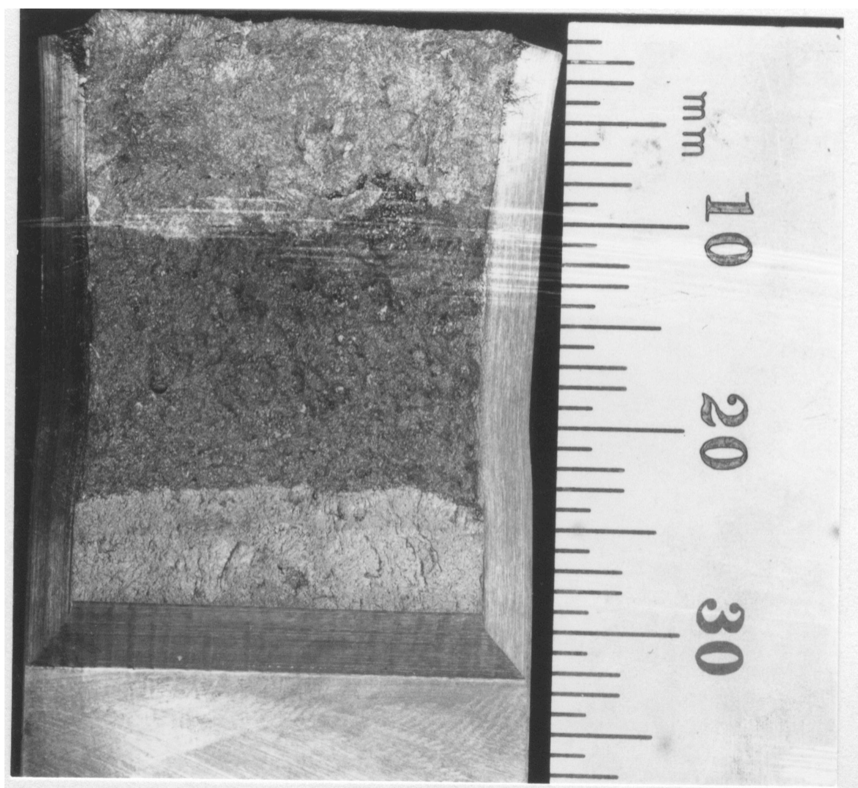

Figure C–59. Fracture surface of the spare pump volute VR aged 10,000 h at 400°C and tested at 290°C

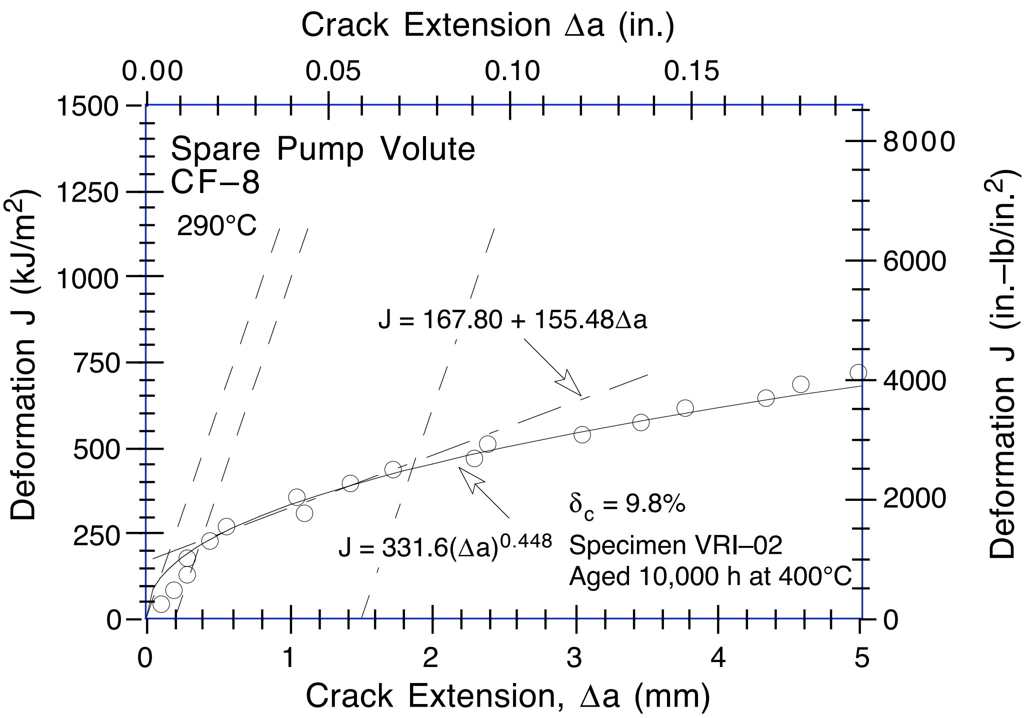

Figure C–60. Deformation J–R Curve at 290°C for spare pump volute VR aged 10,000 h at 400°C

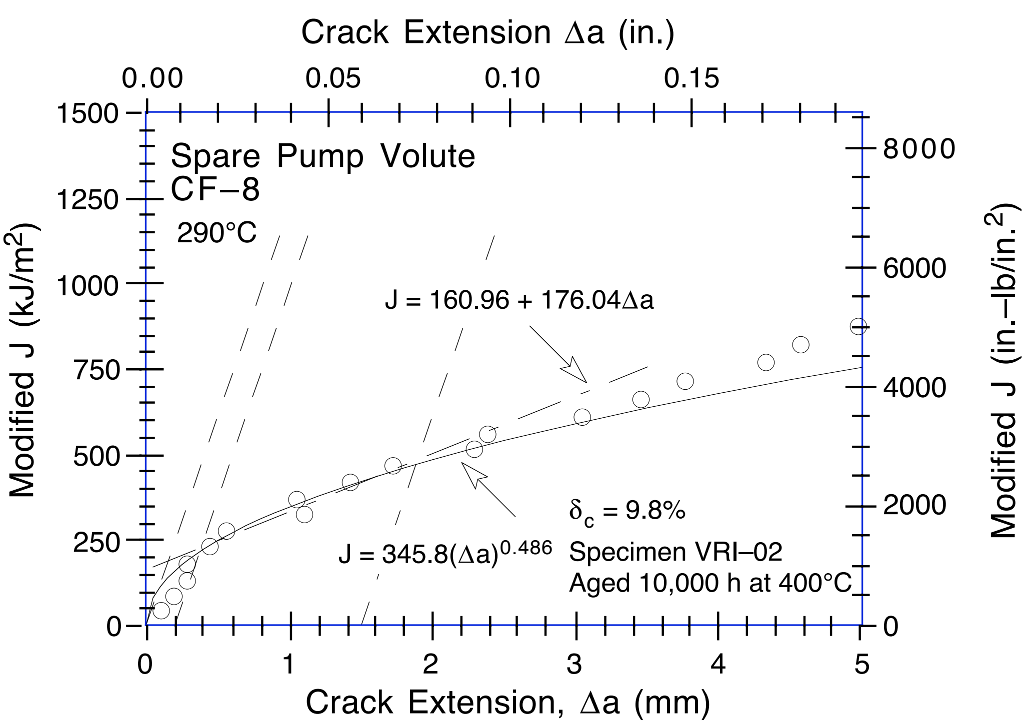

Figure C–61. Modified J–R Curve at 290°C for spare pump volute VR aged 10,000 h at 400°C

Distribution for NUREG/CR–6275 (ANL–94/37)

Internal:

O. K. Chopra (25)
H. M. Chung
T. F. Kassner
C. Malefyt
R. B. Poeppel
W. J. Shack
C. E. Till
R. W. Weeks
TIS Files

External:

NRC, for distribution per R5
ANL Libraries
  ANL–E (2)
  ANL–W
Manager, Chicago Field Office, DOE
Energy Technology Division Review Committee
  H. K. Birnbaum, University of Illinois, Urbana, IL
  R. C. Buchanan, University of Cincinnati, Cincinnati, OH
  M. S. Dresselhaus, Massachusetts Institute of Technology, Cambridge, MA
  B. G. Jones, University of Illinois, Urbana, IL
  C.–Y. Li, Cornell University, Ithaca, NY
  S.–N. Liu, Fremont, CA
  R. E. Smith, SciTech, Inc., Morrisville, NC
D. Atteridge, Battelle Pacific Northwest Laboratory, Richland
W. H. Bamford, Westinghouse Electric Corp., Pittsburgh, PA
K. K. Bandyopadhyay, Brookhaven National Laboratory, Upton, NY.
J. A. Christensen, Battelle Pacific Northwest Laboratories, Richland
N. G. Cofie, Nutech, San Jose, CA
A. Cowan, Risley Nuclear Power Development Labs., Risley, Warrington, UK
W. H. Cullen, Materials Engineering Associates, Inc., Lanham, MD
B. J. L. Darlaston, Berkeley Nuclear Laboratories, Berkeley, Gloucestershire, UK
G. Gage, AEA Technology, Harwell Laboratory, Oxfordshire, UK
J. Gilman, Electric Power Research Inst., Palo Alto, CA
W. Gysel, Georg Fischer, Ltd., Schaffhausen, Switzerland
G. E. Hale, The Welding Institute, Abington, Cambridge, UK
P. Hedgecock, APTECH Engineering Services, Inc., Palo Alto, CA
B. Hemsworth, HM Nuclear Installations Inspectorate, London
C. Hoffmann, ABB CE Nuclear Power, Windsor, CT
J. Jansky, Buro für Technische Beratung, Leonberg, Germany
C. E. Jaske, CC Technologies, Cortest, Columbus, OH
G. J. Licina, Structural Integrity Associates, San Jose, CA
T. R. Mager, Westinghouse Electric Corp., Pittsburgh, PA
H. Mehta, General Electric Co., San Jose, CA
Y. Meyzaud, Framatome, Paris La Defense, France
M. Prager, Materials Properties Council, Inc., New York, NY
P. H. Pumphrey, National Power, Technology and Environment Center, Leatherhead, Surrey, UK

D. Quiñones, Robert Cloud & Associates, Berkeley, CA
C. Y. Rieg, Electricité de France, Villeurbanne Cedex, France
V. N. Shah, EG&G Idaho, Inc., Idaho Falls, Idaho
G. Slama, Framatome, Paris La Defense, France
G. D. W. Smith, Oxford University, Oxford, UK
H. D. Solomon, General Electric Co., Schenectady, NY
D. M. Stevens, Lynchburg Research Center, Babcock & Wilcox Co., Lynchburg, VA
L. Taylor, Nuclear Electric plc., Chelsford Rd., Knutsford, Cheshire, UK
J. C. Van Duysen, Electricité de France, Moret–Sur–Loing, France
S. Yukawa, Boulder, CO

NRC FORM 335 (2–89) NRCM 1102, 3201, 3202

U. S. NUCLEAR REGULATORY COMMISSION

BIBLIOGRAPHIC DATA SHEET

(See instructions on the reverse)

1. REPORT NUMBER *(Assigned by NRC. Add Vol., Supp., Rev., and Addendum Numbers, if any.)*

NUREG/CR–6275
ANL–94/37

2. TITLE AND SUBTITLE

Mechanical Properties of Thermally Aged Cast Stainless Steels from Shippingport Reactor Components

3. DATE REPORT PUBLISHED

MONTH	YEAR
April	1995

4. FIN OR GRANT NUMBER

A2256

5. AUTHOR(S)

O. K. Chopra and W. J. Shack

6. TYPE OF REPORT

Technical

7. PERIOD COVERED *(Inclusive Dates)*

8. PERFORMING ORGANIZATION – NAME AND ADDRESS *(If NRC, provide Division, Office or Region, U.S. Nuclear Regulatory Commission, and mailing address; if contractor, provide name and mailing address.)*

Argonne National Laboratory
9700 South Cass Avenue
Argonne, IL 60439

9. SPONSORING ORGANIZATION – NAME AND ADDRESS *(If NRC, type "Same as above": if contractor, provide NRC Division, Office or Region, U.S. Nuclear Regulatory Commission, and mailing address.)*

Division of Engineering
Office of Nuclear Regulatory Research
U. S. Nuclear Regulatory Commission
Washington, DC 20555

10. SUPPLEMENTARY NOTES

11. ABSTRACT (200 words or less)

Thermal embrittlement of static–cast CF–8 stainless steel components from the decommissioned Shippingport reactor has been characterized. Cast stainless steel materials were obtained from four cold–leg check valves, three hot–leg main shutoff valves, and two pump volutes. The actual time–at–temperature for the materials was ≈13 y at ≈281°C for the hot–leg components and ≈264°C for the cold–leg components. Baseline mechanical properties for as–cast material were determined from tests on either recovery–annealed material or material from the cooler region of the component. The Shippingport materials show modest decreases in fracture toughness and Charpy–impact properties and a small increase in tensile strength because of relatively low service temperatures and ferrite content of the steel. The procedure and correlations developed at Argonne National Laboratory for estimating mechanical properties of cast stainless steels predict accurate or slightly lower values for Charpy–impact energy, tensile flow stress, fracture toughness J–R curve, and J_{IC} of the materials. The kinetics of thermal embrittlement and degree of embrittlement at saturation were established from materials that were aged further in the laboratory. The results were consistent with the estimates. The correlations successfully predicted the mechanical properties of the Ringhals 2 reactor hot– and crossover–leg elbows (CF–8M) after service of ≈15 y and the KRB reactor pump cover plate (CF–8) after ≈8 y of service.

12. KEY WORDS/DESCRIPTORS *(List words or phrases that will assist researchers in locating this report.)*

Shippingport reactor
Cast stainless steel
Thermal aging
Embrittlement
Fracture toughness
J–R curve
Impact strength
Tensile strength
Ramberg–Osgood equation

13. AVAILABILITY STATEMENT

Unlimited

14. SECURITY CLASSIFICATION

(This Page)

Unclassified

(This Report)

Unclassified

15. NUMBER OF PAGES

16. PRICE